

**Andreas Preußer**

Vom Fachbereich VI  
(Raum- und Umweltwissenschaften)  
der Universität Trier  
zur Verleihung des akademischen Grades

**Doktor der Naturwissenschaften (Dr. rer. nat.)**

genehmigte Dissertation

# **Multi-sensor remote sensing of long-term circumpolar polynya characteristics in the Arctic**

Betreuer: Univ.-Prof. Dr. Günther Heinemann  
Berichterstattende: Univ.-Prof. Dr. Günther Heinemann  
Univ.-Prof. Dr. Thomas Udelhoven  
Prof. Dr. Lars Kaleschke (extern)

Wissenschaftliche Aussprache: 14. Juni 2017

Trier, 2017

## Abstract

In recent decades, the Arctic has been undergoing a wide range of fast environmental changes. The sea ice covering the Arctic Ocean not only reacts rapidly to these changes, but also influences and alters the physical properties of the atmospheric boundary layer and the underlying ocean on various scales. In that regard, polynyas, i.e. regions of open water and thin ice within the closed pack ice, play a key role as being regions of enhanced atmosphere-ice-ocean interactions and extensive new ice formation during winter. A precise long-term monitoring and increased efforts to employ long-term and high-resolution satellite data is therefore of high interest for the polar scientific community. The retrieval of thin-ice thickness (TIT) fields from thermal infrared satellite data and atmospheric reanalysis, utilizing a one-dimensional energy balance model, allows for the estimation of the heat loss to the atmosphere and hence, ice-production rates. However, an extended application of this approach is inherently connected with severe challenges that originate predominantly from the disturbing influence of clouds and necessary simplifications in the model set-up, which all need to be carefully considered and compensated for.

The presented thesis addresses these challenges and demonstrates the applicability of thermal infrared TIT distributions for a long-term polynya monitoring, as well as an accurate estimation of ice production in Arctic polynyas at a relatively high spatial resolution. Being written in a cumulative style, the thesis is subdivided into three parts that show the consequent evolution and improvement of the TIT retrieval, based on two regional studies (Storfjorden and North Water (NOW) polynya) and a final large-scale, pan-Arctic study.

The first study on the Storfjorden polynya, situated in the Svalbard archipelago, represents the first long-term investigation on spatial and temporal polynya characteristics that is solely based on daily TIT fields derived from MODIS thermal infrared satellite data and ECMWF ERA-Interim atmospheric reanalysis data. Typical quantities such as polynya area (POLA), the TIT distribution, frequencies of polynya events as well as the total ice production are derived and compared to previous remote sensing and modeling studies. The study includes a first basic approach that aims for a compensation of cloud-induced gaps in daily TIT composites. This coverage-correction (CC) is a mathematically simple upscaling procedure that depends solely on the daily percentage of available MODIS coverage and yields daily POLA with an error-margin of 5 to 6 %.

The NOW polynya in northern Baffin Bay is the main focus region of the second study, which follows two main goals. First, a new statistics-based cloud interpolation scheme (Spatial Feature Reconstruction - SFR) as well as additional cloud-screening procedures are successfully adapted and implemented in the TIT retrieval for usage in Arctic polynya regions. For a 13-yr period, results on polynya characteristics are compared to the CC approach. Furthermore, an investigation on highly variable ice-bridge dynamics in Nares Strait is presented. Second, an analysis of decadal changes of the NOW polynya is carried out, as the additional use of a suite of passive microwave sensors leads to an extended record of 37 consecutive winter seasons, thereby enabling detailed inter-sensor comparisons.

In the final study, the SFR-interpolated daily TIT composites are used to infer spatial and temporal characteristics of 17 circumpolar polynya regions in the Arctic for 2002/2003 to 2014/2015. All polynya regions combined cover an average thin-ice area of  $226.6 \pm 36.1 \times 10^3 \text{ km}^2$  during

---

winter (November to March) and yield an average total wintertime accumulated ice production of about  $1811 \pm 293 \text{ km}^3$ . Regional differences in derived ice production trends are noticeable. The Laptev Sea on the Siberian shelf is presented as a focus region, as frequently appearing polynyas along the fast-ice edge promote high rates of new ice production. New affirming results on a distinct relation to sea-ice area export rates and hence, the Transpolar Drift, are shown.

This new high-resolution pan-Arctic data set can be further utilized and build upon in a variety of atmospheric and oceanographic applications, while still offering room for further improvements such as incorporating high-resolution atmospheric data sets and an optimized lead-detection.

## Zusammenfassung

In den letzten Jahrzehnten unterliegt die Arktis einem breiten Spektrum schneller Umweltveränderungen. Das Meereis, das den Arktischen Ozean bedeckt, reagiert nicht nur sehr schnell auf diese Veränderungen, sondern beeinflusst und verändert gleichsam die physikalischen Eigenschaften der atmosphärischen Grenzschicht und des darunter liegenden Ozeans auf verschiedenen Skalen. In dieser Hinsicht spielen Polynjen, also Gebiete mit dünnem Eis oder offenem Wasser im ansonsten dicken Packeis, eine wichtige Rolle als Regionen erhöhter Atmosphäre-Eis-Ozean-Wechselwirkungen sowie umfassender neuer Eisbildung im Winter. Ein präzises Monitoring sowie verstärkte Bemühungen langfristige und hochauflösende Satellitendaten zu nutzen sind daher für die Polarforschung von grossem Interesse. Die Ableitung von Dünneisdicken (TIT) aus thermal-Infrarot Satellitendaten und atmosphärischen Reanalysedaten mittels eines eindimensionalen Energiebilanzmodells ermöglicht die Abschätzung des Wärmeverlusts zur Atmosphäre und damit Eisproduktionsraten. Eine ausgedehnte Anwendung dieses Ansatzes unterliegt jedoch einigen Herausforderungen, die vor allem aus dem störenden Einfluss der Wolken und notwendigen Vereinfachungen in der Modellkonfiguration resultieren. Diese gilt es sorgfältig zu berücksichtigen und zu kompensieren.

Die hier vorliegende Arbeit befasst sich mit diesen Herausforderungen und zeigt die Anwendbarkeit von thermal-Infrarot TIT-Verteilungen für ein langfristiges Polynja-Monitoring sowie eine hochaufgelöste und präzise Schätzung der Eisproduktion in arktischen Polynjen. Die in kumulativer Form geschriebene Arbeit ist in drei Teile gegliedert, welche die konsequente Weiterentwicklung und Verbesserung der Ableitung von TIT auf Basis von zwei Regionalstudien (Storfjorden und North Water (NOW) Polynja) sowie einer abschliessenden gesamt-Arktischen Studie aufzeigen.

Die erste Studie zur Storfjorden Polynja im Svalbard-Archipel stellt die erste auf täglichen TIT-Feldern basierende Langzeituntersuchung räumlicher und zeitlicher Polynya-Charakteristika dar, die ausschliesslich auf Basis von thermal-Infrarot Satellitendaten des MODIS-Sensors und ECMWF ERA-Interim Reanalysedaten gewonnen wurden. Daraus werden typische Eigenschaften wie die Polynja-Fläche (POLA), TIT-Verteilungen, Auftrittsraten von Polynja-Bereichen sowie die akkumulierte Eisproduktion abgeleitet und mit früheren Fernerkundungs- und Modellierungsstudien verglichen. Die Studie beinhaltet einen ersten grundlegenden Ansatz, um die von Wolken verursachten Lücken in den täglichen TIT-Kompositen zu kompensieren. Diese Abdeckungskorrektur (CC) ist ein mathematisch recht einfaches Skalierungsverfahren, welches basierend auf dem täglichen Prozentsatz der verfügbaren MODIS-Abdeckung die tägliche POLA mit einem Fehler von 5 bis 6% korrigiert.

Die NOW Polynja in der nördlichen Baffin Bucht ist der Schwerpunkt der zweiten Studie, die zwei Hauptziele verfolgt. Das erste Ziel beinhaltet die Anpassung und Implementierung eines neuen statistisch-basierten Wolken-Interpolationsschemas (Spatial Feature Reconstruction - SFR) sowie eines erweiterten Verfahrens zum Ausschluss von Wolken-Artefakten in den MODIS TIT-Kompositen. Für einen Zeitraum von 13 Jahren werden die daraus abgeleiteten Polynya-Merkmale mit denen des CC-Ansatzes verglichen. Darüber hinaus wird auf Basis der täglichen TIT-Komposite eine Untersuchung der hochgradig variablen Eisbrücken-Dynamik in der Nares Strasse präsentiert. Als zweites Hauptziel wird eine Analyse dekadischer Änderungen der NOW Polynja verfolgt. Die dabei zusätzlich verwendeten Daten passiver Mikrowellensensoren erwei-

---

ern den Untersuchungszeitraum auf 37 aufeinanderfolgende Winter, wodurch detaillierte Vergleiche zwischen den Sensoren ermöglicht werden.

In der abschliessenden Studie werden die mittels SFR interpolierten täglichen TIT-Verteilungen genutzt um hochaufgelöste räumliche und zeitliche Eigenschaften von 17 zirkumpolaren Polynjaregionen in der Arktis für den Zeitraum 2002/2003 bis 2014/2015 abzuleiten. Alle Polynjaregionen zusammen weisen im Winter (November bis März) eine durchschnittliche Dünneisfläche von  $226,6 \pm 36,1 \times 10^3 \text{ km}^2$  auf, was eine durchschnittliche akkumulierte Eisproduktion von  $1811 \pm 293 \text{ km}^3$  in diesen Gebieten ermöglicht. Es zeigen sich deutliche regionale Unterschiede in den abgeleiteten Trends der Eisproduktion. Im besonderen Fokus steht die Laptev See im Bereich des sibirischen Schelfs, da die dort regelmässig entlang der Festeiskante auftretenden Polynjen eine recht hohe Eisproduktion aufweisen. Es zeigt sich ein ausgeprägter Zusammenhang zwischen der Eisproduktion in den Polynjen und Meereis-Exportraten aus der Laptev See in die Transpolar-drift.

Dieser neue hochaufgelöste pan-Arktische Datensatz kann nun in einer Vielzahl von atmosphärischen und ozeanographischen Anwendungen genutzt werden, und bietet Raum für weitere Verbesserungen wie etwa die Integration höher-aufgelöster atmosphärischer Datensätze und eine optimierte Eisrinnen-Erkennung.

# Contents

<b>List of Figures</b>	<b>II</b>
<b>List of Abbreviations</b>	<b>III</b>
<b>1 Introduction</b>	<b>1</b>
1.1 The role of sea ice in the Arctic . . . . .	3
1.2 Sea ice and ice formation: Physical properties and processes . . . . .	5
1.3 Polynyas and leads: Hotspots for enhanced atmosphere-ice-ocean interactions . . . . .	8
1.4 A changing Arctic sea-ice cover: Overview and implications for polynyas . . . . .	11
<b>2 Methodical Review: Remote Sensing of Sea Ice and the Monitoring of polynyas</b>	<b>14</b>
2.1 Satellite remote sensing of sea ice . . . . .	15
2.1.1 Optical and thermal-infrared sensors . . . . .	15
2.1.2 Passive microwave radiometers . . . . .	17
2.1.3 Other satellite sensor types used for sea ice remote sensing . . . . .	20
2.2 Satellite observations of polynya characteristics - state of research . . . . .	21
2.2.1 Thermal-infrared thin-ice thickness (TIT) retrieval . . . . .	23
2.2.2 Polynya Signature Simulation Method (PSSM) and SIC thresholds . . . . .	25
2.2.3 Thin-ice thickness retrieval using passive microwave sensors . . . . .	26
2.2.4 Derivation of potential thermodynamic ice production in polynyas . . . . .	26
<b>3 Motivation, objectives and outline of the thesis</b>	<b>28</b>
3.1 Short summary - Publication I (Storfjorden polynya) . . . . .	30
3.2 Short summary - Publication II (North Water polynya) . . . . .	31
3.3 Short summary - Publication III (Circumpolar polynya-regions) . . . . .	32
<b>4 Publication I: Thin-ice dynamics and ice production in the Storfjorden polynya</b>	<b>34</b>
<b>5 Publication II: Multi-Decadal Variability of the North Water Polynya</b>	<b>46</b>
<b>6 Publication III: Circumpolar Thin-Ice Regions and Ice Production in the Arctic</b>	<b>71</b>
<b>7 Synthesis &amp; Outlook</b>	<b>94</b>
<b>Bibliography</b>	<b>98</b>
<b>Curriculum Vitae</b>	<b>112</b>
<b>Acknowledgements</b>	<b>117</b>
<b>Eidesstattliche Erklärung</b>	<b>118</b>

## List of Figures

1.1	Overview map of the Arctic . . . . .	2
1.2	Daily time series of the Arctic sea ice extent . . . . .	4
1.3	Crystal structure of ice Ih . . . . .	6
1.4	Different ice types during ice growth . . . . .	7
1.5	Schematic latent heat polynya . . . . .	9
1.6	Monthly ice extent anomalies between 1979 and 2016 . . . . .	11
1.7	Maps and time series of the sea ice age in the Arctic . . . . .	12
2.1	Spectral regions used for TIR and PMW remote sensing . . . . .	15
2.2	Emissivities of sea ice and sea water . . . . .	18
3.1	Schematic overview of the thesis outline . . . . .	29

## List of Abbreviations

<b>70PT</b>	70% (Percent) SIC Threshold
<b>AD</b>	Arctic Dipole
<b>AMSR-E</b>	Advanced Microwave Scanning Radiometer - Earth Observing System
<b>AMSR2</b>	Advanced Microwave Scanning Radiometer 2
<b>AO</b>	Arctic Oscillation
<b>ASI</b>	ARTIST Sea Ice Algorithm
<b>AVHRR</b>	Advanced Very High Resolution Radiometer
<b>CC</b>	Coverage Correction
<b>CCS</b>	Confident Clear-Sky
<b>CSA</b>	Canadian Space Agency
<b>DCC</b>	Definitive Cloud Cover
<b>DMSP</b>	Defense Meteorological Satellite Program
<b>DLR</b>	Deutsches Zentrum für Luft- und Raumfahrt (German Aerospace Center)
<b>DOY</b>	Day Of Year
<b>ECMWF</b>	European Center for Medium-Range Weather Forecasts
<b>ESA</b>	European Space Agency
<b>ESMR</b>	Electrically Scanning Microwave Radiometer
<b>GCOM-W1</b>	Global Change Observation Mission-Water
<b>GR</b>	Gradient Ratio
<b>GrIS</b>	Greenland Ice Sheet
<b>GSFC</b>	Goddard Space Flight Center
<b>IKAPOS</b>	Investigation of KAtabatic winds and POLynyas during Summer
<b>IP</b>	Ice Production
<b>JAXA</b>	Japan Aerospace Exploration Agency
<b>IST</b>	Ice Surface Temperature
<b>LAP</b>	Laptev Sea Polynya
<b>LiDAR</b>	Light Detection And Ranging
<b>MCC</b>	Medium Cloud Cover
<b>MCP</b>	Mixed Cover Pixels



## List of Abbreviations

---

<b>MODIS</b>	Moderate-Resolution Imaging Spectroradiometer
<b>NASA</b>	National Aeronautics and Space Administration
<b>NAO</b>	North Atlantic Oscillation
<b>NCEP</b>	National Center for Environmental Prediction
<b>NOAA</b>	National Oceanic and Atmospheric Administrations
<b>NOW</b>	North Water
<b>NRT</b>	Near Real Time
<b>NSIDC</b>	National Snow and Ice Data Center
<b>OWA</b>	Open Water Area
<b>P</b>	Polarization difference
<b>PIX</b>	Persistence Index
<b>POLA</b>	Polynya Area
<b>PR</b>	Polarization Ratio
<b>PSSM</b>	Polynya Signature Simulation Method
<b>RADAR</b>	Radio Detection And Ranging
<b>SAR</b>	Synthetic Aperture Radar
<b>SFR</b>	Spatial Feature Reconstruction
<b>SIC</b>	Sea Ice Concentration
<b>SLSTR</b>	Sea and Land Surface Temperature Radiometer
<b>SMMR</b>	Scanning Multichannel Microwave Radiometer
<b>SMOS</b>	Soil Moisture and Ocean Salinity sensor
<b>SSM/I</b>	Special Sensor Microwave / Imager
<b>SSMIS</b>	Special Sensor Microwave Imager/Sounder
<b>STD</b>	Standard Deviation
$T_b$	Brightness Temperature
<b>TIR</b>	Thermal Infrared Radiation
<b>TIT</b>	Thermal-/Thin-Ice Thickness
<b>UCP</b>	Un-Covered pixels
<b>UTC</b>	Universal Coordinated Time

# 1 Introduction

The polar oceans of both Arctic and Antarctic cover around 7% of the earth's surface [Wadhams 2000]. This is quite a significant areal fraction that would on its own justify extensive and regular monitoring efforts. However, recent rapid changes of particularly the Arctic sea ice cover as well as altered atmospheric and oceanic characteristics highlight the need for increased research efforts in this region, as the speed of change is hitherto unprecedented in the observational record. Furthermore, the emerging evidence for mid-latitude linkages [e.g. Francis and Vavrus 2012; Overland et al. 2012; Francis and Vavrus 2015; Cohen et al. 2014] slowly transforms the thinking about these climatic changes, simply speaking, from being 'fairly remote' to 'next to one's doorstep'. Besides the increased attention from basically all areas of natural sciences, also the public media, policy-makers and the gas-, oil- and worldwide shipping industry show more and more interest in the changing Arctic sea ice cover due to the anticipated economic potential during the summer months, as the ice gets thinner and ice-free conditions prevail over larger areas and longer time periods [e.g. Kwok et al. 2009; Stroeve et al. 2011, 2014]. Consequently, a huge scientific focus is set on understanding the observed and ongoing small- and large-scale changes of the Arctic sea ice cover over the recent decades and to develop advanced strategies and models to predict its future development in the 21st century. As most field campaigns and experiments in the polar regions are expensive and complex initiatives under generally harsh environmental conditions, many investigations are carried out by means of regional and large-scale modeling of the atmosphere-sea ice-ocean system, or by utilizing the ever growing data sets from various satellite remote sensing missions that started to become available in the 1970's. Nowadays, these satellite observations play a leading role in monitoring, analyzing and understanding remote climatic changes in the Arctic and Antarctic.

The Arctic Ocean itself is basically an almost closed basin with about  $10 \times 10^6 \text{ km}^2$  in area and about  $13.5 \times 10^6 \text{ km}^3$  in volume [Carmack 1986; Wadhams 2000]. The main path for water exchanges with other oceans is the Fram Strait, a deep passage to the Atlantic Ocean that is framed by the Svalbard archipelago in the East and Greenland in the West. Among other important passages are the Nares Strait between Greenland and Ellesmere Island, as well as several more shallow links with the Atlantic and Pacific Ocean, including the Barents Sea, the Canadian Archipelago and Bering Strait. A quite unique characteristic of the Arctic Ocean is the shallowness over broad and extensive shelf areas north of Russia (extending around 800 km from the coast), so that almost one third of the total ocean area features depths of 100 m or less [Carmack 1986; Wadhams 2000]. As can be seen in Fig. 1.1, those shelf areas (also the narrow regions between Alaska and Greenland) frequently feature so called polynyas, which are areas of open water and thin ice with a huge influence on local physical, chemical and biological properties [Smith et al. 1990; Barber and Massom 2007]. More details on polynyas will be given in Chapter 1.3.

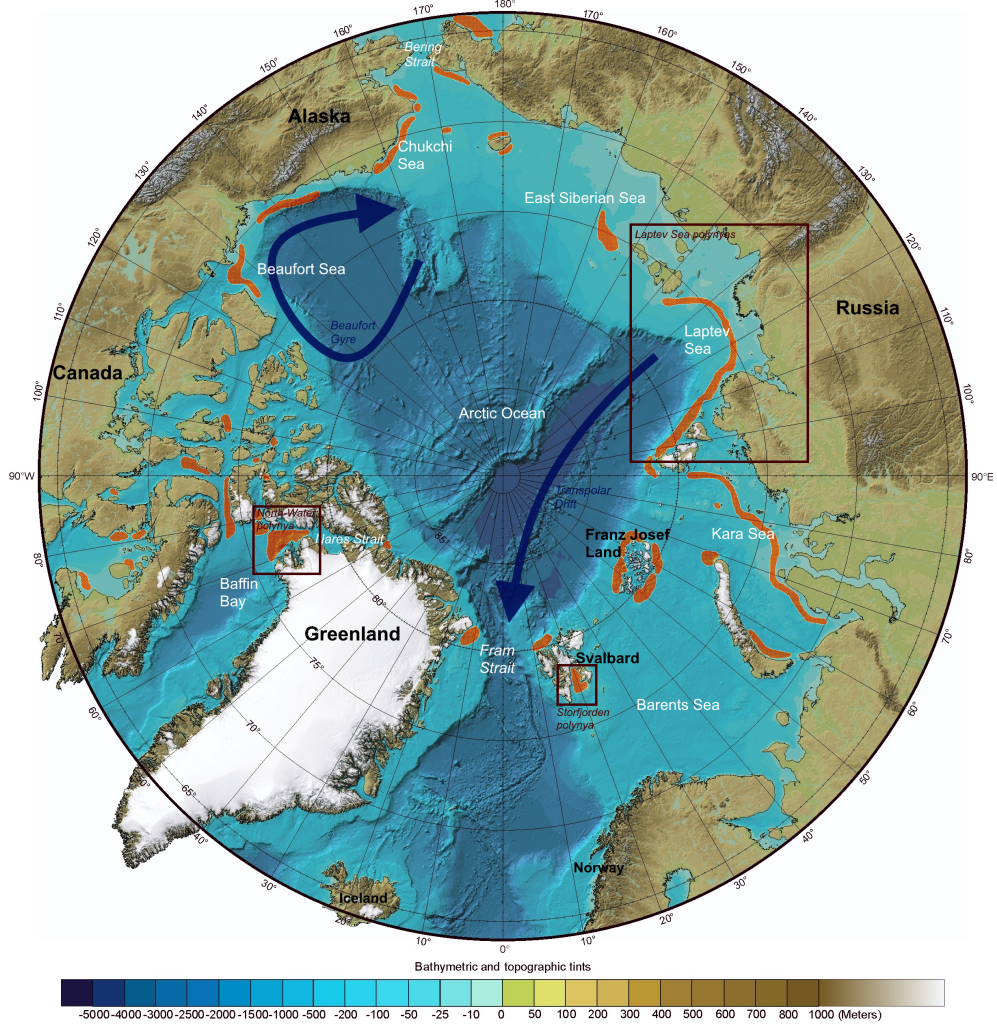


Figure 1.1: The Arctic region, with locations of polynya occurrences indicated as being referred to in Barber and Massom [2007]. Further depicted in blue are the two major circulation patterns, namely the Beaufort Gyre and the Transpolar Drift stream, as well as the main focus areas for the present thesis framed in red. Figure modified from Jakobsson et al. [2012], showing the international bathymetric chart of the Arctic Ocean (IBCAO v3).

Since 1993, a multidisciplinary Russian-German cooperation project (*WTZ RUS: System Laptev Sea Transdrift*; e.g. Kassens et al. [1995]) is investigating the Laptev Sea region on the Siberian shelf as a specifically important part of the Arctic climate system and its distinct connection to a major large-scale drift system - the Transpolar Drift Stream (Fig. 1.1). Sea ice that is formed in open water and thin-ice regions of the Laptev Sea (and adjacent seas) is subsequently incorporated in this mostly wind-driven ice flow and within 1-3 years transported across the Arctic Ocean towards Fram Strait. There, it leaves the Arctic basin and eventually melts into the North Atlantic ocean [e.g. Wadhams 2000; Haas 2010; Smedsrud et al. 2017].

In the most recent project phase (2013 to 2016), one of the main research goals related to high-resolution remote sensing was to get a more comprehensive and long-term picture on ice pro-

duction and generally atmosphere-ice-ocean interactions in polynyas and leads (i.e., open-water and thin-ice areas), which are regarded as regions that influence Transpolar Drift characteristics by generating a substantial amount of ice that is subsequently exported from the shelf areas. Furthermore, a precise and regular monitoring of those regions is of high interest due to their role as being 'windows' [Barber and Massom 2007] between the cold atmosphere (during winter) above and the relatively warm ocean below. In that regard, polynyas and leads play major roles in altering the structure of both the atmospheric boundary layer and the upper ocean layers.

Emerging from this project framework, the prime focus of this thesis is aiming towards the derivation of large-scale and high-resolution thin-ice thickness distributions and the quantification of ice production in Arctic polynya systems by using satellite remote sensing data from the thermal infrared part of the electromagnetic spectrum, measured by the Moderate Resolution Imaging Spectroradiometer (MODIS), in combination with atmospheric reanalysis data (European Center for Medium-range Weather Forecast (ECMWF) ERA-Interim, Dee et al. [2011]). The hereby obtained new results build upon the work of earlier project phases [Willmes et al. 2010, 2011; Adams et al. 2013] and feature recent methodological improvements that evolved in concert with conceptually similar regional remote sensing studies in Antarctica [Paul et al. 2015b, a].

This first introductory chapter aims to give a comprehensive overview on sea-ice fundamentals, both on a large and small scale, a general description of sea-ice features that promote interactions between the ocean, ice and atmosphere, i.e. thin-ice regions, and an overview on recently observed and projected changes in the Arctic climate system. Based on this background, Chapter 2 will focus on a methodical review on remote sensing sensors, data, techniques and principles that are used to monitor sea ice in general and thin-ice regions in specific. This will then serve as the framework for the following chapters, as Chapter 3 highlights the general motivation and associated objectives of the present thesis. It also summarizes the three peer-reviewed publications that all together build the major part of this thesis in Chapters 4 to 6. The final Chapter 7 will summarize the main conclusions and achievements that emerged from these publications and give directions on how the presented work could be further built upon and improved.

### 1.1 The role of sea ice in the Arctic

Every year, the sea ice cover in the Arctic experiences some of the most noticeable seasonal changes of any surface type on the Earth. Certainly the most obvious change is the variation in sea ice extent, ranging from around 4 million  $km^2$  in September at its annual minimum after the summer melt to about 15 million  $km^2$  in March (Fig. 1.2), the month featuring the peak winter-extent where most of the Arctic basin is ice covered [Shokr and Sinha 2015]. Additionally, seasonally and spatially changing physical properties and surface characteristics of sea ice do directly influence a wide range of climatological, meteorological and oceanographic properties, ranging from local to larger spatial scales. Thereby, sea ice plays a key role within the global climate system. The heat exchange between the usually cold winter atmosphere and relatively warm ocean underneath are mainly determined by the physical properties of sea ice. Of particular importance are its thermal properties as well as the released or acquired heat of fusion

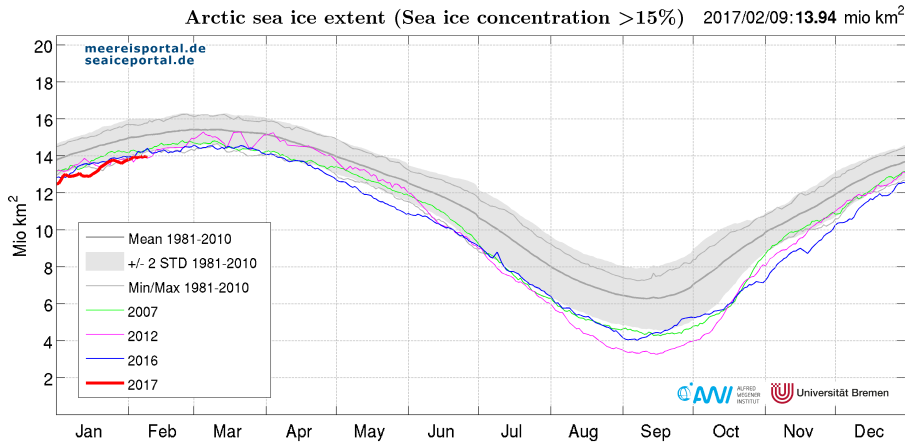


Figure 1.2: Daily sea ice extent in the Arctic, illustrated for three years with the lowest single day September values recorded (2007, 2012, 2016; colored lines) and the current year 2017 (red line). The average course for the period 1981 to 2010, the two-times standard deviation (STD) as well as daily minimum and maximum values are additionally indicated in thick and thin grey lines as well as grey shadowing, respectively. Figure from [www.seaiceportal.de](http://www.seaiceportal.de) (accessed February 10, 2017).

during the freezing and melting of ice, respectively [Shokr and Sinha 2015]. Due to the low thermal conductivity of sea ice, the ocean-atmosphere heat exchange is reduced when sea ice is present so that it basically acts as an insulator. This is already the case for very thin ice, as even an ice layer of only around 10 cm thickness reduces the heat exchange by more than 50% [Maykut 1978, 1982], and generally affects moisture-, momentum- and gas-exchange processes. Furthermore, as the latent heat of fusion of ice/water is one of the highest of all substances, the annual freezing and melting of sea ice triggers a huge heat exchange that affects local weather systems and even climate on a regional scale [Shokr and Sinha 2015].

The most important optical property of sea ice is its high albedo, representing the highest among all surfaces on earth, especially when the ice is covered by snow. Compared to less frequently present open ocean surfaces (around 0.06), the high albedo of often snow-covered sea ice (ranging from 0.4 to 0.9) is the main driver of the ice-covered polar regions staying cold, as most of the incident solar radiation is reflected. As will be shown in Chapter 1.4, the climatic conditions in the Arctic are changing, which has already led to a significant decrease in sea ice extent. It is expected that this decrease continues in the upcoming decades, as increasingly ice-free conditions promote a positive feedback mechanism that is triggered by the sharp contrast in albedo. As the fraction of low albedo ocean areas increases, more heat gets absorbed by the upper ocean layers, thereby amplifying further melting and more absorption [Shokr and Sinha 2015].

In a general sense, the polar regions serve as the cold end of a huge heat engine, where large amounts of absorbed incoming solar radiation from equatorial latitudes are transported north and south by a complex system of global ocean currents and atmospheric circulations. In higher latitudes, the stored oceanic heat is lost to the atmosphere through the open water fraction of sea ice, whereby the actual loss rate is determined by certain variables such as the sea ice extent, the ice thickness and consistency of the ice cover [Wadhams 2000]. This process interacts with

the general atmospheric circulation, which is responsible for generating most weather systems over north-latitude areas [Shokr and Sinha 2015].

In turn, distinct atmospheric and oceanic circulation patterns strongly influence the motion of sea ice, which rarely remains stationary when not attached to the shoreline (the latter being referred to 'landfast ice'). Motion-induced convergence or divergence of the ice cover frequently causes the ice to pile up (termed 'pressure ridges') or open up (termed 'leads', 'cracks' or 'polynyas'; compare Ch. 1.3), thereby strongly modifying physical parameters of sea ice, i.e. surface temperature, surface roughness, emissivity, etc., in a spatial and temporal sense [Shokr and Sinha 2015]. As a consequence, these alterations again feed back to atmospheric and oceanic dynamics.

Sea ice affects the ocean circulation through the annual cycle of freezing and thawing. When new ice forms and/or grows during winter, salt is rejected to the underlying water column. This vertical movement of cold, salty and hence dense water, driven by the gradient in density, initiates a large-scale pattern of seawater motion around the world, the so called 'thermohaline circulation'. In turn, the melting of large volumes of ice that has drifted away from the polar areas during the summer disturbs this circulation by creating a stable oceanic surface layer with low salinities [Shokr and Sinha 2015].

Equally important, sea ice plays a crucial role for the polar biosphere, as a variety of species make use of it as habitat or shelter, for breeding, feeding, and nursery or as a hunting ground. These species range from microorganisms (algae and bacteria) to different fish, birds and marine mammals (e.g., polar bear, walrus, some species of whales and ice-associated seals) [Shokr and Sinha 2015].

## 1.2 Sea ice and ice formation: Physical properties and processes

As briefly mentioned in the beginning of this chapter, the monitoring and documentation of large-scale changes in the sea ice cover of the polar regions is often done using various types of remote sensing data (compare Ch. 2 for more details). However, even the highest-resolution sensors onboard specialized satellites or aircrafts (operating at fairly low altitudes with limited spatial coverage) are only able to resolve details down to the meter scale. In order to get an understanding of the processes relating to and depending on the large scale behavior of sea ice, the evolution of the ice structure and properties needs to be known at even finer scales due to their role as the driving factors for sea ice growth and decay as well as being highly relevant regarding the interpretation of remotely sensed data/images [Petrich and Eicken 2010].

Sea water, the origin for most of the sea ice found in polar waters (sea-ice formation through snowfall, often found around Antarctica, will not be further discussed in the following), is quite an atypical and complex substance. One of the unique characteristics of water in general is that the density of its frozen state is lower than in its liquid phase, which causes ice to float on lakes and seas and not sink down into its melt, as most other solids do [Weeks and Ackley 1986]. This characteristic behavior is the result of the crystal lattice structure of ice 'Ih' (Fig. 1.3).

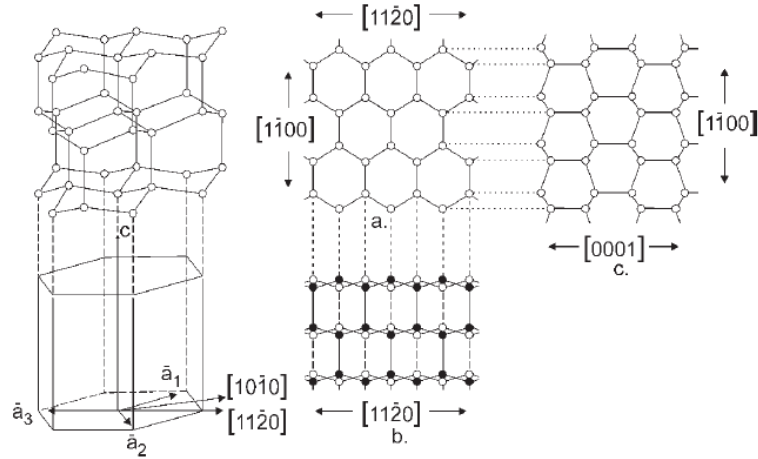


Figure 1.3: Crystal structure of ice Ih, with the  $c$ -axis ( $[0001]$ ) being indicated at the left and right panel. In the center panels, the views along (top) and perpendicular (bottom) to the  $c$ -axis is shown (taken from Weeks and Ackley [1986]). Numbers in form of four digits refer to the Miller indices for planes and directions in a hexagonal crystalline system [see Hobbs 1974; Weeks and Ackley 1986; Shokr and Sinha 2015].

In theory, water can appear in a dozen of different modifications (pressure- and temperature-dependent), but the 'h' in ice 'Ih' refers to a crystal symmetry in the hexagonal system resulting from the freezing of water under equilibrium conditions naturally found at the Earth's surface [Petrich and Eicken 2010]. In the ice crystal lattice, the water molecules arrange tetrahedrally, with the so called 'basal plane' featuring a sixfold symmetry along the  $a$ -axis. The principal crystallographic axis (also  $c$ -axis) is oriented normal perpendicular to this basal plane. While the interface of the basal plane is smooth on a molecular level, as only two atomic bonds need to be broken, the plane normal to the basal plane requires at least four bonds to break and is hence regarded as a rough interface [Weeks and Ackley 1986; Petrich and Eicken 2010]. This results in different interface kinetics and, hence, in a pronounced anisotropy (i.e., directional dependency) in growth rates and general ice-mechanical properties [Wadhams 2000; Petrich and Eicken 2010].

Besides water (hydrogen and oxygen;  $H_2O$ ), which comprises about 965 to 975.3 kg of every 1000kg of sea water (depending on salinity), the main constituents of sea water are dissolved salt ions ( $Na^+$ ,  $K^+$ ,  $Ca^{2+}$ ,  $Mg^{2+}$ ,  $Cl^-$ ,  $SO_4^{2-}$ ,  $CO_3^{2-}$ ) with distinct fractional contributions [Weeks 2010; Petrich and Eicken 2010]. Compared to lake (i.e. fresh) water, which is essentially non-saline, the presence of salt in sea water vastly modifies several characteristics of ice formation.

When sea water that exceeds a salinity-threshold of 24.7 psu (practical salinity units; equivalent to parts per thousand) is cooled from above, the salinity of the water lowers its temperature of maximum density until it is below the freezing temperature [Wadhams 2000; Weeks 2010]. The cooling by the atmosphere will therefore always create a dense surface layer, hence forcing convection with the warmer water below. This convection takes place over the whole polar surface layer up to the pycnocline around 100-150 m depth (and shallower over Arctic shelf regions), where a jump in density is observed. When the whole surface layer is cooled down to

the freezing point ( $-1.8^{\circ}\text{C}$ ), the temperature induced convection comes to an end and ice starts to form [Wadhams 2000]. Most areas of the Arctic Ocean easily exceed a salinity of 24.7 psu, which marks the critical value to separate brackish water and sea water. Due to some areas with an extensive river discharge during summer (e.g., Ob and Yenisei in the southern Kara Sea, Lena in the southeastern Laptev Sea), there are exceptions where the salinity is less than the critical value. This favors ice formation to take place earlier in autumn. In the course of winter, however, ice production on these shelf regions subsequently increases the salinity and density of these waters, thereby causing it to sink and ventilate the water column [Wadhams 2000].

The actual formation process of sea ice differs from calm to rough ocean regimes (compare Fig 1.4). Initially, sea ice that forms at the surface consists of a skim of separable crystals and tiny ice platelets, which float flat on the water surface and have diameters of around 2-3 mm. Their c-axis is orientated vertically, so they grow outwards laterally until they become unstable and develop long dendritic crystals, which have again a vertically orientated c-axis. Due to their fragile nature, these so called frazil ice crystals quickly break up and form a dense suspension in the upper ocean layer called and grease ice [Wadhams 2000].

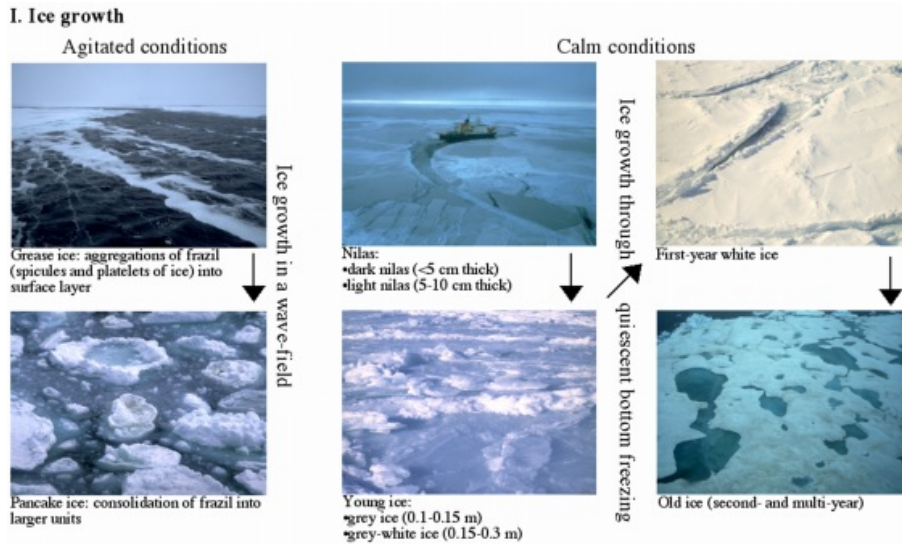


Figure 1.4: Different ice types during ice growth under rough (left side) and calm (right side) conditions [Petrich and Eicken 2010].

When no turbulence is apparent, the frazil ice freezes together and forms a continuous sheet of thin young ice (grey to grey-white colour), which is also referred to as dark and light nilas in its very early stage (less than about 10 cm thickness). With further freezing and increasing thickness, the ice includes more and more air and sea water inclusions, so the color of the ice changes from transparent (i.e. dark) to white. Following this initial formation stage, a subsequent and differing process called congelation growth occurs. In this stage, water molecules freeze on to the bottom of the existing sea ice cover, thereby leading to first year ice (FY) which can reach thicknesses up to 1.5 to 2 m [Wadhams 2000].

Under rough and wavy conditions, the turbulence generated by the wave-field maintains the dense suspension of newly formed ice, rather than forming nilas. The frazil ice crystals orbit



in the wave field and undergo cyclic compression phases, where they can freeze together to form small coherent floes of ice. When these grow larger through the addition of further frazil ice, the ice type is called pancake ice, originating from their characteristic shape with raised rims. With increasing distance to the ice edge, the pancakes grow gradually until they finally freeze together in groups (consolidated pancake ice). The bottom morphology of pancake ice is quite different compared to other sea ice types because of the rafting and collisions during the consolidation process, resulting in a rough bottom surface topography and high thickness values [Wadhams 2000]. After the initial formation of a continuous ice sheet, the growth of ice crystals in contact with the ice-water interface continues downwards by freezing of water molecules from the downside [Wadhams 2000]. The latter process is much easier for ice crystals with a horizontal c-axis than for those with a vertical c-axis leading to a preferred laminar growth. Typically, ice crystals at the top of a FY-ice sheet are randomly orientated followed by a transition to a zone of long vertical columnar crystals with horizontal c-axis. This columnar structure is typical for congelation growth and a striking visible feature of FY-ice [Wadhams 2000].

As stated above, a high fraction of the salt in the sea water is rejected during the freezing process [Wadhams 2000; Petrich and Eicken 2010]. The remaining salt accumulates in form of a highly saline solution called brine between the rows of ice dendrites, and as these advance, the brine gets trapped and isolated in brine pockets. Hence, sea ice rarely exists of pure ice, but remains at a bulk salinity of between 0 and 15 psu [Weeks 2010]. With the development of brine drainage channels, the brine concentration decreases with increasing age of the ice [Wadhams 2000].

Old ice that survives more than one winter is called Multi-Year ice (MY) [Wadhams 2000]. In the Arctic, around half of the sea ice cover used to consist of MY-ice because of relatively slow drift- and circulation-patterns, including the Beaufort Gyre (7-10 years) and the Transpolar Drift Stream expelling in the East Greenland Current (1-3 years). However, the fraction of MY-ice has decreased to about 20 to 30 % in recent years (compare Ch. 1.4). When the ice has reached a thickness of around three meters after several winters, the summer melt fairly equals the winter growth and the thickness starts to oscillate in an annual cycle. Typical properties of MY-ice are a lower conductivity, a rougher surface and an overall low salinity which makes it much stronger than FY-ice [Wadhams 2000].

### **1.3 Polynyas and leads: Hotspots for enhanced atmosphere-ice-ocean interactions**

Interactions between the atmosphere, sea ice and ocean play a crucial role at higher latitudes, as they ultimately influence and provide feedback on large-scale and long-term dynamics of the atmospheric and oceanic circulation, as well as the sea-ice mass balance. Generally, these interactions are quantified as atmosphere-ocean fluxes, which represent the exchange of energy and material between the atmospheric boundary layer (ABL) and the ocean [Bourassa et al. 2013]. These exchanges comprise net fluxes of momentum from wind (-stress), energy (downward and reflected shortwave radiation, downward and emitted longwave radiation, latent heat flux, and sensible heat flux), and mass (moisture, gases, aerosols), with their individual magnitude being highly variable in space and time. Radiative fluxes feature unique characteristics at

higher latitudes, as they vary largely depending on cloud cover, aerosol characteristics and the availability of shortwave radiation in the transition periods between summer and winter. Among the other fluxes, wind stress, sensible and latent heat fluxes as well as the gas and aerosol exchange can be classified as turbulent fluxes [Bourassa et al. 2013].

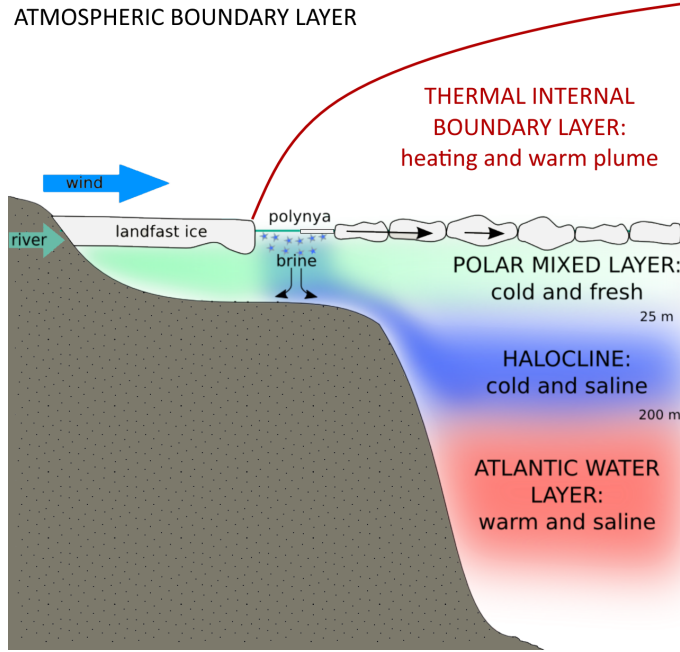


Figure 1.5: Simplified schematic to illustrate the advection mechanism for the formation of cold and salty halocline waters in a latent heat polynya, as well as the development of a thermal internal boundary layer (TIBL) in the lower atmospheric boundary layer (ABL) through the heat release during ice formation. Image modified from Itkin et al. [2015].

In the polar regions, increased low-level wind speeds can be linked to both small-scale features such as polar lows, and also large-scale features like warm-core seclusions (i.e., mature extratropical cyclones). On a local scale, both features can be further amplified by the topography (e.g. channeling effects). Especially at (but not limited to) coastlines or wintertime fast-ice edges, high wind speeds cause vastly increased air-sea / air-ice momentum exchanges that promote the formation of so called polynyas (originating from the russian term for 'hole in the ice') [Bourassa et al. 2013]. In a general sense, polynyas are defined as persistent and recurring thin-ice and/or open water areas in the seasonal ice zone, which tend to form at more or less fixed locations where climatologically a more compact and thick ice cover could be expected [Smith et al. 1990; Martin 2001]. Due to the highly variable nature of atmosphere-ocean fluxes, also the timing, duration and areal extent of a polynya can have large variations from daily to interannual time-scales [Morales-Maqueda et al. 2004]. Traditionally, polynyas are categorized into a latent heat (also 'wind-driven' or 'coastal' polynyas) and sensible heat type (also 'open ocean' polynyas), with some polynyas showing documented or assumed hybrid characteristics [e.g. Smith et al. 1990; Melling et al. 2015; Hirano et al. 2016].

The continuous removal of newly formed sea ice towards the lee-ward polynya margin by strong winds and/or ocean currents is the main origin of latent heat polynyas (Fig. 1.5). The resulting net heat loss to the cold atmosphere, while locally modifying the ABL structure to a convective regime [Ebner et al. 2011; Gutjahr et al. 2016] rather than being stable or near-neutral over sea ice for most of the year [Persson and Vihma 2017], is balanced by ice formation, which provides the latent heat of fusion of ice. The heat loss to the atmosphere during winter can be two orders of magnitude larger than the heat flux through an adjacent thick ice cover [Maykut 1982] and may increase local air temperatures by several degrees, thereby enabling the formation of a thermal internal boundary layer (Fig. 1.5) [e.g. Lüpkes et al. 2008; Tetzlaff et al. 2015]. These large fluxes are, however, rarely maintained for a long period of time as these open water and/or thin-ice areas quickly freeze over and/or thicken [Shokr and Sinha 2015]. The amount of ice formed can thereby reach substantial magnitudes until the removal of new ice ceases in concert with the forcing mechanism, and further thickening of the ice cover is limited to congelation growth. Hence, latent heat polynyas are hotspot regions for the (local) sea ice mass budget and, consequently, deep water formation through the brine release during ice growth (compare Ch. 1.2). Much of the world oceans' deep and bottom water is thought to be formed in polar latitudes as a result of ice formation and growth [Aagaard et al. 1981; Winsor and Björk 2000; Shokr and Sinha 2015], and major changes in the amount of newly formed sea ice can potentially disrupt ocean circulations [Maykut 1978; Carmack 1986; Shokr and Sinha 2015]. In the Arctic Ocean, the generally cold upper halocline layer (Fig. 1.5) is maintained by lateral advection from the continental shelves, where dense and saline shelf water is produced during freezing with an pronounced salinization of the water column originating from coastal polynyas [Aagaard et al. 1981].

Polynyas that are exclusively formed by a sensible heat mechanism, where the oceanic sensible heat flux locally prevents ice formation [Smith et al. 1990], are quite rare in the northern hemisphere. However, certain polynya regions are thought to be temporarily influenced by this mechanism, despite the circumstance that direct observations of these hybrid-characteristics are sparse. Besides from increasing the difficulty to retrieve an accurate quantification of ice formation (more details in Ch. 2.2.4), this highlights the need for increased efforts to quantify ocean heat fluxes through in-situ measurements.

Leads, on the other hand, are linear or elongated cracks (i.e., thin ice and open water) in the ice cover that also originate from diverging ice motions [Smith et al. 1990; Barber and Massom 2007]. A recent study on Arctic lead dynamics underlined that these features are highly variable both in space (contrary to polynyas) and time [Willmes and Heinemann 2016]. However, their effect on the atmosphere and ocean through heat loss and ice formation has yet to be fully quantified.

During winter, the surface temperature of the Arctic sea ice can reach values down to  $-40^{\circ}\text{C}$ . In contrast, open-water and thin-ice areas in polynyas and leads are characterized by surface temperatures around or near the freezing point of sea water ( $-1.8^{\circ}\text{C}$ ), making the ice-covered ocean regions among the largest spatially changing surface temperature on Earth [Shokr and Sinha 2015]. Hence, a precise characterization and monitoring of the spatial distribution of ice surface temperature (IST) is an important task in order to improve weather and climate

simulations, as well as related satellite investigations, in particular during winter. Concluding, polynyas and leads can be regarded as highly important climatic features, and the locations of appearance as well as the spatial distribution of thin ice within their margins are particularly important to regional or even global climate models [Shokr and Sinha 2015].

## 1.4 A changing Arctic sea-ice cover: Overview and implications for polynyas

In recent years and decades, the Arctic is undergoing fast and strongly noticeable climatic changes, with direct implications for the sea ice cover and the Arctic cryosphere in general. In particular, polynyas and leads are highly sensitive to climatic changes due to their direct connection to the ocean and lower atmospheric boundary layer.

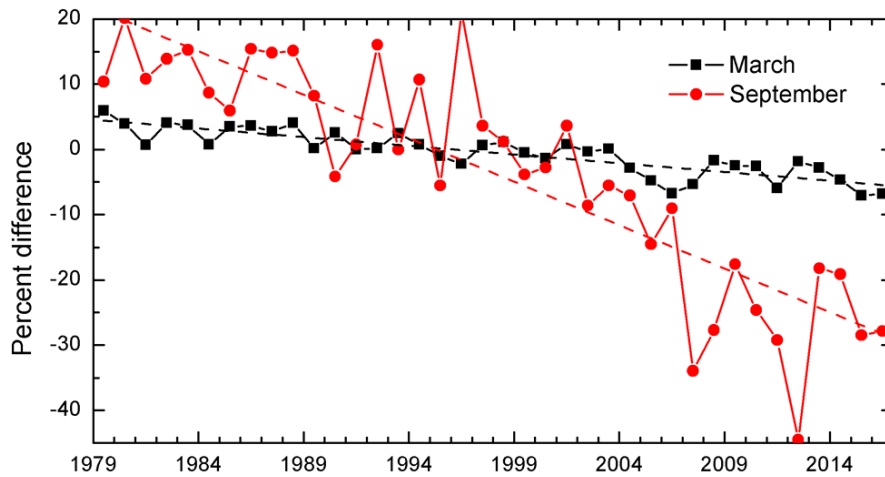


Figure 1.6: Ice extent anomalies in the months of March (maximum ice extent) and September (minimum ice extent), illustrated for the period from 1979 to 2016. The initial time series of sea ice extent is based on estimates produced by the National Snow and Ice Data Center (NSIDC) Sea Ice Index [Fetterer et al. 2002]. For each year, the anomaly is depicted as the difference (in %) in ice extent relative to the average values for the reference period 1981 to 2010. The black and red lines are least squares linear regression lines for March and September, respectively, with their slopes indicating ice losses of 2.7% and 13.3% per decade. Both trends are significant at the 99% confidence level [Perovich et al. 2016].

Most apparently, the Arctic sea ice extent, which is commonly defined as the cumulative ocean area where satellite-derived sea ice concentrations exceed a threshold of 15%), shows a strong downward trend over the period of regular satellite observations (1979 - today), despite large year-to-year variations. As presented in Fig. 1.6, this downward trend in extent is highest in September (-13.3% per decade relative to the 1981-2010 average), but essentially exists for all months (e.g., -2.7% per decade in March). Although not linearly related, the sea ice volume (often calculated from the Pan-Arctic Ice Ocean Modeling and Assimilation System (PIOMAS)

- Zhang and Rothrock [2003]) apparently features a similar downward trend [e.g. Kwok et al. 2009; Laxon et al. 2013; Serreze and Stroeve 2015].

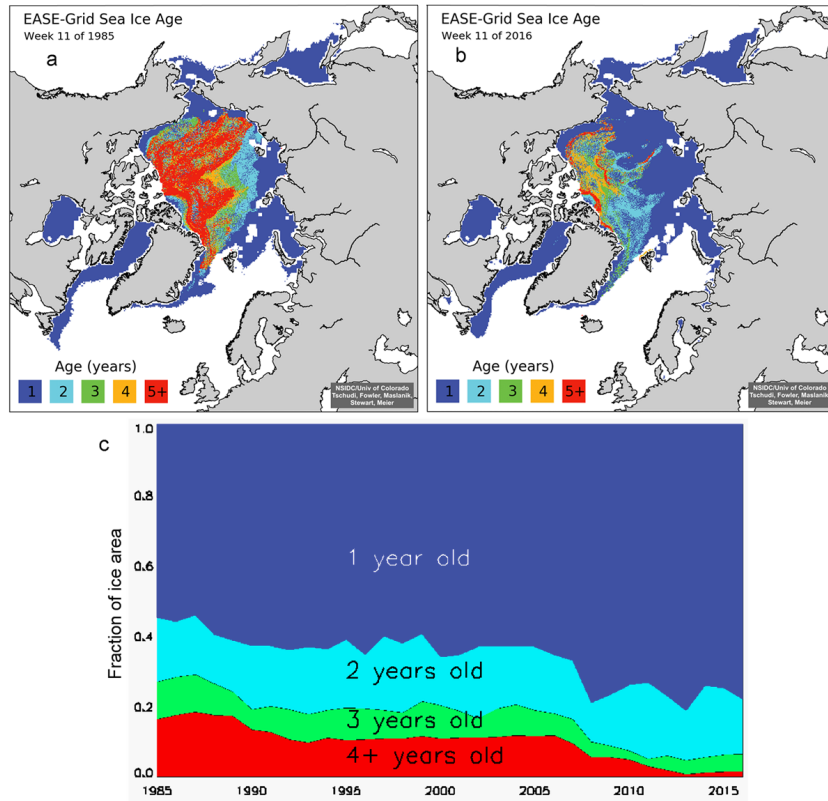


Figure 1.7: Maps of the sea ice age in the Arctic for a) March 1985 [Tschudi and Meier 2016], b) March 2016, and c) time series of sea ice age fractions for the period 1985 to 2016. The fractions in (c) are presented as fractions (fraction\*100 = percent) of the total sea ice areal coverage [Perovich et al. 2016].

Despite the relatively short record of satellite measurements of sea ice (compare Ch. 2), available time series reveal a steepening of the downward trend in sea ice extent since approximately the middle of the 1990s [Serreze and Stroeve 2015]. It is assumed that the preferred loss of old and thick MY ice is one of the main contributors to this trend, as the proportion of relatively thin and young FY ice in the sea ice cover increases [e.g. Comiso 2010; Stroeve et al. 2011]. Figure 1.7 illustrates this by showing information on the age of sea ice in the Arctic, derived from a Lagrangian tracking of individual ice parcels [Serreze and Stroeve 2015; Tschudi and Meier 2016]. The comparison of the distributions in March 1985 and March 2016 clearly shows the loss of old MY ice (older than 4 years) over large portions of the Arctic basin, but most extensively in the Pacific sector [Maslanik et al. 2007, 2011]. As of 2016, the thickest and oldest sea ice is limited to the area north of the Canadian Arctic Archipelago and north of Greenland. Fitting into this context, various observational studies describe a general thinning of the sea ice cover in several regions throughout the Arctic [e.g. Haas et al. 2008; Kwok et al. 2009; Kwok and Rothrock 2009; Hansen et al. 2013; Krumpen et al. 2016] which subsequently enables the sea ice to melt faster, increases its proneness to fracture and enhances the general mobility and drift speed [e.g. Spreen et al. 2011; Kwok et al. 2013].

Stroeve et al. [2011] note that this thinning is, however, only one aspect of the general downward trend in sea ice extent. Another main contribution and potentially a main driver for these trends is a significant atmospheric warming in the Arctic region in all seasons (but strongest in autumn and winter), which reduces the possibility of an ice thickness recovery through especially cold winters. In addition, increasing temperatures lead to a lengthening of the melting season, thereby enhancing the effect of the ice-albedo feedback [Serreze and Stroeve 2015]. This warming is often referred to as one aspect of the polar or Arctic amplification, implying a particular strong increase of the near-surface temperature in the northern latitudes, with rates doubling those of lower latitudes [e.g. Cohen et al. 2014]. According to Cohen et al. [2014], among the contributions to Arctic amplification are local radiative effects from greenhouse-gas forcing [e.g. Stroeve et al. 2011], changes in the snow- and ice-albedo feedback throughout the cryosphere [e.g. Perovich et al. 2007; Serreze and Barry 2011], aerosol concentration changes and black carbon deposition on snow and ice [Shindell and Faluvegi 2009], increasing amounts of cloud cover and a moister atmosphere [e.g. Francis and Hunter 2006; Boisvert and Stroeve 2015], as well as a relatively less increasing emitted longwave radiation in the Arctic when compared to equivalent temperature increases in the tropics [Pithan and Mauritsen 2014]. Especially the effect of the positive ice-albedo feedback, meaning that more energy is absorbed in the increasing fraction of low-albedo open ocean areas during spring and summer, has already resulted in 4 to 5 °C sea surface temperature anomalies in newly ice-free regions [Wood et al. 2013; Cohen et al. 2014]. Hence, the freeze-up of sea ice has been delayed in recent years [Markus et al. 2009; Stroeve et al. 2014] and fast-ice extents as well as duration are decreasing [Yu et al. 2014]. Overall, the extent of changes in the Arctic is highly pronounced, so that several studies (as reviewed by Overland and Wang [2013]) predict a nearly ice-free Arctic Ocean during summer in the upcoming two to three decades.

A thinner, thus more fragile and mobile, sea ice cover and the evident warming in the Arctic have direct implications for polynyas and leads due to their high sensitivity to external forcing mechanisms, i.e. high wind speeds and ocean currents. Recent changes in large-scale atmospheric dynamics, as proposed e.g. by Rigor et al. [2002], already provide the potential to imprint on polynya and lead characteristics in the eastern Arctic. As an example, recent autumn seasons featured extensive open water and thin ice areas as a result of a particularly late freeze-up, thereby fostering large heat losses from the ocean to the atmosphere and consequently, increasing rates of new ice formation. While this stabilizing feedback could potentially act against the recently observed steepening of the downward trend in September sea ice extent, it is apparently not sufficient to counterbalance other accelerating feedback processes [Serreze and Stroeve 2015]. The general response of polynyas and leads to a changing climate and, more specifically, changing sea ice properties is rather complex, as the local forcing mechanisms for thin-ice formation are highly variable throughout the Arctic [Smith and Barber 2007]. However, it can be clearly stated that the presence of thin-ice will be definitely influenced by the earlier mentioned increase in surface temperatures, a lengthening of the melting season and the increased role of the ice-albedo feedback during spring and summer. Further, changes in the location and duration of polynya activity can be expected, especially for those which depends on the stability and existence of specific physical features such as an ice bridge (e.g. North Water polynya) or fast ice (e.g. North-east water polynya, flaw-leads in the eastern Arctic) [Smith and Barber 2007].

## 2 Methodical Review: Remote Sensing of Sea Ice and the Monitoring of polynyas

In a more general sense, the principle of remote sensing can be described as a gathering of information (i.e., reflected, emitted or scattered radiation) about objects or surfaces, without actually physically touching them. However, in order to do so, the relation between the electromagnetic radiation received at a satellite- or air-borne sensor and the physical properties of the surface needs to be characterized as precisely as possible [Rees 2006]. In case of sea ice, its complex structure as well as both spatially and temporarily highly variable physical properties lead to equally complex signatures received at a satellite sensor that require careful data processing and interpretation [Lubin and Massom 2006]. Sea ice remote sensing generally focuses on measuring electromagnetic radiation in so-called atmospheric windows located in the visible (VIS) to near-infrared (NIR), thermal infrared (TIR) and microwave part of the electromagnetic spectrum, utilizing the partly high transparency of the atmosphere in those wavelength-ranges [Spreeen and Kern 2017].

Remote sensing systems can be subdivided into active and passive sensors. Active sensors follow the principle of providing an electromagnetic signal themselves and record the reflected or backscattered radiation from the Earth's surface. Passive sensors, on the other hand, record electromagnetic radiation that is either reflected (VIS and NIR range) or emitted (TIR and microwave range) from the Earth's surface. Among the features characterizing the data collected by remote sensing platforms are sensor-specific spatial, temporal, spectral and radiometric resolutions [Tedesco 2015].

Due to the mostly difficult and expensive accessibility of the polar regions, remote sensing systems are a natural fit and therefore in many cases essential for investigations in those extensive areas. However, the numerous different sensor systems available to date are, depending on the purpose or requirements, not equally well suited to derive information on cryospheric surfaces, and even more specifically - sea ice. Consequently, one main aspect of this chapter is to give an idea of how sea ice is interacting with electromagnetic radiation measured by satellite sensors and how this is represented in remote sensing data sets.

In the context of this thesis, the characterization of Arctic polynyas is mainly conducted using optical data from the thermal infrared region of the electromagnetic spectrum as well as passive microwave remote sensing data. Hence, the beginning of this methodical chapter will concentrate on describing these satellite sensors in more detail, together with their individual benefits, disadvantages and error-sources. Further, it will point out the physical properties of sea ice that influence remote sensing measurements and give a broader look on sea-ice characteristics that can be generally derived from satellite data sets. The second part of this chapter will put emphasis on giving an overview on past remote sensing efforts on Arctic polynyas as well as regularly used monitoring techniques for thin ice in the polar regions.

## 2.1 Satellite remote sensing of sea ice

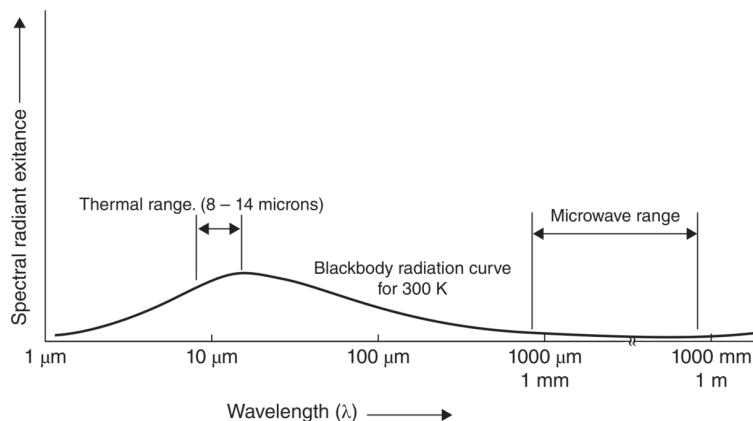


Figure 2.1: Spectral regions used for thermal and passive microwave remote sensing (Tedesco [2015], adapted from Lillesand et al. [2007]).

### 2.1.1 Optical and thermal-infrared sensors

Sensors that operate in the thermal infrared portion of the electromagnetic spectra (i.e., in particular 8-14  $\mu\text{m}$ ) detect the radiation emitted by a surface or object as a result of its physical temperature [Tedesco 2015]. However, in comparison to the VIS and reflected IR range (0.35 to 3  $\mu\text{m}$ ), the longer wavelength and consequently lower energy associated with the photons leads to several necessary modifications of the detectors, such as an increased detector-size. This comes at the cost of a generally coarser spatial resolution when compared to sensors that operate in the high-energy visible and near infrared portion of the electromagnetic spectra. Despite that and certain limitations for surface observations originating from temperature signals of superimposed cloud cover, thermal infrared radiometers like the Advanced Very High Resolution Radiometer (AVHRR) or the Moderate Resolution Imaging Spectroradiometer (MODIS) are frequently used for a variety of atmospheric, oceanic and land-surface applications [Jensen 2007]. For the present thesis, the majority of results were achieved from the use of MODIS data products, so a few characteristics of the instrument will be given in the following. MODIS is a passive optical remote sensing system that is currently deployed on two satellite platforms from the National Aeronautics and Space Administrations (NASA) Earth Observing System (EOS) mission, namely AQUA (launched in May 2002) and TERRA (launched in December 1999). MODIS is measuring electromagnetic radiation with a wavelength between 0.4 and 14.4  $\mu\text{m}$  (VIS to TIR), subdivided into 36 discrete spectral bands (20 bands from 0.4 to 3  $\mu\text{m}$ , 16 bands from 3 to 15  $\mu\text{m}$ ). Thereby, spatial resolutions vary from 250 m up to 1 km at nadir, with coarser resolutions in the TIR region. A nominal swath width of 2330 km is achieved through a field of view of  $\pm 55^\circ$  off-nadir. However, the swath edges suffer from panoramic distortion effects that decrease the spatial resolution off-nadir [Lubin and Massom 2006]. Due to a sun-synchronous polar orbit at an altitude of 705 km, the polar regions are covered several times a day and both



sensors combined are able to capture the entire surface of the earth every 1-2 days [Hall et al. 2004; Rees 2006; Riggs et al. 2006; Jensen 2007].

Satellite sensors in the TIR range such as MODIS observe brightness temperatures ( $T_b$ ), which are converted from the radiance (i.e., emitted energy) received at the satellite by an inversion of Planck's equation. In effect, brightness temperatures are defined as 'the temperature that a blackbody in thermal equilibrium with its surrounding would have to match the intensity of a grey body at a given frequency' [Tedesco 2015; Shokr and Sinha 2015]. In the TIR range, the radiation being emitted from a blackbody is proportional to the fourth power of the physical temperature  $T$  (according to the Stefan-Boltzmann law). With the emissivity  $\epsilon$  being defined as the ratio of the emitted radiation of a given body (i.e., greybody;  $R_G$ ) to the radiation from a blackbody at the same physical temperature ( $R_B$ ) [Shokr and Sinha 2015], the relation between  $T$  and  $T_b$  (Eq. 2.2) can be expressed via Eq. 2.1:

$$\epsilon = \frac{R_G}{R_B} = \frac{\sigma \cdot T_b^4}{\sigma \cdot T^4} = \left[ \frac{T_b}{T} \right]^4 \quad (2.1)$$

with  $\sigma$  being the Stefan-Boltzmann constant ( $5.671 \times 10^{-8} \text{ W m}^{-2} \text{ K}^{-4}$ ), and hence

$$T_b = \epsilon^{\frac{1}{4}} \cdot T \quad (2.2)$$

It can be seen from Eq. 2.2 that in the TIR range,  $T_b$  is less sensitive to changes in emissivity and reacts more to changes in the physical temperature of the surface [Shokr and Sinha 2015]. However, the derivation of the surface temperature requires careful atmospheric corrections as well as detailed information on the surface emissivity and its angular dependence. In case of sea ice, the emissivity in the TIR range is generally larger than 0.96 and even close to unity for snow. It is not affected by the ice thickness and mostly determined by the upper millimeters of the ice (or snow) layer [Lubin and Massom 2006].

TIR data is frequently used for the detection and mapping of sea ice under polar nighttime conditions as the surface temperature of different ice types is considerably different from that of open water Lubin and Massom [2006]. The ability to derive ice-surface temperatures (IST) on large scales is a highly useful tool for the detection and monitoring of thin-ice areas. Further, IST is an important parameter in regional and large-scale modeling, and it can provide useful information on snow metamorphosis- and melt-processes as well as on the thickness of thin ice (Ch. 2.2.1) and ice-growth rates (Ch. 2.2.4) through calculations of the atmosphere-ocean heat exchange [e.g. Yu and Rothrock 1996; Yu and Lindsay 2003; Hall et al. 2004; Willmes et al. 2010, 2011]. Sea-ice concentrations can be derived from MODIS IST by setting the temperature of the ice in relation to an assumed constant temperature of open water [Drüe and Heinemann 2004, 2005]. In addition and more recently, local anomalies of MODIS IST were successfully used to derive long-term statistics of lead-occurrences in the Arctic Ocean [Willmes and Heinemann 2015, 2016]. In case of MODIS, IST are calculated from level 1B calibrated brightness temperatures ( $T_b$ ) (band 31 at  $11.03 \mu\text{m}$  ( $T_{11}$ ) & band 32 at  $12.02 \mu\text{m}$  ( $T_{12}$ )) using a split-window technique in form of a simple regression model [Hall et al. 2004]:

$$IST = a + b \cdot T_{11} + c \cdot (T_{11} - T_{12}) + d \cdot [(T_{11} - T_{12}) \cdot (\sec\theta - 1)] \quad (2.3)$$

with the regression coefficients  $a$ ,  $b$ ,  $c$  and  $d$  being specifically determined for the Arctic and Antarctic as well as three different temperature ranges, and  $\theta$  being the sensor scan angle. The center-wavelengths of both used bands are located within atmospheric water vapor windows. Due to a different attenuation behavior of the radiation in these two bands, the  $T_b$  difference contains information about the amount of water vapor in the atmosphere that can be used for a correction of irritating atmospheric effects [Hall et al. 2004; Adams 2012]. For ideal clear-sky conditions with a low amount of water vapor in the atmosphere, the IST accuracy is given with 1-3 K. However, advanced methods for cloud detection and masking play an important role in affecting the IST accuracy, as any cloud or partially cloudy conditions severely decrease the accuracy [Hall et al. 2004; Riggs et al. 2006].

### 2.1.2 Passive microwave radiometers

Passive microwave radiometers operate in a frequency range of 0.3 to 300 GHz and measure the energy that is naturally emitted by the earth, oceans and atmosphere. Likewise to thermal infrared radiometers, these sensors typically record brightness temperatures ( $T_b$ ). However, in the microwave frequency range and for objects with a temperature range to be expected on the earth's surface, it is possible to apply the Rayleigh-Jeans approximation, yielding the brightness temperature with

$$T_b = \epsilon \cdot T \quad (2.4)$$

where  $\epsilon$  denotes to the object-specific emissivity, dependent on wavelength and polarization, and  $T$  to the object's physical temperature. Furthermore, the emissivity is largely dependent on geophysical quantities such as salinity, roughness, porosity and air content in case of sea ice [Lubin and Massom 2006; Willmes et al. 2014]. More specifically, the combination of four parameters determines the microwave emissive (and scattering) properties of sea ice and its potential snow cover: the complex dielectric constant, dielectric discontinuities such as gas bubbles, the surface roughness and the orientation of the ice/snow surface relative to the azimuth angle of the sensor. Most notably, the complex dielectric constant  $\epsilon^*$  is of major importance to understand microwave signatures of snow and ice in the polar regions [Lubin and Massom 2006]. As complex number, it is defined as:

$$\epsilon^* = \epsilon_0 \cdot (\epsilon' - i\epsilon'') \quad (2.5)$$

with  $\epsilon_0$  being the free-space dielectric constant.  $\epsilon'$  and  $\epsilon''$  are the real and relative imaginary part, respectively.  $\epsilon'$  is the relative dielectric constant or relative permittivity ( $i = \sqrt{-1}$ ) that sets the absolute backscatter level, while  $\epsilon''$  refers to the frequency- and temperature-dependent dielectric loss factor that describes how much energy is lost in the material volume (i.e., frequency-dependent penetration depth), once it passes a dielectric interface [Lubin and Massom 2006]. Regarding the complex nature of sea ice and its dielectric properties, it is widely considered as a medium consisting of pure ice, air and liquid brine. Hence, its complex dielectric constant is mainly influenced by the density of ice, the brine volume as well as their individual dielectric properties and volume fractions [Weeks and Ackley 1986; Lubin and Massom 2006]. For young and first-year (FY) ice, the salinity in the upper layers is generally high, which leads to an

increased absorption, lower reflection and a shallow penetration depth for microwave radiation through high values of both  $\epsilon'$  and  $\epsilon''$ . Hence, the emissivity for young and FY-ice is higher than that of MY-ice (compare Fig. 2.2). MY-ice is generally less saline in the upper layers and features brine pockets in lower layers. Both  $\epsilon'$  and  $\epsilon''$  are generally lower, which enables an increased penetration depth and therefore increased volume scattering through dielectric discontinuities in the ice (e.g. air bubbles). Consequently, the emissivity is also lower and the recorded  $T_b$  for a given physical temperature of MY-ice decreases [Woodhouse 2006; Lubin and Massom 2006].

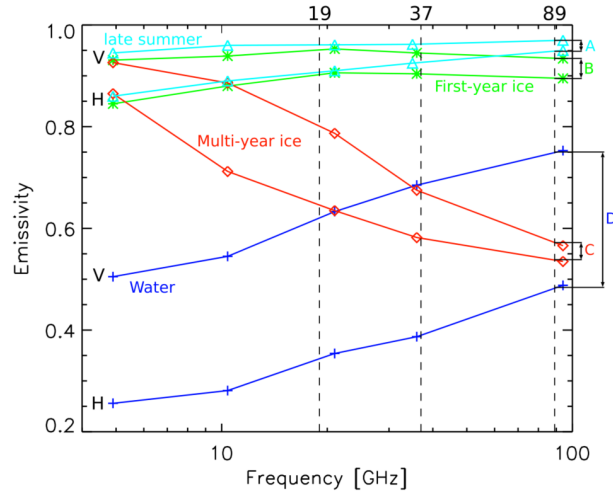


Figure 2.2: Differences in horizontally (H) and vertically (V) polarized frequency-dependent emissivities for different sea ice stages and sea water. Values are retrieved from two field campaigns at an incident angle of  $50^\circ$ . Frequencies from often used satellite channels (19, 37 and 89 GHz) are indicated. Figure by Spreen et al. [2008].

Polarization is a characteristic property for the propagation and scattering of energy in the microwave range. As noted above, it largely influences the recorded signal of an object or surface. In general, electromagnetic radiation consists of electrical and magnetic waves. Polarization describes the locus of the electrical field vector in the plane perpendicular to the direction of propagation, as electromagnetic waves are transversal waves with an x- and y-component [Lubin and Massom 2006; Woodhouse 2006]. With the Earth's surface as reference, a predominant deflection in x-direction is being referred to as horizontal polarization (H), while a predominant deflection in y-direction is known as vertical polarization (V) [Woodhouse 2006]. For sea ice and snow, it is important to note that horizontally and vertically polarized waves interact in a different manner with the target, yielding different emissivities with varying age of the ice and frequency [Lubin and Massom 2006], as becomes apparent in Fig. 2.2.

The low frequencies in the microwave range enable the detection of surface features with hardly any influence from clouds, as most particle sizes found in the atmosphere are smaller than the wavelengths in the microwave range [Rees 2006]. This represents a huge advantage, as the possibility to collect data independent from local weather-conditions and the availability of solar illumination enable high temporal resolutions that are especially valuable regarding the often cloud-covered polar regions and polar night conditions. On the contrary side, however, less available energy in this low frequency range leads to very coarse spatial resolutions (typically

ranging between 3 to 50 km) that may introduce errors from mixed signals wherever there is a sharp contrast in surface type (e.g. in coastal areas). To some extent, this is compensated by the large spatial coverage from spaceborne microwave sensors [Tedesco 2015].

For a regular monitoring of polar sea ice cover in both Arctic and Antarctic, the indispensable 'work-horses' in the passive microwave range are a series of sensors deployed on the Nimbus-7 and the Defense Meteorological Satellite Program (DMSP) platforms, which build upon the legacy of the single-frequency Nimbus-5 Electrically Scanning Microwave Radiometer (ESMR; 1972 to 1976). As of today, these sensors span a nearly continuous time series of almost 40 years, based on measurements from the Scanning Multichannel Microwave Radiometer (Nimbus-7 SMMR; 1978-1986; ten channels between 6.6 and 37 GHz), a series of Special Sensor Microwave / Imager (DMSP-F8,-F10, -F11, -F13 and -F15 SSM/I; 1987-2009; seven channels between 19.4 and 85.5 GHz) and the Special Sensor Microwave Imager Sounder (DMSP-F17 SSMIS; 2003-today; 24 channels between 19.4 and 183 GHz). A conceptually very similar sensor is the Advanced Microwave Scanning Radiometer - Earth Observing System (AMSR-E) on-board the AQUA satellite platform (2002-2011; 12 channels between 6.9 and 89 GHz), as well as its successor on-board the JAXA Global Change Observation Mission-Water (GCOM-W1, 'Shizuku') platform, the Advanced Microwave Scanning Radiometer-2 (2012-today; 14 channels between 6.9 and 89 GHz).

One of the most important and well-known applications for passive microwave data is the derivation of sea-ice concentrations (SIC), which represent the areal fraction (in %) of sea ice in a given grid cell with a known surface area. There is a large number of different retrieval algorithms [Andersen et al. 2007; Ivanova et al. 2014], with each one inhabiting individual strengths and weaknesses for different ice regimes. In general, these algorithms make use of brightness temperature ratios or differences from one or multiple channels, thereby utilizing frequency- and polarization-dependent differences in emissivity (Fig. 2.2) between the spectral endmembers open water, FY- and MY-ice [Lubin and Massom 2006]. Most commonly used are vertically polarized  $T_b$  around 19 and 37 GHz, as the difference in emissivity between water and ice in the 19 GHz channel is large, whereas at 37 GHz the difference between FY- and MY-ice is large [Ivanova et al. 2014].

Further often utilized characteristics are two ratios, with both being dependent on the frequency ( $\nu$ ) and polarization ( $p$ ): the polarization ratio (PR; Eq. 2.6) and gradient ratio (GR; Eq. 2.7).

$$PR_{\nu,p} = \frac{T_b(\nu, V) - T_b(\nu, H)}{T_b(\nu, V) + T_b(\nu, H)} \quad (2.6)$$

$$GR_{\nu_1,\nu_2,p} = \frac{T_b(\nu_1,p) - T_b(\nu_2,p)}{T_b(\nu_1,p) + T_b(\nu_2,p)} \quad (2.7)$$

$$P_{\nu,p} = T_b(\nu, V) - T_b(\nu, H) \quad (2.8)$$

While the PR is mostly used to differentiate between open water and generally sea ice (based on the difference in horizontally and vertically received radiation), the GR is widely used to distinguish sea ice of different age (Young-/FY-/MY-ice) as the  $T_b$  difference between ice types

increases with increasing frequency (Fig 2.2). Generally, the use of ratios yields the advantage of being less sensitive to variations in the physical temperature variations in the emitting layer of ice or snow [Ivanova et al. 2014]. As an example, the frequently used NASA Team algorithm [Markus and Cavalieri 2000] uses both PR and GR to derive SIC.

Other algorithms, such as the ARTIST sea ice (ASI) algorithm [Spren et al. 2008; Beitsch et al. 2014], make additional use of the polarization difference (P; Eq. 2.8) at the high-frequency channels (near 90 GHz) to distinguish water (larger difference) and ice (smaller difference). In case of the ASI algorithm, two tie-points are required to derive sea-ice concentration estimates, with one tie-point representing the P of open water (SIC = 0%) and the other the P of consolidated ice (SIC = 100%). The final SIC are then interpolated using a third order polynomial. Despite the circumstance that the high-frequency channels around 90GHz are influenced by water-vapor and clouds, which requires the application of a weather filter using the low-frequency channels [Spren et al. 2008], these frequencies yield the advantage of increased spatial resolutions (ASI: SIC with  $6.25 \times 6.25 \text{ km}^2$ ).

The Soil Moisture and Ocean Salinity (SMOS) sensor, operated by the European Space Agency (ESA) and launched in 2009, is another passive microwave radiometer that, compared to the more widely used sensors listed above, measures in a lower frequency range (L-band; 1.4 GHz). Besides its initially intended purpose of giving new insights on the global soil moisture and ocean salinity characteristics, Kaleschke et al. [2010] presented a physical approach that related the sensitivity of brightness temperatures at 1.4 GHz to the sea-ice salinity and temperature, which enables the retrieval of thin-ice thicknesses up to around 50 cm independent of solar illumination and weather effects. However, the use of L-band frequencies comes at the cost of a quite coarse spatial resolution of 30 to 50 km [Spren and Kern 2017]. A series of follow-up studies [e.g. Kaleschke et al. 2012; Tian-Kunze et al. 2014; Huntemann et al. 2014; Kaleschke et al. 2016] provided additional empirical background on the procedure towards an operational distribution service.

### 2.1.3 Other satellite sensor types used for sea ice remote sensing

The previous two sub-chapters were mostly meant to give an overview on sea ice remote sensing techniques that are relevant for the detection of thin ice in the context of this thesis. However, there are certainly more aspects from the field of sea ice remote sensing that would require further explanations and details that go beyond the scope of this methodical chapter. Nevertheless, a few important principles and sensors will be shortly introduced in the following with links and references to studies that can provide more detail.

Similar to passive microwave radiometers, the use of active microwave remote sensing techniques, including scatterometry and RADAR (radio detection and ranging), is also very common for sea ice investigations. Thereby, the phase state and salinity of sea ice, quite similar to emissivity, have a significant influence on the backscatter of microwave energy emitted from the sensors. Thereby, more energy is scattered by sea ice, compared to the ocean. For sea ice applications, scatterometers (e.g. the NASA QuickSCAT (1999 to 2009) or the ESA ASCAT (2009 to today)) are mostly used for coarse-resolution estimates of sea ice extent and the retrieval of first-year and

multi-year ice types due to their high sensitivity to the salt content of sea ice which decreases with age [Tedesco 2015].

A bit more frequently and in some cases operationally used, Synthetic Aperture Radar (SAR) instruments are imaging sensors that respond to sea ice in a similar manner to scatterometers. SAR sensors provide the advantage of a much higher spatial resolution (1 to 1000 m). Hence, they are capable to detect small-scale processes in the sea-ice cover, including ice deformation and the opening of leads and polynyas [Tedesco 2015]. The high spatial resolution is achieved through artificially constructing a long radar antenna by utilizing the along-track movement of the satellite. On the downside, SAR sensors generally suffer from poor temporal resolutions (i.e., long revisit-times) due to their comparatively small areal coverage. SAR systems are most commonly used for deriving small-scale sea ice motion with high accuracy as well as subdividing different ice types depending on volume scattering and their surface-roughness (i.e., scattering behavior) [Spren and Kern 2017]. Among the most commonly utilized SAR satellite platforms are RADARSAT-1/-2 with a C-band SAR (1995 to 2013 / 2007 to today; operated by the Canadian Space Agency (CSA)), TerraSAR-X with a X-band SAR (2007 to today; operated by the German Aerospace Center (DLR)) and Sentinel-1A with a C-band SAR (2014 to today; operated by ESA).

For a large scale retrieval of the ice thickness distribution, spaceborne laser (i.e., LiDAR - Light Detection and Ranging) and RADAR altimeters are used. They are able to detect the ice freeboard, i.e. the part of the sea ice above the ocean surface. Early satellite missions (e.g. ERS-1) started in the early 1990s, with the latest satellite radar altimeter mission being Cryosat-2, which is operated by ESA since 2010. In general, altimeters send out an electromagnetic pulse to the earth's surface, from where it reflected back to the sensor. Both the amplitude and the traveling time of the returned signal as well as the exact position of the satellite in space are then needed to derive surface elevation estimates relative to an Earth ellipsoid model, which can be converted to ice freeboard and subsequently ice thickness during extensive post-processing steps [Spren and Kern 2017]. More details on these procedures and, most importantly, derived ice-thickness and uncertainty information can be found in e.g. Zwally et al. [2002]; Kwok et al. [2009]; Laxon et al. [2013]; Kurtz et al. [2014]; Ricker et al. [2014]. Due to a higher relative uncertainty for thin than for thick sea ice, satellite altimeters are in general not well suited for thin-ice areas. This demands for dedicated data-fusion approaches with other satellite systems in order to retrieve information on a wider ice-thickness range of the sea-ice cover and potentially reduce overall uncertainties [e.g. Kaleschke et al. 2015].

## 2.2 Satellite observations of polynya characteristics - state of research

According to Lubin and Massom [2006], the most fundamental contribution of satellites regarding the monitoring of polynyas (compare Ch. 1.3) is the detection and mapping of the polynya extent (or polynya area - POLA) and its temporal variability. As most imaging satellite remote sensing systems capture the surface of the Earth in form of a two-dimensional spatial domain,

it is certainly the most obvious variable. A precise derivation of POLA (and polynya shape) is essential due to its relevance for polynya formation, evolution and decay, as well as its importance in providing realistic boundary conditions in climate simulations and models [Hollands and Dierking 2016]. Most commonly, POLA is derived using passive microwave systems such as SSM/I-SSMIS or AMSR-E due to their frequent and almost seamless coverage of the polar regions, thereby utilizing either thresholding approaches on sea-ice concentrations or iterative classification strategies (more details in Ch. 2.2.2). Manual classification of either high-resolution optical images or SAR data is another technique to infer the polynya margins as well as different ice regimes and types with high accuracy, but is limited to individual case studies due to high requirements regarding time and user expertise. Hence, it is impractical to apply manual classifications to large and long-term data sets [Hollands and Dierking 2016].

Although often being hampered by clouds, thermal infrared data is a frequently used and highly useful tool for polynya studies due to the ability to derive high-resolution ice-surface temperatures, which can be subsequently used to infer the thickness of thin ice in an energy balance model (compare Ch. 2.2.1). This enables not only the derivation of POLA through applying a thickness-threshold (e.g. 0.2 m; Willmes et al. [2011]; Adams et al. [2013]), but also heat flux calculations for the estimation of ice production (IP) rates (compare Ch.2.2.4). The derived ice thickness from TIR data is often referred to as thermal ice thickness ('TIT'; likewise used in the following for 'thermal ice thickness' and 'thin-ice thickness'), and can be either analyzed on its own (as presented in later chapters) or serve as a reference in empirical passive microwave approaches to derive thin-ice thickness (Ch. 2.2.3). However, while these approaches can yield realistic estimates of the thin-ice thickness distribution and ice production rate, the in-situ validation of these quantities is extremely difficult. Further, larger errors may result from the currently used coarse-resolution atmospheric data sets [Adams et al. 2013].

The list of satellite remote sensing studies dealing with Arctic polynya regions as well as associated ice production and dense-water formation is rather extensive. Hence, only a brief overview on recent studies will be given in the following, with some of the most common remote sensing techniques explained in more detail in sub-chapters 2.2.1 to 2.2.4.

Most remote sensing studies on polynyas focus on using passive microwave data, in order to avoid dealing with cloud effects and other possibly obscuring influences. One of the earlier basin-scale studies by Cavalieri and Martin [1994] used a combination of satellite, oceanographic and atmospheric data to calculate brine fluxes from polynyas over the Alaskan, Canadian and Siberian continental shelf regions and their contribution to the cold halocline layer of the Arctic Ocean. However, the majority of studies concentrated on specific regions, thereby taking into account their individual local formation mechanisms and physical settings. The Chukchi Sea and Laptev Sea are certainly two of the most extensively studied regions, with many of the most frequently used remote sensing techniques for polynyas either being established/developed or further advanced in those areas. Martin et al. [2004, 2005] used data from both SSM/I (1990-2001; 25 km) and AMSR-E (only 2003; 12.5 km) to derive thin-ice thickness distributions (Ch. 2.2.3) and ice production estimates (Ch. 2.2.4) in the Chukchi Sea polynyas. Similar attempts followed by Tamura and Ohshima [2011], Iwamoto et al. [2013] and Iwamoto et al. [2014], thereby utilizing the Chukchi Sea as part of their reference areas to establish and develop new empirical thin-ice algorithms for the use with SSM/I and AMSR-E data on a pan-Arctic scale.

In the Laptev Sea, [Alexandrov et al. 2000] studied the sea-ice circulation and the ice export to the Arctic Ocean using sea-ice motion vectors derived from radar and SSM/I data for two single winter seasons. Willmes et al. [2010] performed a cross-validation of different polynya monitoring techniques in the Laptev Sea polynyas, including thin-ice thicknesses derived from passive microwave sensors (Ch. 2.2.3) and the thermal infrared AVHRR sensor (Ch. 2.2.1), respectively. Later, Willmes et al. [2011] used a combination of an empirically derived MODIS thin-ice thickness distribution, polynya areas as classified from SSM/I SIC and atmospheric reanalysis data to calculate wintertime ice production in the Laptev Sea polynyas for the period 1979 to 2008. Based on this time series of polynya area, Krumpfen et al. [2013] presented a first evidence for a linkage between the extent of the Laptev Sea polynyas and the area of ice exported from the Laptev Sea during winter. Other notable studies that were based on passive microwave estimates of polynya area or thin-ice thickness include Barber et al. [2001] (North-Water polynya), Arrigo [2004] (Cape Bathurst polynya), Kern [2008] (Kara Sea), Jardon et al. [2014] (Storfjorden polynya), and Barber and Massom [2007], with the latter presenting a comprehensive overview on locations of polynya occurrences in the northern hemisphere (compare Fig. 1.1). In general, a major obstacle for inter-comparisons of the numerous local- and basin-scale remote sensing (and model) studies on Arctic polynya characteristics is an equally wide range of different reference areas, investigation periods and applied methods and parametrizations.

However, Willmes et al. [2010] already indicated that the coarse spatial resolution of commonly used passive microwave channels provokes sources of error in the narrow flaw polynyas of the Laptev Sea (i.e., located at fast-ice edges), induced by mixed signals and associated spill-over effects at the polynya-margins or completely missed polynya events. Following that argumentation, the usage of high-resolution thermal infrared data should provide an increased spatial accuracy in polynya detection, given that cloud-induced disturbances are sufficiently addressed. Hitherto, however, the retrieval and usage of thin-ice thicknesses from thermal infrared data was mostly limited to case studies or single winter seasons [e.g. Yu and Rothrock 1996; Yu and Lindsay 2003; Drucker et al. 2003] or as an empirical reference for passive microwave algorithms. Hence, as will be outlined in Ch. 3, an expanded application of high-resolution thermal infrared data is one of the major motivations for the present thesis.

### **2.2.1 Thermal-infrared thin-ice thickness (TIT) retrieval**

The sea-ice thickness distribution is an important quantity to characterize sea ice covered regions [Wadhams 2000], as already small differences in ice thickness (a few centimeters) lead to strong alterations in terms of heat exchange between the ocean and the atmosphere [Ebner et al. 2011]. Hence, the heat exchange in thin ice areas (i.e., polynyas) is much larger than in areas with thicker ice, which makes the knowledge on the spatio-temporal distribution of polynyas and leads in the Arctic Ocean a key aspect of climate monitoring and modeling.

For most of the results of the present thesis, an approach following the work of Yu and Rothrock [1996], Yu and Lindsay [2003] and Drucker et al. [2003] was used, together with significant improvements and modifications from Willmes et al. [2010, 2011] and Adams et al. [2013]. The method utilizes the inverse relationship between ice surface temperature (IST) and thickness of



thin ice, meaning that the IST increases with decreasing (thin-) ice thickness [Yu and Rothrock 1996; Drucker et al. 2003]. This also implies that the IST of thin ice (without snow cover) is closer to the freezing point of the upper ocean layer than it is to the lower atmosphere's temperature [Drucker et al. 2003; Kwok et al. 2007].

The thin-ice thickness is calculated using a one-dimensional energy balance model, which assumes a linear temperature profile through the ice and constant water temperature at the boundary between ice and ocean, set to be at its freezing point ( $T_f = 271.35$  K). In addition, the ice is assumed to be free of snow (as observed for parts of the Laptev Sea by Adams [2012]). The model does not explicitly discriminate between different ice types.

The ice thickness is derived from MODIS or AVHRR IST and atmospheric reanalysis data, such as ERA-Interim [Dee et al. 2011] or NCEP2 [Kanamitsu et al. 2002]. In case of thin ice, the conductive heat flux through the ice ( $Q_{ice}$ ) equals the total heat flux to the atmosphere ( $Q_{atm}$ ). This implies that the energy loss at the ice-surface is compensated for solely by the conductive heat flux  $Q_{ice}$ .  $Q_{atm}$  and  $Q_{ice}$  are presented in Equations 2.9 and 2.10:

$$Q_{atm} = Q_0 - H_0 - E_0 \quad (2.9)$$

$$Q_{ice} = \kappa_{ice} \cdot \frac{(T_{surf} - T_f)}{h_{ice}} \quad (2.10)$$

Where  $Q_0$  is the total radiation balance,  $H_0$  and  $E_0$  are the turbulent fluxes of sensible heat and latent heat, respectively,  $\kappa_{ice}$  is the thermal conductivity of sea ice,  $T_{surf}$  is the surface temperature,  $T_f$  the freezing point of sea water and  $h_{ice}$  is the ice thickness. Ice thicknesses are only calculated when  $Q_{atm}$  is negative (energy loss of the surface). Because of difficulties with the parametrization of shortwave radiation terms [Adams 2012] and to avoid dealing with snow and ice albedo effects, only nighttime scenes are incorporated into the calculations. Hence, the radiation balance  $Q_0$  simplifies to:

$$Q_0 = L \downarrow - L \uparrow \quad (2.11)$$

Therein, the down- and upwards directed long wave radiation terms  $L \downarrow$  and  $L \uparrow$  can be calculated using the Stefan-Boltzmann law:

$$L \downarrow = \epsilon_{atm} \cdot \sigma \cdot T_{2m}^4 \quad \text{and} \quad L \uparrow = \epsilon_s \cdot \sigma \cdot T_{surf}^4 \quad (2.12)$$

With  $\sigma$  being the Stefan-Boltzmann constant ( $\sigma = 5.671 \times 10^{-8} \text{ Wm}^{-2} \text{ K}^{-4}$ ) in both equations (Eq. 2.12),  $L \uparrow$  is calculated using the satellite-derived IST as  $T_{surf}$  and the surface emissivity  $\epsilon_s$  set to 1.  $L \downarrow$  can be obtained using atmospheric reanalysis 2m-temperatures for  $T_{2m}$  and the atmospheric emissivity  $\epsilon_{atm}$  is calculated following Jin et al. [2006]. Turbulent fluxes of sensible ( $H_0$ ) and latent ( $E_0$ ) heat in Eq. 2.9 are calculated using an iterative bulk approach by Launiainen and Vihma [1990], where near surface stratification is considered (using Monin-Obukhov similarity theory and associated universal functions) for the heat transfer coefficients  $C_H$  and  $C_E$ :

$$H_0 = \rho \cdot c_p \cdot V_{2m} \cdot C_H \cdot (T_{surf} - T_{2m}) \quad (2.13)$$

$$E_0 = \rho \cdot L_v \cdot V_{2m} \cdot C_E \cdot (q_{surf} - q_{2m}) \quad (2.14)$$

Here,  $\rho$  is the density of air,  $c_p$  is the specific heat capacity (for constant pressure) of air ( $c_p = 1003.5 \text{ W s kg}^{-1} \text{ K}^{-1}$ ),  $V_{2m}$  is the mean horizontal wind speed at a level of 2m (interpolated from standard reanalysis variables  $u_{10m}$  and  $v_{10m}$  components by using a constant roughness length of  $z_0 = 1 \times 10^{-3}$ ),  $L_v$  is the latent heat of vaporization ( $L_v = 2.5 \times 10^6 \text{ J kg}^{-1}$ ) and  $T_{surf/2m}$  and  $q_{surf/2m}$  are the temperature and specific humidity at 2m height / at the surface, with the latter two being calculated using the reanalysis 2m dew point temperatures ( $T_{d,2m}$ ) and mean sea level pressure ( $p_{msl}$ ). As could be shown by Adams et al. [2013], the standard approach using constant heat transfer coefficients tends to underestimate the ice thickness by approximately 7cm on average, when compared to an iteratively and pixel wise calculated heat transfer coefficient.

The final ice thickness  $h_{ice}$  is obtained by setting the total atmospheric flux  $Q_{atm}$  (Eq. 2.9) equal to the conductive heat flux through the ice ( $Q_{ice}$ ; Eq. 2.10), and Eq. 2.10 is solved for the ice thickness  $h_{ice}$ :

$$h_{ice} = \kappa_{ice} \cdot \frac{(T_{surf} - T_f)}{Q_{atm}} \quad (2.15)$$

In Eq. 2.15, the thermal conductivity is set to  $\kappa_{ice} = 2.03 \text{ Wm}^{-2}\text{K}^{-1}$  [Drucker et al. 2003; Tamura et al. 2007]. As already mentioned, the procedure is only applicable to clear sky conditions as clouds and fog over polynyas, leads and/or open water strongly influence the accuracy the recorded IST signal [Riggs et al. 2006]. In general, further analysis is limited to TIT values  $\leq 0.2 \text{ m}$ , as this range is generally regarded sufficient to get reliable results for ice production [Adams et al. 2013; Yu and Rothrock 1996; Tamura et al. 2007; Tamura and Ohshima 2011]. In addition, the uncertainty for the TIT retrieval increases considerably for thicker ice, as was shown in a sensitivity analysis by Adams et al. [2013] ( $\pm 1.0$ ,  $\pm 2.1$  and  $\pm 5.3 \text{ cm}$  for TIT classes 0-5, 5-10 and 10-20 cm, respectively). The swath-wise calculated TIT is afterwards merged into daily composites, from which ice production rates and other quantities can be estimated. In order to do so, an additional cloud-screening needs to be applied as the MODIS cloud mask often contains misclassifications and ambiguities from undetected clouds and sea smoke during nighttime. Further, the daily composites frequently feature cloud-induced gaps, so that fair comparisons to mostly cloud-insensitive satellite data sets require the application of dedicated interpolation schemes, which are presented in detail in Chapters 4 to 6.

### 2.2.2 Polynya Signature Simulation Method (PSSM) and Sea ice concentration thresholds applied on passive microwave data

The usage of passive microwave data to derive the areal extent of a polynya (i.e., to classify passive microwave brightness temperatures into regions of open water, thin and thicker ice) typically follows two different approaches. The first approach is highly straightforward and simply relies on calculated sea-ice concentrations (SIC), as a SIC threshold of or around 70% (70PT; [e.g. Kern 2008; Adams et al. 2011]) has proven to delineate polynya margins fairly well. However, results may vary depending on the utilized SIC algorithm [Kwok et al. 2007].

A more frequently applied approach is the Polynya Signature Simulation Method (PSSM; Markus and Burns [1995]; Willmes et al. [2010, 2011]), which derives POLA with a classification strategy applied on brightness temperatures from the 36/37 (less atmospheric disturbance) and

85/89 (high resolution) GHz channels (frequencies for SSM/I and AMSR-E, respectively). In the PSSM, first a threshold is applied on the polarization ratio (PR) at the higher frequency range (85/89/91 GHz) to get an initial guess for the open water area. Then, the best match between the simulated and measured PR at the lower frequency range (36/37 GHz) is iteratively estimated to achieve a classified image (thin ice / polynya and thicker ice) at a spatial resolution of 6.25 km<sup>2</sup> (AMSR-E) or 12.5 km<sup>2</sup> (SSM/I). The upper value for ice thickness of the PSSM-derived polynya area is subject to regional variability and was previously estimated with 0.2 m for a case study in the Laptev Sea [Willmes et al. 2010] and 0.2–0.25 m for southern-hemisphere polynyas in the Ross Sea [Kern et al. 2007]. As part of the present thesis, both the performance of the 70PT and the PSSM were evaluated anew in a study on the North Water polynya, situated north-west of Greenland (Ch. 5; Preußner et al. [2015a]).

### 2.2.3 Thin-ice thickness retrieval using passive microwave sensors

The calculation of thin-ice thickness using passive microwave brightness temperatures (SSM/I-SSMIS, AMSR-E, AMSR2) commonly follows the principle of empirically linking polarization ratios (PR) of  $T_b$ , influenced by the change in salinity with ice thickness [Naoki et al. 2008], to reference thin-ice thicknesses derived by thermal infrared sensors such as AVHRR or MODIS [e.g. Cavalieri 1994; Tamura et al. 2007, 2008; Willmes et al. 2010; Tamura and Ohshima 2011; Iwamoto et al. 2013, 2014]. As PR values at a given frequency decrease as the sea ice thickens, the relation to the ice thickness can be expressed through linear or exponential regressions [Tamura and Ohshima 2011]. Other similar approaches are based on a simple ratio between the horizontally and vertically polarized  $T_b$  at 36 and 37 GHz [Martin et al. 2004, 2005; Willmes et al. 2010] or  $T_b$  at 89 GHz [Willmes et al. 2010].

However, while these passive microwave approaches all carry the advantages of a frequent and mostly cloud-independent coverage, problems and ambiguities can occur due to their coarse spatial resolutions (ranging from 6.25 to 25 km) and inherent mixed-pixels in coastal areas, atmospheric influences in the near 90 GHz frequency range as well as similar PR-ranges for thin-ice and fast-ice areas, requiring dedicated masking procedures [e.g. Iwamoto et al. 2013, 2014].

### 2.2.4 Derivation of potential thermodynamic ice production in polynyas

The calculation of potential thermodynamic ice production requires an accurate characterization of the distribution of thin-ice and open water within the margins of a detected polynya. The previous chapters showed how this can be done using either optical (i.e., TIR) sensors or passive microwave radiometers. The term 'thermodynamic' implies, that calculated estimates represent the amount of ice that would be formed under ideal thermodynamic conditions, i.e. with no dynamic contribution to ice growth such as ridging and rafting, and assuming a uniform layer of ice within a grid cell of varying spatial extent. The currently used approach of omitting an oceanic heat flux from below, which would lower the amount of heat loss to the atmosphere, leads to the term 'potential'.

From a geophysical perspective, ice production rates are the most interesting parameter that can be derived for thin-ice areas, as they are directly related to other physical processes such as the lateral ice transport out of and into a certain polynya region [Hollands and Dierking 2016]. In addition, the amount of new ice determines the feedback to the underlying ocean column through salt rejection (compare Ch. 1.2 and Ch. 1.3).

A common approach to calculate ice production rates is using information on the ice thickness (distribution) in combination with meteorological data from atmospheric reanalysis data sets, such as the ECMWF ERA-Interim [Dee et al. 2011] or NCEP2 [Kanamitsu et al. 2002] reanalysis. Despite coarse spatial resolutions and ultimately large uncertainties of these data sets, a wide range of earlier remote sensing studies [e.g. Renfrew et al. 2002; Martin et al. 2005; Tamura et al. 2007; Willmes et al. 2011; Tamura and Ohshima 2011; Iwamoto et al. 2014] and model studies [e.g. Ebner et al. 2011; Bauer et al. 2013; Jardon et al. 2014] as well as the present thesis followed this approach as it currently the only viable option when investigating large and remote spatial domains with a lack of in-situ data.

In general, ice production rates are derived by assuming that the entire heat loss at the ice surface to the overlying atmosphere contributes to new ice formation [Tamura et al. 2007, 2008; Willmes et al. 2011].

$$\frac{\partial h}{\partial t} = \frac{-\bar{Q}_{ice}}{\rho_{ice} \cdot L_f} \quad (2.16)$$

Equation 2.16 provides the ice production rate  $\frac{\partial h}{\partial t}$ , with  $\rho_{ice}$  being the density of the ice ( $\rho_{ice} = 910 \text{ kg/m}^3$ ; Timco and Frederking [1996]) and  $L_f$  being the latent heat of fusion of sea ice ( $L_f = 0.334 \text{ MJ/kg}$ ; [e.g. Tamura and Ohshima 2011]). The conductive heat flux through the ice  $Q_{ice}$  (compare Ch. 2.2.1, Eq. 2.10) can be retrieved if the ice thickness and ice surface temperature is known. However, the usage of fixed values for  $\rho_{ice}$  and  $L_f$  is of course a simplification that introduces an additional error source arising from spatially and temporally varying conditions for ice formation.

The in-situ validation of ice production rates in thin-ice areas is a highly difficult task, especially during wintertime. Hence, ice production derived by the above described approach should currently be regarded as a potential upper limit for thermodynamically induced ice growth.

### 3 Motivation, objectives and outline of the thesis

A major objective of the Laptev Sea Transdrift project (2013-2016), introduced in Ch. 1, was the quantification of pan-Arctic sea ice production based on daily derived thin-ice thickness (TIT) fields. As could be seen in the previous chapter, earlier studies and investigations dealing with the derivation of TIT and potential thermodynamic ice production from either thermal infrared or passive microwave sensors were in most cases limited in either a spatial or temporal sense. Hence, the main topics that are addressed in this thesis can be outlined as follows:

1. Refine methods and procedures of Adams et al. [2013] and Willmes et al. [2011] and apply the thin-ice thickness algorithm to a 12-yr data set in an active Arctic polynya region (Storfjorden polynya / Svalbard) to infer ice production rates
2. Perform a long-term comparison between MODIS thermal infrared data and polynya properties derived from passive microwave sensors (SMMR-SSMI/S, AMSR-E and AMSR2) and evaluate differences considering an improved treatment of cloud gaps (North Water (NOW) polynya)
3. Apply the most recent version of the TIT retrieval to the pan-Arctic region north of 68°N for 2002/2003 to 2014/2015 and investigate observed patterns in ice production as well as interconnections to the Transpolar Drift system

Regarding the first point, the studies by Adams et al. [2013] and Willmes et al. [2011] were mostly concentrating on improving the heat flux parametrization, with the main focus area being the Laptev Sea region. By transferring the thereby established concepts (see Ch. 2.2.1) into a streamlined new version of the thin-ice thickness retrieval, a data set spanning 12 winter seasons of daily TIT composites could be analyzed and ice production rates were subsequently derived. In addition, a first attempt of compensating for cloud-gaps in the daily MODIS composites and hence POLA and IP estimates was introduced. Building upon the study by Paul et al. [2015b], where a new scheme for cloud-gap interpolation was presented (co-authored by the candidate), the following study concentrated on a multi-sensor comparison regarding the characteristics of the NOW polynya over a 37-yr period. The direct comparison between rather cloud-insensitive passive microwave estimates and corresponding cloud-corrected MODIS estimates yielded interesting insights regarding differences in POLA and the capability to observe polynya-opening and -closing events. Ultimately, the continuously improved version of the TIT retrieval was applied to the pan-Arctic domain (featuring all areas north of 68°N) in order to get a more detailed picture on polynya dynamics over a period of 13 winter seasons. To date, this represents by far the largest domain on which this procedure to derive TIT has been applied. By covering such a large area and considering the length of the data record, derived trends in thermodynamic ice production revealed distinct hemispheric differences between polynyas in the western and the

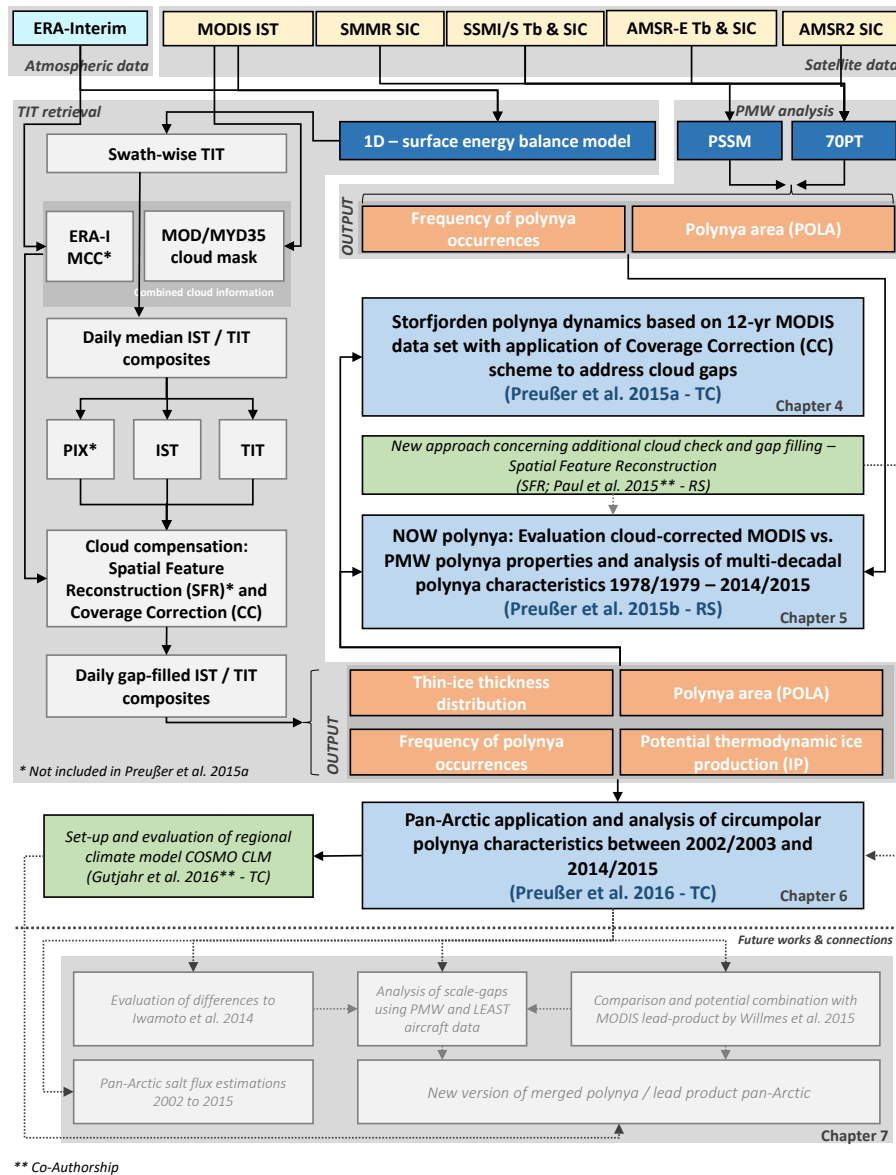


Figure 3.1: Overview on the different input data sets (yellow and light blue boxes) and methods (dark blue boxes plus grey flowchart in the upper part of the figure) that were utilized for this thesis. The blue boxes refer to the here presented thesis chapters: Storfjorden polynya dynamics based on 12-yr MODIS data set with application of Coverage Correction (CC) scheme to address cloud gaps (Chapter 4), the evaluation of cloud-corrected MODIS and passive microwave (PMW) derived polynya properties during the analysis of multi-decadal polynya characteristics between 1978/1979 to 2014/2015 in the North Water (NOW) polynya (Chapter 5), and pan-Arctic application of improved MODIS thin-ice retrievals for the analysis of circumpolar polynya characteristics between 2002/2003 and 2014/2015 (Chapter 6). Orange boxes show derived polynya properties. Inter-dependencies and potential linkages with studies that were co-authored by the candidate are indicated in green. An overview of potential future research activities related to the present thesis (Chapter 7) is given at the bottom of this figure.

eastern Arctic. Further, the data set could be utilized in a study on regional climate modeling in the Laptev Sea by Gutjahr et al. [2016], where the derived long-term thin-ice thickness distribution served as a reference for the initial model set-up and comparisons to the model-derived ice production could be supported.

Chapters 4 to 6 consist of three peer-reviewed and published publications with a first-authorship, following the concept of a cumulative dissertation style. Beforehand, the following three subsections will briefly summarize the content of each publication supported with an overview of the used satellite and meteorological data sets as well as schematics of the underlying concepts/procedures that were used to achieve the above outlined thesis objectives (Fig. 3.1).

### 3.1 Short summary - Publication I (Storfjorden polynya)

As depicted in previous chapters, earlier studies that analyzed (Arctic) polynya dynamics using thermal infrared remote sensing data were either focusing on regional process studies for single winter seasons or fixed to a certain geographic location. Very often, the derivation of thin-ice thicknesses from high resolution TIR data solely served the purpose of producing reference data that is subsequently used to derive empirical relationships with coarser resolution passive microwave data. Chapter 2.1.2 showed that this has been motivated by the advantages of a regular global coverage as well as more or less cloud and illumination insensitivity. The effect of clouds on TIR data is twofold, as they produce data gaps when correctly identified by the MODIS cloud mask as well as possibly erroneous IST values when nighttime clouds remain undetected. However, one of the main purposes of this study was to demonstrate that the utilization of TIR thin-ice thicknesses is also a feasible approach to analyze multiple winter seasons in a highly dynamic Arctic polynya region, despite cloud-induced ambiguities and gaps in the TIR data. Hence, spatial and temporal characteristics of the Storfjorden polynya, a regularly forming area of thin-ice in between the islands Spitsbergen, Barentsøya and Edgeøya in the Svalbard archipelago, have been investigated for the period of 2002/2003 to 2013/2014. This was the first time that such a long-term investigation was carried out using only TIR satellite data.

Thin-ice thicknesses up to 50 cm can be calculated using MODIS ice-surface temperatures (IST) combined with ECMWF ERA-Interim atmospheric reanalysis data in an energy-balance model, as for thin ice the atmospheric heat flux (i.e., total energy loss from the surface to the atmosphere) is considered to be balanced by the conductive heat flux through the ice. As depicted in Ch. 2.2.1, the model requires a number of necessary assumptions, such as a linear temperature profile through the thin, hence snow-free, sea-ice, with the bottom-temperature (i.e., ice-ocean interface) considered as being constant at the freezing point of sea water.

Typical quantities like polynya area, the thin-ice thickness distribution, frequencies of polynya-occurrences as well as the total ice production were derived and compared to previous remote sensing and modeling studies. These previous studies on the Storfjorden area suggested an overall minor importance regarding overall ice production in Arctic polynyas, but this region was chosen on purpose. Besides being a well documented and investigated study area, which

allows to set the MODIS results in a proper context, the comparatively small spatial extents of the Storfjorden polynya should profit from the enhanced resolution imagery. As a first approach to address the cloud-induced gaps in daily TIT composites, a basic coverage-correction (CC) scheme was applied that is based on a mathematically simple upscaling procedure, depending on the daily percentage of MODIS IST coverage. On average, both polynya area and ice production are thereby increased by about 30%. Achieved results complement previous studies in the Storfjorden region [e.g. Skogseth et al. 2004, 2005; Hendricks et al. 2011] and underline the importance of this polynya considering the total amount of ice production and accompanied salt release each winter season, despite its comparatively small spatial extent.

## 3.2 Short summary - Publication II (North Water polynya)

The follow-up study built upon the established methodology from Preußner et al. [2015b], but featured two significant additions / modifications. First, a newly developed statistic-based cloud interpolation scheme (Spatial Feature Reconstruction - SFR; Paul et al. [2015b]) as well as additional cloud-screening procedures (Persistence Index (PIX) based on the sub-daily thin-ice persistence; cloud-filter by applying a threshold on ERA-Interim medium cloud-cover (MCC) fields) were successfully adapted and implemented for usage in Arctic polynya regions, so that a detailed comparison to the coverage-correction (CC) approach could be carried out. Second, a suite of passive microwave sensors were added to the investigation, as the analysis of decadal changes in the North Water region was one of the major goals for this study. The latter also enabled detailed inter-sensor comparisons, which ultimately gave an idea on the performance of cloud-correction techniques as well as new insights into passive microwave derived metrics. The North Water (NOW) Polynya is a regularly-forming and previously well investigated area of open-water and thin-ice, located between northwestern Greenland and Ellesmere Island (Canada) at the northern tip of Baffin Bay. Due to its large spatial extent, even in the midst of winter, as well as its high latitude location, it is a highly important area for a variety of physical and biological processes.

In this study, a long-term analysis of polynya dynamics and ice production in the NOW polynya was presented for all winter seasons between 1978/1979 and 2014/2015. In order to do so, remote sensing data from both passive microwave (AMSR-E, AMSR2, SMMR/SSM/I-SSMIS) and thermal infrared (MODIS) sensors were analyzed to infer characteristic polynya quantities, such as the total polynya area (POLA), the frequency of polynya-occurrences and thermodynamic ice production (IP), on various spatial resolutions and temporal scales. In order to allow comparisons between MODIS and passive microwave estimates, two well-working approaches were applied to overcome difficulties with falsely-classified and/or undetected cloud-covered pixels. It showed that all incorporated sensors were able to capture the overall seasonal development of the polynya very well. Differences occurred mainly in terms of the areal extent of the NOW polynya, as the capability to resolve smaller thin-ice features decreases with increasing grid resolutions (up to 25 km in case of SMMR/SSMIS sea-ice concentrations). Thereby, daily POLA derived by MODIS exceeds the passive microwave estimates in most cases, presumably with leads and thin-ice areas in close proximity to the coasts of Greenland and Ellesmere Island being the main



sources for this difference. However, application of the PSSM method (compare Ch.2.2.2) on SSM/I-SSMIS brightness temperatures yielded estimates that agreed well with corresponding cloud-corrected MODIS numbers.

Overall, this multi-sensor study proved that daily gap-filled MODIS composites can indeed be used for long-term polynya studies. While the differences between solely applying the CC approach and the additional use of temporal interpolation (SFR) was generally small in case of the NOW polynya, including the latter added confidence to the MODIS retrievals by relying on both spatially and temporarily variable, thereby physically more meaningful, statistics. Long-term time series of POLA (1978/1979 to 2014/2015) and IP (2002/2003 to 2014/2015), as well as thin-ice characteristics in Nares Strait complement atmospheric and oceanographic observations and model efforts in the NOW region over the last decades. A future synthesis of atmospheric and oceanographic modeling and remote sensing observations could help to explain the changes that are taking place in the NOW region since the 1990s and ongoing as documented in this study.

### 3.3 Short summary - Publication III (Circumpolar polynya-regions)

For the final publication, established methods and concepts from the previous two studies concerning the derivation of daily gap-filled MODIS composites were applied to a vastly increased spatial domain, that features all Arctic ocean areas north of 68°N. The period of investigation consisted of 13 winter seasons (2002/2003 to 2014/2015), and a total of 17 different polynya regions across the Arctic were analyzed with the aim to infer long term spatial and temporal characteristics.

The study showed that all 17 polynya regions combined cover an average thin-ice area of  $226.6 \pm 36.1 \times 10^3 \text{ km}^2$  during winter (November to March). This allows for an average total wintertime accumulated ice production of about  $1811 \pm 293 \text{ km}^3$ , with the Kara Sea region and the North Water polynya (both 15%), polynyas at the western side of Novaya Zemlya (20%) as well as scattered smaller polynyas in the Canadian Arctic Archipelago (all combined 12%) being the main contributors. Compared to an earlier study on pan-Arctic ice production in polynyas [Iwamoto et al. 2014], the estimate on the average total ice production is about 52-54% larger. However, differences in the regarded time frame, reference areas, sensor-specifics as well as a potential bias due to cloud cover and/or the exclusive assumption of clear-sky conditions contribute to this difference. Hence, a more profound statement on these discrepancies would require a more detailed and direct comparison of both data sets.

Overall, indications of hemispheric differences in ice production trends were noticeable with several regions in the eastern Arctic showing strong increases in wintertime IP, especially in recent years. While the NOW polynya behaved similar (as depicted in Preußner et al. [2015a]), other polynyas in the western Arctic showed a higher interannual variability in terms of POLA and IP. A major focus was set on the Laptev Sea region in the eastern Arctic, as it is known for being one of the core areas for ice production in the Arctic with a distinct connection to Transpolar Drift characteristics. With the most significant positive IP trend among all polynyas

(+ 6.8 km<sup>3</sup>/yr), an overall share of about 5% to the total IP in Arctic polynyas and a significant relation with sea-ice area export rates [Krumpen et al. 2013] between 2002/2003 and 2014/2015, our results once more underlined the significant role of the Laptev Sea. Despite existing limitations originating from the use of thermal infrared remote sensing data during winter, this new data set of 13 consecutive winter seasons is considered to be a huge step forward for a spatially accurate characterization of Arctic polynya dynamics and the associated sea-ice budget related to wintertime sea-ice production.

## **4 Publication I: Thin-ice dynamics and ice production in the Storfjorden polynya for winter seasons 2002/2003 to 2013/2014 using MODIS thermal infrared imagery**

Written by

**Andreas Preußer**, Sascha Willmes, Günther Heinemann and Stephan Paul

Published: 21 May 2015

This paper is reprinted from the journal 'The Cryosphere' (TC) with permission from Copernicus Publishing under the Creative Commons by Attribution (CC-BY) license 3.0 [Preußer et al. 2015b].

The candidate's contribution to this paper was that he carried out the complete analysis and drafted the manuscript, including the preparation of all figures and tables. All co-authors were, with varying degree, involved in the initial set-up of the algorithm and contributed to the writing of the manuscript.

The Cryosphere, 9, 1063–1073, 2015  
www.the-cryosphere.net/9/1063/2015/  
doi:10.5194/tc-9-1063-2015  
© Author(s) 2015. CC Attribution 3.0 License.



# Thin-ice dynamics and ice production in the Storfjorden polynya for winter seasons 2002/2003–2013/2014 using MODIS thermal infrared imagery

A. Preußner, S. Willmes, G. Heinemann, and S. Paul

Dept. of Environmental Meteorology, Faculty of Regional and Environmental Sciences,  
University of Trier, Trier, Germany

Correspondence to: A. Preußner (preusser@uni-trier.de)

Received: 10 October 2014 – Published in The Cryosphere Discuss.: 13 November 2014

Revised: 13 April 2015 – Accepted: 16 April 2015 – Published: 21 May 2015

**Abstract.** Spatial and temporal characteristics of the Storfjorden polynya, which forms regularly in the proximity of the islands Spitsbergen, Barentsøya and Edgeøya in the Svalbard archipelago under the influence of strong northeasterly winds, have been investigated for the period of 2002/2003 to 2013/2014 using thermal infrared satellite imagery. Thin-ice thicknesses were calculated from MODIS ice-surface temperatures combined with ECMWF ERA-Interim atmospheric reanalysis data in an energy-balance model. Associated quantities like polynya area and total ice production were derived and compared to previous remote sensing and modeling studies. A basic coverage-correction scheme was applied to account for cloud gaps in the daily composites. On average, both polynya area and ice production are thereby increased by about 30%. The sea ice in the Storfjorden area experiences a late fall freeze-up in several years over the 12-winter period, which becomes most apparent through an increasing frequency of large thin-ice areas until the end of December. In the course of an average winter season, ice thicknesses below 10 cm are dominating within the Storfjorden basin. During the regarded period, the mean polynya area is  $4555.7 \pm 1542.9 \text{ km}^2$ . Maximum daily ice production rates can reach as high as  $26 \text{ cm d}^{-1}$ , while the average ice production is estimated at  $28.3 \pm 8.5 \text{ km}^3$  per winter and therefore lower than in previous studies. Despite this comparatively short record of 12 winter seasons, a significant positive trend of  $20.2 \text{ km}^3$  per decade could be detected, which originates primarily from a delayed freeze-up in November and December in recent winter seasons. This contrasts earlier reports of a slightly negative trend in accumulated ice production prior to 2002. Although featuring more pronounced in-

terannual variations between 2004/2005 and 2011/2012, our estimates underline the importance of this relatively small coastal polynya system considering its contribution to the cold halocline layer through salt release during ice-formation processes. In addition, calculated quasi-daily thin-ice thickness charts represent a valuable data set for atmosphere and ocean modeling applications.

## 1 Introduction

Recurrent polynyas are considered to play an important role for sea-ice production and ocean circulation (Barber and Massom, 2007). The knowledge of ice production (IP) in the Arctic is of vital interest for the understanding of the Arctic climate system and the verification of climate and ocean models. Divergent ice motions due to wind are the main cause for the opening of near-coastal polynyas (Smith et al., 1990). During winter, these areas of open water or thin ice, exposed to the cold atmosphere, are characterized by strong ice production and brine release and modify the atmospheric boundary layer (Ebner et al., 2011; Bauer et al., 2013). The timing, duration and size of a polynya can often have large interannual variations because of the general interannual variability of atmosphere–ice–ocean interaction processes (Morales-Maqueda et al., 2004). A precise derivation of the thin-ice thickness (TIT) distribution, the areal extent of a polynya (here defined as open water and thin ice below 0.2 m) and the amount of local sea-ice production is therefore an important step towards a comprehensive understanding of

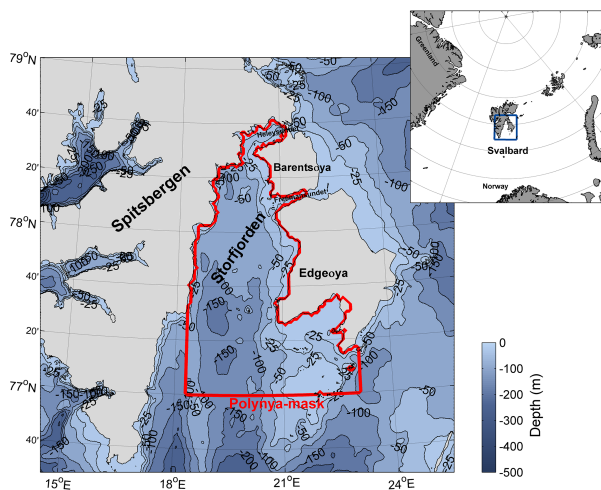


**Figure 1.** Map of the Svalbard archipelago in western Barents Sea. The study region is located in Storfjorden, which is surrounded by the main island Spitsbergen in the west and Barentsøya/Edgeøya in the east. The applied polynya mask is marked in red, enclosing the Storfjorden basin north of the sill at 77° N. Bathymetric data by Jakobsson et al. (2012) (IBCAO v3.0).

physical processes in the Arctic shelf regions and the Arctic sea-ice cover in general. Ice production in thin-ice regions can either be estimated by the use of remote sensing methods (Willmes et al., 2010) or by using model approaches (Ebner et al., 2011; Krumpen et al., 2011; Bauer et al., 2013). The use of thermal infrared and microwave remote sensing data offers the opportunity for daily monitoring of thin-ice thicknesses and their distribution on large spatial scales (Yu and Rothrock, 1996; Willmes et al., 2010; Adams et al., 2013).

Storfjorden (see Fig. 1), situated in the southeastern part of the Svalbard archipelago between the main island of Spitsbergen in the west and Barentsøya/Edgeøya in the east, is a region of high coastal polynya activity during winter, as reported by a number of earlier studies (e.g., Haarpaintner et al., 2001; Skogseth et al., 2004). Two shallow straits, Heleysundet and Freemansundet, connect the northern part of Storfjorden with the Barents Sea and show tidally induced currents as well as exchange processes between water masses inside the fjord and the Barents Sea (Skogseth et al., 2013).

Persistent and strong northerly to northeasterly winds are the main cause for larger polynya openings inside Storfjorden. These opening events may result in large volumes of brine-enriched shelf water, which can be significant regarding the total amount of bottom water in the Arctic Ocean by supplying between 5 and 20 % of all the newly formed dense water (Skogseth et al., 2004; Hendricks et al., 2011). Besides thermodynamically induced ice growth in Storfjorden during wintertime, the dynamical part due to rafting and deformation processes may play a substantial role in the overall ice-thickness distribution, as southerly (onshore) winds can

potentially advect sea ice from the Barents Sea into the fjord (Hendricks et al., 2011). An estimation of thermodynamic IP within the open water and thin-ice area (i.e., Storfjorden polynya) has been conducted in previous studies using mainly microwave remote sensing (both passive and active systems) in combination with different model approaches. Therein, values are ranging between 20 and 35–45 km<sup>3</sup> for single winter seasons (November–May) between 1997/1998 and 2000/2001 (Haarpaintner et al., 2001; Skogseth et al., 2004, 2005) and 47 km<sup>3</sup> when averaged over the winter seasons (October/November–June/July) from 2002/2003 to 2011/2012 (Jardon et al., 2014). Iwamoto et al. (2014) state that the Storfjorden polynya contributes with around 4 % to the average total ice volume produced in Arctic polynyas between 2002/2003 and 2010/2011 (September to May).

While these estimates make the Storfjorden area appear to be of minor importance regarding overall ice production in Arctic polynyas, we chose this region due to several distinct requirements. These included the availability of a number of related polynya studies in order to set our estimates into a proper context as well as the comparatively small spatial extent of the Storfjorden polynya to profit from the enhanced resolution imagery.

Based on daily empirically derived ice-thickness distributions in thin-ice areas at a comparatively high spatial resolution, we perform a broad investigation on the associated quantities polynya area (POLA) and ice production for the period between 2002/2003 and 2013/2014 using high-resolution Moderate Resolution Imaging Spectroradiometer (MODIS) thermal infrared data. The presented results will develop a more comprehensive understanding of the polynya dynamics in Storfjorden as well as associated processes over both annual and interannual timescales (in the course of this paper, the term “annual” refers to one winter season from November to March). Furthermore, results will contribute to pan-arctic studies of polynya dynamics.

## 2 Data and methods

### 2.1 MODIS ice-surface temperatures

Thin-ice thickness are computed using the MOD/MYD29 sea-ice product (Hall et al., 2004; Riggs et al., 2006) derived from MODIS satellite data. We used data from both MODIS instruments on board the Terra and Aqua polar-orbiting satellite platforms. They are available from the National Snow and Ice Data Center (NSIDC) located in Boulder, USA (<ftp://n5eil01u.ecs.nsidc.org/SAN/>). The product contains swath data of ice-surface temperatures (ISTs). Swath-based ISTs have a spatial resolution of 1 km × 1 km at nadir. The accuracy of the MOD/MYD29 ISTs is given with 1–3 K (Hall et al., 2004).

For our analysis, swaths covering the Storfjorden area were extracted using metadata information for each MODIS

**Table 1.** Total number of individual MODIS swaths, which were incorporated into the thin-ice thickness (TIT) calculations. Numbers are given for each winter season from November to March.

Winter season	Number of MODIS swaths
2002–2003	4054
2003–2004	4023
2004–2005	4062
2005–2006	4073
2006–2007	3990
2007–2008	4069
2008–2009	4135
2009–2010	4142
2010–2011	4205
2011–2012	4129
2012–2013	4137
2013–2014	4244
Sum	49 263

swath, resulting in 27 individual swaths per day on average for later composite generation. These composites solely consist of nighttime scenes to exclude the influence of incident shortwave radiation (Yu and Lindsay, 2003; Adams et al., 2013; cf. Sect. 2.3 and 2.3.1). The total number of incorporated MODIS swaths is illustrated in Table 1. As MODIS swath data presumably suffer from inherent panoramic distortion effects, all IST swaths were mapped onto a  $2\text{ km} \times 2\text{ km}$  ( $0.018^\circ$ ) equirectangular grid covering the southern part of Svalbard ( $75\text{--}80^\circ\text{ N}$ ,  $10\text{--}30^\circ\text{ E}$ ).

A polynya mask (red area in Fig. 1) is applied in order to cover an area comparable to previous studies (Skogseth et al., 2004, 2005; Jardon et al., 2014), as well as to limit the probability of remaining hidden cloud artifacts. The mask comprises a total area of  $12\,594\text{ km}^2$  and has its southern limit at  $77^\circ\text{ N}$  (following Skogseth et al., 2004), where a 120 m deep sill serves as kind of a boundary for the accumulation of brine-enriched shelf water in the Storfjorden basin (see Fig. 1).

## 2.2 ERA-Interim reanalysis

For the calculation of thin-ice thicknesses, atmospheric variables from the ERA-Interim reanalysis product (Dee et al., 2011) are used to provide 2 m temperature, 2 m dew point temperature, 10 m wind speed components ( $u$  and  $v$ ) and the mean sea-level pressure at a temporal resolution of 6 h. The data set is provided by the European Center for Medium-Range Weather Forecasts (ECMWF) in a horizontal resolution of  $0.75^\circ$  ( $\sim 79\text{ km}$ ). As the satellite data set is by far spatially higher resolved than the atmospheric data set, a linear interpolation of the ERA-Interim data is performed to match the MODIS data. In the course of the TIT calculations, each MODIS swath is linked to the closest time step of the atmospheric fields.

## 2.3 Thin-ice thickness retrieval using a 1-D thermodynamic surface energy model

In order to derive daily TIT distributions, we use an approach that follows the work of Yu and Rothrock (1996), Yu and Lindsay (2003) and Drucker et al. (2003), with most recent improvements and modifications made by Willmes et al. (2010, 2011) and Adams et al. (2013). The applied method utilizes the distinct relationship between IST and thickness of thin ice depending on atmospheric energy fluxes. The IST of very thin ice (with no snow cover) is close to the freezing point of the upper ocean layer and decreasing IST can be observed for thicker ice (Drucker et al., 2003; Kwok et al., 2007). However, IST is governed by atmospheric radiation fluxes and turbulent fluxes of heat, which does not allow for a simple relationship between IST and ice thickness. The ice thickness  $h_{\text{ice}}$  (likewise abbreviated “TIT” for thin ice in the course of this paper) is therefore calculated using a 1-D thermodynamic sea-ice model.

Several assumptions have to be made to apply this model. First, the temperature profile through the ice is assumed to be linear. This approximation is valid for  $h_{\text{ice}} \leq 0.5\text{ m}$  (Drucker et al., 2003). Second, the water temperature at the boundary between ice and ocean is constant and at its freezing point ( $T_f = 271.35\text{ K}$ ). Third, the ice is assumed to be free of snow. The ice thickness is calculated by using MODIS IST and ERA-Interim reanalysis data. The method is based on the condition, that the conductive heat flux through the ice ( $Q_{\text{ice}}$ , Eq. 1) equals the total heat flux to the atmosphere ( $Q_{\text{atm}}$ , Eq. 2). This implies that all energy loss at the ice-surface is compensated by the conductive heat flux  $Q_{\text{ice}}$ .

$$Q_{\text{ice}} = \kappa_{\text{ice}} \times \frac{(T_{\text{surf}} - T_f)}{h_{\text{ice}}}, \quad (1)$$

$$Q_{\text{atm}} = Q_0 - H_0 - E_0, \quad (2)$$

where  $Q_0$  is the net radiation balance,  $H_0$  and  $E_0$  are the turbulent fluxes of sensible heat and latent heat, respectively,  $\kappa_{\text{ice}}$  is the thermal conductivity of sea ice,  $T_{\text{surf}}$  is the surface temperature,  $T_f$  is the freezing point of sea water and  $h_{\text{ice}}$  is the ice thickness. Because of difficulties with the parametrization of shortwave radiation terms (Adams et al., 2013), only nighttime scenes were incorporated into the calculations (by checking the solar incidence angle on a pixel-by-pixel basis), so that the radiation balance  $Q_0$  simplifies to the long-wave radiation terms  $L \downarrow$  and  $L \uparrow$ . Upwelling long-wave radiation  $L \uparrow$  is calculated using the IST from MOD/MYD29 with the surface emissivity  $\epsilon_s$  set to 1.  $L \downarrow$  can be obtained using ERA-Interim 2 m temperatures and the atmospheric emissivity  $\epsilon_{\text{atm}}$ , calculated using the formulation of Jin et al. (2006). Turbulent fluxes of sensible ( $H_0$ ) and latent ( $E_0$ ) heat in Eq. (2) are calculated using an iterative bulk approach by Launiainen and Vihma (1990), where near-surface stratification is considered using Monin–Obukhov similarity theory and associated universal functions for the

heat transfer coefficients  $C_H$  and  $C_E$ . The 10 m wind speed is interpolated to the 2 m level. A constant roughness length for momentum  $z_0 = 1 \times 10^{-3}$  m is used. As could be shown by Adams et al. (2013), the standard approach used in previous studies using constant heat transfer coefficients tends to underestimate the ice thickness by approximately 7 cm on average, when compared to an iteratively calculated heat transfer coefficient. To obtain the ice thickness ( $h_{ice}$ ), the total atmospheric flux  $Q_{atm}$  (Eq. 2) is set equal to the conductive heat flux through the ice ( $Q_{ice}$ ; Eq. 1), and Eq. (1) is solved for  $h_{ice}$  using a value for the thermal conductivity of  $\kappa_{ice} = 2.03 \text{ W m}^{-2} \text{ K}^{-1}$  (Drucker et al., 2003).

Calculated ice thicknesses are assumed to be uniform at a given pixel location and therefore hypothetical (Tamura and Ohshima, 2011). The described method is only applicable to clear sky conditions, as clouds and fog strongly influence the accuracy of the recorded ISTs (Riggs et al., 2006).

In a sensitivity analysis of the above described method, Adams et al. (2013) state an uncertainty for the ice-thickness retrieval of  $\pm 1.0$ ,  $\pm 2.1$  and  $\pm 5.3$  cm for TIT classes 0–5, 5–10 and 10–20 cm, respectively. Therefore, we constrain our analysis to ice thicknesses  $\leq 0.2$  m, as this range is regarded sufficient to get reliable results for ice production (Yu and Rothrock, 1996; Adams et al., 2013).

### 2.3.1 Calculation of daily thin-ice thickness composites

From all available MODIS swaths covering the Storfjorden polynya region, daily composites of ISTs and thin-ice thicknesses were computed. The TIT is first calculated from each swath on its own with the procedure described in Sect. 2.3. Subsequently, the mean TIT is computed pixel-wise and stored with its corresponding IST value.

By using daily composites, the daily IST coverage (percentage of pixels within the polynya mask that feature at least one valid IST value, based on all MOD/MYD29 swaths covering the Storfjorden region on a given day) is significantly increased compared to single swaths, reaching an average value of 82 % for the winter seasons 2002/2003 to 2013/2014. Figure 2 shows the seasonal and interannual variability of IST coverage. Noteworthy is a very low coverage in November to early January 2009/2010, as well as generally less frequent coverage at the beginning (November) and end (March) of each winter season. The latter effect originates from the previously stated restriction to nighttime scenes and consequently a reduction in the amount of available MODIS swaths. Hence, it is also the main reason why the months of October and April were left out in our investigations.

### 2.3.2 Derivation of ice production and polynya area

Following Tamura et al. (2007, 2008) and Willmes et al. (2011), daily ice production rates are calculated from the heat loss at the ice surface by assuming that the entire heat loss to

the overlying atmosphere contributes to new ice formation.

$$\frac{\partial h}{\partial t} = \frac{-\bar{Q}_{ice}}{\rho_{ice} \times L_f} \quad (3)$$

Therein,  $\frac{\partial h}{\partial t}$  stands for the ice production rate,  $\bar{Q}_{ice}$  is the daily mean conductive heat flux through the ice,  $\rho_{ice}$  is the density of sea ice (taken as  $\rho_{ice} = 910 \text{ kg m}^{-3}$ ) and  $L_f$  is the latent heat of fusion of ice ( $L_f = 0.334 \text{ MJ kg}^{-1}$ ; e.g., Tamura and Ohshima, 2011). Note that the negative sign in the right side of Eq. (3) handles the convention that  $Q_{atm}$  is considered positive when the surface gains energy, as well as considering that ice production only takes place when there is a net energy loss from the surface. Multiplying  $\frac{\partial h}{\partial t}$  with the areal extent of each pixel in the regarded region yields the volume IP rate  $\frac{\partial V}{\partial t}$ . IP rates are calculated for each pixel with an ice thickness  $\leq 0.2$  m and afterwards extrapolated to daily rates for later accumulation and/or averaging. Considering the total polynya area, a threshold of  $h_{ice} \leq 0.2$  m is applied to identify pixels containing thin ice in the daily composites as part of the POLA. The total area of those pixels is then accumulated to obtain the total daily POLA in square kilometers.

### 2.3.3 IST coverage correction

Cloud-induced gaps in our daily IST and TIT composites are a serious problem when we want to compare our initially calculated POLA and IP to estimates from other studies in which the use of active and passive microwave remote sensing systems largely reduces the effect of atmospheric disturbances.

To overcome these difficulties, a simple scaling approach is applied that works under the assumption that pixels in the uncovered part of the masked (Fig. 1) daily composites also contribute to the total POLA by the same proportion as those areas that are covered by a IST signal.

The initially calculated daily POLA is therefore scaled by a factor  $F$ :

$$F = 1/\text{coverage}, \quad (4)$$

$$\text{POLA}_{CC} = \text{POLA} \times F. \quad (5)$$

The coverage in Eq. (4) could range from 0 to 1, but we apply the correction only for coverages exceeding 0.5. Similarly, estimated IP values are also scaled by the same factor yielding a corrected ice production  $\text{IP}_{CC}$ .

Application of this correction scheme is limited to cases where the daily IST coverage (compare Fig. 2) within the fjord (i.e., the predefined polynya mask) surpasses a threshold of 50 %. By using this threshold, unrealistically high  $\text{POLA}_{CC}$  and  $\text{IP}_{CC}$  values are avoided. Otherwise, both  $\text{POLA}_{CC}$  and  $\text{IP}_{CC}$  are linearly interpolated using bounding days with a coverage fulfilling this precondition.

In order to test the performance of the cloud-correction method, we selected a total of six case studies from Jan-

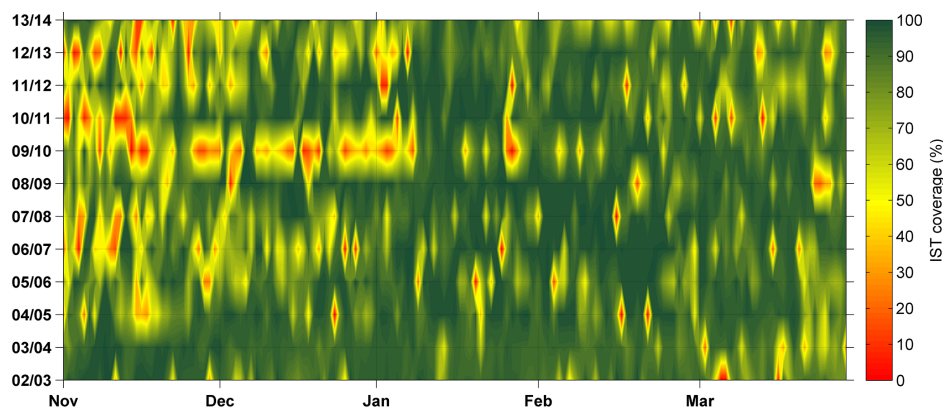


**Figure 2.** Interannual overview of the daily ice-surface temperature (IST) coverage (in %) within the applied polynya mask (compare Fig. 1). Values are derived from daily MODIS IST composites for the complete investigation period from 2002/2003 to 2013/2014 (November–March).

uary 2009 (DOY 002, 020, 024, 025, 026, 030) which feature near-clear-sky conditions (IST coverage  $\geq 99\%$ ). The coverage correction has been applied for each case study after randomly removing 45 % of the pixels within the polynya mask for 1000 realizations. The resulting deviation (in percent) from the “true” polynya area from all case studies combined is shown in Fig. 3. POLA<sub>CC</sub> deviations almost perfectly follow a typical normal (Gaussian) distribution, with a mean value of 0.77 % and a standard error of 5–6 % of the daily POLA.

Because the correction of IP values uses the same scaling factor  $F$ , the retrieved error margins can also be regarded as the uncertainty of our IP<sub>CC</sub> estimates.

### 3 Results

The bars in Fig. 4 show the mean relative contribution of each ice-thickness class from the total number of pixels with a TIT  $\leq 0.2$  m between the winter seasons 2002/2003 and 2013/2014. A temporal differentiation between the beginning of the freezing season (November–December) and the end of the freezing season (January–March) as well as a combined distribution for the whole winter period is given. Error bars refer to  $\pm 1$  standard deviation (SD) of the interannual averaged distribution frequencies. Between November and March, ice thinner than 0.02 m contributes around 15 % to the total polynya area in an average winter season. Due to a higher sensitivity of open water and very thin ice for sea smoke effects and consequently an exclusion of thin-ice pixels by the cloud mask, this thickness class is potentially biased (Willmes et al., 2011). The average ice thickness within the polynya mask is  $10 \pm 1.8$  cm. Thicker ice classes ( $> 0.1$  m) cover around half of the entire Storfjorden polynya in January to March and show overall lower contributions at the beginning of the freezing season. This follows from the

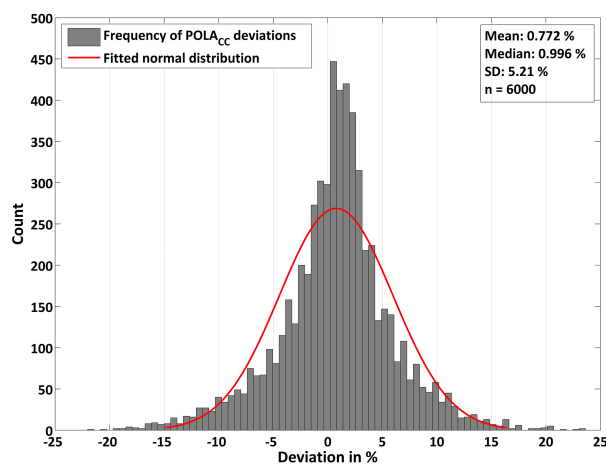


**Figure 3.** Histogram of coverage-corrected polynya area (POLA<sub>CC</sub>) deviations, based on six near-clear-sky case studies from January 2009 (DOY: 002, 020, 024, 025, 026, 030). For each case study, the coverage correction was repeated several times ( $n = 1000 \times 6$ ), after randomly removing 45 % of the pixels within the applied polynya mask. The red curve illustrates a fitted normal distribution.

high contribution of very thin ice in November to December, where over 60 % of the total POLA consists of ice thinner than 0.1 m. SD is highest in the lowest thickness classes ( $< 0.04$  m) and appears to be lower towards the end of the freezing season, possibly indicating a stronger seasonal variability of ice-thickness distributions within the polynya in November and December over the 12-year record (also apparent in relative TIT frequencies for November–December; Fig. 5).

Spatial distributions of the relative TIT frequency for 2002/2003 to 2013/2014 are presented as a seasonal comparison between the beginning of each freezing season



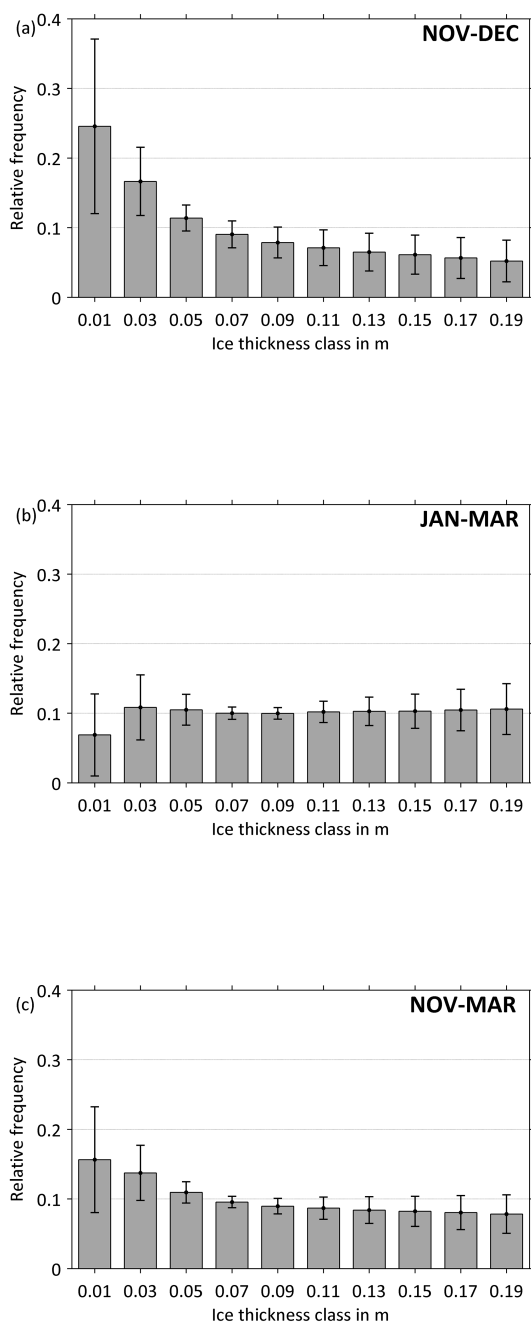


**Figure 4.** Relative thin-ice thickness (TIT) distribution in the Storfjorden polynya, with ice-thickness classes of 2 cm range ( $x$  axis). Input data are based on daily TIT composites. The bars indicate the mean relative distribution of each thickness class from the total number of TIT  $\leq 0.2$  m appearances between the winter seasons 2002/2003 and 2013/2014. Error bars refer to  $\pm 1$  SD. Besides an overview of the complete freezing season from November to March (c), it is further separated between the months November and December (a) as well as January to March (b).

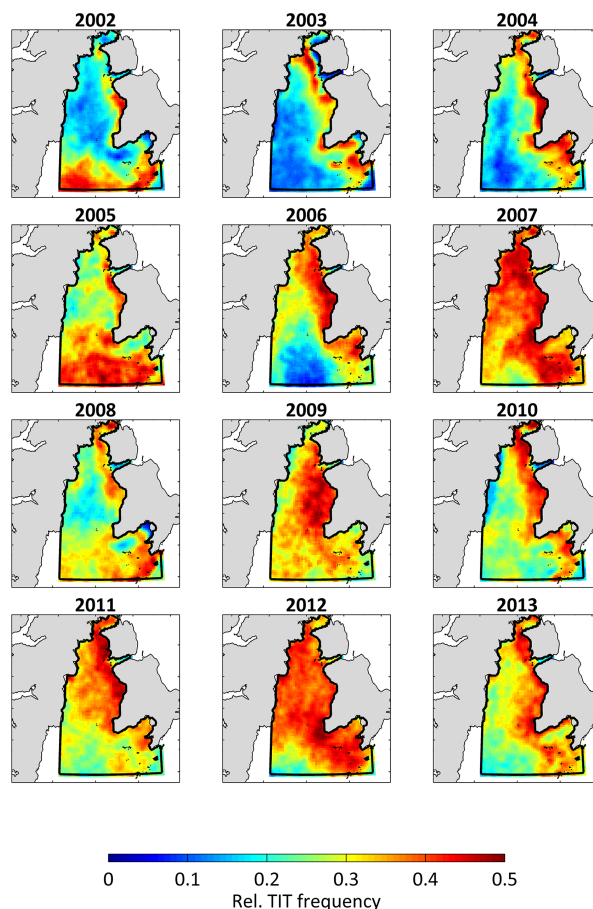


**Figure 5.** Early freezing season (November to December) relative frequency distribution of thin-ice thicknesses  $\leq 0.2$  m for 2002 to 2013, based on daily TIT composites.

(November–December, Fig. 5) and the end of each freezing season (January–March, Fig. 6). Therein, a pixel value of, e.g., 0.25 means that on 25 % of all days, a TIT threshold of 0.2 m was not exceeded. Following the previously stated definition of a polynya, these pixels represent the number of polynya occurrences in the given period. Figure 6 shows that the main regions for polynya development towards the end of the freezing season are at the lee sides of Barentsøya and Edgeøya at the eastern side of the fjord, extending more (2006–2008, 2010, 2012–2014) or less (2003–2005, 2009, 2011) further southwestwards.

At the beginning of the freezing season (Fig. 5), annual distributions show a more variable pattern of TIT frequencies. In some years (e.g., 2007, 2009, 2012), frequencies exceeding 0.3 cover large areas within the masked area in Storfjorden, which might be an effect of a late fall freeze-up and subsequently longer periods with thin ice and open water in the fjord. In other years (e.g., 2003, 2004), the observed pattern of high TIT frequencies is similar to typical polynya

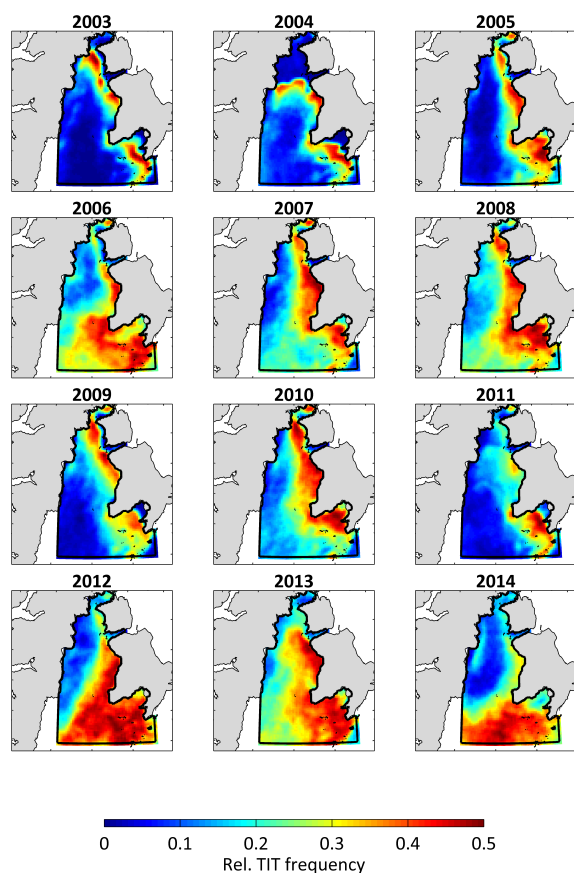


**Figure 6.** Late freezing season (January to March) relative frequency distribution of thin-ice thicknesses  $\leq 0.2$  m for 2003 to 2014, based on daily TIT composites.

locations between January and March, indicating an earlier freeze-up of the ice cover in Storfjorden.

Frequent TIT occurrences in the southern part of Storfjorden could originate from a generally northwards retreating ice edge in Storfjorden in some of the regarded winter seasons. This becomes most obvious in 2006, 2008 and 2012 to 2014 (Fig. 6). Low values ( $< 0.05$ ) at the (north) western side of Storfjorden towards the end of a freezing season (Fig. 6) further indicate typical fast-ice areas, which are most pronounced in the years 2003, 2004, 2005, 2007, 2009 and 2011.

The daily coverage-corrected (CC) polynya area ( $POLA_{CC}$ ) for all winters (November–March) between 2002/2003 and 2013/2014 is presented in Fig. 7. Highest  $POLA_{CC}$  values are generally found in November and December, which might be an effect of the already mentioned late fall freeze-up and therefore very thin newly formed ice (compare Figs. 4a and 5) in large parts of Storfjorden. From 2006 to 2008 and 2012 to 2013, this effect even extends

**Table 2.** Accumulated ice production (IP) in cubic kilometers per winter and average polynya area (POLA) in square kilometers for each winter season (November to March) in the Storfjorden polynya, together with the interannual average (mean) and its standard deviation (SD). CC denotes values after coverage correction, with relative increase compared to uncorrected values in brackets. All values are calculated within the predefined polynya mask (Fig. 1).

	Acc. IP ( $\text{km}^3$ )	Acc. IP <sub>CC</sub> ( $\text{km}^3$ )	POLA ( $\text{km}^2$ )	POLA <sub>CC</sub> ( $\text{km}^2$ )
2002–2003	13.9	16.1 (+16 %)	2185.2	2429.6 (+11 %)
2003–2004	15.2	16.7 (+10 %)	2186.6	2382.0 (+9 %)
2004–2005	19.2	23.7 (+24 %)	2684.7	3296.6 (+23 %)
2005–2006	20.6	25.1 (+22 %)	3934.8	4750.6 (+21 %)
2006–2007	19.4	25.3 (+31 %)	3473.9	4524.2 (+30 %)
2007–2008	27.4	33.1 (+21 %)	4491.0	5472.5 (+22 %)
2008–2009	21.6	24.6 (+14 %)	2965.4	3353.3 (+13 %)
2009–2010	17.3	30.0 (+73 %)	3390.1	6357.0 (+88 %)
2010–2011	23.2	31.9 (+38 %)	2996.0	4024.7 (+34 %)
2011–2012	21.5	29.6 (+38 %)	4087.6	5001.5 (+22 %)
2012–2013	36.0	47.2 (+31 %)	5592.4	7388.0 (+32 %)
2013–2014	25.4	36.5 (+44 %)	4154.3	5688.4 (+37 %)
Mean	21.7	28.3 (+30 %)	3511.8	4555.7 (+29 %)
SD	5.9	8.5	999.6	1542.9

well into January with a series of large  $POLA_{CC}$  events ( $> 5000 \text{ km}^2$ ) developing in February and March.

The mean (November to March) POLA for the entire regarded period amounts to  $3511.8 \pm 999.6 \text{ km}^2$ , with an increase of 29 % for  $POLA_{CC}$  when the presented coverage correction is applied. Around 60 % of this area consists of ice thinner than 10 cm. A complete overview on wintertime mean POLA and  $POLA_{CC}$  values is given in Table 2.

A spatial overview of the resulting accumulated daily ice production rates (in  $\text{m winter}^{-1}$ ), averaged between 2002/2003 and 2013/2014 is presented in Fig. 8. Largest values occur in regions which also show high TIT frequencies (Fig. 6). The average ice production in the western part of Storfjorden is generally lower, as thin ice in these areas is mainly present at the beginning of the freezing season.

Maximum daily ice production rates in the fjord can reach as high as  $26 \text{ cm d}^{-1}$  (winter season 2006/2007), with the highest rates occurring on average in the northern part of Storfjorden (north of  $77.5^\circ \text{ N}$ ).

Figure 9 shows values of accumulated ice production per winter season from November to March, both with and without applied coverage correction. The impact of seasonal differences is highlighted in yellowish and blueish colored bars. A detailed overview for each winter season is additionally given in Table 2. On average, the correction scheme increases the wintertime ice production by approximately 30 %. While the average IP value is  $28.3 \pm 8.5 \text{ km}^3$  (CC;  $21.7 \pm 5.9 \text{ km}^3$  for no CC), a high interannual variability of ice production is found, with values as low as  $16.1 \text{ km}^3$  (CC; no CC –16 %) in 2002/2003 and up to  $47.2 \text{ km}^3$  (CC; no

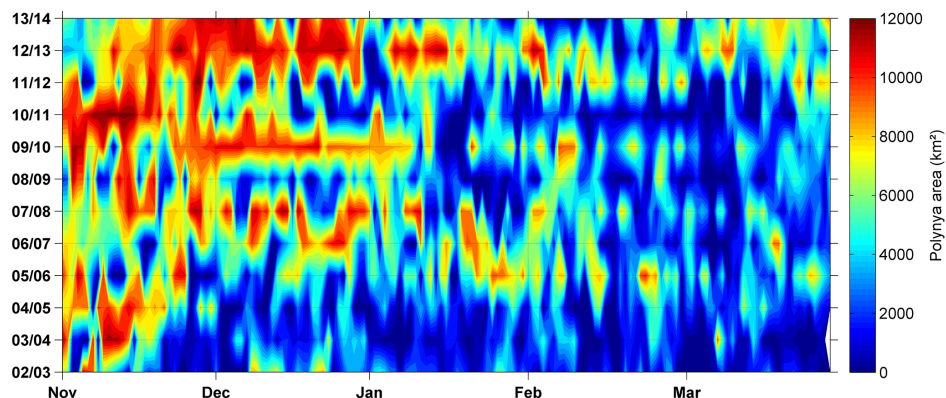


**Figure 7.** Hovmöller diagram of daily coverage-corrected polynya area (POLACC;  $TIT \leq 0.2$  m) in the Storfjorden polynya between 2002/2003 and 2013/2014.

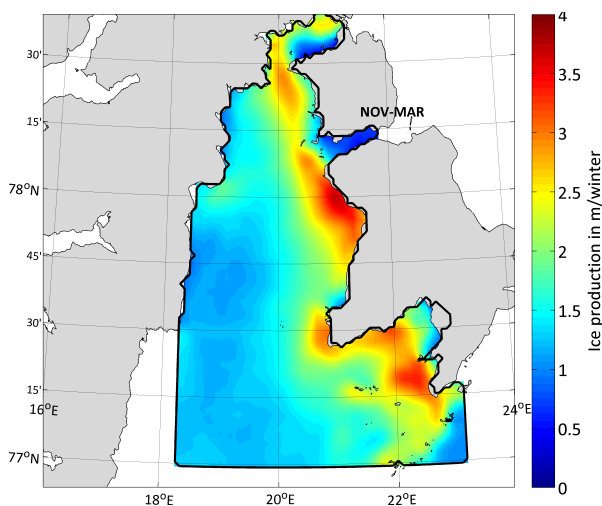


**Figure 8.** Spatial distribution of the interannual mean accumulated ice production (IP) rate in  $\text{m winter}^{-1}$ . Values are first accumulated for each winter season from November to March and afterwards averaged for 2002/2003 to 2013/2014.

CC  $-31\%$ ) in 2012/2013. Large increases in IP occur from winter 2003/2004 to 2004/2005 (CC:  $+7.0 \text{ km}^3$ ) and again from winter 2011/2012 to 2012/2013 (CC:  $+17.6 \text{ km}^3$ ). This could originate from the increasing extent of thin-ice areas in January–March 2005 and 2013 compared to the same period in 2004 and 2012 (Fig. 6). Regardless of an applied coverage correction, a significant ( $p \leq 0.05$ ) positive trend of  $1.2\text{--}2.0 \text{ km}^3 \text{ yr}^{-1}$  over the examined 12-winter period can be observed. It shows that this trend in overall (November–March) IPCC originates primarily from a significant positive trend (CC:  $1.29 \text{ km}^3 \text{ yr}^{-1}$ ,  $p = 9.05 \times 10^{-4}$ ) at the beginning of winter (November–December), while the period from January to March shows no significant trend (CC:  $0.73 \text{ km}^3 \text{ yr}^{-1}$ ,  $p = 0.052$ ). This could be an effect of an observable shift

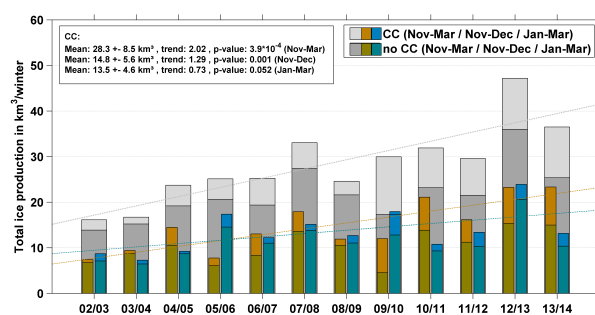


**Figure 9.** Annual wintertime accumulated ice production in the Storfjorden polynya, given in cubic kilometers per winter. Estimations are based on daily heat flux calculations using the daily derived thin-ice thickness (TIT) composites. Special emphasis is given to the effect of an applied coverage correction (CC). Dotted lines show linear trend estimations for IPCC. Colored bars show a seasonal comparison between November and December (yellowish) and January and March (blueish).

towards more thin ice in November–December, which is most probably connected to the later appearing fall freeze-up and consequently a lot of open water and very thin ice in the southern part of the applied polynya-mask. A similar explanation can be given for the high ice production in 2012/2013, where the Storfjorden area features high frequencies of  $TIT \leq 0.2$  m throughout the whole winter season from November to March.

#### 4 Discussion

In Skogseth et al. (2004, 2005), a manual classification of several ERS-2 synthetic aperture radar (SAR) images from 1998 to 2002 was performed to derive parameters for a wind-driven polynya width model (Haarpaintner et al., 2001), which gives estimates of ice production and brine-enriched shelf water based on satellite imagery, wind data from nearby

weather stations and surface hydrography. Ice production was calculated from surface heat balance and includes contributions from open water (frazil ice), thin ice as well as fast and pack ice inside the Storfjorden basin north of 77° N. This setup was later extended to a 33-year record of modeled total ice production covering the winters 1970 to 2002 using model parameters derived from the examined 5-winter period (Skogseth et al., 2005). While the average total ice production for 1998 to 2002 was estimated to  $43.6 \pm 9.7 \text{ km}^3$ , it was slightly lower for the 33-year time series with only  $39.9 \pm 11.7 \text{ km}^3$ . When comparing these numbers to our average  $\text{IP}_{\text{CC}}$  estimate of  $28.3 \pm 8.5 \text{ km}^3$  for 2002/2003 to 2013/2014, one has to keep in mind that Skogseth et al. (2004, 2005) also include ice production under fast and pack ice inside the fjord, while our study concentrates on open water and thin-ice areas only. Assuming an average contribution of 25 % from fast-ice and pack-ice areas (Table 3 in Skogseth et al., 2005) and after reducing annually accumulated total ice production accordingly, the average ice production (1970 to 2002) inside open water and thin-ice areas of Skogseth et al. (2005) is lowered to approximately  $30 \pm 9 \text{ km}^3$  which is within the standard deviation presented here. Skogseth et al. (2005) give some further information on the interannual variability of ice production within the Storfjorden polynya, although it is stated that the uncertainty for the 33-year time series is increased. The presented 33-year time series shows a slightly negative and non-significant trend of approximately  $-2 \text{ km}^3 \text{ decade}^{-1}$ , while the last 12 winter seasons presented here show a positive trend of  $2.02 \text{ km}^3 \text{ yr}^{-1}$  during the analyzed period. However, the long-term model estimates by Skogseth et al. (2005) indicate the presence of multi-decadal fluctuations.

Jardon et al. (2014) developed an ice production model which uses Advanced Microwave Scanning Radiometer – Earth Observing System (AMSR-E) sea-ice concentration data to derive daily open water fractions. Heat flux calculations over water were performed using ERA-Interim reanalysis data in a bulk algorithm. In contrast to our results, their estimates of POLA and IP incorporate both frazil ice growth as well as ice growth under ice thicker than 20 cm. In comparison, our results should profit from the enhanced resolution of MODIS and daily derived TIT distributions. Nevertheless, derived POLA from  $\text{TIT} \leq 0.2 \text{ m}$  in our study compares well with POLA derived from AMSR-E sea-ice concentration data. Both wintertime mean POLA and  $\text{POLA}_{\text{CC}}$  are within the 25th and 75th percentile of the estimated open water area by Jardon et al. (2014) in almost every winter season except for 2004/2005 and 2010/2011, during which both values derived by MODIS exceed the 75th percentile. Discrepancies in derived total ice production are obvious but can be partly explained by differences in the regarded time frame of each winter season. While Jardon et al. (2014) analyze the full period with sea ice in the fjord (roughly October/November to June/July), we focus on the November to March period. Even when we reduce the presented IP val-

ues by the amount of frazil ice that is formed in the months April–July, which in 2006/2007 (example shown in Jardon et al., 2014) contributed around 15 % to the total volume of frazil ice in this particular winter season, the time series differ on average by approx. 40 %. Therefore, Jardon et al. (2014) presents higher IP values in all winter seasons except 2004/2005 and 2010/2011, but overall the interannual variability is comparable.

The studies by Tamura and Ohshima (2011) and Iwamoto et al. (2014) face similar restrictions concerning the spatial resolution of the applied passive microwave data from Special Sensor Microwave Imager (SSM/I) and AMSR-E, which is most apparent in smaller polynyas such as in Storfjorden. In Tamura and Ohshima (2011), an average ice production of  $137 \pm 35 \text{ km}^3$  for the period 1992–2007 (September–May) is presented. This value largely exceeds our estimates as well as those by Skogseth et al. (2005) and Jardon et al. (2014), most probably due to the discrepancies in spatial resolution of the input data. More recent numbers by Iwamoto et al. (2014), who use an updated algorithm based on MODIS and AMSR-E satellite data as well as ERA-Interim reanalysis, are also lower than those in Tamura and Ohshima (2011), with the mean annual (also September–May) ice production between 2002/2003 and 2010/2011 estimated as  $47 \pm 5 \text{ km}^3$  (roughly  $40 \text{ km}^3$  for November–March; based on presented monthly mean values). A positive trend of  $3 \text{ km}^3$  per decade is presented which is much smaller than our value of  $18.7 \text{ km}^3$  per decade based on the same period from 2002/2003 to 2010/2011. Although Iwamoto et al. (2014) provide enhancements in terms of spatial resolution and the inclusion of land fast-ice detection in comparison to Tamura and Ohshima (2011), our estimates are still exceeded in every winter season. The presented interannual variability is similar to our study, with 2005/2006 and 2008/2009 being the only winter seasons with a strongly contrasting development. Both Tamura and Ohshima (2011) and Iwamoto et al. (2014) apply noticeably larger polynya masks to derive ice production values in the Storfjorden area which extend well into the Greenland and Barents Sea regions and far beyond Storfjorden itself. This omission of local characteristics in the Storfjorden basin in addition to a differing base period, which spans the months from September to May, could therefore explain part of the difference. However, the use of coarse-resolution passive microwave data certainly leads to a higher uncertainty of IP estimates, while the sign of the bias cannot be determined here. It will depend on the distribution of thin ice within the sensor's footprint and potential land spillover effects.

## 5 Summary and conclusions

In this study, we presented a comprehensive overview of daily thin-ice thickness distributions and resulting thermodynamic ice production rates for the Storfjorden polynya, located in the southern part of the Svalbard archipelago. The

investigation period covers the winter seasons 2002/2003–2013/2014 from November to March. Our results are complementary to previous studies in the Storfjorden region (e.g., Skogseth et al., 2004, 2005; Hendricks et al., 2011) and underline the importance of this polynya considering the total amount of ice production and accompanied salt release each winter season, despite its comparatively small spatial extent. Within the polynya, ice thicknesses below 10 cm dominate in the course of an average winter season and cover larger areas in the eastern part of Storfjorden. This enables ice production rates, which sum up to an average value of  $28.3 \pm 8.5 \text{ km}^3$  per winter season. There is a positive trend in accumulated ice production over the last 12 winter seasons which contrasts earlier indications of a slightly negative trend prior to 2002 (Skogseth et al., 2005).

Compared to other studies which rely on active and passive microwave remote sensing, the use of MODIS ice-surface temperatures has distinct drawbacks considering the effect of clouds, which produce data gaps when correctly identified by the MODIS cloud mask and possibly erroneous IST values when nighttime clouds remain undetected. By composing daily composites, data gaps in the Storfjorden region were minimized, resulting in an average IST coverage of 82% within the applied polynya mask. The application of a coverage-correction scheme yielded plausible adjustments of approximately 30% to the total polynya area and ice production, although its current basic approach offers room for future improvements such as including long-term spatial statistics. Still, this comprehensive data set will be of high value for a variety of climate and ocean applications, including the provision of quasi-daily high-resolution thin-ice thickness charts for regional climate and ocean models.

*Acknowledgements.* The authors want to thank the National Snow and Ice Data Center (NSIDC) as well as the European Center for Medium-Range Weather Forecasts (ECMWF) for providing the MODIS sea-ice product and the ERA-Interim atmospheric reanalysis data. This work was part of the German-Russian cooperation “WTZ RUS: System Laptev Sea: TRANSDRIFT” funded by the Federal Ministry of Education and Research (BMBF) under grant 03G0833D. We would like to thank the three anonymous referees and Christian Haas for their very detailed and helpful reviews.

Edited by: C. Haas

## References

- Adams, S., Willmes, S., Schroeder, D., Heinemann, G., Bauer, M., and Krumpfen, T.: Improvement and sensitivity analysis of thermal thin-ice retrievals, *IEEE T. Geosci. Remote*, 51, 3306–3318, doi:10.1109/tgrs.2012.2219539, 2013.
- Barber, D. G. and Massom, R. A.: The Role of Sea Ice in Arctic and Antarctic Polynyas, in: *Polynyas – Windows to the World*, in: *The Role of Sea Ice in Arctic and Antarctic Polynyas*, edited by: Smith, W. O. and Barber, D. G., 1–54, Elsevier Oceanography Series, doi:10.1016/s0422-9894(06)74001-6, 2007.
- Bauer, M., Schröder, D., Heinemann, G., Willmes, S., and Ebner, L.: Quantifying polynya ice production in the Laptev Sea with the COSMO model, *Polar Res.*, 32, 20922, doi:10.3402/polar.v32i0.20922, 2013.
- Dee, D. P., Uppala, S. M., Simmons, A. J., Berrisford, P., Poli, P., Kobayashi, S., Andrae, U., Balmaseda, M. A., Balsamo, G., Bauer, P., Bechtold, P., Beljaars, A. C. M., van de Berg, L., Bidlot, J., Bormann, N., Delsol, C., Dragani, R., Fuentes, M., Geer, A. J., Haimberger, L., Healy, S. B., Hersbach, H., Hólm, E. V., Isaksen, I., Kållberg, P., Köhler, M., Matricardi, M., McNally, A. P., Monge-Sanz, B. M., Morcrette, J.-J., Park, B.-K., Peubey, C., de Rosnay, P., Tavolato, C., Thépaut, J.-N., and Vitart, F.: The ERA-Interim reanalysis: configuration and performance of the data assimilation system, *Q. J. Roy. Meteor. Soc.*, 137, 553–597, doi:10.1002/qj.828, 2011.
- Drucker, R., Martin, S., and Moritz, R.: Observations of ice thickness and frazil ice in the St. Lawrence Island polynya from satellite imagery, upward looking sonar, and salinity/temperature moorings, *J. Geophys. Res.*, 108, 3149, doi:10.1029/2001jc001213, 2003.
- Ebner, L., Schröder, D., and Heinemann, G.: Impact of Laptev Sea flaw polynyas on the atmospheric boundary layer and ice production using idealized mesoscale simulations, *Polar Res.*, 30, 7210, doi:10.3402/polar.v30i0.7210, 2011.
- Haarpaintner, J., Gascard, J.-C., and Haugan, P. M.: Ice production and brine formation in Storfjorden, Svalbard, *J. Geophys. Res.-Oceans*, 106, 14001–14013, doi:10.1029/1999jc000133, 2001.
- Hall, D., Key, J., Casey, K., Riggs, G., and Cavalieri, D.: Sea ice surface temperature product from MODIS, *IEEE T. Geosci. Remote*, 42, 1076–1087, doi:10.1109/tgrs.2004.825587, 2004.
- Hendricks, S., Gerland, S., Smedsrud, L., Haas, C., Pfaffhuber, A., and Nilsen, F.: Sea-ice thickness variability in Storfjorden, Svalbard, *Ann. Glaciol.*, 52, 61–68, doi:10.3189/172756411795931561, 2011.
- Iwamoto, K., Ohshima, K. I., and Tamura, T.: Improved mapping of sea ice production in the Arctic Ocean using AMSR-E thin ice thickness algorithm, *J. Geophys. Res.-Oceans*, 119, 3574–3594, doi:10.1002/2013jc009749, 2014.
- Jakobsson, M., Mayer, L., Coakley, B., Dowdeswell, J. A., Forbes, S., Fridman, B., Hodnesdal, H., Noormets, R., Pedersen, R., Rebesco, M., Schenke, H. W., Zarayskaya, Y., Accettella, D., Armstrong, A., Anderson, R. M., Bienhoff, P., Camerlenghi, A., Church, I., Edwards, M., Gardner, J. V., Hall, J. K., Hell, B., Hestvik, O., Kristoffersen, Y., Marcussen, C., Mohammad, R., Mosher, D., Nghiem, S. V., Pedrosa, M. T., Travaglini, P. G., and Weatherall, P.: The international bathymetric chart of the Arctic Ocean (IBCAO) version 3.0, *Geophys. Res. Lett.*, 39, 12, doi:10.1029/2012gl052219, 2012.
- Jardon, F., Vivier, F., Bouruet-Aubertot, P., Lourenço, A., Cuypers, Y., and Willmes, S.: Ice production in Storfjorden (Svalbard) estimated from a model based on AMSR-E observations: Impact on water mass properties, *J. Geophys. Res.-Oceans*, 119, 377–393, doi:10.1002/2013jc009322, 2014.
- Jin, X., Barber, D., and Papakyriakou, T.: A new clear-sky downward longwave radiative flux parameterization for Arctic areas based on rawinsonde data, *J. Geophys. Res.*, 111, D24104, doi:10.1029/2005jd007039, 2006.

- Kruppen, T., Hölemann, J. A., Willmes, S., Maqueda, M., Busche, T., Dmitrenko, I. A., Gerdes, R., Haas, C., Heinemann, G., Hendricks, S., Kassens, H., Rabenstein, L., and Schröder, D.: Sea ice production and water mass modification in the eastern Laptev Sea, *J. Geophys. Res.-Oceans*, 116, C05014, doi:10.1029/2010JC006545, 2011.
- Kwok, R., Comiso, J. C., Martin, S., and Drucker, R.: Ross Sea polynyas: Response of ice concentration retrievals to large areas of thin ice, *J. Geophys. Res.*, 112, C12012, doi:10.1029/2006jc003967, 2007.
- Launiainen, J. and Vihma, T.: Derivation of turbulent surface fluxes – An iterative flux-profile method allowing arbitrary observing heights, *Environ. Softw.*, 5, 113–124, doi:10.1016/0266-9838(90)90021-w, 1990.
- Morales-Maqueda, M., Willmott, A., and Biggs, N.: Polynya dynamics: A review of observations and modeling, *Rev. Geophys.*, 42, 1–37, doi:10.1029/2002rg000116, 2004.
- Riggs, G., Hall, D., and Salomonson, V.: MODIS Sea Ice Products User Guide to Collection 5, National Snow and Ice Data Center, University of Colorado, Boulder, CO 80309-0449 USA, available at: [http://nsidc.org/data/docs/daac/modis\\_v5/dorothy\\_ice\\_doc.pdf](http://nsidc.org/data/docs/daac/modis_v5/dorothy_ice_doc.pdf) (last access: 11 May 2015), 2006.
- Skogseth, R., Haugan, P., and Haarpaintner, J.: Ice and brine production in Storfjorden from four winters of satellite and in situ observations and modeling, *J. Geophys. Res.-Oceans*, 109, C10008, doi:10.1029/2004jc002384, 2004.
- Skogseth, R., Fer, I., and Haugan, P. M.: Dense-Water Production and Overflow from an Arctic Coastal Polynya in Storfjorden, *The Nordic Seas: An Integrated Perspective*, 73–88, doi:10.1029/158gm07, 2005.
- Skogseth, R., McPhee, M. G., Nilsen, F., and Smedsrud, L. H.: Creation and tidal advection of a cold salinity front in Storfjorden: 1. Polynya dynamics, *J. Geophys. Res.-Oceans*, 118, 3278–3291, doi:10.1002/jgrc.20231, 2013.
- Smith, S. D., Muench, R. D., and Pease, C. H.: Polynyas and leads: An overview of physical processes and environment, *J. Geophys. Res.*, 95, 9461–9479, doi:10.1029/jc095ic06p09461, 1990.
- Tamura, T. and Ohshima, K. I.: Mapping of sea ice production in the Arctic coastal polynyas, *J. Geophys. Res.*, 116, C07030, doi:10.1029/2010jc006586, 2011.
- Tamura, T., Ohshima, K. I., Markus, T., Cavalieri, D. J., Nihashi, S., and Hirasawa, N.: Estimation of Thin Ice Thickness and Detection of Fast Ice from SSM/I Data in the Antarctic Ocean, *J. Atmos. Ocean. Tech.*, 24, 1757–1772, doi:10.1175/jtech2113.1, 2007.
- Tamura, T., Ohshima, K. I., and Nihashi, S.: Mapping of sea ice production for Antarctic coastal polynyas, *Geophys. Res. Lett.*, 35, L07606, doi:10.1029/2007gl032903, 2008.
- Willmes, S., Kruppen, T., Adams, S., Rabenstein, L., Haas, C., Hoelemann, J., Hendricks, S., and Heinemann, G.: Cross-validation of polynya monitoring methods from multisensor satellite and airborne data: a case study for the Laptev Sea, *Can. J. Remote Sens.*, 36, S196–S210, doi:10.5589/m10-012, 2010.
- Willmes, S., Adams, S., Schröder, D., and Heinemann, G.: Spatio-temporal variability of polynya dynamics and ice production in the Laptev Sea between the winters of 1979/80 and 2007/08, *Polar Res.*, 30, 5971, doi:10.3402/polar.v30i0.5971, 2011.
- Yu, Y. and Lindsay, R.: Comparison of thin ice thickness distributions derived from RADARSAT Geophysical Processor System and advanced very high resolution radiometer data sets, *J. Geophys. Res.*, 108, 3387, doi:10.1029/2002jc001319, 2003.
- Yu, Y. and Rothrock, D. A.: Thin ice thickness from satellite thermal imagery, *J. Geophys. Res.*, 101, 25753–25766, doi:10.1029/96jc02242, 1996.

## **5 Publication II: Multi-Decadal Variability of Polynya Characteristics and Ice Production in the North Water Polynya by Means of Passive Microwave and Thermal Infrared Satellite Imagery**

Written by

**Andreas Preußer**, Günther Heinemann, Sascha Willmes and Stephan Paul

Published: 27 November 2015

This paper is reprinted from the journal 'Remote Sensing' (Remote Sens.) with permission from MDPI under the Creative Commons by Attribution (CC-BY) license 4.0 [Preußer et al. 2015a].

The candidate's contribution to this paper was that he carried out the complete analysis and drafted the manuscript, including the preparation of all figures and tables. All co-authors were, with varying degrees, involved in the initial set-up of the algorithm and contributed to the writing of the manuscript.



Article

# Multi-Decadal Variability of Polynya Characteristics and Ice Production in the North Water Polynya by Means of Passive Microwave and Thermal Infrared Satellite Imagery

Andreas Preußner \*, Günther Heinemann, Sascha Willmes and Stephan Paul

Received: 16 September 2015 / Accepted: 12 November 2015 / Published: 27 November 2015

Academic Editors: Walt Meier, Mark Tschudi, Magaly Koch and Prasad S. Thenkabail

Department of Environmental Meteorology, Faculty of Regional and Environmental Sciences, University of Trier, Behringstr. 21, 54296 Trier, Germany; heinemann@uni-trier.de (G.H.); willmes@uni-trier.de (S.W.); paul@uni-trier.de (S.P.)

\* Correspondence: preusser@uni-trier.de; Tel.: +49-(0)651-201-4630; Fax +49-(0)651-201-3817

**Abstract:** The North Water (NOW) Polynya is a regularly-forming area of open-water and thin-ice, located between northwestern Greenland and Ellesmere Island (Canada) at the northern tip of Baffin Bay. Due to its large spatial extent, it is of high importance for a variety of physical and biological processes, especially in wintertime. Here, we present a long-term remote sensing study for the winter seasons 1978/1979 to 2014/2015. Polynya characteristics are inferred from (1) sea ice concentrations and brightness temperatures from passive microwave satellite sensors (Advanced Microwave Scanning Radiometer (AMSR-E and AMSR2), Scanning Multichannel Microwave Radiometer (SMMR), Special Sensor Microwave Imager/Sounder (SSM/I-SSMIS)) and (2) thin-ice thickness distributions, which are calculated using MODIS ice-surface temperatures and European Center for Medium-Range Weather Forecasts (ECMWF) atmospheric reanalysis data in a 1D thermodynamic energy-balance model. Daily ice production rates are retrieved for each winter season from 2002/2003 to 2014/2015, assuming that all heat loss at the ice surface is balanced by ice growth. Two different cloud-cover correction schemes are applied on daily polynya area and ice production values to account for cloud gaps in the MODIS composites. Our results indicate that the NOW polynya experienced significant seasonal changes over the last three decades considering the overall frequency of polynya occurrences, as well as their spatial extent. In the 1980s, there were prolonged periods of a more or less closed ice cover in northern Baffin Bay in winter. This changed towards an average opening on more than 85% of the days between November and March during the last decade. Noticeably, the sea ice cover in the NOW polynya region shows signs of a later-appearing fall freeze-up, starting in the late 1990s. Different methods to obtain daily polynya area using passive microwave AMSR-E/AMSR2 data and SSM/I-SSMIS data were applied. A comparison with MODIS data (thin-ice thickness  $\leq 20$  cm) shows that the wintertime polynya area estimates derived by MODIS are about 30 to 40% higher than those derived using the polynya signature simulation method (PSSM) with AMSR-E data. In turn, the difference in polynya area between PSSM and a sea ice concentration (SIC) threshold of 70% is fairly low (approximately 10%) when applied to AMSR-E data. For the coarse-resolution SSM/I-SSMIS data, this difference is much larger, particularly in November and December. Instead of a sea ice concentration threshold, the PSSM method should be used for SSM/I-SSMIS data. Depending on the type of cloud-cover correction, the calculated ice production based on MODIS data reaches an average value of  $264.4 \pm 65.1$  km<sup>3</sup> to  $275.7 \pm 67.4$  km<sup>3</sup> (2002/2003 to 2014/2015) and shows a high interannual variability. Our achieved long-term results underline the major importance of the NOW polynya considering its influence on Arctic ice production and associated atmosphere/ocean processes.



**Keywords:** MODIS; polynya; sea ice; passive microwave; Baffin Bay; Nares Strait; ice bridge

---

## 1. Introduction

Polynyas are distinct features of the sea ice cover in the polar regions. These areas of open water and thin ice are playing a crucial role in altering a variety of local physical, biological and chemical processes at the boundary between atmosphere and ocean [1]. Particularly during wintertime, large energy loss to the atmosphere occurs at these locations, which is associated with strong ice production and brine release. These processes have strong implications for both the atmospheric boundary layer, as well as the underlying ocean layers. The knowledge of wintertime sea ice production in the Arctic is therefore of vital interest for the understanding of the Arctic climate system and the verification of climate and ocean models. The main cause for polynya openings in the Arctic shelf regions is divergent ice motions due to wind stress [2]. Consequently, the timing, duration and size of a polynya can often have large interannual variations [3], and a precise and regular monitoring of thin-ice areas is needed in order to detect long-term changes and linkages to other environmental compartments. Since the late 1970s, remote sensing approaches using passive microwave and thermal infrared data have offered valuable tools for these tasks.

The North Water (NOW) Polynya appears regularly in the northern part of Baffin Bay in the proximity of Smith Sound. It is bounded by Ellesmere Island (Canada) in the West and Greenland in the East (Figure 1 [4]). As the NOW polynya is one of the largest polynyas in the Northern Hemisphere with a huge impact on local biological and physical processes [5], it was intensively studied in the past decades with strong efforts in the years 1997 to 2000 (International NOW-study, [6,7]). In the north, the NOW polynya is generally bounded by an ice bridge, which forms regularly in winter at the southern end of the Nares Strait (at Smith Sound). With its formation, the ice bridge controls the sea ice outflow from the Lincoln Sea through Nares Strait and Kane Basin down to Baffin Bay in the south [8]. The southern boundary of the polynya is not defined that strictly, as it varies drastically in the course of the winter season [2]. After the initial formation of the ice bridge at Smith Sound, the sea ice south of it experiences a strong advection due to strong northerly winds from the Nares Strait and prevailing southerly ocean currents [8]. During late spring, the polynya opens up until it merges with the melted ocean area in the Baffin Bay in June/July. The NOW polynya can be categorized as a latent heat-type polynya, *i.e.*, the energy loss to the atmosphere is compensated by the release of latent heat by sea ice formation. According to Barber *et al.* [8], air temperatures show an east-west temperature gradient, with higher values at the eastern side of the polynya (Greenland) than on the western side (Canada). This leads to a slower sea ice formation and lower ice thicknesses in the east, as well as an earlier melt-onset in summer [9]. Additionally, the eastern side is thought to be under the influence of the West Greenland current, which transports relatively warm and salty water from the south to the sea surface and is responsible for a cyclonic ocean circulation in northern Baffin Bay. According to Melling *et al.* [10] and Mundy and Barber [9], this does not contribute to the formation of the polynya, but instead to its maintenance. A less saline and cold ocean surface in Baffin Bay is maintained by water of Arctic origin entering via three straits (including Nares Strait) in the north [11].

This multi-sensor study uses a long-term record of Moderate-Resolution Imaging Spectroradiometer (MODIS)-derived ice-thickness distributions in thin-ice areas at a comparatively high spatial resolution of  $2 \times 2 \text{ km}^2$ , as well as long-term records of coarse-resolution Scanning Multichannel Microwave Radiometer (SMMR), Special Sensor Microwave Imager/Sounder (SSM/I-SSMIS) and Advanced Microwave Scanning Radiometer (AMSR-E and AMSR2) passive microwave data (Section 2; see Table 1 [12–19]). By comparing different sensors and methods, our study will give further insight into sensor-specific differences in monitoring thin-ice areas in the polar regions (Section 3.1). We then perform a detailed investigation on the associated quantities

polynya area and ice-production (MODIS data starting in 2002) for the period between 1978/1979 and 2014/2015 (Sections 3.2 and 3.3). Thereby, our results will be discussed and compared to earlier remote sensing studies, e.g., [8,20,21]. In addition, MODIS-derived ice-thickness distributions in Nares Strait will be used to infer ice bridge characteristics related to the formation of the North Water (NOW) Polynya (Section 3.4). Our study will aid in getting a more comprehensive understanding of multi-decadal polynya dynamics in the North Water region, as well as associated physical processes over both annual (one winter season from November to March) and interannual timescales.

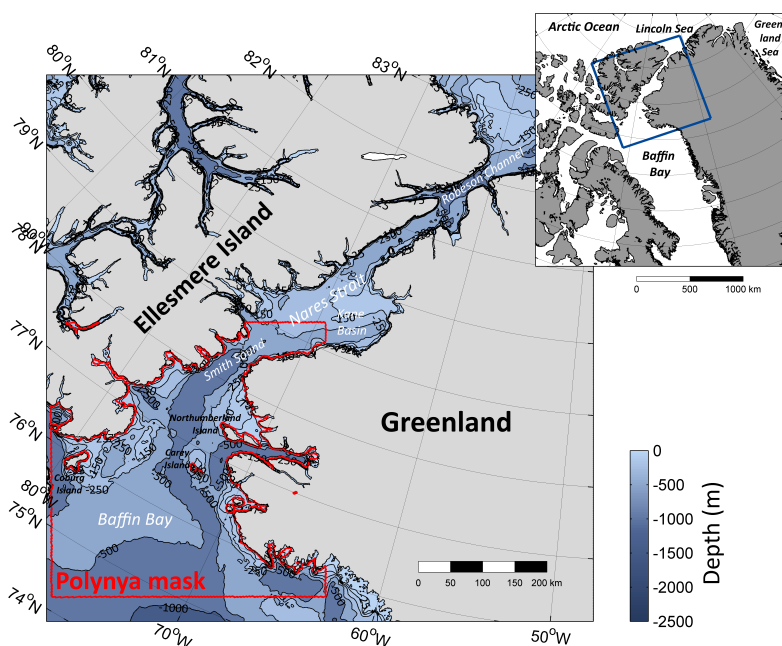


**Figure 1.** Map of the northern part of Baffin Bay, Nares Strait and Lincoln Sea, all surrounded by Ellesmere Island (Canada) in the west and Greenland in the east. The applied polynya mask is marked in red, enclosing the typical location of the North Water Polynya in wintertime, north of  $74^{\circ}\text{N}$  and indicating the main study region south of Smith Sound. Bathymetric data by Jakobsson *et al.* [4] (IBCAO v3.0).

**Table 1.** Overview of sensors, platforms, acquisition sources, raw data and derived parameters, the analyzed period and the effective spatial resolution on the grid for all of the satellite data that are used in this study (IST = ice surface temperature, TIT = thin-ice thickness,  $T_B$  = brightness temperature, SIC = sea ice concentration, POLA = polynya area, IP = ice production; subscripts of derived parameters denote different methods: 70PT (70% SIC threshold), PSSM (polynya signature simulation method), CC (coverage correction) and SFR (spatial feature reconstruction); see Sections 2.5 and 2.6 for details).

Sensor	Platform	Source	Retrieved Variables	Derived Parameters	Period	Spatial Resolution on Grid
MODIS	Aqua/Terra	NSIDC [12]	IST	TIT $POLA_{CC}$ , $IP_{CC}$ $POLA_{SFR}$ , $IP_{SFR}$	2002 to 2015	$2 \times 2 \text{ km}^2$
AMSR-E	Aqua/ADEOS-II	NSIDC [13,14]	$T_B89V$ , $T_B89H$ $T_B36V$ , $T_B36H$	$POLA_{AMSR,PSSM}$	2002 to 2011	$6.25 \times 6.25 \text{ km}^2$ $12.5 \times 12.5 \text{ km}^2$
AMSR2	GCOM-W1	Univ. of Hamburg [15]	SIC	$POLA_{AMSR,70PT}$	2012 to 2015	$6.25 \times 6.25 \text{ km}^2$
SMMR	Nimbus-7	Univ. of Bremen [15]	SIC	$POLA_{AMSR,70PT}$	1978 to 1986	$25 \times 25 \text{ km}^2$
SSM/I and SSMIS	DMSP	NSIDC [16–19]	$T_B85/91V$ , $T_B85/91H$ $T_B37V$ , $T_B37H$	$POLA_{SSMI,PSSM}$	1987 to 2015	$12.5 \times 12.5 \text{ km}^2$ $25 \times 25 \text{ km}^2$
			SIC	$POLA_{SSMI,70PT}$		$25 \times 25 \text{ km}^2$

## 2. Data and Methods

### 2.1. Remote Sensing Data

#### 2.1.1. SMMR and SSM/I-SSMIS

To achieve a long-term satellite record ranging over the period of November 1978 to March 2015, we use sea ice concentrations (SIC) generated from passive microwave brightness temperature ( $T_B$ ) data from the Nimbus-7 SMMR, the Defense Meteorological Satellite Program (DMSP)-F8, -F11 and -F13 SSM/I and the DMSP-F17 SSMIS, provided at a grid cell size of  $25 \times 25 \text{ km}^2$  [16]. SIC are calculated using the NASA Team algorithm developed at the Goddard Space Flight Center (GSFC) and are provided on a daily basis from 1987 onwards. SMMR SIC are provided every other day and need to be linearly interpolated from bounding days to achieve a continuous time series. To increase consistency between changing satellites and sensor systems, the dataset includes adjustments of sea ice algorithm tie points by matching geophysical parameters [16,22].

In addition, we use DMSP SSM/I-SSMIS daily polar-gridded brightness temperatures from the 37.0 GHz and 85.5 GHz (on SSM/I)/91.7 GHz (on SSMIS) channels in both horizontal and vertical polarization [19]. While the channels from the latter two frequencies are gridded at a spatial resolution of  $12.5 \times 12.5 \text{ km}^2$ , the 37.0-GHz data are available at a spatial resolution of  $25 \times 25 \text{ km}^2$  (compare Table 1). Brightness temperature data from SSM/I-SSMIS feature dedicated inter- and cross-calibrations between changing DMSP platforms [19].

As the datasets by Cavalieri *et al.* [16] and Maslanik and Stroeve [19] are updated on an annual basis only, daily SIC and brightness temperatures for 2015 are taken from near real-time (NRT) datasets by Maslanik and Stroeve [18] and Cavalieri *et al.* [17] to be able to include the most recent winter season 2014/2015 in our analysis.

#### 2.1.2. AMSR-E and AMSR2

Daily  $T_B$  data from the AMSR-E instrument on board the Aqua satellite platform is available from June 2002 to October 2011. We use horizontally- and vertically-polarized  $T_B$  from the 89.0-GHz [13] and 36.0-GHz [14] frequency channels at a spatial resolution of  $6.25 \times 6.25 \text{ km}^2$  and  $12.5 \times 12.5 \text{ km}^2$ , respectively.

Sea ice concentrations are provided for the same period from the University of Hamburg and are calculated using the ARTIST sea ice (ASI) algorithm [15]. Due to the inclusion of the 89.0-GHz data (smaller footprint, but more likely weather influenced), they are available at a spatial resolution of  $6.25 \times 6.25 \text{ km}^2$ .

Data from the AMSR2 on board the JAXA Global Change Observation Mission-Water (GCOM-W1, “Shizuku”) satellite platform are available from 2012 onwards, which leaves a gap of approximately one year after its predecessor AMSR-E. Hence, for the winter seasons 2012/2013 and 2014/2015, we are able to use AMSR2 ASI SIC from the University of Bremen [15], as the SIC algorithm could be easily transferred to AMSR2 due to the same frequency channels, as well as similar spatial resolutions and orbital configurations. However, the derivation of AMSR2 SIC using the ASI algorithm currently uses the same parameters as was used for AMSR-E. Therefore, these data have to be treated with caution, as no independent validation has been performed so far.

#### 2.1.3. MODIS Ice Surface Temperatures

For the derivation of thin-ice thickness (TIT), we use the MOD/MYD29 sea ice product [12,23] derived from MODIS satellite data. We incorporate data from both MODIS instruments on board the Terra and Aqua polar-orbiting satellite platforms. The product features swath data of ice surface temperatures (ISTs) with a spatial resolution of  $1 \times 1 \text{ km}^2$  at nadir and includes the MODIS cloud mask (MOD35; [24]). Overall, the accuracy of the MOD/MYD29 ISTs is given with 1 to 3 K [23].

Swaths covering the NOW area were extracted using metadata information for each MODIS swath. Afterwards, all IST swaths were mapped onto a  $2 \times 2 \text{ km}^2$  ( $0.018^\circ\text{LAT} \times 0.07^\circ\text{LON}$ ) equirectangular grid covering the northern part of Baffin Bay ( $74^\circ\text{N}$  to  $79.5^\circ\text{N}$ ,  $62^\circ\text{W}$  to  $86^\circ\text{W}$ ).

## 2.2. ERA-Interim Atmospheric Reanalysis Data

For the calculation of TIT, atmospheric variables from the ERA-Interim reanalysis product [25] are used to provide 2-m-temperature, 2-m-dew point temperature, 10-m-wind speed components ( $u$  and  $v$ ) and the mean sea-level pressure at a resolution of 6 h. The dataset is provided by the European Center for Medium-Range Weather Forecasts (ECMWF) in a horizontal resolution of  $0.75^\circ$ , (approximately 79 km). A linear interpolation of the ERA-Interim data is necessary to match the spatial resolution of MODIS data. For the thin-ice thickness (TIT) calculations, single MODIS swaths are linked to the closest time step of the atmospheric data fields.

In order to reduce errors originating from misclassifications of the nighttime MOD35 cloud mask, we additionally utilize ERA-Interim medium cloud cover (MCC) information. As was shown by Liu and Key [26], the ERA-Interim MCC fields correspond closely to the MODIS-derived cloud patterns, both in winter and summer, and can therefore be used as an additional quality control during the TIT retrieval.

## 2.3. MODIS Thin-Ice Thickness Retrieval Using a Surface Energy-Balance Model

In order to derive daily TIT distributions, we use an approach that follows the work of Yu and Rothrock [27], Yu and Lindsay [28] and Drucker *et al.* [29]. Ice surface temperature (IST) and the thickness of thin ice are related to atmospheric radiation fluxes and turbulent fluxes of heat via a one-dimensional energy-balance model. The original method of Yu and Rothrock [27] was improved and modified by Willmes *et al.* [30] and Adams *et al.* [31]. The latest version of the applied algorithm is described in detail in Preußner *et al.* [32] and Paul *et al.* [33]. The procedure to derive TIT is only applicable to clear sky conditions, as clouds and fog strongly influence the accuracy of the recorded IST [12]. In addition, only nighttime scenes are used to exclude ambiguities from incident short-wave radiation [28,31]. A sensitivity analysis of the TIT retrieval by Adams *et al.* [31] revealed an uncertainty of  $\pm 1.0 \text{ cm}$ ,  $\pm 2.1 \text{ cm}$  and  $\pm 5.3 \text{ cm}$  for TIT Classes 0 to 5 cm, 5 to 10 cm and 10 to 20 cm, respectively. As a thickness range of  $\text{TIT} \leq 0.2 \text{ m}$  is regarded to be sufficient for reliable estimates on thermodynamic ice production in polynyas [27,31], we constrain our analysis accordingly.

## 2.4. Calculation of Daily TIT Composites

In general, a less frequent coverage can be observed at the beginning (November) and end (March) of each winter season, which originates primarily from the previously-stated restriction to nighttime scenes and consequently a reduction in the amount of available MODIS swaths. This is also a limiting factor in our investigations regarding the time period in each winter season.

From all available MODIS swaths covering the NOW polynya region (Table 2), daily composites of IST and TIT were computed to increase the daily coverage of our area of interest. The TIT is first calculated from each swath on its own with the procedure described in Section 2.3. Subsequently, the median TIT is computed pixel-wise and stored with its corresponding IST value, as well as the daily energy-balance components.

The MODIS cloud mask can have difficulties in detecting thin clouds and sea smoke during nighttime [24], which may influence the capability to observe “real” thin-ice features. Therefore, ERA-Interim MCC fields are used for additional cloud-cover information during the composite generation. Thereby, areas in the ERA-Interim data that exceed a cloud-fraction threshold of 75% are considered as cloud covered. In order to achieve an enhanced quality measure for each pixel in the daily composites, four individual classes can be defined based on the combined MODIS and ERA-Interim cloud information and assigned to each pixel in the area of interest. They range from (1) confident clear-sky pixels (ccs; clear-sky MODIS and ERA-Interim) over (2) mixed-covered

pixels (mcp; ratio between clear-sky input swaths and the total number of input swaths per pixel) to (3) definitive cloud-covered pixels (both in MODIS and ERA-Interim) and (4) completely uncovered pixels. As was introduced in Paul *et al.* [33], we also make use of an additional cloud-cover check that looks at the persistence of a pixel that was classified as thin ice ( $TIT \leq 0.2$  m). While misclassified thin-ice detections are associated with a low persistence due to movements on short time scales, “real” thin-ice features (*i.e.*, polynyas) in the sea ice cover show a higher spatial and temporal persistence. This is expressed by a pixel-wise persistence index (PIX), which is defined as the ratio between the total number of MODIS swaths that featured thin-ice and the total number of swaths that featured clear-sky conditions on that pixel position. These additional quality attributes (cloud cover/persistence) for each pixel in the daily composites are utilized in the spatial feature reconstruction algorithm (compare Section 2.6). An overview of MODIS coverage statistics is given in Table 2.

**Table 2.** MODIS coverage statistics for the period from 2002/2003 to 2014/2015. The second column shows the amount of incorporated MODIS swaths for each winter season (November to March), as well as the total amount for all years combined. COV1 represents the average daily coverage (decimal cover fraction ranging from 0 to 1) of confident clear-sky pixels, while high- (>0.5) and low- (<0.5; min. 1 IST value per day) persistence mcp (mixed-cover pixels) indicate cases where either MODIS or ERA-Interim medium cloud cover features cloud signals in the daily composites. COV4 shows the achieved coverage after application of the spatial feature reconstruction (SFR) approach (compare Section 2.6). All numbers are retrieved based on daily composites and are calculated within the predefined polynya mask.

	Number of MODIS Swaths	Avg. COV1 (Confident Clear-Sky)	Avg. COV2 (High-Persistence Mcp)	Avg. COV3 (Low-Persistence Mcp)	Avg. COV4 (Incl. SFR Areas)
2002 to 2003	4040	0.74	0.86	0.90	0.97
2003 to 2004	4009	0.69	0.79	0.83	0.94
2004 to 2005	4067	0.72	0.82	0.86	0.97
2005 to 2006	4133	0.78	0.88	0.93	0.98
2006 to 2007	4086	0.77	0.85	0.88	0.97
2007 to 2008	4108	0.77	0.87	0.90	0.97
2008 to 2009	4079	0.79	0.86	0.90	0.97
2009 to 2010	4130	0.70	0.81	0.85	0.96
2010 to 2011	4098	0.65	0.76	0.81	0.96
2011 to 2012	4170	0.77	0.86	0.88	0.98
2012 to 2013	4153	0.73	0.86	0.90	0.98
2013 to 2014	4132	0.83	0.90	0.92	0.97
2014 to 2015	3417	0.84	0.90	0.92	0.98
Total/Average	52,622	0.75	0.85	0.88	0.97

### 2.5. Derivation of Ice Production and Polynya Area

When calculating ice production and polynya area, we apply a polynya mask (red area in Figure 1) in order to cover a reference area that is comparable to previous studies. The mask comprises a total area of approximately 110,000 km<sup>2</sup> and has its southern limit around 74°N.

From all available daily MODIS composites, we calculate ice production rates by assuming that the entire heat loss at the ice surface to the overlying atmosphere contributes to new ice formation [34–36].

$$\frac{\partial h}{\partial t} = \frac{-\bar{Q}_{ice}}{\rho_{ice} * L_f} \quad (1)$$

In Equation (1),  $\frac{\partial h}{\partial t}$  represents the ice production rate,  $\bar{Q}_{ice}$  is the daily mean conductive heat flux through the ice,  $\rho_{ice}$  is the density of sea ice ( $\rho_{ice} = 910$  kg/m<sup>3</sup>) and  $L_f$  is the latent heat of fusion of ice ( $L_f = 0.334$  MJ/kg; e.g., [20]). The negative sign in the right side of Equation (1) handles

the convention that the atmospheric heat flux is positive when the surface gains energy, as well as assuring that ice production exclusively takes place when there is a net energy loss from the surface. According to the surface energy balance, the heat flux  $\bar{Q}_{ice}$  is equal to the total atmospheric heat loss (sum of net radiation, turbulent latent and sensible heat flux). The ocean heat flux is not considered. The volume ice production rate  $\frac{\partial V}{\partial t}$  (IP) is calculated by multiplying  $\frac{\partial h}{\partial t}$  with the areal extent of each pixel in the regarded region. Ice production rates are calculated for each pixel with a TIT  $\leq 0.2$  m and afterwards extrapolated to daily rates for later accumulation and averaging. The total area of thin-ice pixels, *i.e.*, featuring a TIT  $\leq 0.2$  m in the applied polynya mask, is accumulated to obtain the total daily POLA in km<sup>2</sup>.

The usage of passive microwave data followed two different approaches towards deriving polynya area (POLA) from AMSR-E and SMMR/SSM/I. The first approach uses a SIC-threshold of 70% (70PT; *e.g.*, [37]), while the second approach utilizes a modified version of the polynya signature simulation method (PSSM; [30,36,38]) to derive POLA with a classification strategy applied on brightness temperatures from the 36/37- (less atmospheric disturbance) and 85/89- (high resolution) GHz frequency range (frequencies for SSM/I and AMSR-E, respectively). The PSSM applies a threshold on the polarization ratio (PR) at the higher frequency range (85/89/91 GHz) to get an initial guess for the open water area. Afterwards, the best match between the simulated and measured PR at the lower frequency range (36/37 GHz) is iteratively estimated to achieve a classified (thin ice/polynya and thicker ice) image at 6.25 km<sup>2</sup> (AMSR-E) or 12.5 km<sup>2</sup> (SSM/I). The upper value for ice thickness of the PSSM-derived polynya area is subject to regional variability and was previously estimated with 0.2 m for a case study in the Laptev Sea [30] and 0.2 to 0.25 m for Southern Hemisphere polynyas in the Ross Sea [39].

#### 2.6. IST-Coverage Correction and Spatial Feature Reconstruction

Despite the effort of selecting cloud-free pixels for calculating daily TIT and IST composites from MODIS swath data, cloud-induced gaps still occur. This limits direct comparisons with passive microwave remote sensing data, which are more or less cloud-insensitive.

Two distinct approaches are applied to overcome these difficulties. The first one is a relatively simple scaling approach (“coverage-correction” (CC)) that works under the assumption that pixels in the cloud-covered part of the daily composites (polynya mask applied; Figure 2) also contribute to the total POLA by approximately the same proportion as clear-sky areas. Hence, the initially calculated daily POLA and ice production (IP) are scaled according to the IST-coverage (here defined as the percentage of pixels within the polynya mask that features at least one valid IST value, *i.e.*, confident clear-sky and mixed-covered pixels; compare Table 2) to yield corrected daily values ( $POLA_{CC}$  and  $IP_{CC}$ ).

The CC approach is only applied to days where the daily IST coverage within the polynya mask exceeds a threshold of 50% to avoid unrealistically high values. In the case of a coverage  $\leq 50\%$ ,  $POLA_{CC}$  and  $IP_{CC}$  are linearly interpolated using bounding days. An error-margin of 5 to 6% of the daily POLA by using the CC method was stated in Preußner *et al.* [32].

The second approach is based on the “spatial feature reconstruction” (SFR) algorithm by Paul *et al.* [40], which was developed to increase the information about cloud-covered areas under fast-changing environmental conditions and utilizes all available cloud-cover and PIX information (compare Section 2.4). Cloud-induced gaps in the daily TIT composites are compared to the surrounding six days, and a probability of thin-ice occurrence is derived using a weighted composite of the surrounding days. Several case studies in the Brunt Ice Shelf region of Antarctica showed that the algorithm performed very good by reproducing artificially cloud-covered thin-ice areas with an average spatial correlation of 0.83 [40]. We apply this procedure on areas with identified low-quality data (low persistence, cloud covered) to fill the gaps with new information on potential thin-ice occurrences. Thereby, the daily coverage is increased to around 97% on average (2002/2003 to 2014/2015; compare Table 2). Likewise with respect to Paul *et al.* [33], also TIT and IST values

are pixel-wise assigned by a weighted average of the surrounding six days. Afterwards, remaining coverage gaps (e.g., prolonged periods of stable cloud cover, *i.e.*, no coverage on more than three consecutive days) are filled by additionally applying the above-described CC approach.

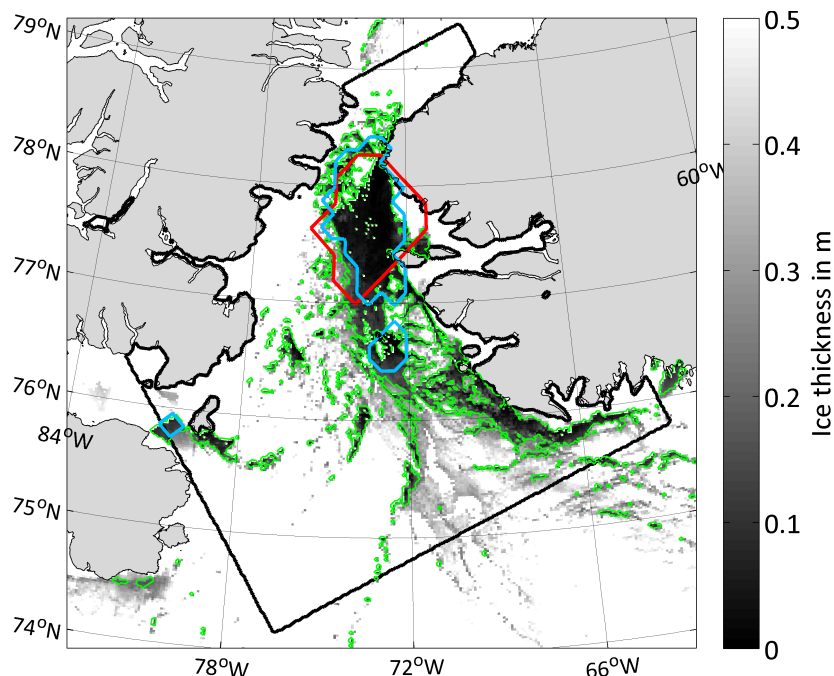


**Figure 2.** MODIS thin-ice thicknesses (TIT up to 0.5 m) on 14 March 2009, 1055UTC. The black boundary marks the applied polynya mask, while the sensor-specific retrieved POLA is indicated by colored contours for MODIS (TIT  $\leq$  0.2 m; green contour; 2 km), SSM/I 70PT (red contour; 25 km) and SSM/I PSSM (light-blue contour; 12.5 km).

### 3. Results and Discussion

#### 3.1. Sensor Differences in the POLA Retrieval

Concerning the upper value for ice thickness of the PSSM-derived POLA in the NOW region, Figure 3 shows a similar analysis as in Kern *et al.* [39] and Willmes *et al.* [30] for both SSM/I, as well as AMSR-E/AMSR2 for the period 2002 to 2015. We notice that the vast majority of thin-ice pixels in the NOW polynya region as defined by PSSM and 70PT does not exceed the 0.2-m threshold, which is in accordance with previous studies, while at the same time, a significant amount of outliers exists. In the case of PSSM, the average TIT amounts to  $11.2 \pm 9.0$  cm and  $10.8 \pm 8.6$  cm for SSM/I-SSMIS and AMSR-E, respectively. When using a 70% SIC-threshold to derive POLA (70PT), similar values of  $12.4 \pm 9.1$  cm (SSM/I-SSMIS) and  $9.7 \pm 7.8$  cm (AMSR-E/AMSR2) are calculated. As these values are gathered over the complete polynya area as prescribed by PSSM and 70PT, these TIT can be seen as areal averages.

Differences in the retrieved POLA (AMSR-E/2 *vs.* SMMR/SSM/I-SSMIS *vs.* MODIS) can be mostly attributed to the sensor-specific capability to resolve small thin-ice features, such as small coastal polynyas and leads, *i.e.*, the spatial resolution of each sensor. Figure 2 illustrates this effect quite nicely by showing an example (14 March 2009) of the retrieved POLA for MODIS (TIT  $\leq$  0.2 m; green contour; 2 km), SSM/I 70PT (red contour; 25 km) and SSM/I PSSM (blue contour; 12.5 km). While the passive microwave estimates on that given day are comparable (PSSM: 7463 km<sup>2</sup>; 70PT: 6691 km<sup>2</sup>), the MODIS-estimates more than double those values (no CC: 17,804 km<sup>2</sup>; CC (IST-coverage 92.3%): 19,290 km<sup>2</sup>).

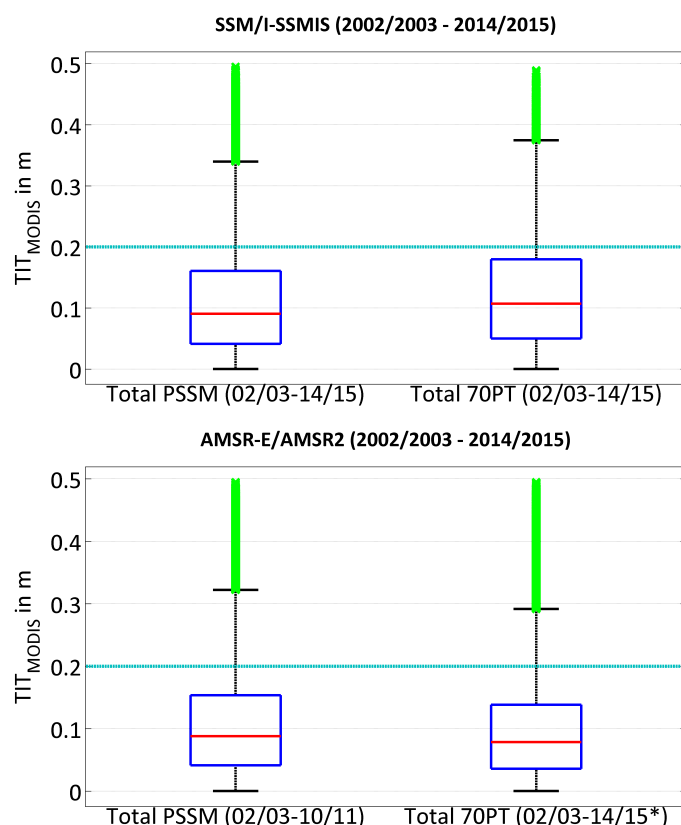


**Figure 3.** Box-plots of the daily TIT distribution in polynya areas as detected by passive microwave sensors (upper panel: SSM/I-SSMIS; lower panel: AMSR-E/AMSR2). Boxes on the left side show the MODIS TIT distribution in the PSSM polynya area, while the right-hand boxes show the equivalent information for the 70PT method. The light blue horizontal bar marks the 0.2-m TIT-threshold for the MODIS POLA-retrieval. Red bars indicate the median within the 25th and 75th percentile (inter-quartile range; blue boxes). The whisker length has a default value of 1.5-times the inter-quartile range, and outliers are marked in green (\* no AMSR-E/AMSR2 sea ice concentrations available for November to March 2011/2012).

### 3.2. Assessment of Long-Term POLA Development

As the coarse-resolution SMMR/SSM/I-SSMIS SIC dataset features by far the longest available satellite record (1978 to 2015), Figure 4 shows the daily development of  $POLA_{SSM,70PT}$  estimates for the NOW polynya. This time series of 37 consecutive winter seasons covers a comparatively long period of time and is therefore better suited for climatological studies than the MODIS and AMSR-E/AMSR2 estimates, which feature only the last 13 winter seasons. It gets clear that the NOW polynya changed significantly during the last three decades, regardless of the absolute accuracy of the underlying SIC dataset [16]. Until the mid-1990s, the overall polynya-activity was very weak. Larger polynya events occurred mainly at the beginning of a freezing season (November), while the remaining months only featured sparse periods with enhanced activity. Overall, a shift to a later fall freeze-up is observed in the last 15 to 16 years, where the polynya exceeds areal extents of 40,000 to 50,000 km<sup>2</sup> until the end of December. In addition, also the remaining months of these years show large polynya events. Less polynya activity is generally observed towards the end of an average winter season.



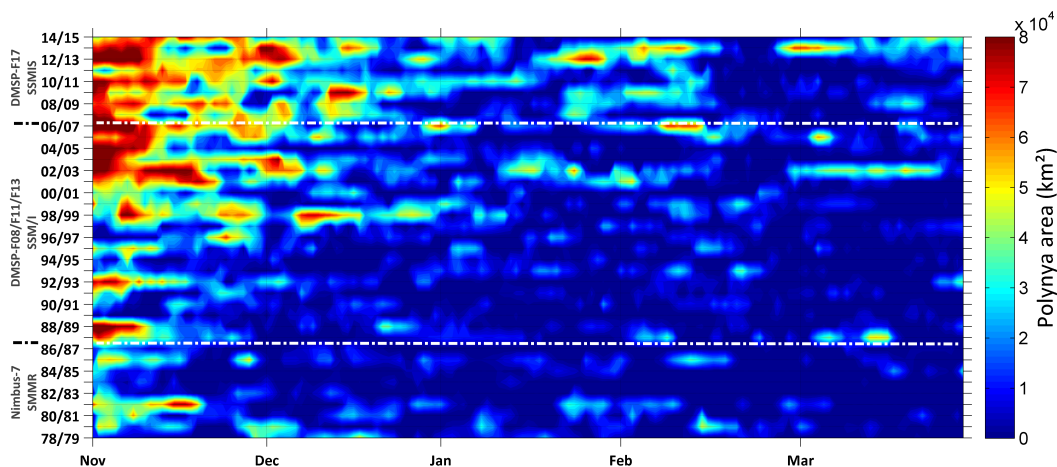


**Figure 4.** Hovmöller diagram of daily polynya area ( $POLA_{SSMI,70PT}$ ) in the North Water Polynya between 1978/1979 and 2014/2015. White horizontal dotted lines indicate changing sensors in the sea ice concentration (SIC) dataset by Cavalieri *et al.* [16].

Figure 5 shows spatial overviews of the relative frequency of polynya/thin-ice occurrences on a monthly basis (November to March) based on daily  $POLA_{SSMI,70PT}$  estimates,  $POLA_{SSMI,PSSM}$  estimates and MODIS TIT (using SFR for gap filling). The upper three rows roughly represent the 1980s (1978/1979 to 1989/1990), the 1990s (1990/1991 to 2001/2002) and the 2000s (2002/2003 to 2014/2015) periods to detect decadal changes of the sea ice in northern Baffin Bay. The lower two rows show equivalent information for the 2000s period based on  $POLA_{SSMI,PSSM}$  and MODIS. In the 1980s, the NOW polynya features an overall low activity. These first 12 winter seasons show appearance rates of around 70% (21 d) in November down to approximately 30% (9 d) in February and March in the area of Smith Sound. The main polynya activity during this period is limited to areas north of  $76^{\circ}\text{N}$  (maximum extent in November). During the 1990s and even more the 2000s, this region vastly expands down to approximately  $74^{\circ}\text{N}$ . Even in January to March, appearance rates of over 20% to 30% extend down to around  $76^{\circ}\text{N}$ . Remarkably, the monthly duration of the polynya in the proximity of Smith Sound increases towards 60% (17 to 19 d) in January to March and up to 90% to 100% (28 to 31 d) in November to December. The finer resolving counterparts from MODIS, SSM/I-SSMIS (PSSM) (Figure 5; 2000s period) and AMSR-E/AMSR2 (not shown) are certainly able to provide more precise regional differentiations. Not only in the case of MODIS (relative frequencies of TIT  $\leq 0.2$  m), observed patterns are in accordance with earlier studies (e.g., [8,20,21]) and underline the previously-stated observations based on coarse-resolution SMMR and SSM/I-SSMIS 70PT data. In addition, the detection of small-scale features, like the clearly visible shape of the ice bridge at Smith Sound, as well as larger thin-ice areas at the eastern side of the polynya, profits from the enhanced spatial resolution of MODIS. Also noticeable is a quite large area with values ranging from around 35% to 60% south of Ellesmere Island (eastern entrance of Jones Sound).

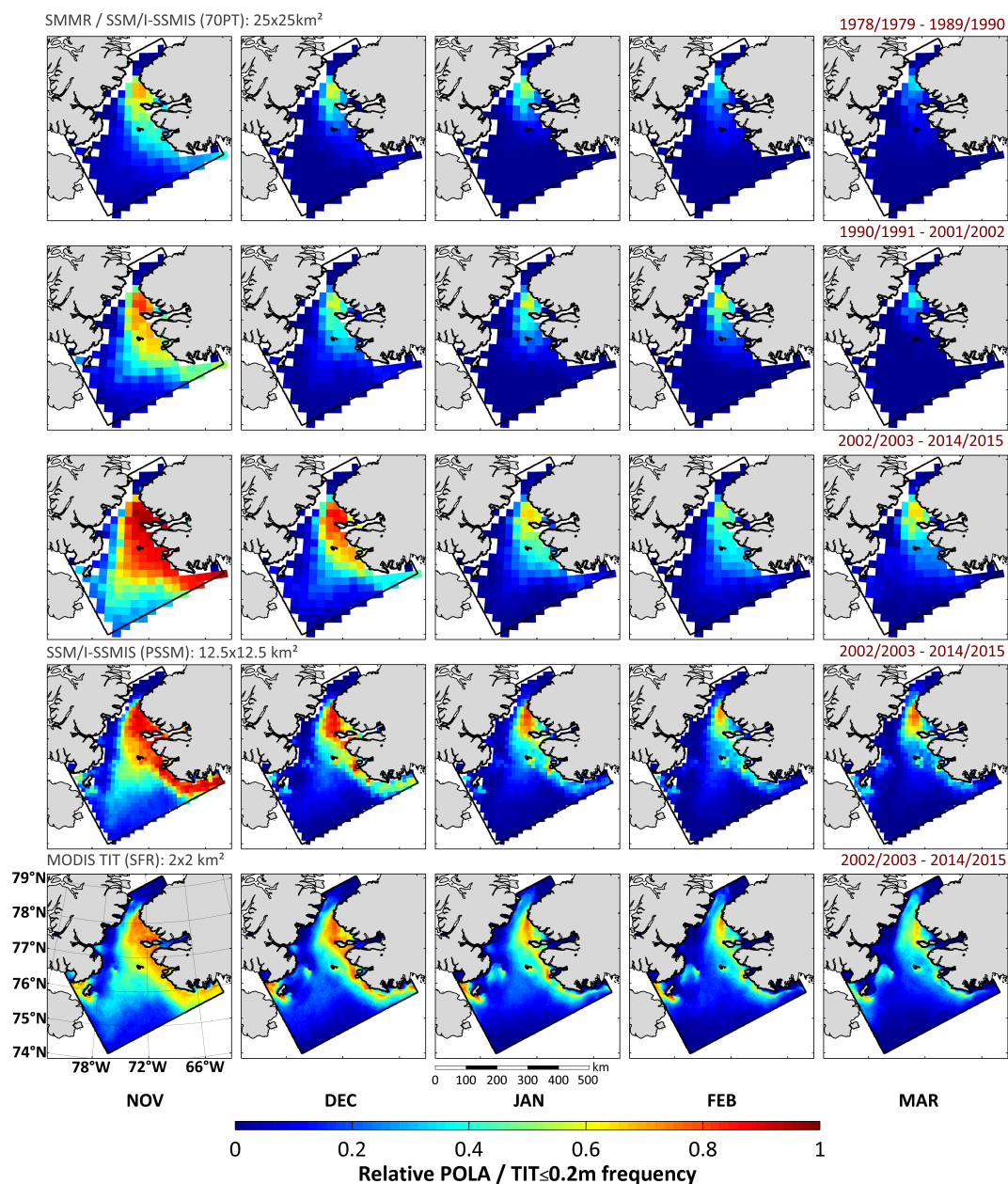


**Figure 5.** Average monthly relative frequency distribution of polynya-pixels as classified by the 70PT-method (SMMR/SSM/I-SSMIS; top three rows), the PSSM method (SSM/I-SSMIS); fourth row) and based on MODIS thin-ice thicknesses  $\leq 0.2$  m (daily TIT composites with applied spatial feature reconstruction (SFR); bottom row). Note the reference period over which the monthly relative frequency distributions are calculated, as indicated in the the upper right corner of each row.

Figure 6 sums up the previous findings for the whole regarded period from 1978 to 2015. It shows the amount of open polynya days (based on POLA estimates from MODIS (CC/SFR), AMSR-E/AMSR2 and SMMR/SSM/I-SSMIS (both 70PT/PSSM)) exceeding a certain areal threshold (POLA  $\geq 1500/5000/20,000/50,000$  km<sup>2</sup>). In the upper panel (POLA  $\geq 1500$  km<sup>2</sup>), days that are falling below a threshold of 1500 km<sup>2</sup>, *i.e.*, an almost closed polynya, can be depicted by the difference of given values to the total number of days each winter season (November to March; 151/152 d). In recent winters, the number of very small to almost closed polynyas seems to vanish almost

completely (except for the SMMR/SSM/I-SSMIS 70PT retrievals). On the other hand, the number of larger polynyas increases significantly from approximately 1997/1998 onwards, especially those exceeding a threshold of 20,000 km<sup>2</sup>. Noteworthy is the higher amount of detected polynyas larger than 20,000 km<sup>2</sup> from MODIS and a good agreement between MODIS and the passive microwave estimates for very large polynyas (≥50,000 km<sup>2</sup>).

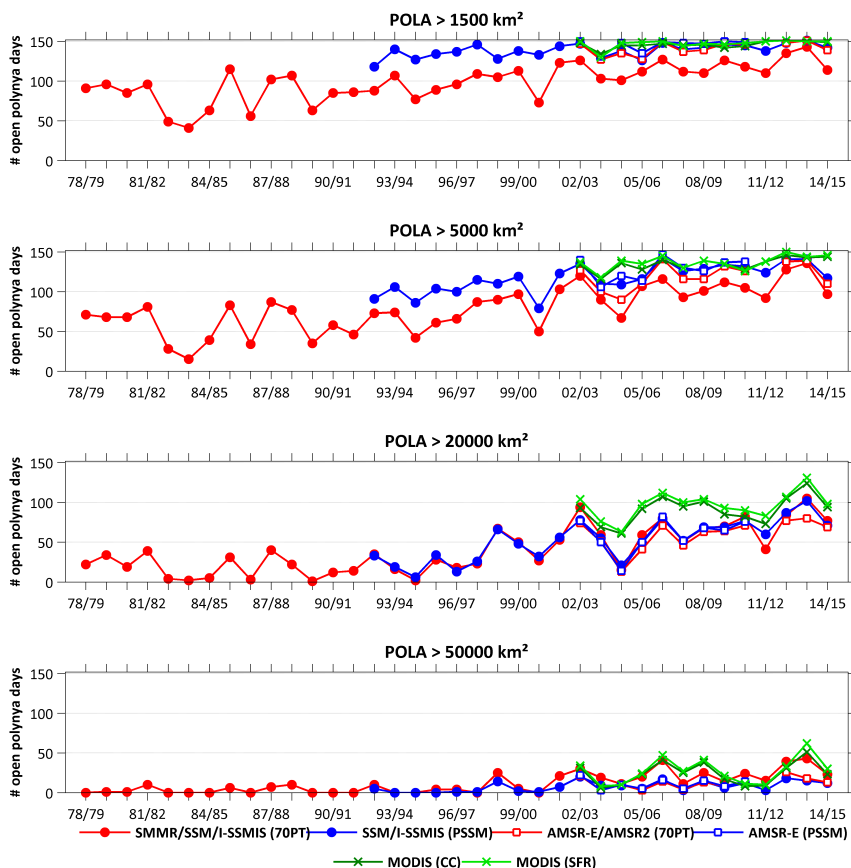


**Figure 6.** Number of polynya days with an area of  $\geq 1500$  km<sup>2</sup>,  $\geq 5000$  km<sup>2</sup>,  $\geq 20,000$  km<sup>2</sup> and  $\geq 50,000$  km<sup>2</sup> within the applied polynya mask. A comparison is made between POLA estimations based on daily MODIS TIT composites (CC: dark green crosses; SFR: light green crosses) and passive microwave sensors (SMMR/SSM/I-SSMIS 70PT: filled red circles; AMSR-E/AMSR2 70PT: unfilled red squares; SSM/I-SSMIS PSSM: filled blue circles; AMSR-E PSSM: unfilled blue squares). The numbers indicate the amount of polynya days for each area threshold from zero.

A comparison of the wintertime mean POLA for all available sensors and retrieval-schemes is presented in Figure 7 for the complete record of 37 winter seasons. In this long-term context, we find coherent patterns between all incorporated satellites and sensors, although absolute mean values are differing. Further, a tendency towards larger areal extents of the NOW polynya becomes very obvious. As could be seen before, the winter seasons around 1996/1997 to 1997/1998 seem to be the periods where the NOW polynya starts to expand from an average level of around 7000 km<sup>2</sup> in the 1980s and early 1990s up to almost doubled average values in recent years.

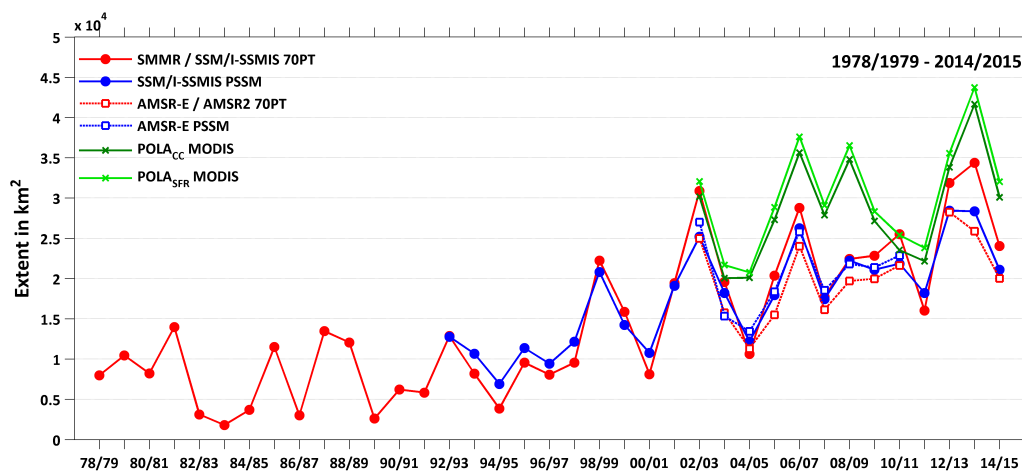


**Figure 7.** Average wintertime (November to March) polynya area (POLA) for the period from 1978/1979 to 2014/2015. A comparison is made between POLA estimations based on daily MODIS TIT composites (CC: dark green crosses; SFR: light green crosses) and passive microwave sensors (SMMR/SSM/I-SSMIS 70PT: filled red circles; AMSR-E/AMSR2 70PT: unfilled red squares; SSM/I-SSMIS PSSM: filled blue circles; AMSR-E PSSM: unfilled blue squares).

This sudden “POLA shift” during the mid-1990s may be related to the clear warming trend in northwestern Greenland from 1994 onwards [41] (associated with an increasing amount of blocking events (high-pressure anomalies) over the Greenland Ice Sheet (GrIS), e.g., [42]). The North Atlantic Oscillation (NAO) and Arctic Oscillation (AO) are well known and widely used indices that characterize large-scale atmospheric variability in the Northern Hemisphere. While featuring significant interannual and seasonal variability, the NAO experienced a transition to a prevailing more negative phase in 1995/1996, which so far peaked in the most negative wintertime NAO index in 2009/2010 [43]. These negative phases are associated with a high-pressure anomaly/ridges over the GrIS, which can bring relatively warm southerly winds from lower latitudes to the western side of Greenland [44]. Although the NAO and AO are very similar from a conceptual point of view and do strongly correlate ( $r > 0.8$ ), the recently declining nature of the summer NAO is not replicated in the AO index [45]. Instead, both indexes show enhanced wintertime variability in recent years [45,46]. However, extreme negative phases, like in 2009/2010, are evident in both the NAO and AO index. Stroeve *et al.* [46] highlights that winter months (December to January) for the period 1979 to 2009 with a strongly negative AO index tend to show positive air temperature (925-hPa level) anomalies and negative SIC anomalies over Greenland, Baffin Bay, Canada and Alaska. A steady increase in autumn and winter air temperatures from 1995/1996 onwards could slow down or limit ice growth during freeze-up and, hence, lead to prolonged periods with very thin ice in northern Baffin Bay. Following this argumentation, increasing POLA and a later fall freeze-up align well. Therefore, besides having a potentially large influence on summer melt rates on the GrIS and land surface [41], we assume that increased winter warming and associated negative NAO phases are also linked to sea ice and polynya characteristics in the NOW region.

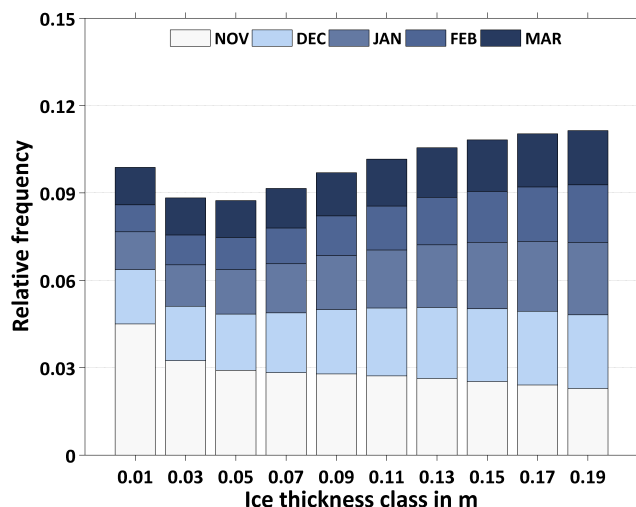
Overall, it can be noted, that MODIS, as well as both AMSR-E PSSM and SSM/I-SSMIS PSSM all capture the general seasonal development of polynya opening events in good agreement (compare Table 3). In several cases, MODIS-derived POLA exceeds the passive microwave estimates by a factor of 1.5 to two, especially for polynyas below 40,000 km<sup>2</sup>. When comparing individual winter seasons, a large interannual variability can be observed.

**Table 3.** Comparison of calculated monthly mean polynya area (POLA; in  $10^3 \text{ km}^2$ ) from different sensor types (SSM/I-SSMIS, AMSR-E, MODIS) and methods, averaged over the overlapping period from 2002/2003 to 2010/2011 (November to March). Cloud-cover corrections have been applied to the MODIS data where CC denotes the values after coverage correction and SFR denotes the values after the spatial feature reconstruction (compare Section 2.6). All values are calculated within the predefined polynya mask (Figure 1).

	SSM/I-SSMIS 70PT ( $10^3 \text{ km}^2$ )	SSM/I-SSMIS PSSM ( $10^3 \text{ km}^2$ )	AMSR-E 70PT ( $10^3 \text{ km}^2$ )	AMSR-E PSSM ( $10^3 \text{ km}^2$ )	MODIS CC ( $10^3 \text{ km}^2$ )	MODIS SFR ( $10^3 \text{ km}^2$ )
November	50.5	39.3	38.5	39.1	39.3	42.8
December	25.6	21.6	20.5	22.5	29.0	30.8
January	12.9	15.6	13.5	15.3	26.9	28.1
February	11.4	12.6	10.8	13.5	21.8	22.5
March	10.0	12.2	10.5	12.1	19.9	20.3
Mean	22.1	20.3	18.8	20.5	27.4	28.9
SD	17.0	11.3	11.8	11.2	7.6	8.8

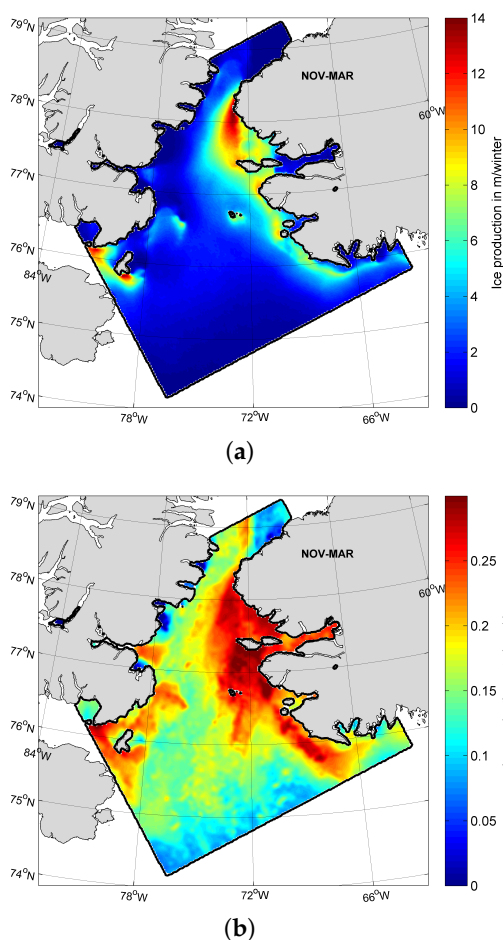
### 3.3. Thin-Ice Thickness Distribution and Thermodynamic Ice Production for 2002/2003 to 2014/2015

Figure 8 shows a histogram of the total wintertime relative TIT distribution for ice thicknesses below 0.2 m, based on median daily composites. Colors indicate monthly differences. Between November and March, ice thinner than 0.04 m contributes around 9 to 10% to the total polynya area in an average winter season, with the largest proportion being present in November during freeze-up. Thicker ice classes ( $>0.1 \text{ m}$ ) show higher contributions of around 10 to 11% in total, therefore covering more than half of the entire NOW polynya predominately from January to March. Concerning the thin-ice thickness distribution in the NOW-polynya region, there is only sparse information available in recent literature. As Ingram *et al.* [5] states, an improved characterization of the ice-thickness distribution is one of the main aspects that needs to be further investigated in the NOW region to get more viable information about the magnitude of heat exchange between ocean and atmosphere. Nevertheless, some information on sea ice types and associated ice thicknesses in the North Water region can be found in an older study by Steffen [47]. This study had the purpose of investigating the general ice conditions in the winters of 1978/1979 and 1980/1981 by means of an aerial survey performing radiometric temperature measurements of the sea surface. From these measurements, distinct ice types were classified, and their proportion to the sea ice cover was derived. According to Steffen [47], more than 50% of the NOW polynya (in his study called “Smith Sound polynya”) was covered by young ice (0.1 m to 0.3 m), nilas (0 m to 0.1 m) and open water in the months November to January. This is roughly in accordance to the estimated relative TIT frequencies ( $\text{TIT} \leq 0.2 \text{ m}$ ) for November to December derived in this study, where values up to 65% are visible south of Smith Sound. Steffen [47] also states that in February and March, more white ice ( $>0.3 \text{ m}$ ) was present during their flight campaigns. This fits the conclusion made earlier that there is less polynya activity in the NOW region towards the end of the freezing season (Figures 4 and 5). While there is no direct comparison available for the TIT distribution shown in Figure 8, the study of Steffen [47] also gives an indication that the derived proportion of very thin ice is not far off from his observations (see his Table 3; categories “ice-free” and “dark nilas” combined), despite a possible bias in this thickness class due to inherent cloud and sea smoke effects [36].



**Figure 8.** Histogram of the relative thin-ice thickness (TIT) distribution in the NOW polynya, with ice-thickness classes of the 2-cm range ( $x$  axis). Input data are based on daily TIT composites covering the complete freezing season from November to March. The bars indicate the relative distribution of each thickness class from the total number of TIT  $\leq 0.2$ -m appearances between the winter seasons 2002/2003 and 2014/2015. Contributions of each month with respect to the whole winter season for each thickness class are indicated by the blueish colors (see the legend).

Based on the calculated thin-ice distributions, daily averaged net surface heat loss and associated ice production (rates) are pixel-wise calculated. Spatial overviews of interannual (2002/2003 to 2014/2015) average wintertime ice production (in  $\text{m}\cdot\text{winter}^{-1}$ ) and the daily maximum ice production rates (in  $\text{m}\cdot\text{d}^{-1}$ ) are shown in Figure 9 with the purpose of locating regional differences and typical spatial patterns. The highest values of accumulated ice production (up to 13 to 14  $\text{m}\cdot\text{winter}^{-1}$ ; Figure 9a) occur directly south of the Greenland side of Smith Sound (lee-side) and slightly lower values (around 5 to 8  $\text{m}\cdot\text{winter}^{-1}$ ) in proximity of the West Greenland coast. These values compare well to Iwamoto *et al.* [21], who state a maximum rate of 13  $\text{m}\cdot\text{winter}^{-1}$  and are therefore lower than the 19  $\text{m}\cdot\text{winter}^{-1}$  stated by Tamura and Ohshima [20]. Maximum daily rates at these locations can exceed 20 to 25 cm per day, in certain areas even reaching values as high as 30 cm per day (e.g., south of Northumberland Island at approximately  $77^\circ\text{N}$ ,  $72^\circ\text{W}$ ; Figure 9b). It has to be noted that the typical location of the ice bridge at Smith Sound (see the following Section 3.3) is well visible and recognizable by its characteristic arch-like shape. However, the main location for high ice formation rates is found at the eastern exit of Smith Sound, indicating the importance of the gap flow dynamics for the polynya formation in that area [48]. Other prominent features are large areas of high ice production between Ellesmere Island and Devon Island in the west of the polynya domain near Coburg Island. While potentially belonging to individual smaller polynya systems (as implied by Barber and Massom [1]), these areas are included in our NOW polynya estimates.



**Figure 9.** Spatial distribution of (a) the average accumulated ice production (IP, in  $\text{m}\cdot\text{winter}^{-1}$ ) rate, as well as (b) the maximum daily ice production rate (in  $\text{m}\cdot\text{d}^{-1}$ ) in the North Water Polynya for winter seasons (November to March) 2002/2003 to 2014/2015.

In Figure 10a,b, average wintertime energy fluxes from the heat flux calculations are shown together with the total accumulated ice production (CC/SFR) per winter season from November to March. A detailed overview on ice production and polynya area (CC/SFR) for each winter season is additionally given in Table 4. Overall, the average fluxes from both net long-wave radiation and latent heat show almost no interannual variability by ranging around  $95 \text{ W}\cdot\text{m}^{-2}$  and  $25 \text{ W}\cdot\text{m}^{-2}$ , respectively. The net energy balance during wintertime is therefore strongly controlled by the contribution of the sensible heat flux. In the NOW region, average values for H are ranging between  $91 \text{ W}\cdot\text{m}^{-2}$  (2010/2011) and  $119 \text{ W}\cdot\text{m}^{-2}$  (2004/2005). Concerning wintertime ice production in the NOW polynya, results from the two correction schemes (CC/SFR) are overall differing by approximately 4%. The average  $\text{IP}_{\text{SFR}}$  value amounts to  $275.7 \pm 67.4 \text{ km}^3$  (CC:  $264.4 \pm 65.1 \text{ km}^3$ ). We note a high interannual variability of ice production, with values as low as  $190.2 \text{ km}^3$  (SFR; CC  $-6.9\%$ ) in 2003/2004 and up to  $405.7 \text{ km}^3$  (SFR; CC  $-3.9\%$ ) in 2013/2014. Large increases in IP occur from winter 2005/2006 to 2006/2007 (SFR:  $+108 \text{ km}^3$ ) and again from winter 2011/2012 to 2012/2013 (SFR:  $+106 \text{ km}^3$ ). Regardless of the applied cloud-cover correction, a non-significant positive trend of  $5.9 \text{ km}^3\cdot\text{yr}^{-1}$  can be observed over the examined 13 winters' record. The high ice production in 2013/2014 can be partly explained by continuously high frequencies of  $\text{TIT} \leq 0.2 \text{ m}$  and, therefore, several large polynya events in the NOW area throughout the whole winter season from November to March.

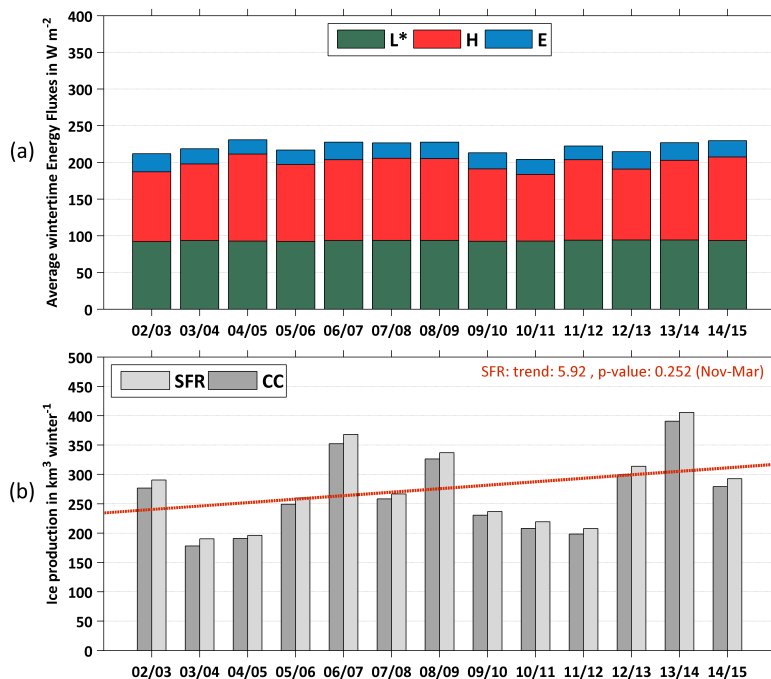


**Figure 10.** (a) Average wintertime (November to March) energy fluxes of net long-wave radiation ( $L^*$ ), sensible ( $H$ ) and latent ( $E$ ) heat (all in  $\text{W}\cdot\text{m}^{-2}$ ) within the applied polynya mask. (b) Annual wintertime accumulated ice production (IP) in the NOW polynya (in  $\text{km}^3\cdot\text{winter}^{-1}$ ) for 2002/2003 to 2014/2015. Estimations of IP are based on heat flux calculations using the daily derived TIT composites. Special emphasis is given to the effect of an applied cloud-cover correction (CC/SFR). The red dotted line shows a linear trend estimation for  $\text{IP}_{\text{SFR}}$ .

**Table 4.** Accumulated ice production in  $\text{km}^3$  per winter and average polynya area (in  $10^3 \text{ km}^2$ ) for each winter season (November to March) from 2002/2003 to 2014/2015 in the North Water Polynya, together with the interannual average (mean) and its standard deviation (SD). Cloud-cover corrections have been applied where CC denotes the values after coverage correction and SFR denotes the values after the spatial feature reconstruction (see the text). All values are derived from daily MODIS TIT composites after application of the predefined polynya mask (Figure 1).

	Acc. $\text{IP}_{\text{CC}}$ ( $\text{km}^3$ )	Acc. $\text{IP}_{\text{SFR}}$ ( $\text{km}^3$ )	$\text{POLA}_{\text{CC}}$ ( $10^3 \text{ km}^2$ )	$\text{POLA}_{\text{SFR}}$ ( $10^3 \text{ km}^2$ )
2002 to 2003	276.6	290.3	30.2	32.1
2003 to 2004	178.0	190.2	20.0	21.7
2004 to 2005	191.0	196.2	20.1	20.8
2005 to 2006	249.2	259.8	27.3	28.8
2006 to 2007	352.2	368.2	35.6	37.6
2007 to 2008	258.2	266.6	27.9	29.1
2008 to 2009	326.2	337.1	34.8	36.5
2009 to 2010	230.5	236.7	27.2	28.3
2010 to 2011	208.1	219.1	23.5	25.4
2011 to 2012	198.3	207.8	22.2	23.8
2012 to 2013	299.4	313.9	33.8	35.6
2013 to 2014	390.6	405.7	41.7	43.7
2014 to 2015	279.1	292.6	30.1	32.0
Mean	264.4	275.7	28.8	30.4
SD	65.1	67.4	6.5	6.7



Comparative numbers from previous studies in terms of ice production are hard to find for the NOW polynya. There are recent studies by Tamura and Ohshima [20] (hereafter TO11) and Iwamoto *et al.* [21] (hereafter I14), who both estimated pan-Arctic ice production in polynyas. Their estimated ice production values are based on newly-developed thin-ice algorithms, which use either SSM/I or AMSR-E brightness-temperature data to calculate thin-ice thicknesses. These algorithms are based on empirical approaches, which incorporate either Advanced Very High Resolution Radiometer (AVHRR) or MODIS-calculated reference-thicknesses (TIT). Similar to our study, these estimated ice thicknesses are then combined with heat-flux calculations (NCEP2 [49]/ERA-Interim reanalysis serving as the atmospheric dataset) to achieve ice production.

For the NOW polynya, TO11 [20] and I14 [21] state an average ice production of  $353 \pm 69 \text{ km}^3$  (1992/1993 to 2007/2008) and  $186 \pm 34 \text{ km}^3$  (2002/2003 to 2010/2011), respectively. The base-period of these studies is extended by four months each winter season compared to our study (November to March), and the applied polynya masks are differing (similar to the comparisons in [32]), which makes direct comparisons challenging. For the same averaging interval as I14 and based on  $\text{IP}_{\text{SFR}}$ , we achieve a 41% higher value of  $263 \pm 61 \text{ km}^3$ . We assume that the values derived here are more accurate, as they profit from the enhanced resolution of MODIS. Additionally, they are presumably far less influenced by ambiguities in heat loss calculations by leaving out the months of September, October, April and May. Regarding the large ice production in TO11 [20], the study of I14 [21] refers to a “thin-bias”, which is explained by differences in the applied atmospheric reanalysis data (NCEP2 *vs.* ERA-Interim). Thereby, larger calculated heat loss and thinner TIT are explained by a lower bias in 2-m-air temperature and a higher bias in wind speed when NCEP2 is compared to ERA-Interim in the the Arctic Ocean domain (also evident in Lindsay *et al.* [50]). Part of the difference from I14 is thought to originate from a smaller areal extent of their polynya mask, which excludes the area of high IP at the eastern entrance of Jones Sound (around  $76^\circ\text{N}$ ,  $81^\circ\text{W}$ ; compare Figure 9). We also applied a smaller polynya mask, which excluded the Jones Sound area for earlier investigations on the NOW polynya, which resulted in slightly lower IP (CC) estimates (about 8%). Taking this into consideration, our presented average accumulated IP values would get closer to I14, while still being higher.

Both TO11 and I14 [20,21] state that polynyas located around the Canada Basin (including the NOW polynya) show the largest ice production values in the early stage of the freezing period (October to December), which afterwards gradually decrease towards March. This is also revealed in our data and can be explained by more consolidated pack ice in northern Baffin Bay and several fast-ice areas around Ellesmere Island at the end of a freezing season, which limit the west- and south-ward expansion of the NOW polynya.

#### 3.4. Ice Bridge Dynamics in Nares Strait (2002/2003 to 2014/2015)

According to Kwok *et al.* [51], ice bridges typically form at two distinct locations along Nares Strait. A deeper understanding of the involved mechanisms and temporal patterns is of high value, as the movement of sea ice through Nares Strait and, therefore, the export of old multi-year ice from the north of Greenland is strongly controlled by the timing and location of ice bridge formation.

In the context of the present study, the most prominent location is certainly Smith Sound at the southern exit of the channel, as it usually is associated with the formation of the NOW polynya (e.g., [5,8]). According to Barber *et al.* [8], the timing of wintertime ice bridge formation at Smith Sound is quite variable by occurring sometime between November and March. Barber *et al.* [8] analyze time series of SIC north and south of the typical ice bridge location to infer characteristic development stages in the course of a year. While a similar analysis using our data worked reasonably well for the southern ice bridge at Smith Sound, we were not able to apply this analysis to the northern ice bridge locations at Robeson Channel (compare Figure 1), presumably due to the coarse resolution of the passive microwave data.

As an alternative approach we decided to take a closer look at the annual (November to March; 151/152 days in total) relative occurrences of MODIS TIT  $\leq 0.2 \text{ m}$ , in order to relate typical thin-ice

locations to nearby ice bridge patterns. The spatial overviews for the winter seasons 2002/2003 to 2014/2015 are presented in Figure 11. The observed locations of an arch-type pattern during each winter season are marked with a white arrow. The southern ice bridge at Smith Sound is present in every winter season, except the period from 2008/2009 to 2009/2010. Contrary to Kwok *et al.* [51], who also had a closer look at the behavior of the ice bridges in Nares Strait, we cannot confirm the absence of the southern ice bridge in 2006/2007, which was stated as the main reason for a sea ice export anomaly through Nares Strait in 2007. It was assumed that the movement of sea ice was not suppressed by any kind of blocking features both at Smith Sound in the south and Robeson Channel roughly 450 km further north. While the latter is also observable in our study (high TIT frequencies in the northerly part of Nares Strait), an arch-type TIT pattern at the southern end of Nares Strait was present during the whole winter season from November to March, although its location is very variable. In addition, daily TIT maps reveal several events where large patches of ice broke off at Smith Sound and drifting further south, thereby still indicating a less stable ice bridge and enhanced sea ice export at the Canadian side of the channel.

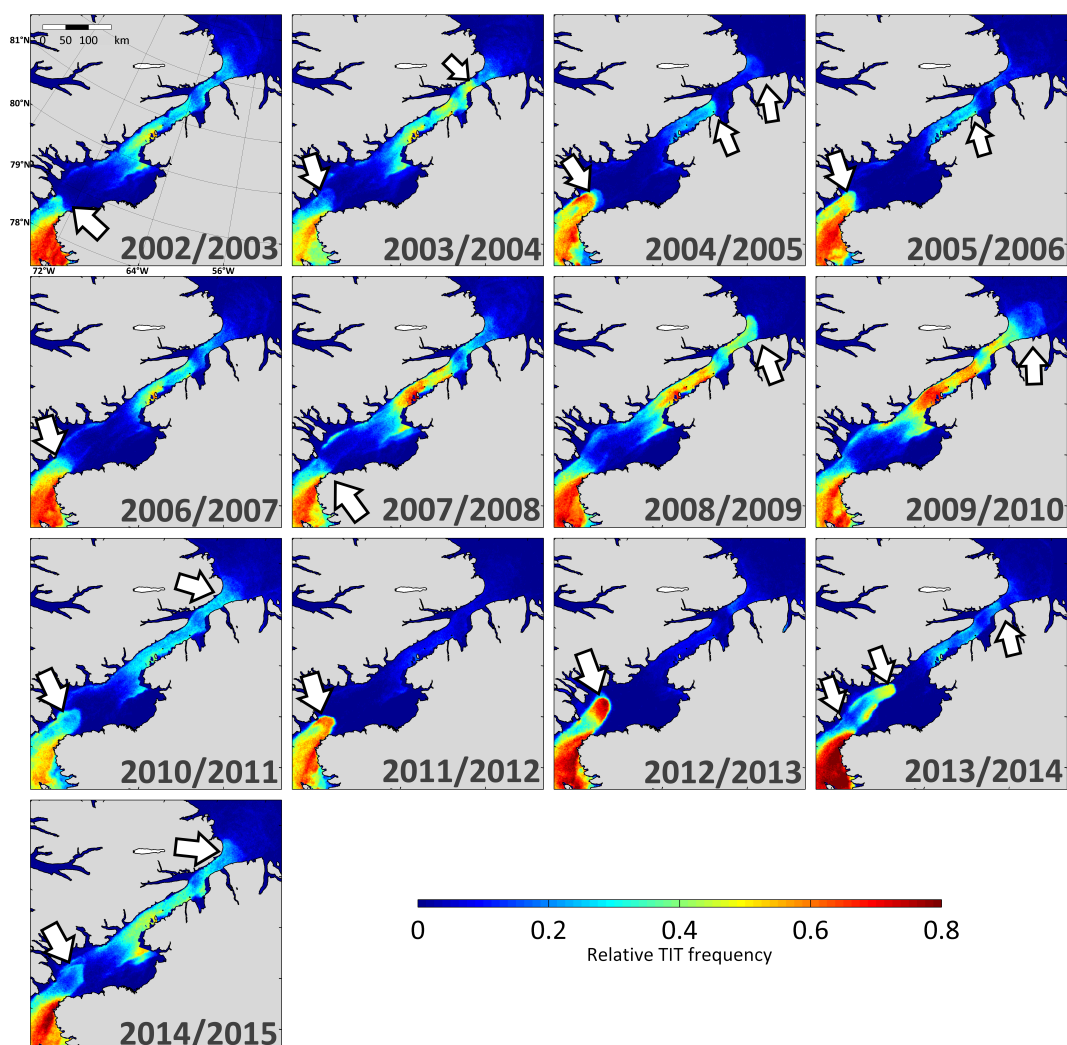


**Figure 11.** Relative frequency distribution of thin-ice thickness  $\leq 0.2$  m in northern Baffin Bay/Smith Sound, Nares Strait and Lincoln Sea for the complete freezing seasons (November to March) 2002/2003 to 2014/2015, based on daily TIT composites. Observed sites of ice bridge appearances between November and March are indicated by white arrows.

Barber *et al.* [8] stated that the formation of an ice bridge at Smith Sound seemed to be less regular in the 1990s compared to the 1980s, with a tendency to form later and break up earlier. As we only regard the case of ice bridge formation during winter, we cannot comment on the timing of ice bridge break-up for the 2000s and ongoing. Regarding the later appearing ice bridge formation, we noted a large monthly variability of TIT frequencies in Nares Strait over the last 13 winter seasons, but no sign of a temporal shift.

Using SAR (Synthetic Aperture Radar) satellite imagery from RADARSAT, Kwok *et al.* [51] estimated the average timing of ice bridge formation at Smith Sound to be around 2 February ( $\pm 44$  d), blocking the ice movement in Nares Strait on average for  $184 \pm 10$  d until the summer melt period. Based on monthly TIT frequency distributions (2002/2003 to 2014/2015; not shown), we can confirm that the most regular ice bridge development starts from February onwards. In addition, more than half of the winters between 2002/2003 and 2014/2015 already feature an ice bridge in November and December.

Unfortunately, we are not able to directly relate the ice bridge formation in Nares Strait to the development of the NOW polynya during winter. Years with high wintertime POLA and IP do not necessarily coincide with long ice bridge periods and *vice versa*. Hence, we expect that the ice bridge at Smith Sound becomes more important around April to June, when the NOW-polynya starts to expand southward.

#### 4. Summary and Conclusions

In this study, we present a long-term analysis of polynya dynamics and ice production in the NOW polynya for the winter seasons 1978/1979 to 2014/2015. For that purpose, we analyzed remote sensing data from both passive microwave (AMSR-E, AMSR2, SMMR/SSM/I-SSMIS) and thermal infrared (MODIS) sensors to infer characteristic polynya quantities, such as the total polynya area (POLA) and thermodynamic ice production (IP), on various spatial resolutions and temporal scales. In order to allow comparisons between MODIS and passive microwave estimates, two well-working approaches are applied to overcome difficulties with falsely-classified and/or undetected cloud-covered pixels. All sensors capture the overall seasonal development of the polynya very well, with differences occurring mainly in terms of polynya sizes due to the varying capability to resolve smaller thin-ice features. Thereby, daily POLA derived by MODIS exceeds the passive microwave estimates in most cases, as leads and areas in close proximity to the coasts of Greenland and Ellesmere Island contribute to the estimations. This results in about 30 to 40% higher average POLA estimates compared to the ones derived by AMSR-E. MODIS estimates can even exceed the POLA values derived by SSM/I, depending on the type of calculation (70PT/PSSM). In addition, land spillover effects are reduced compared to coarse-resolution passive microwave estimates of POLA, which is especially valuable for areas with a very rugged coastline, such as Greenland. While the difference in POLA between the 70PT and PSSM approach is fairly low (approximately 10%) for AMSR-E, it can be much larger for the coarse-resolution SSM/I-SSMIS data, especially in November and December, when large thin-ice areas dominate the NOW region. As a compromise between a long-term satellite record and a good agreement with the comparatively high-resolution MODIS estimates, the PSSM method should be used instead of the 70PT method with SSM/I-SSMIS data to calculate POLA over longer time scales.

Compared to earlier studies in the NOW polynya region, the results presented in this study extend the time series and use a multi-sensor approach. The derived location of predominant thin-ice occurrences (*i.e.*, POLA) is in accordance with other studies and focuses on the Smith Sound area with ice bridge and gap flow mechanics as the responsible formation mechanisms. Our results confirm earlier observations by Steffen [47] regarding high polynya activity at the beginning of the freezing period and less polynya activity towards the end of the freezing season and give new insights on a steady increase in polynya area since the mid-1990s. We suggest a potential connection of this sudden shift to a predominately negative phase of the NAO since 1995/1996. However, a more

detailed analysis on this topic is beyond the scope of this study and should be implemented in a future atmospheric study. Comparative numbers for the ice production in the NOW polynya are given in Tamura and Ohshima [20] and Iwamoto *et al.* [21]. Their estimations derived from coarse-resolution SSM/I and AMSR-E data are either by far higher [20] than the results presented here from MODIS IST data or clearly lower [21], which is (at least to some extent and also considering an apparent “thin-bias” in [20]) expected to originate from the shortened investigation period in this study (leaving out September, October, April and May) and different polynya masks [21].

Increased thin-ice frequencies in Nares Strait could be linked to nearby ice bridge formation by revealing distinct spatial patterns. Unfortunately, we could not deduce a clear relation to our calculated polynya metrics and instead assume an increased importance of the ice bridges in Nares Strait towards spring and summer.

Long-term time series of POLA (1978/1979 to 2014/2015) and IP (2002/2003 to 2014/2015), as well as thin-ice characteristics in Nares Strait complement atmospheric and oceanographic observations and model efforts in the NOW region over the last decades. A future synthesis of atmospheric and oceanographic modeling and remote sensing observations might help to explain the obvious changes that are taking place in the NOW region since the 1990s and ongoing. Although the atmospheric part is the essential formation mechanism for the NOW polynya, e.g., [5,8,20], a more detailed analysis of the ocean heat budget (influenced by the Arctic ocean and different water masses in Baffin Bay, like the relatively warm West Greenland Current [11]) and potential implications could certainly help to obtain a complete picture. Supplementary data are available at <http://dx.doi.org/10.1594/PANGAEA.854921>.

**Acknowledgments:** The authors want to thank the National Snow and Ice Data Center (NSIDC), as well as the European Center for Medium-Range Weather Forecasts (ECMWF) for providing the passive microwave brightness temperature data, the MODIS Sea Ice product (<ftp://n5eil01u.ecs.nsidc.org/SAN/>) and the ERA-Interim atmospheric reanalysis data. The University of Bremen and the University of Hamburg are also kindly acknowledged for providing the passive microwave sea ice concentration data. We would like to thank the referees for their valuable comments and suggestions during the review. This work was funded by the Federal Ministry of Education and Research (Bundesministerium für Bildung und Forschung - BMBF) under Grant 03G0833D.

**Author Contributions:** Andreas Preußner carried out the complete analysis and drafted the manuscript. Sascha Willmes and Stephan Paul assisted in the satellite data analysis and the SFR approach. All three co-authors, including Günther Heinemann, contributed to the writing of the manuscript. The final draft of the manuscript was revised and approved by all of the authors.

**Conflicts of Interest:** The authors declare no conflict of interest.

## Abbreviations

70PT	70% sea ice concentration threshold	MODIS	Moderate Resolution Imaging Spectroradiometer
ADEOS-II	Advanced Earth Observing Satellite; also known as Midori II	NAO	North Atlantic Oscillation
AMSR-E	Advanced Microwave Scanning Radiometer -Earth Observing System	NASA	National Aeronautics and Space Administration
AMSR2	Advanced Microwave Scanning Radiometer 2	NCEP2	National Center for Environmental Prediction-Reanalysis 2
AO	Arctic Oscillation	NOW	North Water
ASI	ARTIST Sea Ice	NRT	near real time
AVHRR	Advanced Very High Resolution Radiometer	NSIDC	National Snow and Ice Data Center
CC	coverage correction	PIX	persistence index
CCS	confident clear-sky	POLA	polynya area
DMSP	Defense Meteorological Satellite Program	PR	polarization ratio
ECMWF	European Center for Medium Range Weather Forecast	PSSM	polynya signature simulation method
GCOM-W1	Global Change Observation Mission-Water	SAR	Synthetic Aperture Radar
GrIS	Greenland Ice Sheet	SFR	spatial feature reconstruction
GSFC	Goddard Space Flight Center	SIC	sea ice concentration
IP	ice production	SMMR	Scanning Multichannel Microwave Radiometer
IST	ice surface temperature	SSM/I	Special Sensor Microwave/Imager
JAXA	Japan Aerospace Exploration Agency	SSMIS	Special Sensor Microwave Imager/Sounder
MCC	medium cloud cover	$T_B$	brightness temperature
MCP	mixed cover pixels	TIT	thin-ice thickness

## References

1. Barber, D.G.; Massom, R.A. The role of sea ice in Arctic and Antarctic polynyas. In *Polynyas—Windows to the World*; Smith, W.O., Barber, D.G., Eds.; Elsevier Oceanography Series: Amsterdam, The Netherlands, 2007; pp. 1–54.
2. Smith, S.D.; Muench, R.D.; Pease, C.H. Polynyas and leads: An overview of physical processes and environment. *J. Geophys. Res.* **1990**, *95*, 9461–9479.
3. Morales-Maqueda, M.; Willmott, A.; Biggs, N. Polynya dynamics: A review of observations and modeling. *Rev. Geophys.* **2004**, *42*, 1–37.
4. Jakobsson, M.; Mayer, L.; Coakley, B.; Dowdeswell, J.A.; Forbes, S.; Fridman, B.; Hodnesdal, H.; Noormets, R.; Pedersen, R.; Rebesco, M.; *et al.* The international bathymetric chart of the Arctic Ocean (IBCAO) version 3.0. *Geophys. Res. Lett.* **2012**, *39*, doi:10.1029/2012GL052219.
5. Ingram, R.G.; Bâcle, J.; Barber, D.G.; Gratton, Y.; Melling, H. An overview of physical processes in the North Water. *Deep-Sea Res. Pt II* **2002**, *49*, 4893–4906.
6. Barber, D.; Marsden, R.; Minnett, P.; Ingram, G.; Fortier, L. Physical processes within the North Water (NOW) polynya. *Atmos. Ocean* **2001**, *39*, 163–166.
7. Deming, J.W.; Fortier, L.; Fukuchi, M. The International North Water Polynya Study (NOW): A brief overview. *Deep-Sea Res. Pt II* **2002**, *49*, 4887–4892.
8. Barber, D.; Hanesiak, J.; Chan, W.; Piwowar, J. Sea-ice and meteorological conditions in Northern Baffin Bay and the North Water polynya between 1979 and 1996. *Atmos. Ocean* **2001**, *39*, 343–359.
9. Mundy, C.; Barber, D. On the relationship between spatial patterns of sea-ice type and the mechanisms which create and maintain the North Water (NOW) polynya. *Atmos. Ocean* **2001**, *39*, 327–341.
10. Melling, H.; Gratton, Y.; Ingram, G. Ocean circulation within the North Water polynya of Baffin Bay. *Atmos. Ocean* **2001**, *39*, 301–325.
11. Yao, T.; Tang, C. The formation and maintenance of the North Water polynya. *Atmos. Ocean* **2003**, *41*, 187–201.
12. Riggs, G.; Hall, D.; Salomonson, V. *MODIS Sea Ice Products User Guide to Collection 5*; National Snow and Ice Data Center, University of Colorado: Boulder, CO, USA, 2006.
13. Cavalieri, D.J.; Markus, T.; Comiso, J.C. *AMSR-E/Aqua Daily L3 6.25 km 89 GHz Brightness Temperature Polar Grids. Version 3. 2002–2011*; NASA National Snow and Ice Data Center Distributed Active Archive Center: Boulder, CO, USA, 2014.
14. Cavalieri, D.J.; Markus, T.; Comiso, J.C. *AMSR-E/Aqua Daily L3 12.5 km Brightness Temperature, Sea Ice Concentration, & Snow Depth Polar Grids. Version 3. 2002–2011*; NASA National Snow and Ice Data Center Distributed Active Archive Center: Boulder, CO, USA, 2014.
15. Spreen, G.; Kaleschke, L.; Heygster, G. Sea ice remote sensing using AMSR-E 89 GHz channels. *J. Geophys. Res.* **2008**, *113*, doi:10.1029/2005JC003384.
16. Cavalieri, D.J.; Parkinson, C.L.; Gloersen, P.; Zwally, H. *Sea Ice Concentrations from Nimbus-7 SMMR and DMSP SSM/I-SSMIS Passive Microwave Data. 1978–2014*; NASA National Snow and Ice Data Center Distributed Active Archive Center: Boulder, CO, USA, 1996.
17. Cavalieri, D.J.; Gloersen, P.; Zwally, H.; Maslanik, J.; Stroeve, J. *Near-Real-Time DMSP SSMIS Daily Polar Gridded Brightness Temperatures. 2015*; NASA National Snow and Ice Data Center Distributed Active Archive Center: Boulder, CO, USA, 1999.
18. Maslanik, J.; Stroeve, J. *Near-Real-Time DMSP SSMIS Daily Polar Gridded Sea Ice Concentrations. 2015*; NASA National Snow and Ice Data Center Distributed Active Archive Center: Boulder, CO, USA, 1999.
19. Maslanik, J.; Stroeve, J. *DMSP SSM/I-SSMIS Daily Polar Gridded Brightness Temperatures. Version 4. 1992–2014*; NASA National Snow and Ice Data Center Distributed Active Archive Center: Boulder, CO, USA, 2004.
20. Tamura, T.; Ohshima, K.I. Mapping of sea ice production in the Arctic coastal polynyas. *J. Geophys. Res.* **2011**, *116*, C07030.
21. Iwamoto, K.; Ohshima, K.I.; Tamura, T. Improved mapping of sea ice production in the Arctic Ocean using AMSR-E thin ice thickness algorithm. *J. Geophys. Res. Oceans* **2014**, *119*, 3574–3594.

22. Cavalieri, D.J.; Parkinson, C.L.; Gloersen, P.; Comiso, J.C.; Zwally, H.J. Deriving long-term time series of sea ice cover from satellite passive-microwave multisensor data sets. *J. Geophys. Res. Oceans* **1999**, *104*, 15803–15814.
23. Hall, D.; Key, J.; Casey, K.; Riggs, G.; Cavalieri, D. Sea ice surface temperature product from MODIS. *IEEE Trans. Geosci. Remote Sens.* **2004**, *42*, 1076–1087.
24. Ackerman, S.; Frey, R.; Strabala, K.; Liu, Y.; Gumley, L.; Baum, B.; Menzel, P. *Discriminating Clear-Sky from Cloud with MODIS Algorithm Theoretical Basis Document (MOD35)*, Version 6.1; Technical Report for MODIS Cloud Mask Team, Cooperative Institute for Meteorological Satellite Studies, University of Wisconsin: Wisconsin, WI, USA, 2010.
25. Dee, D.P.; Uppala, S.M.; Simmons, A.J.; Berrisford, P.; Poli, P.; Kobayashi, S.; Andrae, U.; Balmaseda, M.A.; Balsamo, G.; Bauer, P.; et al. The ERA-Interim reanalysis: Configuration and performance of the data assimilation system. *Q. J. R. Meteor. Soc.* **2011**, *137*, 553–597.
26. Liu, Y.; Key, J.R. Less winter cloud aids summer 2013 Arctic sea ice return from 2012 minimum. *Environ. Res. Lett.* **2014**, *9*, 044002.
27. Yu, Y.; Rothrock, D.A. Thin ice thickness from satellite thermal imagery. *J. Geophys. Res.* **1996**, *101*, 25753–25766.
28. Yu, Y.; Lindsay, R. Comparison of thin ice thickness distributions derived from RADARSAT Geophysical Processor System and advanced very high resolution radiometer data sets. *J. Geophys. Res.* **2003**, *108*, doi:10.1029/2002JC001319.
29. Drucker, R.; Martin, S.; Moritz, R. Observations of ice thickness and frazil ice in the St. Lawrence Island polynya from satellite imagery, upward looking sonar, and salinity/temperature moorings. *J. Geophys. Res.* **2003**, *108*, doi:10.1029/2001JC001213.
30. Willmes, S.; Krumpen, T.; Adams, S.; Rabenstein, L.; Haas, C.; Hoelemann, J.; Hendricks, S.; Heinemann, G. Cross-validation of polynya monitoring methods from multisensor satellite and airborne data: a case study for the Laptev Sea. *Can. J. Remote Sens.* **2010**, *36*, S196–S210.
31. Adams, S.; Willmes, S.; Schroeder, D.; Heinemann, G.; Bauer, M.; Krumpen, T. Improvement and sensitivity analysis of thermal thin-ice retrievals. *IEEE Trans. Geosci. Remote Sens.* **2013**, *51*, 3306–3318.
32. Preußner, A.; Willmes, S.; Heinemann, G.; Paul, S. Thin-ice dynamics and ice production in the Storfjorden polynya for winter seasons 2002/2003–2013/2014 using MODIS thermal infrared imagery. *Cryosphere* **2015**, *9*, 1063–1073.
33. Paul, S.; Willmes, S.; Heinemann, G. Long-term coastal-polynya dynamics in the Southern Weddell Sea from MODIS thermal-infrared imagery. *Cryosphere* **2015**, *9*, 2027–2041.
34. Tamura, T.; Ohshima, K.I.; Markus, T.; Cavalieri, D.J.; Nihashi, S.; Hirasawa, N. Estimation of thin ice thickness and detection of fast ice from SSM/I Data in the Antarctic Ocean. *J. Atmos. Oceanic Technol.* **2007**, *24*, 1757–1772.
35. Tamura, T.; Ohshima, K.I.; Nihashi, S. Mapping of sea ice production for Antarctic coastal polynyas. *Geophys. Res. Lett.* **2008**, *35*, L07606.
36. Willmes, S.; Adams, S.; Schröder, D.; Heinemann, G. Spatio-temporal variability of polynya dynamics and ice production in the Laptev Sea between the winters of 1979/80 and 2007/08. *Polar Res.* **2011**, *30*, doi:10.3402/polar.v30i0.5971.
37. Adams, S.; Willmes, S.; Heinemann, G.; Rozman, P.; Timmermann, R.; Schröder, D. Evaluation of simulated sea-ice concentrations from sea-ice/ocean models using satellite data and polynya classification methods. *Polar Res.* **2011**, *30*, doi:10.3402/polar.v30i0.7124.
38. Markus, T.; Burns, B.A. A method to estimate subpixel-scale coastal polynyas with satellite passive microwave data. *J. Geophys. Res.* **1995**, *100*, 4473–4487.
39. Kern, S.; Spreen, G.; Kaleschke, L.; de La Rosa, S.; Heygster, G. Polynya Signature Simulation Method polynya area in comparison to AMSR-E 89 GHz sea-ice concentrations in the Ross Sea and off the Adélie Coast, Antarctica, for 2002–05: First results. *Ann. Glaciol.* **2007**, *46*, 409–418.
40. Paul, S.; Willmes, S.; Gutjahr, O.; Preußner, A.; Heinemann, G. Spatial feature reconstruction of cloud-covered areas in daily MODIS composites. *Remote Sens.* **2015**, *7*, 5042–5056.
41. Box, J.E.; Cohen, A.E. Upper-air temperatures around Greenland: 1964–2005. *Geophys. Res. Lett.* **2006**, *33*, L12706.

42. Overland, J.E.; Francis, J.A.; Hanna, E.; Wang, M. The recent shift in early summer Arctic atmospheric circulation. *Geophys. Res. Lett.* **2012**, *39*, doi:10.1029/2012GL053268.
43. Osborn, T.J. Winter 2009/2010 temperatures and a record-breaking North Atlantic Oscillation index. *Weather* **2011**, *66*, 19–21.
44. Häkkinen, S.; Hall, D.K.; Shuman, C.A.; Worthen, D.L.; DiGirolamo, N.E. Greenland ice sheet melt from MODIS and associated atmospheric variability. *Geophys. res. lett.* **2014**, *41*, 1600–1607.
45. Hanna, E.; Cropper, T.E.; Jones, P.D.; Scaife, A.A.; Allan, R. Recent seasonal asymmetric changes in the NAO (a marked summer decline and increased winter variability) and associated changes in the AO and Greenland Blocking Index. *Int. J. Climatol.* **2014**, *35*, doi:10.1002/joc.4157.
46. Stroeve, J.C.; Maslanik, J.; Serreze, M.C.; Rigor, I.; Meier, W.; Fowler, C. Sea ice response to an extreme negative phase of the Arctic Oscillation during winter 2009/2010. *Geophys. Res. Lett.* **2011**, *38*, L02502.
47. Steffen, K. Ice conditions of an Arctic polynya: North Water in winter. *J. Glaciol.* **1986**, *32*, 383–390.
48. Samelson, R.; Barbour, P. Low-level jets, orographic effects, and extreme events in Nares Strait: A model-based mesoscale climatology. *Mon. Wea. Rev.* **2008**, *136*, 4746–4759.
49. Kanamitsu, M.; Ebisuzaki, W.; Woollen, J.; Yang, S.K.; Hnilo, J.; Fiorino, M.; Potter, G. NCEP-DOE AMIP-II Reanalysis (R-2). *Bull. Amer. Meteor. Soc.* **2002**, *83*, 1631–1643.
50. Lindsay, R.; Wensnahan, M.; Schweiger, A.; Zhang, J. Evaluation of seven different atmospheric reanalysis products in the Arctic. *J. Climate* **2014**, *27*, 2588–2606.
51. Kwok, R.; Toudal Pedersen, L.; Gudmandsen, P.; Pang, S.S. Large sea ice outflow into the Nares Strait in 2007. *Geophys. Res. Lett.* **2010**, *37*. L03502.



© 2015 by the authors; licensee MDPI, Basel, Switzerland. This article is an open access article distributed under the terms and conditions of the Creative Commons by Attribution (CC-BY) license (<http://creativecommons.org/licenses/by/4.0/>).

## **6 Publication III: Circumpolar Thin-Ice Regions and Ice Production in the Arctic: Results from MODIS Thermal Infrared Imagery for 2002/2003 to 2014/2015 with a regional focus on the Laptev Sea**

Written by

**Andreas Preußer**, Günther Heinemann, Sascha Willmes and Stephan Paul

Published: 15 December 2016

This paper is reprinted from the journal 'The Cryosphere' (TC) with permission from Copernicus Publishing under the Creative Commons by Attribution (CC-BY) license 3.0 [Preußer et al. 2016].

The candidates contribution to this paper was that he carried out the complete analysis and drafted the manuscript, including the preparation all figures and tables. All co-authors were, with varying degree, involved in the initial set-up of the algorithm and contributed to the writing of the manuscript.



The Cryosphere, 10, 3021–3042, 2016  
www.the-cryosphere.net/10/3021/2016/  
doi:10.5194/tc-10-3021-2016  
© Author(s) 2016. CC Attribution 3.0 License.



## Circumpolar polynya regions and ice production in the Arctic: results from MODIS thermal infrared imagery from 2002/2003 to 2014/2015 with a regional focus on the Laptev Sea

Andreas Preußer<sup>1</sup>, Günther Heinemann<sup>1</sup>, Sascha Willmes<sup>1</sup>, and Stephan Paul<sup>2</sup>

<sup>1</sup>Department of Environmental Meteorology, Fac. of Regional and Environmental Sciences, University of Trier, Behringstr. 21, Trier, 54296, Germany

<sup>2</sup>Alfred Wegener Institute, Helmholtz Centre for Polar and Marine Research, Am Handelshafen 12, 27570 Bremerhaven, Germany

Correspondence to: Andreas Preußer (preusser@uni-trier.de)

Received: 31 May 2016 – Published in The Cryosphere Discuss.: 21 July 2016

Revised: 14 November 2016 – Accepted: 23 November 2016 – Published: 15 December 2016

**Abstract.** High-resolution MODIS thermal infrared satellite data are used to infer spatial and temporal characteristics of 17 prominent coastal polynya regions over the entire Arctic basin. Thin-ice thickness (TIT) distributions ( $\leq 20$  cm) are calculated from MODIS ice-surface temperatures, combined with ECMWF ERA-Interim atmospheric reanalysis data in an energy balance model for 13 winter seasons (2002/2003 to 2014/2015; November to March). From all available MODIS swath data, daily thin-ice thickness composites are computed in order to derive quantities such as polynya area and total thermodynamic (i.e., potential) ice production. A gap-filling approach is applied to account for cloud and data gaps in the MODIS composites. All polynya regions combined cover an average thin-ice area of  $226.6 \pm 36.1 \times 10^3$  km<sup>2</sup> in winter. This allows for an average total winter-accumulated ice production of about  $1811 \pm 293$  km<sup>3</sup>, whereby the Kara Sea region, the North Water polynya (both 15%), polynyas on the western side of Novaya Zemlya (20%), as well as scattered smaller polynyas in the Canadian Arctic Archipelago (all combined 12%) are the main contributors. Other well-known sites of polynya formation (Laptev Sea, Chukchi Sea) show smaller contributions and range between 2 and 5%. We notice distinct differences to earlier studies on pan-Arctic polynya characteristics, originating in some part from the use of high-resolution MODIS data, as the capability to resolve small-scale ( $> 2$  km) polynyas and also large leads are increased. Despite the short record of 13 winter seasons, positive trends in ice production are detected for several regions

of the eastern Arctic (most significantly in the Laptev Sea region with an increase of  $6.8$  km<sup>3</sup> yr<sup>-1</sup>) and the North Water polynya, while other polynyas in the western Arctic show a more pronounced variability with varying trends. We emphasize the role of the Laptev Sea polynyas as being a major influence on Transpolar Drift characteristics through a distinct relation between increasing ice production and ice area export. Overall, our study presents a spatially highly accurate characterization of circumpolar polynya dynamics and ice production, which should be valuable for future modeling efforts of atmosphere–ice–ocean interactions in the Arctic.

### 1 Introduction

The sea-ice cover in the Arctic is subject to continuous changes through a variety of thermodynamic and dynamic processes, which are driven by atmosphere and ocean dynamics. Areas of open water and thin ice, i.e., polynyas and leads, are characteristic features in this icescape with a huge influence on local physical, biological and chemical processes at the interface between the atmosphere and the ocean (Barber and Massom, 2007).

Especially during winter, the presence of open water and thin ice leads to increased ocean-to-atmosphere heat fluxes, thereby allowing new ice production and brine release as well as generally strong modifications of both the atmospheric boundary layer and upper ocean layers (Ebner et al., 2011;

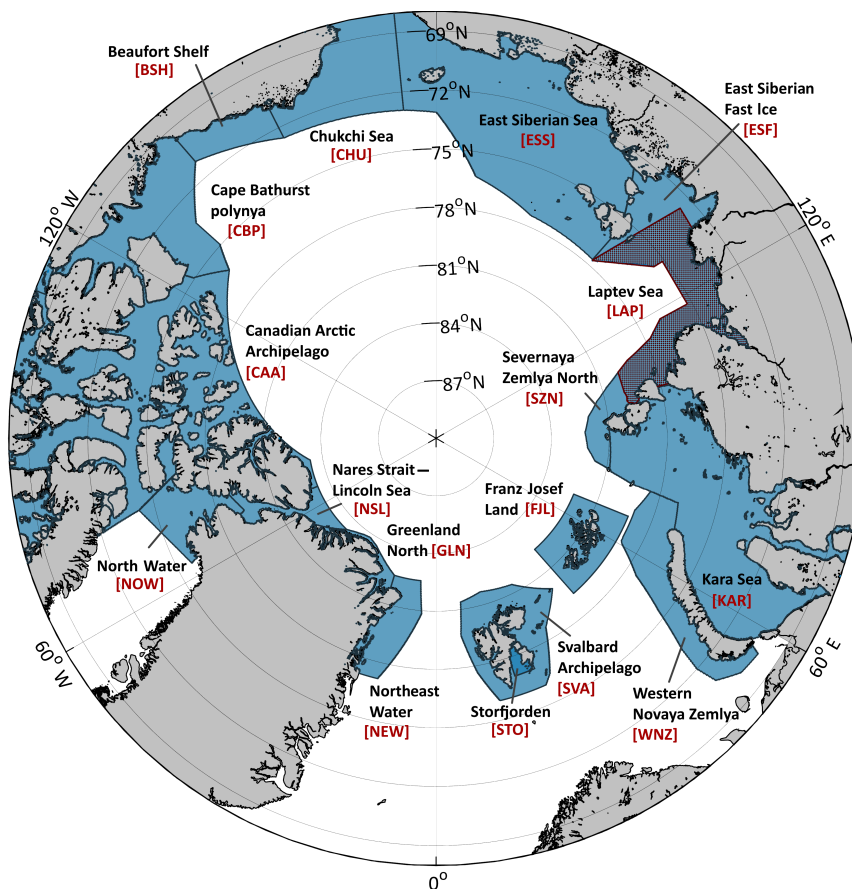


**Figure 1.** Map of all investigated areas of interest located in the Arctic, north of 68° N. Except for the Laptev Sea (red frame), all other applied polynya masks are marked in blue and enclose the typical location of each polynya in wintertime.

Gutjahr et al., 2016). Hence, an accurate assessment of winter sea-ice production in the Arctic is of vital interest for the understanding of Arctic sea-ice dynamics, the annual sea-ice mass balance and, in general, for the verification of climate and ocean models. In the case of the Arctic, it is widely considered that the main mechanism for polynya and lead openings is divergent ice motions caused by wind-induced stress (Smith et al., 1990). Therefore, most Arctic polynyas can be found adjacent to or in the proximity of a fixed obstacle such as the coastline, attached land-fast ice or ice bridges under offshore-wind conditions (Williams et al., 2007). While the time of formation, the duration and the spatial extent of a polynya can be highly variable from year to year, their location of formation is generally rather stable (Morales-Maqueda et al., 2004). Leads are, in contrast, far more variable both in space and time (Willmes and Heinemann, 2016). Regular monitoring of these open-water and thin-ice areas with a high spatial accuracy is therefore a crucial step to be able to detect long-term changes, potential linkages and feedbacks to other environmental compartments as well as spatial and temporal patterns.

Based on the inventory of Barber and Massom (2007), we here define a total of 17 individual polynya regions in the Arctic north of 68° N (Fig. 1). Some of these areas are designed to match reference areas in previous studies (e.g., Kern, 2008). The areal extent, i.e. the total ocean area, of each subregion is depicted in Table 1. The vast majority of polynyas in our study are located around the Arctic shelf areas, with the largest fraction in the Siberian shelf region (East Siberian Sea (ESS), Laptev Sea (LAP), Severnaya Zemlya North (SZN), Kara Sea (KAR) and Western Novaya Zemlya (WNZ)). Other well-known sites of polynya formation are the North Water (NOW) polynya in northern Baffin Bay, several other frequently appearing thin-ice zones around northern Greenland (Nares Strait–Lincoln Sea (NSL), Greenland North (GLN), Northeast Water (NEW) polynya), the Storfjorden (STO) polynya in the Svalbard Archipelago (SVA), a number of smaller polynya locations around Franz Josef Land (FJL), the Canadian Arctic Archipelago (CAA), as well as the Beaufort Shelf (BSH), Cape Bathurst polynya (CBP) and Chukchi Sea (CHU). The marginal ice zone (MIZ) in the Fram Strait and northern Barents Sea is mostly excluded

**Table 1.** Areal extents (i.e., total ocean area) of all applied polynya masks in km<sup>2</sup>. Furthermore, the interannual average amount of MODIS swaths that could be used for calculating daily composites in a given region is indicated, together with the interannual average daily MODIS coverage (decimal cover fraction ranging from 0 to 1 with their respective standard deviations) before (COV2) and after (COV4) application of the spatial feature reconstruction (SFR) for each polynya region from 2002–2003 to 2014–2015 (November to March). The abbreviation “ccs” denotes confident clear-sky coverage, while “HQ mcp” are high-quality mixed-cover pixels where either MODIS or ERA-Interim medium cloud cover feature reconstruction cloud signals in the daily composites. In addition, the average thin-ice thickness (TIT, in cm) inside each polynya region (for all TIT ≤ 0.2 m) is given together with its standard deviation. An overview on all applied predefined polynya masks is given in Fig. 1.

Region	Total ocean area (10 <sup>3</sup> km <sup>2</sup> )	Avg. number of MODIS swaths (d <sup>-1</sup> )	COV2		COV4	Avg. TIT (cm)
			(ccs, HQ mcp)	(ccs, HQ mcp, SFR)		
Beaufort Shelf (BSH)	91.6	6	0.76 ± 0.03		0.97 ± 0.02	14.0 ± 0.5
Canadian Arctic Archipelago (CAA)	719.6	14	0.82 ± 0.03		0.96 ± 0.01	13.7 ± 0.2
Cape Bathurst (CBP)	311.6	10	0.81 ± 0.03		0.98 ± 0.01	14.1 ± 0.4
Chukchi Sea (CHU)	286.0	5	0.55 ± 0.04		0.79 ± 0.03	12.8 ± 0.4
East Siberian Fast Ice (ESF)	110.1	8	0.77 ± 0.04		0.96 ± 0.01	14.3 ± 0.3
East Siberian Sea (ESS)	904.1	9	0.70 ± 0.03		0.92 ± 0.01	14.0 ± 0.3
Franz Josef Land (FJL)	140.1	13	0.79 ± 0.04		0.97 ± 0.02	11.7 ± 0.8
Greenland North (GLN)	33.8	13	0.67 ± 0.04		0.81 ± 0.04	16.3 ± 0.4
Kara Sea (KAR)	725.5	14	0.75 ± 0.04		0.95 ± 0.02	11.7 ± 1.1
Laptev Sea (LAP)	281.1	12	0.80 ± 0.03		0.98 ± 0.01	13.5 ± 0.5
Northeast Water (NEW)	112.0	13	0.81 ± 0.03		0.98 ± 0.01	13.7 ± 0.5
North Water (NOW)	110.1	13	0.85 ± 0.04		0.97 ± 0.01	11.5 ± 0.5
Nares Strait–Lincoln Sea (NSL)	55.5	14	0.83 ± 0.03		0.96 ± 0.01	13.6 ± 1.0
Storfjorden (STO)	11.7	9	0.75 ± 0.04		0.95 ± 0.03	9.2 ± 1.7
Svalbard Archipelago (SVA+STO)	204.3	13	0.68 ± 0.06		0.90 ± 0.04	7.2 ± 1.0
Severnaya Zemlya North (SZN)	65.3	12	0.80 ± 0.04		0.98 ± 0.01	13.5 ± 0.6
Western Novaya Zemlya (WNZ)	211.6	12	0.60 ± 0.07		0.83 ± 0.04	6.8 ± 1.6
Total	436.2	73*	0.75 ± 0.04		0.93 ± 0.02	12.7 ± 0.6

\* Not the sum of all regions, as single MODIS swaths may cover multiple regions at the same time.

in our investigations due to a variety of potential ambiguities originating from ocean heat fluxes and a high interannual variability of the MIZ in terms of location and extent. However, in order to ensure consistency with previous studies, the MIZ is to some extent included in the CHU, STO, NOW, WNZ and KAR areas. For those regions, this implies that the characteristics derived here may contain periods with extensive ice-free conditions, first and foremost in early winter.

Pan-Arctic estimations of daily thin-ice thickness (TIT) and ice production in polynyas were previously published by Tamura and Ohshima (2011) and Iwamoto et al. (2014), who both presented newly developed empirical thin-ice algorithms. Therein, commonly used passive microwave remote sensing data from the Special Sensor Microwave/Imager (SSM/I) and Advanced Microwave Scanning Radiometer-EOS (AMSR-E) satellite sensors are related to reference thin-ice thicknesses from Advanced Very High Resolution Radiometer (AVHRR) and Moderate Resolution Imaging Spectroradiometer (MODIS) thermal infrared data, based on a characteristic inverse relationship between the surface brine volume fraction and the thickness of sea ice (Iwamoto et al.,

2014). In both studies, the advantages of passive microwave systems (complete daily coverage in the Arctic with almost no influence of clouds) come at the cost of quite coarse spatial resolutions (6.25–25 km), which strongly limit the ability to resolve small and/or narrow thin-ice areas in close proximity to coastlines or along fast-ice edges (Preußer et al., 2015a).

According to Willmes et al. (2011), a retrieval of long-term ice production is challenging for several reasons. The derivation of polynya area needs to be addressed with spatial and temporal resolutions that are sufficient for capturing the seasonal and regional dynamics of polynya events (Winsor and Björk, 2000; Morales-Maqueda et al., 2004; Tamura et al., 2008; Willmes et al., 2010). Furthermore, the heat loss over the polynya has to be calculated, which requires detailed information about the fraction of open water, the ice thickness and its distribution within the polynya. The distribution of thin-ice largely affects the heat loss by providing feedback on the ice-surface temperature, thereby altering the vertical temperature gradients both through the ice as well as towards the lower atmospheric boundary layer. No less important, an accurate calculation of heat loss requires a state-of-

the-art approach regarding the parametrization of the surface energy balance, turbulent fluxes of latent and sensible heat and the conductive heat flux through the ice. Thus, detailed (i.e., region-specific and ideally highly resolved) information on meteorological quantities and correct formulations for the turbulent exchange coefficient for heat ( $C_H$ ) are of particular importance (Gutjahr et al., 2016).

In order to address those challenges, the prime focus of this study is aimed towards the derivation of daily spatial thin-ice thickness distributions, which allows for a pan-Arctic retrieval of associated quantities like polynya area and thermodynamic ice production. We make use of a high-resolution long-term record of thermal-infrared data from MODIS, as measured ice-surface temperatures can be combined with atmospheric reanalysis data in a 1-D energy balance model (Adams et al., 2013) to obtain ice thicknesses up to 50 cm (Sect. 3.1). Based on these daily distributions and taking into account the necessary compensation for inherent cloud and data gaps (Sect. 3.2), the amount of new sea-ice formation can be determined (Sect. 3.3). In Sect. 4, our achieved results will be presented and discussed before closing this paper with final conclusions and prospects for further investigations. In recent studies using the same methodology based on MODIS data, we focused on the Storfjorden polynya (Preußner et al., 2015b) and NOW polynya (Preußner et al., 2015a). The present study has a strong focus on the Laptev Sea region due to significant changes over the last decade (Sect. 4.2) as well as its role as a central component of the Transpolar Drift, a large-scale drift system where ice from the Siberian coastal regions is advected across the Arctic Ocean and through the Fram Strait.

## 2 Data

### 2.1 MODIS ice-surface temperatures

The MOD/MYD29 Collection 5 sea-ice product (Hall et al., 2004; Riggs et al., 2006) is used to derive thin-ice thickness (TIT) from MODIS satellite data. It features swath data of ice-surface temperatures (ISTs) from both MODIS instruments on board the Terra and Aqua polar-orbiting satellite platforms. All swath data offer a spatial resolution of  $1 \times 1 \text{ km}^2$  at nadir and include a basic cloud-screening procedure using the MODIS cloud mask (MOD/MYD35; Ackerman et al., 2010). In general, the accuracy of the MOD/MYD29 ISTs is given with 1–3 K (Hall et al., 2004). All IST swaths covering the Arctic Ocean and adjacent seas were extracted using metadata information for each MODIS swath. Subsequently, single swaths were mapped onto a common equirectangular (reference) grid covering all areas north of  $68^\circ \text{N}$ , with the output resolution set at 2 km in order to account for the decreasing spatial resolution of the MODIS sensor off-nadir. For our analysis between 2002/2003 and 2014/2015 (November to March), we used a total of 143 000

MODIS swaths for the complete Arctic domain, averaging at 73 scenes per day. The average number of MODIS scenes per day and per polynya region are additionally listed in Table 1.

### 2.2 ERA-Interim atmospheric reanalysis data

In order to provide the necessary atmospheric input for the applied surface energy balance model, the following variables from the European Center for Medium-Range Weather Forecasts (ECMWF) ERA-Interim reanalysis product (Dee et al., 2011) are used: 2 m temperature, 2 m dew point temperature, 10 m wind speed and mean sea-level pressure. As the use of the MOD/MYD35 cloud mask during nighttime often contains misclassifications and ambiguities from undetected clouds and sea smoke, we additionally utilize ERA-Interim medium cloud cover (MCC) information. The study of Liu and Key (2014) demonstrated that the ERA-Interim MCC fields correspond closely to the MODIS-derived cloud patterns throughout the seasons and can therefore be used as an additional quality control during the TIT retrieval. The temporal resolution of all variables is 6 h, so that each single MODIS swath can be linked to the closest time step of the atmospheric fields from ERA-Interim for the calculation of thin-ice thickness, with the overall average time difference being  $90 \pm 52 \text{ min}$  (max. 180 min). The data set is provided by ECMWF at a spatial resolution of  $0.75^\circ$  (approx. 80 km). All ERA-Interim data fields are linearly interpolated and projected on the common reference grid in order to match the higher spatial resolution of MODIS data.

## 3 Methodology

### 3.1 MODIS thin-ice thickness retrieval using a surface energy balance model

We derive daily TIT distributions up to 50 cm by using an approach that follows the work of Yu and Rothrock (1996), Yu and Lindsay (2003) and Drucker et al. (2003). The core of this approach is a one-dimensional energy balance model, in which IST and the thin-ice thickness are related to atmospheric radiation fluxes and turbulent heat fluxes. The original method of Yu and Rothrock (1996) was first improved and modified by Willmes et al. (2010) and Adams et al. (2013). More recently, the latest modifications of the algorithm are described in detail in Preußner et al. (2015a, b) and Paul et al. (2015b), together with comprehensive information on applied parametrization schemes that are used to calculate atmospheric radiation fluxes and turbulent heat fluxes. A complete overview on the currently used data-processing chain is given in Fig. 2.

There are certain limitations and simplifications attached to this procedure to derive TIT. First, it is only applicable to clear sky conditions, as clouds and sea smoke would strongly alter the recorded IST (Riggs et al., 2006). Second, we only use nighttime scenes to avoid potential ambiguities from in-

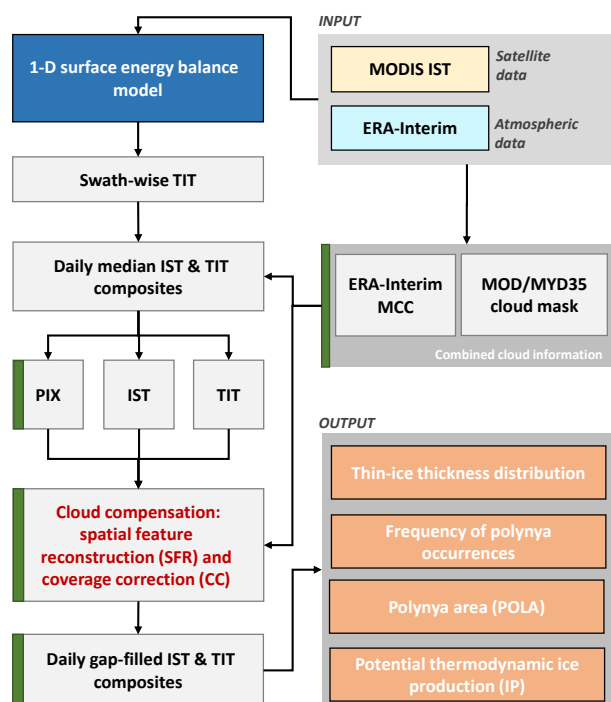


**Figure 2.** Schematic overview on the current version of the MODIS thin-ice thickness (TIT) retrieval scheme based on Paul et al. (2015b) and Preußer et al. (2015a). The most recent updates are marked in green and are mainly aimed towards an additional cloud-cover treatment. Aside from indicated abbreviations, “IST”, “MCC” and “PIX” denote the ice-surface temperature, medium cloud cover and persistence index, respectively.

cident shortwave radiation (Yu and Lindsay, 2003; Adams et al., 2013). Furthermore, newly formed ice is assumed to be free of snow and the temperature profile between the surface (IST) and the lower boundary of the ice (constant; freezing point of sea water) is linear. Following this assumption, the approach does not explicitly discriminate between different ice types within a polynya, as TIT is solely derived from calculating the heat conduction in/through an assumed layer of ice (aside from subsequent gap filling; see Sect. 3.2).

The study of Adams et al. (2013) presented a sensitivity analysis of the TIT retrieval, which revealed average uncertainties of  $\pm 1.0$ ,  $\pm 2.1$  and  $\pm 5.3$  cm for TIT classes 0–5, 5–10 and 10–20 cm, respectively. Between 20 and 50 cm, the uncertainty increases considerably. Therefore, we constrain our analysis accordingly as a thickness range of  $TIT \leq 0.2$  m is widely regarded as a threshold for polynya areas and for estimates of thermodynamic ice production in polynyas (Yu and Rothrock, 1996; Adams et al., 2013; Haid et al., 2015).

### 3.2 Calculation of daily TIT composites and correction of cloud and data gaps

Because of the restriction to nighttime scenes, a less frequent MODIS coverage is present, especially towards the end (February to March) of each winter season. In order to increase the MODIS coverage for all considered areas (Fig. 1), we derive daily composites of IST and TIT from the total number of available MODIS swaths covering the Arctic domain on a given day (compare Sect. 2.1). Following the procedure described in Sect. 3.1, the TIT is first calculated from each single swath on its own. Subsequently, the daily median TIT per pixel is calculated and stored alongside its corresponding IST value and daily median energy-balance components. The median is preferred over a simple average in order to reduce the potential risk of erroneously high or low values in single swaths, originating from unidentified clouds, for example.

As described in Sect. 2.2, we additionally make use of ERA-Interim MCC fields as an indicator for potential cloud coverage during the generation of daily TIT composites. Previous studies showed that a threshold of 75 % cloud cover in the MCC fields is quite effective in identifying, filtering and removing potentially cloud-affected areas (Paul et al., 2015b; Preußer et al., 2015a). The combined MODIS and ERA-Interim cloud information allows for the assignment of four different quality classes for each pixel in the daily composites: (1) confident clear-sky pixels (“ccs”; clear-sky MODIS and ERA-Interim), (2) mixed-covered pixels (“mcp”; ratio between clear-sky input swaths and the total number of input swaths per pixel), (3) definitive cloud-covered pixels (“dcc”; both in MODIS and ERA-Interim) and (4) completely uncovered pixels (“ucp”).

Paul et al. (2015b) introduced an additional cloud-cover check based on the daily persistence of each pixel that is classified as thin ice ( $TIT \leq 0.2$  m). Misclassified thin-ice detections (i.e., clouds) are generally associated with low-persistence values due to their more mobile nature and displacements on sub-daily timescales. In contrast, polynyas show a higher spatial and temporal persistence due to their distinct formation mechanisms (Sect. 1). Leads, however, may be discarded by this criteria, since they generally have a low persistence due to their short lifetime and sea-ice drift caused by wind, ocean currents and tides. Based on these simple but distinct relations, we use a pixel-wise persistence index (PIX), defined as the ratio between the total number of MODIS swaths that feature thin ice at a given pixel location and the total number of swaths that feature clear-sky conditions at the same pixel position.

All derived quality attributes (MCC filter, cloud-cover information, PIX) are utilized in the Spatial Feature Reconstruction (SFR) algorithm (Paul et al., 2015a), which was recently successfully applied on a regional scale in both the Antarctic and Arctic to increase the information about otherwise cloud-covered areas (Paul et al., 2015b; Preußer et al.,

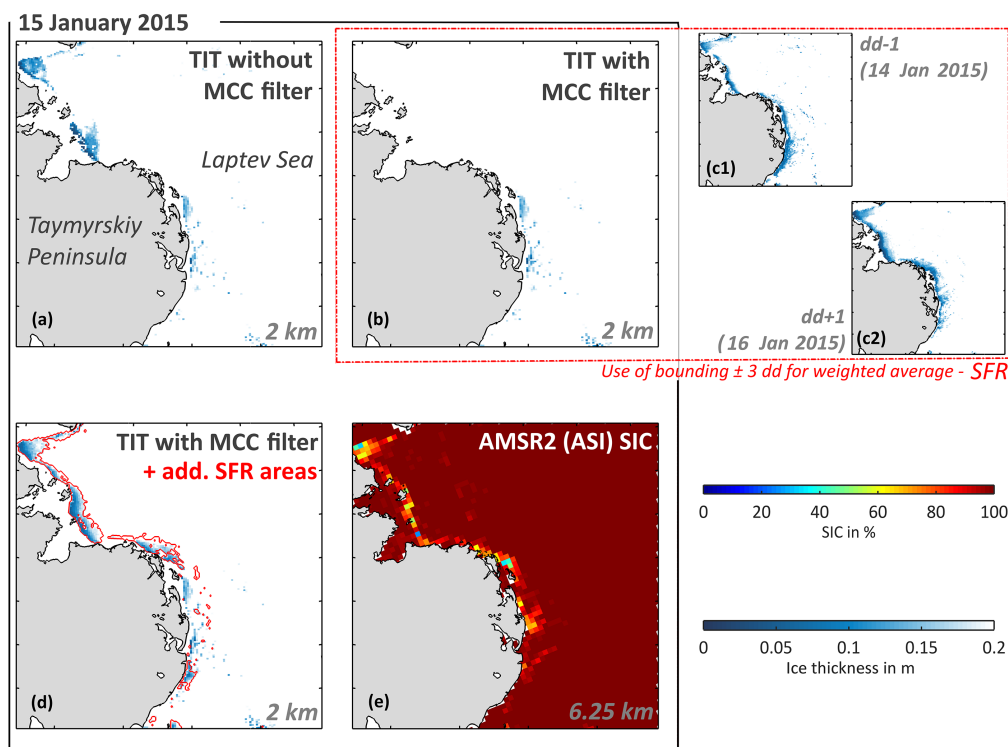


**Figure 3.** Different stages in the MODIS thin-ice thickness (TIT up to 0.2 m) processing chain for a single exemplary day (15 January 2015). Subpanels (a), (b), (c1/c2) and (d) all feature a subset (northwestern Laptev Sea) from daily pan-Arctic TIT composites, with (a) showing the daily TIT without any cloud treatment aside from the MOD35 cloud mask and (b) the resulting TIT distribution after applying the ERA-Interim MCC filter. Panels (c1) and (c2) feature 2 bounding days with a better coverage of thin-ice thickness as a reference for the highest relative contribution in the SFR algorithm. The resulting spatial distribution of TIT after application of SFR is shown in panel (d), with new additional reconstructed areas (up to 20 cm) marked in red. A comparison with Advanced Microwave Scanning Radiometer-2 (AMSR2) ASI sea-ice concentrations (Spren et al., 2008; Beitsch et al., 2014; University of Bremen) from the same date is given in (e). The respective grid resolution is given in the lower right corner of each subpanel.

2015a). The basic principle is that cloud-induced gaps in the daily TIT composites are compared with the TIT of the surrounding 6 days. In doing so, a probability of thin-ice occurrence is derived using a weighted composite of the days surrounding an initial day of interest (DOI). As in previous studies, we applied the following set of weights:  $w_3 = 0.02$  ( $\text{DOI} \pm 3$ ),  $w_2 = 0.16$  ( $\text{DOI} \pm 2$ ) and  $w_1 = 0.32$  ( $\text{DOI} \pm 1$ ). The probability threshold remains fixed at  $\text{th} = 0.34$  and needs to be surpassed in order to assign “new” probable polynya pixels. Paul et al. (2015a) showed that this combination is less restrictive in terms of missing MODIS coverage in close proximity to the initial DOI. The procedure is applied on all areas with identified low-quality data (low persistence, cloud covered), so that indicated gaps can be filled with new information on potential thin-ice occurrences. For these areas, new TIT and IST values are pixel-wise allocated using a weighted average (same set of weights  $w_1$  to  $w_3$  applied) of the surrounding 6 days (Paul et al., 2015b; Preußer et al., 2015a). Table 1 gives an overview on the achieved MODIS coverage before and after application of the SFR al-

gorithm. On a pan-Arctic level, the average (2002/2003 to 2014/2015) MODIS coverage is increased from around 0.75 (confident clear-sky and high-quality mixed-cover pixels featuring clear-sky conditions in more than 50 % of all daily input swaths) to 0.93 (including SFR areas), with certain regions performing better (e.g., CBP, LAP, NEW, SZN) and some other regions noticeably worse (CHU, GLN, WNZ).

A total of 66 case studies in the Brunt Ice Shelf region of Antarctica demonstrated the generally good performance of the algorithm in comparison to more intelligible approaches by realistically reproducing artificially cloud-covered thin-ice areas with an average spatial correlation of 0.83 and a RMSE of 1904 km<sup>2</sup> (Paul et al., 2015a). When compared to reference runs based on equally weighted and in some cases shorter time intervals, the SFR procedure featuring the weights  $w_1$  to  $w_3$  ( $\text{DOI} \pm 3$  days) listed above yielded superior results both in spatial correlation and reconstructed polynya extent, regardless of the temporal polynya evolution (e.g., opening–closing events). As an additional example from the Arctic (northwestern Laptev Sea), Fig. 3 vi-

sualizes the basic principle of the SFR algorithm, together with a qualitative comparison of Advanced Microwave Scanning Radiometer 2 (AMSR2) sea-ice concentration (SIC) data (Spreen et al., 2008; Beitsch et al., 2014). As a first step, the MCC filter eliminates potentially cloud-influenced areas that are in this case located north of the Taymyr Peninsula (Laptev Sea, Russia). One could argue that this filtering is a bit harsh, but we chose a more conservative threshold to minimize the risk of “false” thin-ice pixels. Afterwards, the SFR algorithm is applied and a new gap-filled TIT composite (Fig. 3d) is produced. In this particular example from 15 January 2015, the reconstructed TIT distribution compares well with locations of lower SIC from AMSR2 (Fig. 3e), while maintaining the increased spatial detail at the same time. Based on this example and successful applications in previous works by the authors (Paul et al., 2015a, b; Preußner et al., 2015a), we conclude that the applied schemes to compensate and correct cloud effects work reasonably well on a pan-Arctic scale and allow for a fair comparison to other commonly used remote sensing approaches to infer polynya characteristics, with limitations regarding the reconstruction of leads.

### 3.3 Derivation of ice production and polynya area

Ice production rates are derived by assuming that the entire heat loss at the ice surface to the overlying atmosphere contributes to new ice formation (Tamura et al., 2007, 2008; Willmes et al., 2011). Components for the following equation (Eq. 1) can be taken from calculated and gap-filled daily MODIS composites.

$$\frac{\partial h}{\partial t} = \frac{-\bar{Q}_{\text{ice}}}{\rho_{\text{ice}} \cdot L_f} \quad (1)$$

Therein,  $\frac{\partial h}{\partial t}$  denotes the ice production rate,  $\bar{Q}_{\text{ice}}$  is the daily mean conductive heat flux through the ice,  $\rho_{\text{ice}}$  is the density of the ice ( $\rho_{\text{ice}} = 910 \text{ kg m}^{-3}$ ; Timco and Frederking, 1996) and  $L_f$  is the latent heat of fusion of sea ice ( $L_f = 0.334 \text{ MJ kg}^{-1}$ ; Tamura and Ohshima, 2011). Concerning  $L_f$ , Tamura and Ohshima (2011) noted that an accurate value for areas of high ice production is not known so far. Following the work of Martin (1981), Tamura and Ohshima (2011) argued that frazil ice consists of freshwater ice crystals enclosed within a thin saline layer and that frazil ice production rates are of similar magnitudes to freshwater ice production rates. Consequently, we also use fixed values for  $\rho_{\text{ice}}$  and  $L_f$  in order to ensure comparability with earlier studies focusing on sea-ice production in (Arctic) polynyas (e.g., Willmes et al., 2011; Tamura and Ohshima, 2011; Iwamoto et al., 2014). However, this simplification may introduce an additional error source in our estimates due to spatially and temporally varying conditions for ice formation. Note that the negative sign in Eq. (1) implies that the atmospheric heat flux is positive when the surface gains energy, and at

the same time it assures that ice production only takes place when there is a net energy loss from the surface. According to the surface energy balance, the heat flux  $\bar{Q}_{\text{ice}}$  is equal to the total atmospheric heat loss (sum of net radiation, turbulent latent and sensible heat flux). We do not consider an ocean heat flux, although it might potentially reduce thermodynamic ice growth in certain areas of the Chukchi Sea (Hirano et al., 2016), the Canadian Arctic Archipelago (Hannah et al., 2009; Melling et al., 2015) and northern Baffin Bay (e.g., Steffen, 1985; Yao and Tang, 2003) by as much as 23–27 % in case of the NOW polynya (Tamura and Ohshima, 2011; Iwamoto et al., 2014). The volume ice production rate  $\frac{\partial V}{\partial t}$  (IP) is calculated by multiplying  $\frac{\partial h}{\partial t}$  with the areal extent of each pixel in the regarded region. Ice production rates are calculated for each pixel with a TIT  $\leq 0.2$  m, and afterwards extrapolated to daily rates. However, it has to be noted that daily IP rates inhibit a positive bias due to the exclusive use of both nighttime and clear-sky MODIS scenes. The former is mainly of concern during the late autumn and early spring period when polar night conditions are absent, while the latter circumstance is unavoidable throughout each winter when relying on optical and infrared remote sensing data. Since low-level clouds reduce the net radiative loss by about  $50 \text{ W m}^{-2}$  in polar regions (Heinemann and Rose, 1990; König-Langlo and Augstein, 1994), the restriction to cloud-free conditions in the daily composites results in a positive bias in IP. Considering an average clear-sky fraction of  $73 \pm 8 \%$  per pixel from all input swaths in a given daily composite and assuming that not all clouds are low level, the overestimation of net energy loss by our method can be estimated to be less than  $10 \text{ W m}^{-2}$ , which corresponds to less than 0.4 m IP per winter.

The daily polynya area (POLA, in  $\text{km}^2$ ) in each polynya mask (Fig. 1) is defined as the accumulated total area of all thin-ice pixels with a TIT  $\leq 0.2$  m. Remaining MODIS coverage gaps after the application of the SFR approach (e.g., prolonged periods of persistent cloud cover, meaning no coverage on more than 3 consecutive days) are handled by additionally applying an extrapolation approach (coverage-correction; CC) to calculated POLA and IP estimates, which yields daily values with an error margin of 5 to 6 % (Preußner et al., 2015b). In case of very persistent cloud cover inside the respective reference areas and a resulting daily MODIS coverage below 50 % (i.e., COV4 < 0.5), both daily POLA and IP are linearly interpolated from bounding days.

The complete period from November to March each winter is considered for the calculation of POLA/IP, which implies that the values derived here are potentially influenced by shifts in the timing of freeze onset during the early freezing season (November to December). For potentially MIZ-influenced regions (CHU, SVA, NOW, WNZ, KAR), this has to be considered when comparing metrics derived for the full winter period (November to March).

For topographically complex regions like Greenland and the Arctic fjords, recent studies revealed shortcomings of the

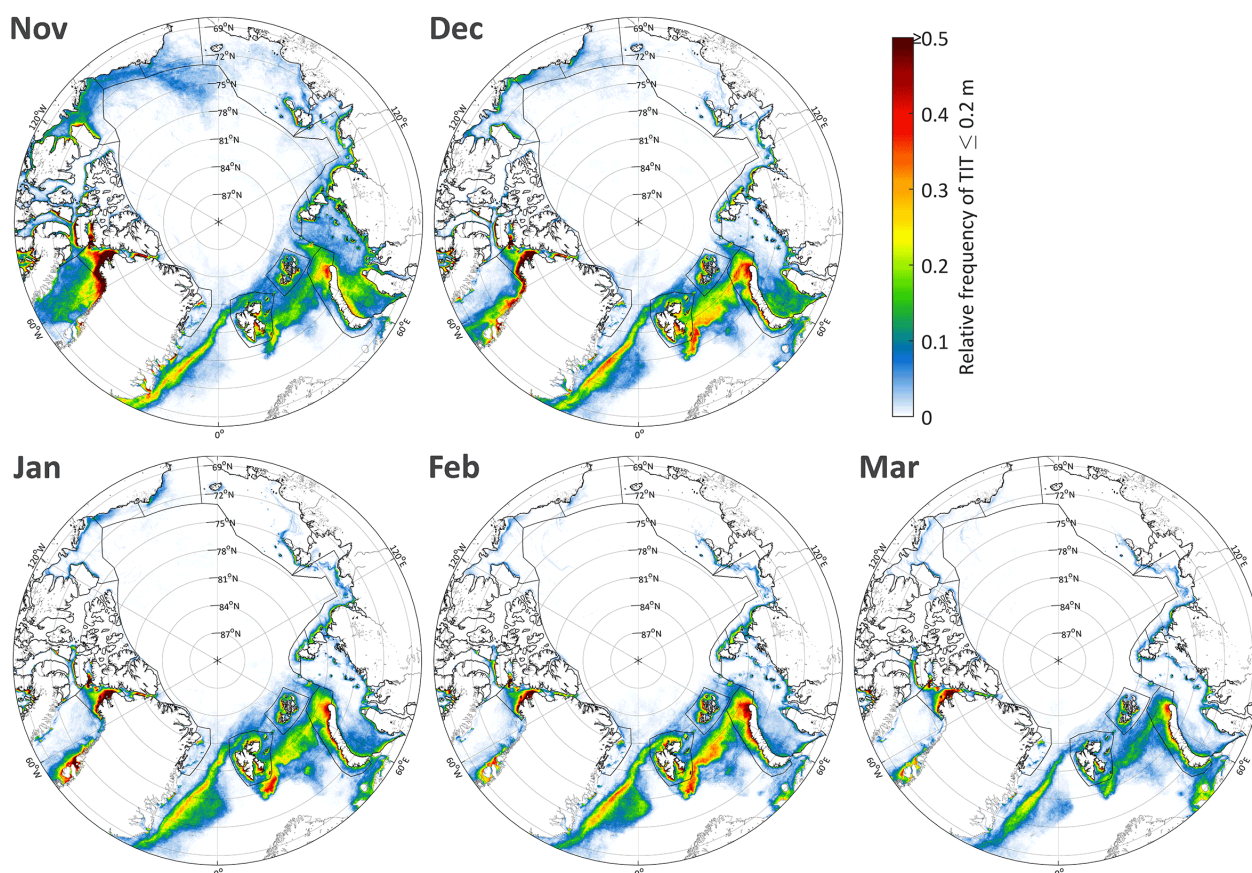


**Figure 4.** Average winter (November to March) frequencies of  $TIT \leq 0.2$  m in the Arctic between winters 2002/2003 and 2014/2015. For each month, frequencies are calculated per pixel as the fraction of days with a  $TIT \leq 0.2$  m relative to the 13-year investigation period. Note that only thin-ice areas within the margins of a given polynya mask (dashed black lines; see Fig. 1) are used for further analysis, while all other areas are discarded. Hence, areas with high TIT frequencies in the MIZ around the Fram Strait and northern Barents Sea are excluded from further analysis due to potential ambiguities originating from ocean heat fluxes and a high interannual variability of the MIZ in terms of location and extent.

coarse-resolution ERA-Interim data regarding the representation of mesoscale spatial features in the wind field, such as tip jets, channeling effects or other topography-induced phenomena related to locally increased wind speeds (e.g., Moore et al., 2016). Thus, ERA-Interim shows a tendency to underestimate peak wind speeds (Moore et al., 2016), which might in some cases induce a negative bias (lower heat fluxes, smaller POLA or less IP) in regions where polynya formation is strongly influenced by the local topography (e.g., CAA, NOW, NEW, SZN). In our study, the usage of ERA-Interim is motivated by ensuring comparability to similar studies (e.g., Iwamoto et al., 2014) as well as the constraint that higher-resolution atmospheric data sets such as the Arctic System Reanalysis (ASRv1 – 30 km; Bromwich et al., 2015) are currently not available for the complete time period from 2002 to 2015.

## 4 Results and discussion

### 4.1 Thin-ice dynamics, polynya area and thermodynamic ice production in the Arctic for 2002/2003 to 2014/2015

Interannual average values for  $TIT \leq 0.2$  m are listed in Table 1 for each polynya region. They range between 6.8 cm (WNZ) and 16.3 cm (GLN), with an overall average of about  $12.7 \pm 0.6$  cm. The underlying long-term time series of average winter TIT within each polynya (not shown) reveal a tendency towards decreasing thin-ice thicknesses in almost every region (e.g., up to 2.5 cm per decade in the Storfjorden polynya), with the only exceptions being the CAA, GLN and NEW.

Monthly thin-ice frequencies, calculated per pixel as the fraction of days with a  $TIT \leq 0.2$  m relative to the 13-year investigation period, are presented in Fig. 4. Frequencies of



larger than 0.5 are primarily found around the Canadian Arctic, first and foremost in the NOW polynya and the eastern CAA. More specifically, coastal areas around Devon Island and southwestern Ellesmere Island (Hells Gate, Cardigan Strait) and larger areas at the eastern exits of Lancaster Sound and Jones Sound are well visible and have previously been related to tidal currents and slightly increased ocean heat fluxes (Hannah et al., 2009; Melling et al., 2015). Other areas with similar magnitudes include the Storfjorden polynya and coastal areas (north)west of Novaya Zemlya. In addition, elongated thin-ice areas along the Siberian shelf (Laptev and Kara seas, frequencies around 0.05 to 0.35 each month) are well delineated. Locations of frequent thin-ice occurrences in the Kara Sea are in accordance with results from the study of Kern (2008). The northern Barents Sea, Franz Josef Land and the Svalbard Archipelago also feature quite high appearance rates of around 0.1 to 0.3. Contrary to earlier reports (Barber and Massom, 2007), the Northeast Water (NEW) polynya in northeastern Greenland (approx. 81° N, 13° W) neither shows any signs of disappearance, nor is it limited to the spring to late autumn period. With average frequencies of around 0.1 to 0.25 each month in winter, it is more likely to be categorized as a regularly forming polynya. Comparatively low frequencies below 0.15 (especially from January to March) are primarily found in the Beaufort and Chukchi seas as well as in the East Siberian Sea. Vast fast-ice areas, e.g., along the Siberian coast, can be detected from monthly TIT frequencies, as these areas usually appear at fixed locations attached to the shore and TIT frequencies tend towards zero as the ice quickly thickens by congelation ice growth. Hence, our 13-year record of monthly TIT-occurrence rates offers the potential to further develop optimized automatic methods for a regular Arctic-wide mapping of monthly fast-ice extents and could thereby complement currently existing approaches from earlier studies (e.g., Yu et al., 2014; Mahoney et al., 2014; Selyuzhenok et al., 2015).

Compared to the study of Willmes and Heinemann (2016), leads are only weakly visible in these long-term averages (frequencies below 0.05–0.1). In Fig. 4, leads are mainly located in the area of the Beaufort Sea and north of Greenland (shear zones), which can be mainly attributed to their relatively high spatial and temporal persistence. Frequent lead occurrences in the East Siberian Sea found by Willmes and Heinemann (2016), for example, are not reflected in our study. In some regions, however, the influence of (shelf) bathymetry and associated ocean currents on the spatial distribution of polynya and lead occurrences is also visible in the TIT frequencies derived here (e.g., eastern exit Vilkitsky Strait, Hanna Shoal on the northern Chukchi Shelf, northern ESS).

In Figs. 5 and 6, the interannual variability of the average POLA (in km<sup>2</sup>) and accumulated IP (in km<sup>3</sup>) is presented for all examined polynya regions. In both figures, the difference between the beginning (November to December) and end (January to March) of the freezing (winter) period is

additionally highlighted. Concerning POLA, it shows that the largest average winter extents are found in the NOW, WNZ and KAR areas. The study of Preußner et al. (2015a) demonstrated that the large POLA values in the NOW region are part of a (non-significant) long-term increase of average polynya extents between 1978 and 2015. In case of polynyas in the proximity of Novaya Zemlya, our average winter value for POLA of around  $42 \times 10^3$  km<sup>2</sup> is fairly close to the respective value from Iwamoto et al. (2014) ( $49 \times 10^3$  km<sup>2</sup>), despite the circumstances that their study covered an extended winter period from September to May and featured a different mask area, which stretched over some part of the western Kara Sea. As mentioned earlier, Kern (2008) presented POLA values for the Kara Sea. His retrievals are based on approximately the same reference area (Fig. 1), which in this case allows for a fair comparison to the numbers presented here. It shows that the average POLA in the late freezing season reveals similar magnitudes in recent years. During the period from 1979 to 2004, the average POLA (in Kern, 2008: January to April) ranged between 1 and  $5 \times 10^4$  km<sup>2</sup> (except for 1995, which was around  $6 \times 10^4$  km<sup>2</sup>), which is close to the range of the results presented here for January to March (Fig. 5; Table 2). Although the estimated positive trend in POLA remains non-significant for the Kara Sea as in Kern (2008), the magnitude of the trend in the late freezing period (January to March, around 9000 km<sup>2</sup> decade<sup>-1</sup>) seems to have increased from 2400 km<sup>2</sup> decade<sup>-1</sup> (Kern, 2008) to around 9000 km<sup>2</sup> decade<sup>-1</sup> over the last 13 years. The interannual POLA variability in all regions is generally pronounced, but it is especially large for smaller polynyas and/or thin-ice regions such as the NSL, NEW and ESS. Concerning seasonal differences, it appears that some regions (e.g., NEW, GLN, LAP, SZN) have the tendency towards larger thin-ice areas during the freeze-up period since the time period of approximately 2006/2007 to 2007/2008. About 8 to 10 polynya regions show distinct positive trends of up to 18 390 km<sup>2</sup> per decade (KAR), with only the LAP, ESF and SZN regions being significant (two-sided *t* test) with  $p \leq 0.05$ . Interestingly, subregions located in the proximity of the Beaufort Gyre (BSH and CBP) indicate very large thin-ice areas between November and December 2007, shortly after the second lowest September sea-ice extent since 1979 (approx. 4.7 million km<sup>2</sup>; Parkinson and Comiso, 2013). This did not appear in a similar way in 2012 (record low of approx. 3.4 million km<sup>2</sup>). A detailed investigation shows that the freeze-up in the Beaufort Sea area was much slower in 2007 and extended until mid-December, while in 2012 the same area was ice-covered by 10 November. The study of Timmermans (2015) linked this significant delay in ice growth to upward mixing processes of ocean heat in the Canada Basin, originating from the release of stored solar heat input following summer 2007. This resulted in large areas with very thin ice (around 170 000 km<sup>2</sup>) from November to December and consequently allowed for huge amounts of

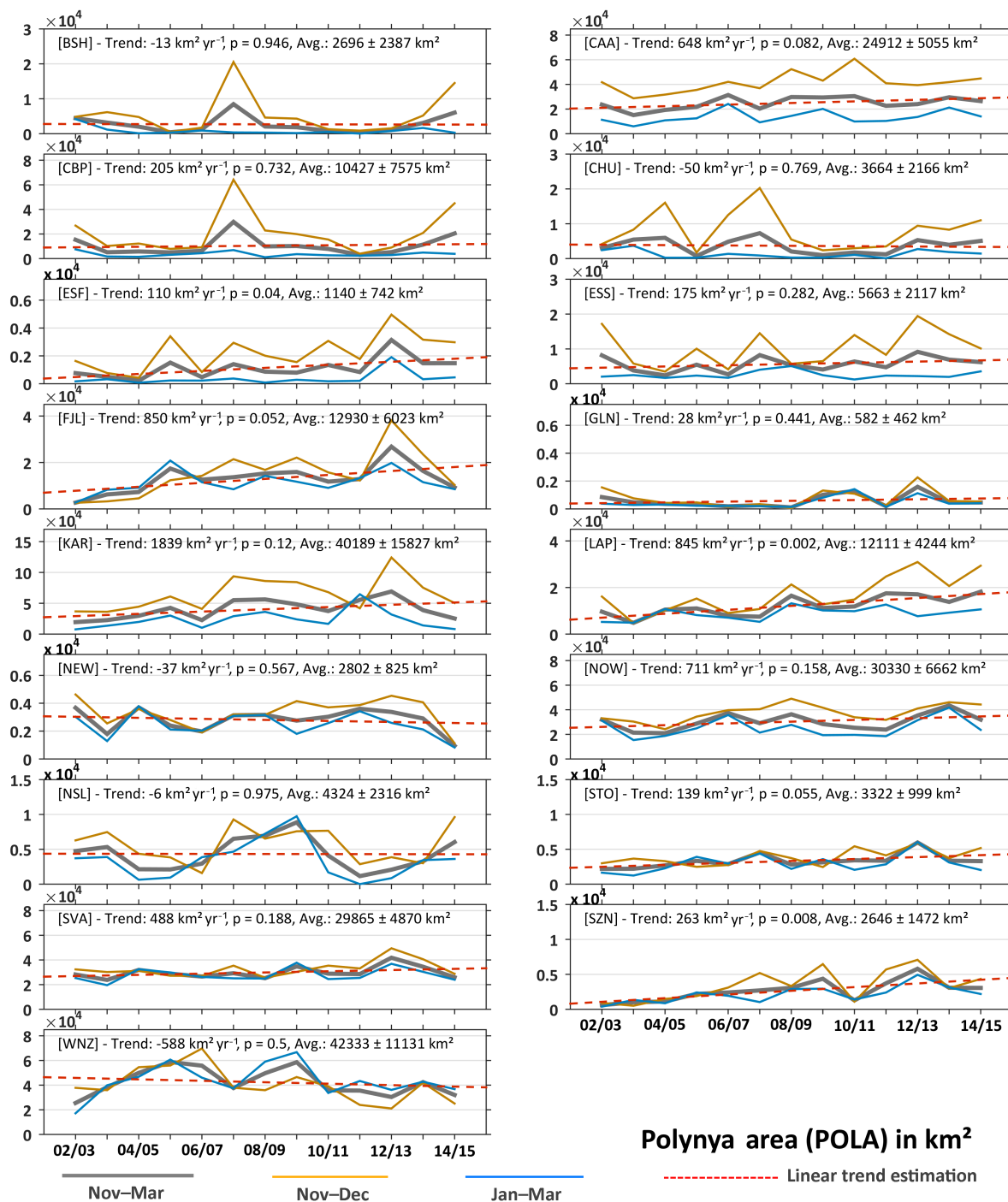


**Figure 5.** Regional time series of the annual average polynya area (POLA; TIT  $\leq 0.2$  m) in  $\text{km}^2$  from 2002/2003 to 2014/2015, together with a seasonal comparison (November to December vs. January to March) and a linear trend estimation. The estimated linear trend (in  $\text{km}^2 \text{ yr}^{-1}$ ), its  $p$  value and the interannual average POLA (in  $\text{km}^2$ ) are additionally listed in each subpanel. Please note the varying scale on each y axis.

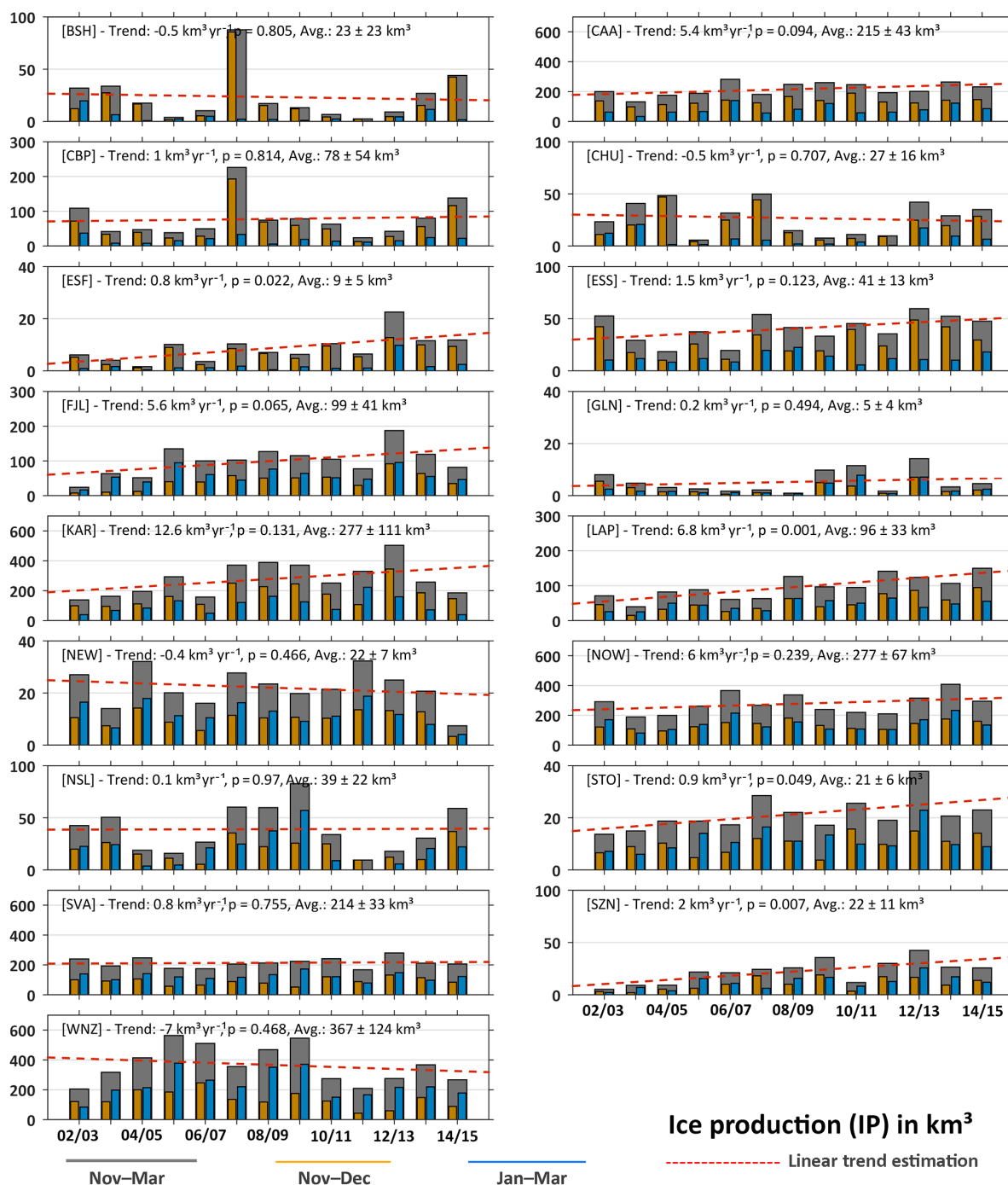


**Figure 6.** Regional time series of the annually accumulated ice production (IP) in  $\text{km}^3$  from 2002/2003 to 2014/2015, together with a seasonal comparison (November to December vs. January to March) and a linear trend estimation. The estimated linear trend (in  $\text{km}^3 \text{yr}^{-1}$ ), its  $p$  value and the interannual average IP (in  $\text{km}^3$ ) are additionally listed in each subpanel. Please note the varying scale on each y axis.

**Table 2.** Average polynya area (POLA) in km<sup>2</sup> in each polynya region between 2002/2003 and 2014/2015 (SFR cloud-cover correction applied). Aside from being based on the available winter period from November to March, it is further separated between the early freezing season (November to December) and the late freezing season (January to March). All values are derived from daily MODIS TIT composites after application of the predefined polynya masks (Fig. 1). Trends are additionally given, where underlined, bold and bold italic numbers denote statistical significance (two-sided *t* test) at the 90, 95 and 99 % levels, respectively.

Region	November to March		November to December		January to March	
	Avg. POLA (10 <sup>3</sup> km <sup>2</sup> )	Trend POLA (km <sup>2</sup> yr <sup>-1</sup> )	Avg. POLA (10 <sup>3</sup> km <sup>2</sup> )	Trend POLA (km <sup>2</sup> yr <sup>-1</sup> )	Avg. POLA (10 <sup>3</sup> km <sup>2</sup> )	Trend POLA (km <sup>2</sup> yr <sup>-1</sup> )
Beaufort Shelf (BSH)	2.7 ± 2.4	-13	5.5 ± 5.8	132	0.8 ± 1.1	-111
Canadian Arctic Archipelago (CAA)	24.9 ± 5.1	<u>648</u>	41.5 ± 8.3	958	13.7 ± 5.2	438
Cape Bathurst (CBP)	10.4 ± 7.6	205	20.6 ± 16.9	581	3.6 ± 2.0	-49
Chukchi Sea (CHU)	3.7 ± 2.2	-50	8.2 ± 5.7	-95	1.3 ± 1.1	-37
East Siberian Fast Ice (ESF)	1.1 ± 0.7	<b>110</b>	2.3 ± 1.3	<b>200</b>	0.4 ± 0.5	48
East Siberian Sea (ESS)	5.7 ± 2.1	175	10.3 ± 5.2	385	2.5 ± 1.1	33
Franz Josef Land (FJL)	12.9 ± 6.0	<u>850</u>	15.2 ± 9.7	<b>1565</b>	11.5 ± 4.9	380
Greenland North (GLN)	0.6 ± 0.5	28	0.8 ± 0.6	14	0.5 ± 0.4	37
Kara Sea (KAR)	40.2 ± 15.8	1839	64.9 ± 26.8	3209	23.5 ± 15.5	904
Laptev Sea (LAP)	12.1 ± 4.2	<b>845</b>	17.0 ± 8.0	<b>1559</b>	8.8 ± 2.7	<u>362</u>
Northeast Water (NEW)	2.8 ± 0.8	-37	3.3 ± 1.0	-10	2.4 ± 0.9	-55
North Water (NOW)	30.3 ± 6.7	711	37.7 ± 7.1	<b>1072</b>	25.4 ± 7.8	464
Nares Strait–Lincoln Sea (NSL)	4.3 ± 2.3	-6	5.7 ± 2.6	18	3.4 ± 2.8	-22
Storfjorden (STO)	3.3 ± 1.0	<u>139</u>	3.9 ± 1.1	<b>175</b>	2.9 ± 1.3	115
Svalbard Archipelago (SVA+STO)	29.9 ± 4.9	488	32.8 ± 6.5	732	27.9 ± 5.3	327
Severnaya Zemlya North (SZN)	2.6 ± 1.5	<b>263</b>	3.4 ± 2.2	<b>353</b>	2.1 ± 1.2	<b>203</b>
Western Novaya Zemlya (WNZ)	42.3 ± 11.1	-588	40.4 ± 13.8	<u>-1806</u>	43.6 ± 13.0	230
Total	226.6 ± 36.1	<b>5468</b>	309.4 ± 62.6	<u>8864</u>	171.3 ± 32.6	3151

latent and sensible heat to be released from the ocean, leading to extraordinary high IP values in these areas (Fig. 6).

Regarding IP, many of the features described above are also visible in the regional time series of Fig. 6. Contrary to Tamura and Ohshima (2011), the majority of polynya regions show overall positive (up to 126 km<sup>3</sup> per decade (KAR)) or no trends in winter ice production, and only four regions indicate a slight yet insignificant decrease over the last 13 years (BSH, CHU, NEW, WNZ). Complete overviews of calculated average POLA and IP values per region, together with their respective trends, are given in Tables 2 and 3, respectively. These overviews highlight the huge effect that seasonal differences (November to December vs. January to March) have on calculated average values and trends for the complete winter period from November to March. Consequently, the numbers discussed here should be regarded as winter integrals with potentially inherent effects originating from the timing of freeze-up onset. In cases such as the Kara Sea, Franz Josef Land, the Chukchi Sea and the Canadian Arctic Archipelago, for example, large thin-ice and potential open-water areas during the early freezing period in November and December imprint on the total winter averages as well as derived trends of POLA and IP, especially from 2007/2008 onwards. While the majority of polynyas also feature positive trends in the late freezing season from January to March, these trends are for the most part insignificant.

The average total ice production in Arctic polynyas sums up to 1811 ± 293 km<sup>3</sup> per winter. Thus, it lies in between previously determined average values of 2940 ± 373 km<sup>3</sup> (Tamura and Ohshima, 2011; 1992/1993 to 2007/2008) and 1178 ± 65 km<sup>3</sup> (Iwamoto et al., 2014; 2002/2003 to 2010/2011) per winter. We expect that the MODIS-derived quantities offer a valuable increase in both spatial and quantitative accuracy due to the use of high-resolution and gap-filled daily fields of thin-ice thicknesses. A shortening of the averaging interval for the period 2002/2003 to 2010/2011 (as in Iwamoto et al., 2014, but not accounting for differences in covered winter period) marginally reduces the average total ice production derived here by about 1–2 %. In order to assess apparent differences between our data set and the passive microwave data set from Iwamoto et al. (2014), a more direct comparison based on identical reference areas and the same winter period would be necessary.

A spatial overview of the average (2002/2003 to 2014/2015) accumulated ice production per winter (November to March) is presented in Fig. 7. Similar to Fig. 4, the NOW polynya stands out at first glance due to its high average ice production of up to 14 m per winter. However, smaller polynyas in the Canadian Arctic (around Devon Island) feature comparatively high values for ice production. Most other areas in the Arctic produce on average between 1 and 3 m of ice per winter, with a few noticeable exceptions like Franz Josef Land (about 4–5 m per winter), the northern tip of No-

**Table 3.** Average accumulated ice production (IP) in  $\text{km}^3$  in each polynya region between 2002/2003 and 2014/2015 (SFR cloud-cover correction applied). Aside from being based on the available winter period from November to March, it is further separated between the early freezing season (November to December) and the late freezing season (January to March). All values are derived from daily MODIS TIT composites after application of the predefined polynya masks (Fig. 1). Trends are additionally given, where underlined, bold and bold italic numbers denote statistical significance (two-sided  $t$  test) at the 90, 95 and 99 % levels, respectively.

Region	November to March		November to December		January to March	
	Acc. IP ( $\text{km}^3$ )	Trend IP ( $\text{km}^3 \text{yr}^{-1}$ )	Acc. IP ( $\text{km}^3$ )	Trend IP ( $\text{km}^3 \text{yr}^{-1}$ )	Acc. IP ( $\text{km}^3$ )	Trend IP ( $\text{km}^3 \text{yr}^{-1}$ )
Beaufort Shelf (BSH)	23 ± 23	−0.5	19 ± 23	0.0	5 ± 5	−0.4
Canadian Arctic Archipelago (CAA)	215 ± 43	<u>5.4</u>	136 ± 23	2.5	79 ± 31	2.9
Cape Bathurst (CBP)	78 ± 54	1.0	60 ± 48	1.1	18 ± 10	−0.1
Chukchi Sea (CHU)	27 ± 16	−0.5	20 ± 14	−0.3	7 ± 6	−0.2
East Siberian Fast Ice (ESF)	9 ± 5	<b>0.8</b>	7 ± 3	<b>0.6</b>	2 ± 2	0.3
East Siberian Sea (ESS)	41 ± 13	1.5	28 ± 13	1.3	13 ± 5	0.2
Franz Josef Land (FJL)	99 ± 41	<u>5.6</u>	42 ± 24	<b>4.1</b>	57 ± 22	1.5
Greenland North (GLN)	5 ± 4	0.2	3 ± 2	0.0	3 ± 2	0.2
Kara Sea (KAR)	277 ± 111	12.6	174 ± 76	9.0	104 ± 56	3.6
Laptev Sea (LAP)	96 ± 33	<b>6.8</b>	51 ± 24	<b>4.8</b>	45 ± 14	<b>2.0</b>
Northeast Water (NEW)	22 ± 7	−0.4	10 ± 3	0.0	12 ± 4	−0.4
North Water (NOW)	277 ± 67	6.0	135 ± 27	<u>3.4</u>	145 ± 45	2.6
Nares Strait–Lincoln Sea (NSL)	39 ± 22	0.1	20 ± 10	0.2	20 ± 16	−0.1
Storfjorden (STO)	21 ± 6	<b>0.9</b>	10 ± 4	<b>0.5</b>	11 ± 4	0.4
Svalbard Archipelago (SVA+STO)	214 ± 33	0.8	91 ± 24	1.6	123 ± 24	−0.8
Severnaya Zemlya North (SZN)	22 ± 11	<b>2.0</b>	10 ± 6	<b>0.9</b>	12 ± 6	<b>1.1</b>
Western Novaya Zemlya (WNZ)	367 ± 124	−7.0	136 ± 56	−6.8	231 ± 88	−0.2
Total	1811 ± 293	34.5	940 ± 178	<u>22.4</u>	871 ± 175	12.1

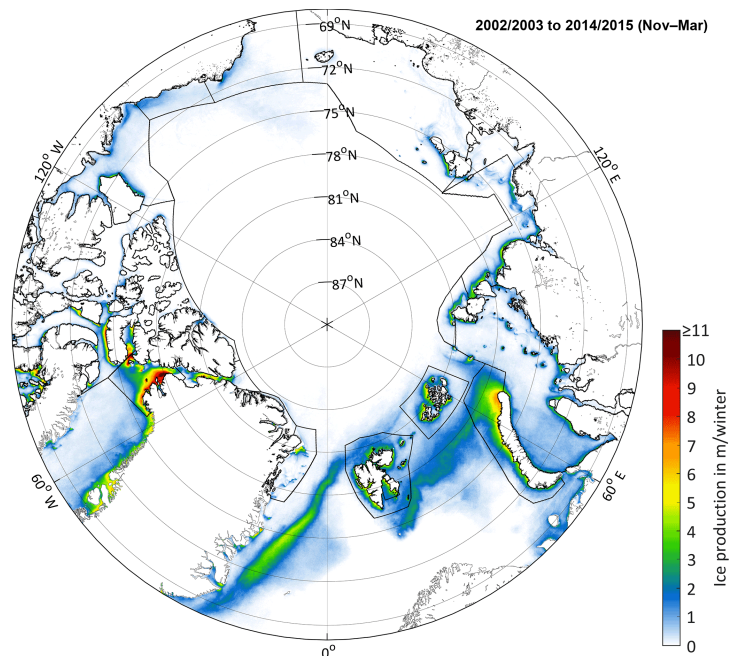


**Figure 7.** Average (2002/2003 to 2014/2015) accumulated ice production (m per winter) during winter (November to March) in the Arctic, north of  $68^\circ \text{N}$ . The margins of applied polynya masks (Fig. 1) are shown in black dashed lines.

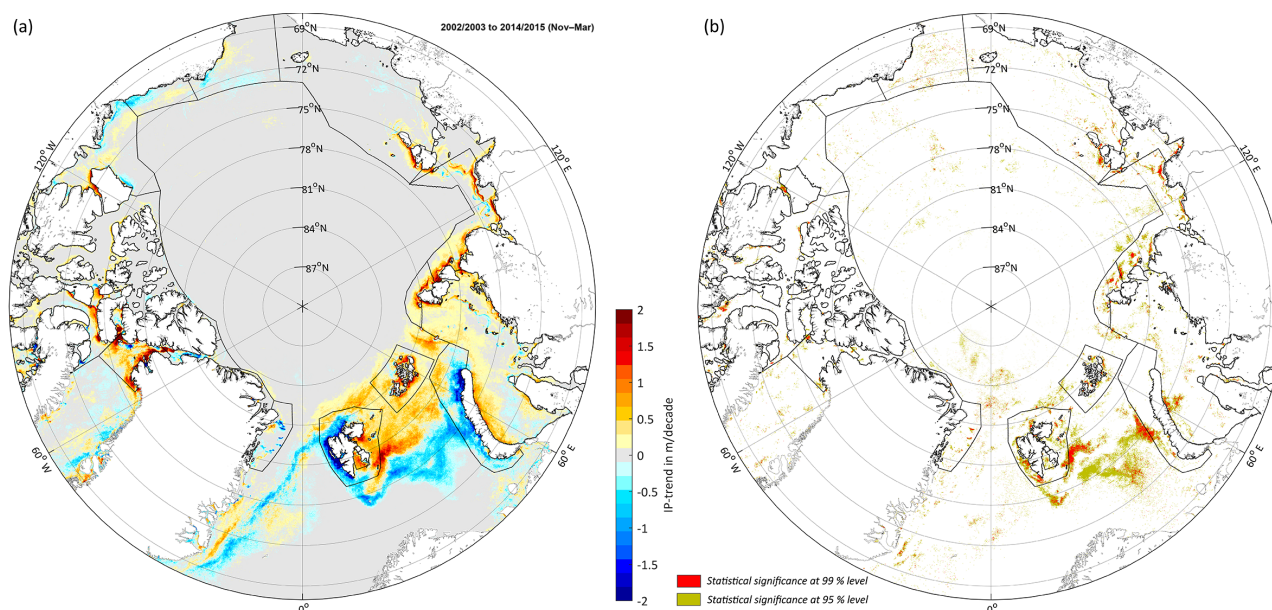


**Figure 8.** (a) Decadal trends (m per decade) of winter (November to March) ice production in the Arctic, north of  $68^{\circ}$  N. Trends are calculated by applying a linear regression to the annual accumulated IP per pixel for the period 2002/2003 to 2014/2015. Areas with statistical significance (based on a two-sided  $t$  test) at the 95 and 99 % level are depicted in (b). The margins of applied polynya masks (Fig. 1) are shown as black dashed lines.

vaya Zemlya (5–7 m per winter) and some coastal areas in the Kara Sea (1–4 m per winter). While the core areas of high ice production show a high resemblance to Iwamoto et al. (2014) with marginal differences in absolute numbers, MODIS is capable of providing enhanced spatial detail. This is especially valuable concerning the narrow thin-ice areas along the coast and fast-ice edges in the eastern part of the Arctic (Kara Sea, Laptev Sea, East Siberian Sea), as these areas are not resolved by the coarse-resolution passive microwave data (6.25 km; Iwamoto et al., 2014). This striking advantage is also reflected in the comparatively narrow fjords and bays or sounds around Greenland and the Canadian Archipelago, where a high ice production of up to 3 m per winter is found. While these observations, mostly related to differences in spatial resolution, could explain the discrepancy described above in average accumulated numbers to some extent (compare Preußner et al., 2015a), the net effect of a lower grid size cannot be quantified here.

Spatial trends between the winter seasons 2002/2003 and 2014/2015 (November to March) can be calculated by applying a linear regression to the annual accumulated IP per pixel. The resulting map is shown in Fig. 8a. Aside from many interesting small-scale patterns, two main conclusions can be drawn from this spatial overview: (1) while the trends identified in the western Arctic show no consistent pattern, large areas of the eastern Arctic are characterized by significant (two-sided  $t$  test; significance levels indicated in Fig. 8b) positive trends that can exceed 2 m per decade and (2) we ob-

serve opposing negative–positive IP trends along the coasts of the Laptev and Kara seas, which could be due to changes in fast-ice extent over the 13-year period. Decreasing fast-ice extents and durations in the eastern Arctic between 1976 and 2007 were recently described by Yu et al. (2014). In addition, Selyuzhenok et al. (2015) analyzed the fast ice in the southeastern Laptev Sea in more detail (1999 to 2013). While their study showed that the winter maximum fast-ice extent (around March to April) as well as the shape and location of the fast-ice edge did not vary significantly over the regarded time period, they likewise presented an overall decrease in the fast-ice season ( $-2.8 \text{ d yr}^{-1}$ ) due to later formation and earlier break-up. These described changes regarding the timing of fast-ice formation in early winter could explain the observed structures of positive–negative trends in the proximity of fast-ice areas.

In order to put these observations into context, we suppose that this characteristic pattern of opposing trends in the western and eastern Arctic as well as the apparently fast-ice-related structures in the Laptev Sea and Kara Sea could be connected to a fall freeze-up that has generally appeared later (Markus et al., 2009; Stroeve et al., 2014) in recent years, which itself is thought to result from a complex mixture and/or interplay of year-round steadily increasing (2 m) air temperatures (e.g., Cohen et al., 2014), distinct large-scale atmospheric patterns (e.g., Rigor et al., 2002) and the overall downward trend of total sea-ice extent and volume in the Arctic (e.g., Schweiger et al., 2011; Laxon et al., 2013).

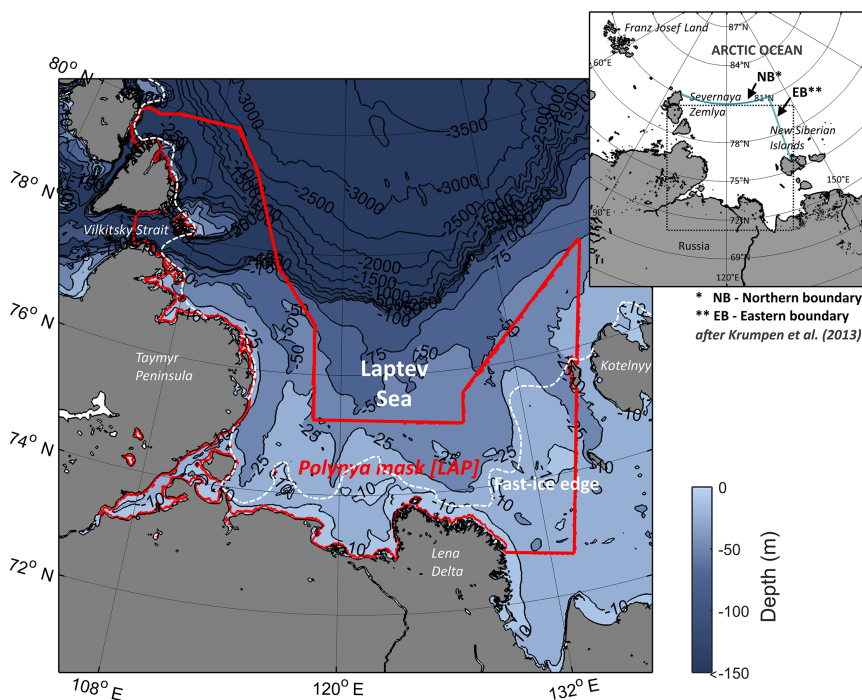


**Figure 9.** The geographical location of the Laptev Sea in the eastern Arctic. The applied polynya mask is marked in red, enclosing the locations of typical polynya formation along the coast and fast-ice edge (dashed white line; position derived from long-term thin-ice frequencies in March; Fig. 4). Flux gates from the study by Krumpfen et al. (2013) at the northern (NB) and eastern (EB) boundary of the Laptev Sea are shown in the inset map (cyan solid lines). Bathymetric data from Jakobsson et al. (2012) (IBCAO v3.0).

The latter implies a tendency towards a more fragile, and thus mobile, sea-ice cover in the Arctic, with a potentially increased sensitivity for external forcing mechanisms (i.e., strong winds and/or ocean currents) that are responsible for thin-ice formation in polynyas and leads. Since the Laptev Sea is one of the main regions with highly pronounced and significant positive trends in both POLA and IP throughout the complete winter period, the following section will take a closer look at polynya dynamics in the region.

#### 4.2 Regional focus – Laptev Sea

One main advantage of the high-resolution MODIS data is the ability to perform detailed investigations on a regional scale across the Arctic. The grid spacing of 2 km allows for the detection of relatively fine, delineated polynya structures and for more accurate statements about areas of high ice production than were possible in previous studies.

The Laptev Sea was previously described as a key region to investigate climatic changes in the Arctic shelf seas (ACIA, 2005), as it is one of the major source areas for sea-ice export into the Transpolar Drift system (Dethleff et al., 1998). As can be seen in Fig. 9, the Laptev Sea is located between the Severnaya Zemlya at the western boundary, the Lena River delta at the southern edge and the New Siberian Islands in the east (approximately 70–80° N, 100–140° E).

The water-mass composition in the Laptev Sea is temporarily quite variable, as there is a huge freshwater inflow during the summer and autumn period (around 750 km<sup>3</sup> per year; Rigor and Colony, 1997) and strong ice formation accompanied by brine rejection in polynyas during winter (Bauch et al., 2012). These processes significantly alter the stratification of the upper ocean layers as well as the salinity levels in the annual cycle. These and other recurring features of the sea-ice and ocean environments were recently illustrated and updated by Janout et al. (2016).

During the freezing period (from roughly October to June), fast ice forms along the coastlines of the Laptev Sea, which usually reaches its maximum areal extent by April. The approximate location of the fast-ice edge at the end of March is depicted in Fig. 9. For drifting sea ice, the fast-ice edge forms an advanced coastline with heavy ridging occurring along this edge during onshore wind events (Rigor and Colony, 1997). The combination of this fast-ice edge and offshore components of the mean wind patterns enable the formation of several flaw-lead polynyas across the Laptev Sea, which can reach widths of up to 200 km (Bareiss and Gørgen, 2005; Martin and Cavalieri, 1989; Ernsdorf et al., 2011; Adams et al., 2013).

When comparing previous studies dealing with ice production rates in the Laptev Sea (Dethleff et al., 1998;

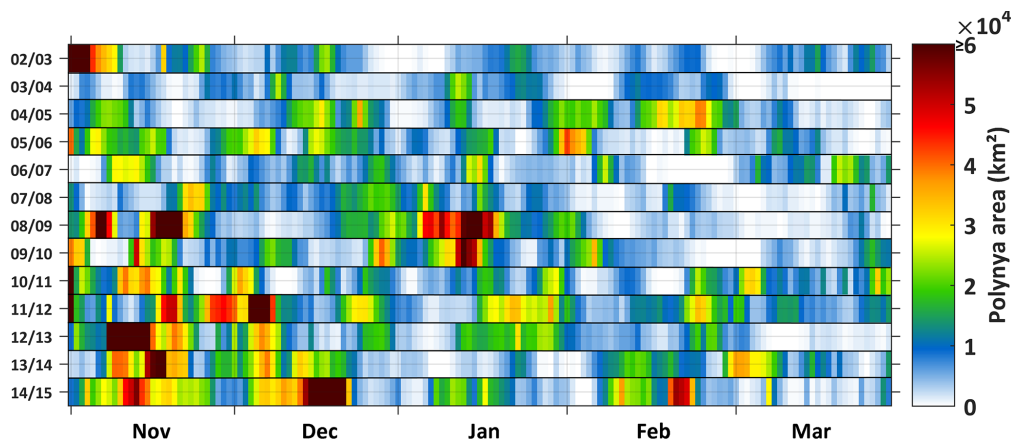


**Figure 10.** The daily polynya area ( $TIT \leq 0.2$  m) in the Laptev Sea region for the winter seasons 2002/2003 to 2014/2015. Values are calculated within the margins of the applied polynya mask (Fig. 1) and saturated at a level of  $6 \times 10^4 \text{ km}^2$  for a better discrimination of lower values.

Winsor and Björk, 2000; Dmitrenko et al., 2009; Willmes et al., 2011; Tamura and Ohshima, 2011; Bauer et al., 2013; Iwamoto et al., 2014; Gutjahr et al., 2016), it becomes clear that there are large differences depending on the applied methods and various data sets. In these studies, values for the accumulated ice production during an average winter season (“extended” winter period from November to April) range between  $55 \text{ km}^3$  (Willmes et al., 2011) for an approach using microwave and thermal infrared remote sensing data in combination with atmospheric reanalysis data and  $258 \text{ km}^3$  (Dethleff et al., 1998) when using a simple relationship between wind direction, wind speed, and polynya area. Estimated average values (September to May) from Tamura and Ohshima (2011) ( $152 \text{ km}^3$ ) and Iwamoto et al. (2014) ( $77 \text{ km}^3$ ) range in between. Although derived for different time periods and slightly varying reference areas, these large discrepancies highlight the relevance of applying improved, high-resolution approaches to quantify sea-ice production.

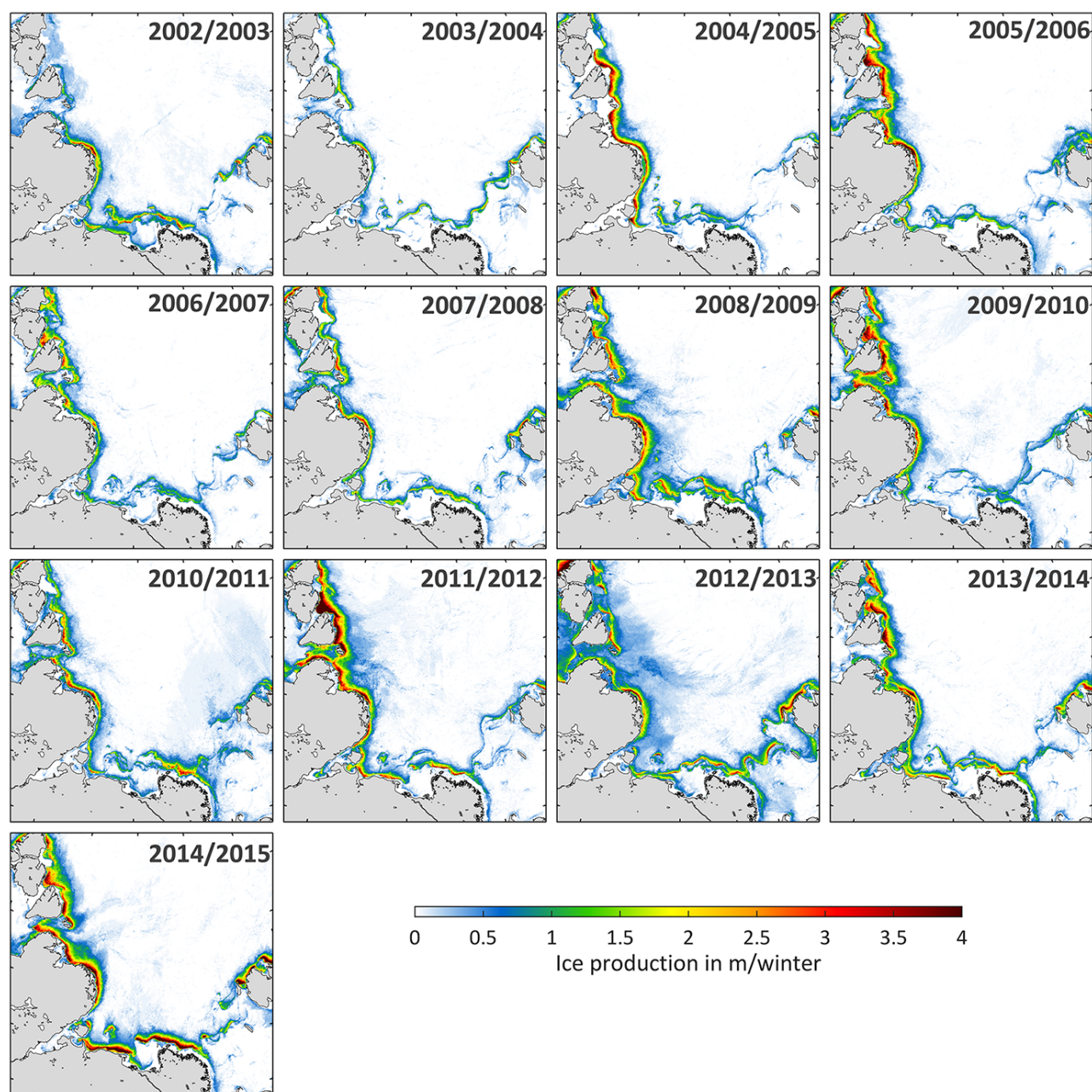
In order to give an overview of the long-term development of thin-ice areas ( $TIT \leq 0.2$  m) in the Laptev Sea, the daily POLA is presented in Fig. 10. It is evident that the largest areas of thin-ice appear on average in November and more recently also in December (compare Table 2). A tendency towards an increased duration of these polynya events can be observed. In the winter seasons 2008/2009 and 2009/2010, large POLA exceeding  $50\,000 \text{ km}^2$  were also observed in January, and another major polynya event can be noted for mid-February 2015. A pronounced seasonal variation is visible for the winter seasons 2004/2005, 2005/2006 and from 2010/2011 onwards, while the other years show less polynya activity (more lengthy periods with a closed polynya; white color in Fig. 10) and overall smaller polynya extents in February and March.

Figure 11 shows an annual comparison (2002/2003 to 2014/2015) of accumulated (November to March) ice pro-

duction (in m per winter) for the Laptev Sea. The highest ice production rates of sometimes more than 4 m per winter occur predominantly in the proximity of the Taymyr Peninsula and Severnaya Zemlya (western Laptev Sea), as well as along the southern fast-ice edge (mainly coastward of the regions with high ice production). However, ice production in the eastern Laptev Sea (west and north of the New Siberian Islands) shows a greater interannual variability. Furthermore, it is striking that the position of the fast-ice edge in Fig. 11 is highly variable over the 13-year record (as in Sect. 4.1, Fig. 8a). However, it has to be noted that certain bands of higher ice production, especially in the southeastern Laptev Sea, reflect the winter evolution of fast ice (compare Seluyzhenok et al., 2015) and are hence primarily related to the early winter period from November to December. Another interesting observation can be made in the Vilkitsky Strait, which is located in the western Laptev Sea south of Severnaya Zemlya (Fig. 9). The distribution of thin-ice areas contributing significantly to the total sea-ice production in that area seems to shift westwards towards the Kara Sea in several years (2005/2006 to 2012/2013 and 2014/2015). In some cases, the shape of these areas resembles an arch-type pattern of an ice bridge mechanism, a feature that commonly appears in the Nares Strait between Ellesmere Island and Greenland, for example (Williams et al., 2007).

Kruppen et al. (2013) discovered that most of the ice being incorporated in the Transpolar Drift originates from the western and central part of the Laptev Sea. Furthermore, it is indicated that the contribution from polynyas, while being generally small, is limited to events in the proximity of the Laptev Sea boundaries. As noted before, the northwestern Laptev Sea shows by far the largest contribution to the total winter ice production in the Laptev Sea polynyas, which implies a potential significant influence on the interannual variability of ice export during winter. In order to check this





**Figure 11.** Overview of winter (November to March) accumulated ice production (m per winter) in the Laptev Sea region between 2002/2003 and 2014/2015.

hypothesis, we compare annual accumulated IP values to independently derived ice-area export (IAE) values (both presented as anomalies and normalized with their standard deviation) in Fig. 12 for 2002/2003 to 2014/2015. IAE values are taken from the updated time series of Krumpfen et al. (2013), where they were calculated as the integral of the product between the eastward and northward component of the ice drift velocity and ice concentration at the northern boundary

(NB) and eastern boundary (EB) of the Laptev Sea, respectively. Similar to a high agreement between polynya area and across-boundary ice export (Krumpfen et al., 2013), there is also a significant correlation between calculated ice production and the areal ice export ( $r = 0.69$  with  $p = 0.009$ ).

The spatial overview of annual ice production (Fig. 11) is supplemented by the previously shown time series of the average winter POLA and accumulated IP per winter (Figs. 5

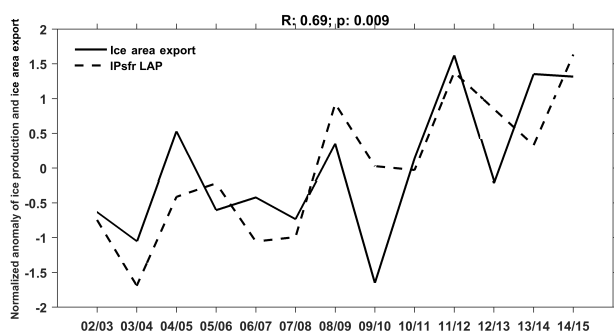


**Figure 12.** Normalized anomalies of accumulated winter ice production (IP of the present study, dashed line) and accumulated ice area export (IAE, solid line) for the winter seasons from 2002/2003 to 2014/2015. IAE data are based on an updated time series from Krumpfen et al. (2013).

and 6, respectively). Both time series of POLA and IP in the Laptev Sea show an overall positive trend (significant with  $p \leq 0.01$ ), which can for the most part be traced back to larger thin-ice areas during the freeze-up period in November and December (as described above, Fig. 10). This is underlined by Tables 2 and 3, which both reveal largest average values of POLA and IP and most significant trends during that period of winter. The average ice production from November to March in the Laptev Sea is estimated with about  $96 \pm 33 \text{ km}^3$  (2002/2003 to 2014/2015), with a positive trend of  $6.8 \text{ km}^3$  per year. Compared to other Arctic polynyas (see Table 3), this corresponds to a share of about 5 % of the total ice production in polynya regions.

As the relative strength of the Transpolar Drift is dependent on atmospheric dynamics, it has previously been linked to atmospheric indices like the Arctic Oscillation (AO) index (Rigor and Wallace, 2004). For the period from 1982 to 2009, the study by Kwok et al. (2013) presented indicators for a net strengthening of both the Transpolar Drift and the Beaufort Gyre as well as a general increase in the Arctic ice drift speed, which is presumably related to a decreasing fraction of thick multiyear (MY) ice. As mentioned before (Sect. 4.1), the latter is thought to be connected to an increased fragility and mobility of the Arctic sea-ice cover, which may have implications for pan-Arctic polynya and lead dynamics. According to Rigor et al. (2002), a positive winter AO promotes both an increased ice transport out of the Arctic Ocean through the Fram Strait and an increased ice transport away from the Siberian coastal areas, thereby leaving open water and thin ice that foster new ice formation. Hence, positive trends in both POLA and IP not only fit well to the previously estimated positive trend in IP from Iwamoto et al. (2014) but also to the positive trend of  $0.85 \times 10^5 \text{ km}^2$  per decade in the Laptev Sea ice area flux (Krumpfen et al., 2013). Other linkages and dependencies with the Arctic sea-ice extent in September (annual minimum), the timing of the freeze on-

set and further connections to large-scale atmospheric circulation patterns are very likely and have been proposed by various previous studies (e.g., Alexandrov et al., 2000; Deser et al., 2000; Rigor et al., 2002; Willmes et al., 2011; Krumpfen et al., 2013). In particular, a significant lengthening of the melt season in recent years, and hence a later freeze-up in autumn, already seems to imprint on the derived POLA (i.e., thin-ice area) and IP estimates in the early winter period (Markus et al., 2009; Parkinson, 2014; Stroeve et al., 2014). In that context, increasing atmosphere and ocean temperatures in autumn and winter were recently reported by Boisvert and Stroeve (2015). These increasing temperatures comprise the potential to alter or shift vertical temperature gradients with consequences for the surface energy balance and ultimately IP. Furthermore, a shortened fast-ice duration and enhanced variability of the fast-ice edge in early winter (Yu et al., 2014; Selyuzhenok et al., 2015) presumably influences the location of flaw leads and consequently high ice production and brine release. Admittedly, all these (potential) interconnections are rather complex and require more detailed investigations that go beyond the scope of the present study. In the context of other reported changes during the spring and summer period (Janout et al., 2016), it may emerge that the overall setup for atmosphere–ice–ocean interactions in the Laptev Sea is gradually changing towards a new state.

## 5 Conclusions

In the present study we analyzed circumpolar polynya dynamics and ice production in the Arctic based on high-resolution MODIS thermal infrared imagery and atmospheric reanalysis from the ERA-Interim data set. Pan-Arctic and daily thin-ice thickness distributions were calculated using a 1-D energy balance model for the period from 2002/2003 to 2014/2015 (November to March). After applying a necessary and well-working gap-filling approach to compensate for cloud and data gaps, the thermodynamic ice production was derived by assuming that all heat loss at the ice surface contributes to the growth of sea ice. We presented results for 17 prominent polynya regions, with a strong focus set on the Laptev Sea region in the eastern Arctic. Despite existing limitations originating from the use of thermal infrared remote sensing data during winter, we think that this new data set of 13 consecutive winter seasons is a huge step forward for a spatially accurate characterization of Arctic polynya dynamics and the associated sea-ice budget related to winter sea-ice production. Our main findings and conclusions are the following:

1. The use of high-resolution MODIS data enables the detection of thin ice much closer to the coast or fast-ice edges, mitigates land spillover effects efficiently and generally increases the capability of resolving small-scale ( $> 2 \text{ km}$ ) thin-ice features such as narrow

polynyas and leads, which therefore contribute to our ice production estimates. This represents an advantage compared to other (passive microwave) data sets.

2. The average winter-accumulated ice production in all 17 polynya regions is estimated to be about  $1811 \pm 293 \text{ km}^3$ . The largest contributions originate from the western proximity of Novaya Zemlya (20 %), the Kara Sea region and the North Water polynya (both 15 %) as well as scattered smaller polynyas in the (eastern) Canadian Arctic Archipelago (all combined around 12 %). By relying on predefined and fixed polynya masks, these IP estimates can include both thermodynamic ice growth within detected polynya margins ( $\text{TIT} \leq 0.2 \text{ m}$ ) as well as ice production in open ocean and/or MIZ areas. However, our estimate of the average total ice production exceeds that of Iwamoto et al. (2014) by about 52–54 %. We note that differences in the regarded time frame, reference areas, sensor specifics as well as a potential bias due to cloud cover and/or the exclusive assumption of clear-sky conditions certainly contribute to this discrepancy.
3. Positive trends in ice production can be detected for several regions of the eastern Arctic (most significant in the Laptev Sea region with an increase of  $6.8 \text{ km}^3 \text{ yr}^{-1}$ ) and the North Water polynya, while other polynyas in the western Arctic show a more pronounced interannual variability. These regionally different trends could potentially originate from changes in the overall sea-ice mobility (i.e., sea-ice drift), a temporal shift of the freeze onset in autumn (leading to larger thin-ice areas in November and December) or distinct large-scale atmospheric setups that promote an increased ice export and enhanced ice production in the Siberian shelf regions during winter.
4. The Laptev Sea region was chosen as a special focus in our study as it is one of the core areas for ice production in the Arctic with a distinct connection to Transpolar Drift characteristics and showing a strong positive trend. Ice production in the Laptev Sea was mapped with enhanced spatial detail, which is especially valuable in this region with narrow and elongated flaw leads close to the fast-ice edge. Our results showed that polynyas in the Laptev Sea contribute at least 5 % to the total potential sea-ice production in Arctic polynyas. While the interannual variability in terms of location and extent seems to be rather high, the positive trends in both POLA and IP time series fit well to results and observations from other recently published studies in the Laptev Sea. A clear relation between increasing sea-ice area export (Krumpfen et al., 2013) and positive trends in IP could be demonstrated, and future comparisons with recently derived volume-flux estimates in the Transpolar Drift (Krumpfen et al., 2016) certainly promise further

insights into the absolute contribution of polynyas to the volume ice export out of the Laptev Sea and adjacent seas.

5. Compared to the MODIS-derived lead product from Willmes and Heinemann (2016), the SFR algorithm used in the present study is not able to adequately reconstruct leads with low spatial and temporal persistence. A thoughtful combination of both concepts is therefore a goal worth achieving for future investigations of thin-ice regions in the polar regions using thermal infrared data from MODIS or other comparable satellite sensors. This would also allow for estimates of IP by leads for the central Arctic Ocean.

## 6 Data availability

Supporting data, featuring time series of daily polynya area and ice production for all 17 polynya regions, are available at doi:10.1594/PANGAEA.869294. Daily maps of derived thin-ice thicknesses and ice production are available on request from the authors (preusser@uni-trier.de).

*Author contributions.* Andreas Preußner carried out the complete analysis and drafted the manuscript. Sascha Willmes and Stephan Paul supported the satellite data analysis and further processing. All coauthors contributed to the writing of the paper. The final draft of the paper was revised and approved by all of the authors.

*Acknowledgements.* The authors want to thank the National Snow and Ice Data Center (NSIDC) as well as the European Center for Medium-Range Weather Forecasts (ECMWF) for providing the MODIS sea ice product (<ftp://n5eil01u.ecs.nsidc.org/SAN/>) and the ERA-Interim atmospheric reanalysis data. The University of Bremen is also kindly acknowledged for providing the AMSR2 passive microwave sea-ice concentration data. The provision of the ice area export data set by Thomas Krumpfen (Alfred Wegener Institute, Bremerhaven, Germany) as well as related discussions are highly acknowledged. Additional thanks to the three referees and the editor Dirk Notz, who helped to improve the paper with their highly valuable comments and suggestions during the review. This work was funded by the Federal Ministry of Education and Research (Bundesministerium für Bildung und Forschung – BMBF) under Grant 03G0833D.

Edited by: D. Notz

Reviewed by: G. Björk, S. Kern, and one anonymous referee

## References

- ACIA: Arctic Climate Impact Assessment. ACIA Overview report, Cambridge University Press, 2005.
- Ackerman, S., Frey, R., Strabala, K., Liu, Y., Gumley, L., Baum, B., and Menzel, P.: Discriminating clear-sky from cloud with MODIS algorithm theoretical basis document (MOD35) Version 6.1, Tech. rep., MODIS Cloud Mask Team, Cooperative Institute for Meteorological Satellite Studies, University of Wisconsin, 2010.
- Adams, S., Willmes, S., Schroeder, D., Heinemann, G., Bauer, M., and Krumpfen, T.: Improvement and sensitivity analysis of thermal thin-ice retrievals, *IEEE T. Geosci. Remote Sens.*, 51, 3306–3318, doi:10.1109/tgrs.2012.2219539, 2013.
- Alexandrov, V. Y., Martin, T., Kolatschek, J., Eicken, H., Kreyscher, M., and Makshtas, A. P.: Sea ice circulation in the Laptev Sea and ice export to the Arctic Ocean: Results from satellite remote sensing and numerical modeling, *J. Geophys. Res.*, 105, 17143–17159, doi:10.1029/2000jc900029, 2000.
- Barber, D. G. and Massom, R. A.: The Role of Sea Ice in Arctic and Antarctic Polynyas, in: *Polynyas – Windows to the World*, edited by: Smith, W. O. and Barber, D. G., chap. The Role of Sea Ice in Arctic and Antarctic Polynyas, 1–54, Elsevier Oceanography Series, doi:10.1016/s0422-9894(06)74001-6, 2007.
- Bareiss, J. and Gørgen, K.: Spatial and temporal variability of sea ice in the Laptev Sea: Analyses and review of satellite passive-microwave data and model results, 1979 to 2002, *Global Planet. Change*, 48, 28–54, doi:10.1016/j.gloplacha.2004.12.004, 2005.
- Bauch, D., Hölemann, J. A., Dmitrenko, I. A., Janout, M. A., Nikulina, A., Kirillov, S. A., Krumpfen, T., Kassens, H., and Timokhov, L.: Impact of Siberian coastal polynyas on shelf-derived Arctic Ocean halocline waters, *J. Geophys. Res.*, 117, C00G12, doi:10.1029/2011JC007282, 2012.
- Bauer, M., Schröder, D., Heinemann, G., Willmes, S., and Ebner, L.: Quantifying polynya ice production in the Laptev Sea with the COSMO model, *Polar Res.*, 32, 20922, doi:10.3402/polar.v32i0.20922, 2013.
- Beitsch, A., Kaleschke, L., and Kern, S.: Investigating High-Resolution AMSR2 Sea Ice Concentrations during the February 2013 Fracture Event in the Beaufort Sea, *Remote Sensing*, 6, 3841–3856, doi:10.3390/rs6053841, 2014.
- Boisvert, L. N. and Stroeve, J. C.: The Arctic is becoming warmer and wetter as revealed by the Atmospheric Infrared Sounder, *Geophys. Res. Lett.*, 42, 4439–4446, doi:10.1002/2015GL063775, 2015GL063775, 2015.
- Bromwich, D. H., Wilson, A. B., Bai, L.-S., Moore, G. W. K., and Bauer, P.: A comparison of the regional Arctic System Reanalysis and the global ERA-Interim Reanalysis for the Arctic, *Q. J. Roy. Meteorol. Soc.*, 142, 644–658, doi:10.1002/qj.2527, 2015.
- Cohen, J., Screen, J. A., Furtado, J. C., Barlow, M., Whittleston, D., Coumou, D., Francis, J., Dethloff, K., Entekhabi, D., Overland, J., and Jones, J.: Recent Arctic amplification and extreme mid-latitude weather, *Nat. Geosci.*, 7, 627–637, doi:10.1038/ngeo2234, 2014.
- Dee, D. P., Uppala, S. M., Simmons, A. J., Berrisford, P., Poli, P., Kobayashi, S., Andrae, U., Balmaseda, M. A., Balsamo, G., Bauer, P., Bechtold, P., Beljaars, A. C. M., van de Berg, L., Bidlot, J., Bormann, N., Delsol, C., Dragani, R., Fuentes, M., Geer, A. J., Haimberger, L., Healy, S. B., Hersbach, H., Hólm, E. V., Isaksen, L., Kållberg, P., Köhler, M., Matricardi, M., McNally,
- A. P., Monge-Sanz, B. M., Morcrette, J.-J., Park, B.-K., Peubey, C., de Rosnay, P., Tavalato, C., Thépaut, J.-N., and Vitart, F.: The ERA-Interim reanalysis: configuration and performance of the data assimilation system, *Q. J. Roy. Meteorol. Soc.*, 137, 553–597, doi:10.1002/qj.828, 2011.
- Deser, C., Walsh, J. E., and Timlin, M. S.: Arctic sea ice variability in the context of recent atmospheric circulation trends, *J. Climate*, 13, 617–633, doi:10.1175/1520-0442(2000)013<0617:ASIVIT>2.0.CO;2, 2000.
- Dethleff, D., Loewe, P., and Kleine, E.: The Laptev Sea flaw lead-detailed investigation on ice formation and export during 1991/1992 winter season, *Cold Reg. Sci. Technol.*, 27, 225–243, doi:10.1016/s0165-232x(98)00005-6, 1998.
- Dmitrenko, I. A., Kirillov, S. A., Tremblay, L. B., Bauch, D., and Willmes, S.: Sea-ice production over the Laptev Sea shelf inferred from historical summer-to-winter hydrographic observations of 1960s–1990s, *Geophys. Res. Lett.*, 36, L13605, doi:10.1029/2009gl038775, 2009.
- Drucker, R., Martin, S., and Moritz, R.: Observations of ice thickness and frazil ice in the St. Lawrence Island polynya from satellite imagery, upward looking sonar, and salinity/temperature moorings, *J. Geophys. Res.*, 108, 3149, doi:10.1029/2001jc001213, 2003.
- Ebner, L., Schröder, D., and Heinemann, G.: Impact of Laptev Sea flaw polynyas on the atmospheric boundary layer and ice production using idealized mesoscale simulations, *Polar Res.*, 30, 7210, doi:10.3402/polar.v30i0.7210, 2011.
- Ernsdorf, T., Schröder, D., Adams, S., Heinemann, G., Timmermann, R., and Danilov, S.: Impact of atmospheric forcing data on simulations of the Laptev Sea polynya dynamics using the sea-ice ocean model FESOM, *J. Geophys. Res.*, 116, C12038, doi:10.1029/2010jc006725, 2011.
- Gutjahr, O., Heinemann, G., Preußner, A., Willmes, S., and Drüe, C.: Sensitivity of ice production estimates in Laptev Sea polynyas to the parameterization of subgrid-scale sea-ice inhomogeneities in COSMO-CLM, *The Cryosphere Discuss.*, doi:10.5194/tc-2016-83, in review, 2016.
- Haid, V., Timmermann, R., Ebner, L., and Heinemann, G.: Atmospheric forcing of coastal polynyas in the south-western Weddell Sea, *Antarct. Sci.*, 27, 388–402, doi:10.1017/s0954102014000893, 2015.
- Hall, D., Key, J., Casey, K., Riggs, G., and Cavalieri, D.: Sea ice surface temperature product from MODIS, *IEEE T. Geosci. Remote Sens.*, 42, 1076–1087, doi:10.1109/tgrs.2004.825587, 2004.
- Hannah, C. G., Dupont, F., and Dunphy, M.: Polynyas and tidal currents in the Canadian Arctic Archipelago, *Arctic*, 62, 83–95, doi:10.14430/arctic115, 2009.
- Heinemann, G. and Rose, L.: Surface energy balance, parameterizations of boundary-layer heights and the application of resistance laws near an Antarctic Ice Shelf front, *Bound.-Lay. Meteorol.*, 51, 123–158, doi:10.1007/bf00120464, 1990.
- Hirano, D., Fukamachi, Y., Watanabe, E., Ohshima, K. I., Iwamoto, K., Mahoney, A. R., Eicken, H., Simizu, D., and Tamura, T.: A wind-driven, hybrid latent and sensible heat coastal polynya off Barrow, Alaska, *J. Geophys. Res.-Oceans*, 121, 980–997, doi:10.1002/2015JC011318, 2016.
- Iwamoto, K., Ohshima, K. I., and Tamura, T.: Improved mapping of sea ice production in the Arctic Ocean using AMSR-E thin ice

- thickness algorithm, *J. Geophys. Res.-Oceans*, 119, 3574–3594, doi:10.1002/2013jc009749, 2014.
- Jakobsson, M., Mayer, L., Coakley, B., Dowdeswell, J. A., Forbes, S., Fridman, B., Hodnesdal, H., Noormets, R., Pedersen, R., Rebesco, M., Schenke, H. W., Zarayskaya, Y., Accettella, D., Armstrong, A., Anderson, R. M., Bienhoff, P., Camerlenghi, A., Church, I., Edwards, M., Gardner, J. V., Hall, J. K., Hell, B., Hestvik, O., Kristoffersen, Y., Marcussen, C., Mohammad, R., Mosher, D., Nghiem, S. V., Pedrosa, M. T., Travaglini, P. G., and Weatherall, P.: The international bathymetric chart of the Arctic Ocean (IBCAO) version 3.0, *Geophys. Res. Lett.*, 39, L12609, doi:10.1029/2012gl052219, 2012.
- Janout, M., Hölemann, J., Juhls, B., Krumpfen, T., Rabe, B., Bauch, D., Wegner, C., Kassens, H., and Timokhov, L.: Episodic warming of near-bottom waters under the Arctic sea ice on the central Laptev Sea shelf, *Geophys. Res. Lett.*, 43, 264–272, doi:10.1002/2015GL066565, 2016.
- Kern, S.: Polynya area in the Kara Sea, Arctic, obtained with microwave radiometry for 1979–2003, *IEEE Geosci. Remote S.*, 5, 171–175, doi:10.1109/lgrs.2008.916831, 2008.
- König-Langlo, G. and Augstein, E.: Parameterization of the downward long-wave radiation at the Earth's surface in polar regions, *Meteorol. Z.*, N.F.3, 343–347, doi:10013/epic.12338, 1994.
- Krumpfen, T., Janout, M., Hodges, K. I., Gerdes, R., Girard-Arduin, F., Hölemann, J. A., and Willmes, S.: Variability and trends in Laptev Sea ice outflow between 1992–2011, *The Cryosphere*, 7, 349–363, doi:10.5194/tc-7-349-2013, 2013.
- Krumpfen, T., Gerdes, R., Haas, C., Hendricks, S., Herber, A., Selyuzhenok, V., Smedsrud, L., and Spreen, G.: Recent summer sea ice thickness surveys in Fram Strait and associated ice volume fluxes, *The Cryosphere*, 10, 523–534, doi:10.5194/tc-10-523-2016, 2016.
- Kwok, R., Spreen, G., and Pang, S.: Arctic sea ice circulation and drift speed: Decadal trends and ocean currents, *J. Geophys. Res.-Oceans*, 118, 2408–2425, doi:10.1002/jgrc.20191, 2013.
- Laxon, S. W., Giles, K. A., Ridout, A. L., Wingham, D. J., Willatt, R., Cullen, R., Kwok, R., Schweiger, A., Zhang, J., Haas, C., Hendricks, S., Krishfield, R., Kurtz, N., Farrell, S., and Davidson, M.: CryoSat-2 estimates of Arctic sea ice thickness and volume, *Geophys. Res. Lett.*, 40, 732–737, doi:10.1002/grl.50193, 2013.
- Liu, Y. and Key, J. R.: Less winter cloud aids summer 2013 Arctic sea ice return from 2012 minimum, *Environ. Res. Lett.*, 9, 044002, doi:10.1088/1748-9326/9/4/044002, 2014.
- Mahoney, A. R., Eicken, H., Gaylord, A. G., and Gens, R.: Landfast sea ice extent in the Chukchi and Beaufort Seas: The annual cycle and decadal variability, *Cold Reg. Sci. Technol.*, 103, 41–56, doi:10.1016/j.coldregions.2014.03.003, 2014.
- Markus, T., Stroeve, J. C., and Miller, J.: Recent changes in Arctic sea ice melt onset, freezeup, and melt season length, *J. Geophys. Res.*, 114, C12024, doi:10.1029/2009jc005436, 2009.
- Martin, S.: Frazil ice in rivers and oceans, *Annu. Rev. Fluid Mech.*, 13, 379–397, doi:10.1146/annurev.fl.13.010181.002115, 1981.
- Martin, S. and Cavalieri, D. J.: Contributions of the Siberian shelf polynyas to the Arctic Ocean intermediate and deep water, *J. Geophys. Res.-Oceans*, 94, 12725–12738, doi:10.1029/jc094ic09p12725, 1989.
- Melling, H., Haas, C., and Brossier, E.: Invisible polynyas: Modulation of fast ice thickness by ocean heat flux on the Canadian polar shelf, *J. Geophys. Res.-Oceans*, 120, 777–795, doi:10.1002/2014jc010404, 2015.
- Moore, G. W. K., Bromwich, D. H., Wilson, A. B., Renfrew, I., and Bai, L.: Arctic System Reanalysis improvements in topographically forced winds near Greenland, *Q. J. Roy. Meteorol. Soc.*, 142, 2033–2045, doi:10.1002/qj.2798, 2016.
- Morales-Maqueda, M., Willmott, A., and Biggs, N.: Polynya dynamics: A review of observations and modeling, *Rev. Geophys.*, 42, 1–37, doi:10.1029/2002rg000116, 2004.
- Parkinson, C. L.: Spatially mapped reductions in the length of the Arctic sea ice season, *Geophys. Res. Lett.*, 41, 4316–4322, doi:10.1002/2014gl060434, 2014.
- Parkinson, C. L. and Comiso, J. C.: On the 2012 record low Arctic sea ice cover: Combined impact of preconditioning and an August storm, *Geophys. Res. Lett.*, 40, 1356–1361, doi:10.1002/grl.50349, 2013.
- Paul, S., Willmes, S., Gutjahr, O., Preußer, A., and Heinemann, G.: Spatial Feature Reconstruction of Cloud-Covered Areas in Daily MODIS Composites, *Remote Sensing*, 7, 5042–5056, doi:10.3390/rs70505042, 2015a.
- Paul, S., Willmes, S., and Heinemann, G.: Long-term coastal-polynya dynamics in the southern Weddell Sea from MODIS thermal-infrared imagery, *The Cryosphere*, 9, 2027–2041, doi:10.5194/tc-9-2027-2015, 2015b.
- Preußer, A., Heinemann, G., Willmes, S., and Paul, S.: Multi-Decadal Variability of Polynya Characteristics and Ice Production in the North Water Polynya by Means of Passive Microwave and Thermal Infrared Satellite Imagery, *Remote Sensing*, 7, 15844–15867, doi:10.3390/rs71215807, 2015a.
- Preußer, A., Willmes, S., Heinemann, G., and Paul, S.: Thin-ice dynamics and ice production in the Storfjorden polynya for winter seasons 2002/2003–2013/2014 using MODIS thermal infrared imagery, *The Cryosphere*, 9, 1063–1073, doi:10.5194/tc-9-1063-2015, 2015b.
- Riggs, G., Hall, D., and Salomonson, V.: MODIS Sea Ice Products User Guide to Collection 5, National Snow and Ice Data Center, University of Colorado, Boulder, CO 80309-0449 USA, [http://nsidc.org/data/docs/daac/modis\\_v5/dorothy\\_ice\\_doc.pdf](http://nsidc.org/data/docs/daac/modis_v5/dorothy_ice_doc.pdf), 2006.
- Rigor, I. and Colony, R.: Sea-ice production and transport of pollutants in the Laptev Sea, 1979–1993, *Sci. Total Environ.*, 202, 89–110, doi:10.1016/s0048-9697(97)00107-1, 1997.
- Rigor, I. G. and Wallace, J. M.: Variations in the age of Arctic sea-ice and summer sea-ice extent, *Geophys. Res. Lett.*, 31, L09401, doi:10.1029/2004gl019492, 2004.
- Rigor, I. G., Wallace, J. M., and Colony, R. L.: Response of sea ice to the Arctic Oscillation, *J. Climate*, 15, 2648–2663, doi:10.1175/1520-0442(2002)015<2648:ROSITT>2.0.CO;2, 2002.
- Schweiger, A., Lindsay, R., Zhang, J., Steele, M., Stern, H., and Kwok, R.: Uncertainty in modeled Arctic sea ice volume, *J. Geophys. Res.*, 116, C00D06, doi:10.1029/2011jc007084, 2011.
- Selyuzhenok, V., Krumpfen, T., Mahoney, A., Janout, M., and Gerdes, R.: Seasonal and interannual variability of fast ice extent in the southeastern Laptev Sea between 1999 and 2013, *J. Geophys. Res.-Oceans*, 120, 7791–7806, doi:10.1002/2015jc011135, 2015.
- Smith, S. D., Muench, R. D., and Pease, C. H.: Polynyas and leads: An overview of physical processes and environment, *J. Geophys. Res.*, 95, 9461–9479, doi:10.1029/jc095ic06p09461, 1990.

- Spreen, G., Kaleschke, L., and Heygster, G.: Sea ice remote sensing using AMSR-E 89 GHz channels, *J. Geophys. Res.*, 113, C02S03, doi:10.1029/2005JC003384, 2008.
- Steffen, K.: Warm water cells in the North Water, northern Baffin Bay during winter, *J. Geophys. Res.-Oceans*, 90, 9129–9136, doi:10.1029/JC090iC05p09129, 1985.
- Stroeve, J., Markus, T., Boisvert, L., Miller, J., and Barrett, A.: Changes in Arctic melt season and implications for sea ice loss, *Geophys. Res. Lett.*, 41, 1216–1225, doi:10.1002/2013gl058951, 2014.
- Tamura, T. and Ohshima, K. I.: Mapping of sea ice production in the Arctic coastal polynyas, *J. Geophys. Res.*, 116, C07030, doi:10.1029/2010jc006586, 2011.
- Tamura, T., Ohshima, K. I., Markus, T., Cavalieri, D. J., Nihashi, S., and Hirasawa, N.: Estimation of Thin Ice Thickness and Detection of Fast Ice from SSM/I Data in the Antarctic Ocean, *J. Atmos. Ocean. Tech.*, 24, 1757–1772, doi:10.1175/jtech2113.1, 2007.
- Tamura, T., Ohshima, K. I., and Nihashi, S.: Mapping of sea ice production for Antarctic coastal polynyas, *Geophys. Res. Lett.*, 35, L07606, doi:10.1029/2007gl032903, 2008.
- Timco, G. and Frederking, R.: A review of sea ice density, *Cold Reg. Sci. Technol.*, 24, 1–6, doi:10.1016/0165-232X(95)00007-X, 1996.
- Timmermans, M.-L.: The impact of stored solar heat on Arctic sea ice growth, *Geophys. Res. Lett.*, 42, 6399–6406, doi:10.1002/2015gl064541, 2015.
- Williams, W. J., Carmack, E. C., and Ingram, R. G.: Physical Oceanography of Polynyas, in: *Polynyas – Windows to the World*, edited by: Smith, W. O. and Barber, D. G., chap. Physical Oceanography of Polynyas, 55–86, Elsevier, doi:10.1016/s0422-9894(06)74002-8, 2007.
- Willmes, S. and Heinemann, G.: Sea-Ice Wintertime Lead Frequencies and Regional Characteristics in the Arctic, 2003–2015, *Remote Sensing*, 8, 4, doi:10.3390/rs8010004, 2016.
- Willmes, S., Krumpen, T., Adams, S., Rabenstein, L., Haas, C., Hoelemann, J., Hendricks, S., and Heinemann, G.: Cross-validation of polynya monitoring methods from multisensor satellite and airborne data: a case study for the Laptev Sea, *Can. J. Remote Sens.*, 36, S196–S210, doi:10.5589/m10-012, 2010.
- Willmes, S., Adams, S., Schröder, D., and Heinemann, G.: Spatio-temporal variability of polynya dynamics and ice production in the Laptev Sea between the winters of 1979/80 and 2007/08, *Polar Res.*, 30, 5971, doi:10.3402/polar.v30i0.5971, 2011.
- Winsor, P. and Björk, G.: Polynya activity in the Arctic Ocean from 1958 to 1997, *J. Geophys. Res.*, 105, 8789–8803, doi:10.1029/1999jc900305, 2000.
- Yao, T. and Tang, C.: The formation and maintenance of the North Water polynya, *Atmosphere-Ocean*, 41, 187–201, doi:10.3137/ao.410301, 2003.
- Yu, Y. and Lindsay, R.: Comparison of thin ice thickness distributions derived from RADARSAT Geophysical Processor System and advanced very high resolution radiometer data sets, *J. Geophys. Res.*, 108, 3387, doi:10.1029/2002jc001319, 2003.
- Yu, Y. and Rothrock, D. A.: Thin ice thickness from satellite thermal imagery, *J. Geophys. Res.*, 101, 25753–25766, doi:10.1029/96jc02242, 1996.
- Yu, Y., Stern, H., Fowler, C., Fetterer, F., and Maslanik, J.: Interannual Variability of Arctic Landfast Ice between 1976 and 2007, *J. Climate*, 27, 227–243, doi:10.1175/jcli-d-13-00178.1, 2014.

## 7 Synthesis & Outlook

In the course of the present (cumulative) thesis, a broad picture of Arctic polynya dynamics was presented. Considering the fast changing Arctic environment, investigations on the role of sea ice in general and thin-ice areas in specific are certainly of high interest to the polar scientific community due to their vast range of interconnections to physical, chemical and biological issues/matters. In order to increase the understanding of those ecological and environmental hotspot regions, the expanded use of high-resolution optical TIR data is a goal worth to achieve as it enables a spatially more accurate derivation of daily TIT distributions and polynya margins than it is possible with other commonly used satellite systems, first and foremost passive microwave radiometers. However, it also imposes a lot of challenges that originate primarily from the disturbing influence of clouds, besides other limitations that emerge from the exclusive use of nighttime and clear-sky data. A main obstacle in that context was the weaker performance of the MODIS cloud mask during nighttime conditions [e.g. Liu and Key 2014]. Hence, as outlined in Ch. 3, one of the primary goals of this thesis was to demonstrate the applicability of this data type to both large-scale and long-term time series of the MODIS sensor and find efficient ways to compensate for the drawbacks of this approach (i.e., cloud cover). Thereby, a more accurate quantification of potential thermodynamic ice production in Arctic polynyas should be possible. In addition, the availability of a long-term MODIS reference data set enables comparisons to traditional polynya monitoring methods, which are commonly based on either sea-ice concentrations or iterative classification strategies from passive microwave radiometers.

The first publication was aimed to address the long-term applicability of MODIS TIR data and presented results on thin-ice dynamics and ice production in the Storfjorden polynya (southern Svalbard archipelago) for the 12 winter seasons between 2002/2003 and 2013/2014. Thin-ice thicknesses up to 50 cm were calculated using MODIS ice-surface temperatures (IST) and ECMWF ERA-Interim atmospheric reanalysis data in an energy-balance model, as for thin ice the atmospheric heat flux (i.e., total energy loss from the surface to the atmosphere) is balanced by the conductive heat flux through the ice. The used method extended upon earlier studies by Willmes et al. [2010, 2011] and Adams et al. [2013] by incorporating less coarse atmospheric reanalysis data and the derivation of daily TIT composites. Cloud-induced gaps in these TIT composites were addressed by introducing a basic coverage-correction (CC) scheme. While being relatively simple in a mathematical sense, this linear extrapolation/upscaling procedure proved to function reasonably well with a standard error of only 5-6%. However, as this procedure relies on the daily percentage of MODIS coverage in a predefined polynya mask, i.e. the proportion of POLA pixels in the covered part of the polynya reference area, it does not consider which areas are cloud covered and, hence, if the scaling makes sense in a physical way. In case of the Storfjorden polynya, the CC-approach increased both the average polynya area ( $4556 \text{ km}^2$ ) and average accumulated ice production ( $28.3 \text{ km}^3$ ) by about 30%, when compared to uncorrected

estimates. Overall, while results were mostly comparable to earlier studies in that region [e.g. Jardon et al. 2014], the study extended upon the spatial detail as well as a more accurate determination of daily thin-ice thickness distribution and with that, a reduced error in heat flux calculations. Alongside with an increasing trend in ice production over the 12-yr period, the importance of this relatively small coastal polynya system considering its potential contribution to the cold halocline layer through salt release during ice-formation processes could be pointed out.

The follow-up study focused on a well-known polynya region between the Canadian Arctic and Greenland - the North Water (NOW) polynya in northern Baffin Bay. The NOW polynya was chosen on purpose, as it represents the largest and most active Arctic polynya (north of 68°N) and has therefore a long history of extended/broad and multi-disciplinary investigations [e.g. Deming et al. 2002]. However, despite its status and ongoing climatic changes, the last time that the sea-ice cover and polynya properties of the NOW polynya were explicitly studied was roughly 15 years ago, which urged for an update and continuation of earlier efforts in that region. Besides extending the MODIS time series by one more winter season, one main advancement in this study compared to the first publication [Preußner et al. 2015b] was a generally more sophisticated treatment of cloud cover by utilizing (1) additional data from ERA-Interim and a daily measure for the persistence of thin ice to reduce the risk of misclassifications by the MODIS cloud mask, and (2) an interpolation scheme ('Spatial Feature Reconstruction' - SFR; Paul et al. [2015b]) that is aimed at reproducing likely polynya pixels based on derived polynya-probabilities from bounding days (details in Ch. 5 and Ch. 6). Although still incorporating the CC-approach to some extent, this SFR-enhanced time series of thin-ice thickness distributions, POLA and IP enabled an evaluation of estimates that were solely based on the CC-approach, i.e. linear extrapolation based on the the daily MODIS coverage in the polynya reference area. Differences were generally small (POLA - IP: around 4-6%), so that it was concluded to rely on SFR estimates in future studies as they add a certain level of confidence (based on spatial and temporal statistics) and a physically solid explanation for necessary corrections. Based on the MODIS data, a 13-yr time series of gap-filled TIT, thus POLA and IP, could be established. Furthermore, the long-term behavior of wintertime ice-bridges in Nares Strait could be obtained from annual frequencies of thin-ice occurrences. As one of the goals for this study was the analysis of the multi-decadal polynya variability, different methods were applied on sea-ice concentrations and brightness temperature data from various passive microwave radiometers (AMSR-E, AMSR2, SMMR, SSM/I-SSMIS) to obtain the frequency of polynya occurrences and POLA, with also enabled cross-comparisons to MODIS-derived quantities. Based on the SMMR / SSM/I-SSMIS time series, starting in 1978/1979, results showed that the NOW polynya experienced significant seasonal changes over the last three decades considering the overall frequency of polynya occurrences and their spatial extent. In the 1980s, there were prolonged periods of a more or less closed ice cover in northern Baffin Bay in winter. During the last decade, this changed towards an average opening on more than 85% of the days between November and March. Since the late 1990s, signs of a later-appearing fall freeze-up became evident. The comparison with MODIS thin-ice thickness data shows that the wintertime polynya area estimates derived by MODIS are about 30 to 40% higher than those derived using the polynya signature simulation method (PSSM) with AMSR-E data. Differences and characteristics of two common microwave



techniques (i.e., 70PT vs. PSSM) could be further revealed, as it turned out that the difference in polynya area between PSSM and a sea ice concentration (SIC) threshold of 70% is fairly low (approximately 10%) when applied to AMSR-E data. For the coarse-resolution SSM/I-SSMIS data and particularly in early winter, this difference is much larger. Hence, a recommendation regarding a long-term polynya monitoring (e.g. to be utilized as boundary conditions in numerical models) could be given in that the PSSM method should be used for SSM/I-SSMIS data to profit both from a long-term data record and realistic, yet potentially underestimated polynya margins.

The final study evolved from Preußer et al. [2015b, a] and focused back to MODIS-derived daily thin-ice thickness distributions, yet vastly expanding upon the covered spatial domain, featuring all ocean areas north of 68°N. Ultimately, the main purpose behind this study was to assess pan-Arctic polynya dynamics at a high spatial resolution and a comparatively long 13-yr data record, as well as their possible connections to the Transpolar Drift system. Both the spatial extent and the length of the data record represented a novelty for this method to retrieve polynya characteristics and allowed for the first pan-Arctic qualitative comparison to comparable passive microwave estimates [Tamura and Ohshima 2011; Iwamoto et al. 2014]. The study used the latest iteration of the TIT retrieval and hence featured improvements from Paul et al. [2015b]; Preußer et al. [2015a] regarding the treatment of cloud-cover and daily gap-filling (SFR). In total, 17 major polynya regions were analyzed based on newly derived estimates of the frequency of polynya occurrences, POLA and IP. In winter, all regions combined cover an average (2002/2003 to 2014/2015) thin-ice area of  $226.6 \pm 36.1 \times 10^3 \text{ km}^2$ , enabling an average accumulated ice production of around  $1811 \pm 293 \text{ km}^3$  per winter. The main areas for high ice production were the Kara Sea region and the North Water polynya (both 15%), polynyas at the western side of Novaya Zemlya (20%) as well as scattered smaller polynyas in the Canadian Arctic Archipelago (all combined 12%). It had to be noted, however, that the influence of large open-water areas during the freeze-up period on the derived IP could be quite significant for some of these regions. The share of other well-known polynya regions (e.g. Laptev Sea, Chukchi Sea) to the total ice production was smaller and ranged around 2 and 5%. The use of high resolution MODIS data showed distinct advantages in narrow fjords as well as in proximity of coastlines and fast-ice edges. Further, the capability to resolve larger leads was increased. However, short-lived leads in the central Arctic Ocean were overall underestimated due to a strict persistence criteria of 50%, meaning that more than half of the MODIS swaths covering a pixel on a given day had to feature a thin-ice signal. Although the data record of 13 winter-seasons is relatively short, positive trends in ice production were calculated for several regions of the eastern Arctic (most significant in the Laptev Sea region with an increase of  $6.8 \text{ km}^3/\text{yr}$ ) and the North Water polynya (not significant). Polynyas in the western Arctic showed generally a higher variability. A special focus was set on the Laptev Sea region, as it remains one of the core areas for ice production in the Arctic (total share around 5%) with a strong positive trend and a distinct connection to Transpolar Drift characteristics. Concerning the latter, a clear relation between increasing sea-ice area export [Krumpfen et al. 2013] and positive trends in IP could be highlighted. Overall, the study contained a spatially highly accurate characterization of circumpolar polynya dynamics and ice production, with presumably high value for future modeling efforts on atmosphere-sea ice-ocean interactions.

Taking a step back and looking at all three publications in total, the consequent evolution of the applied scheme to derive thin-ice thicknesses becomes obvious. Starting from the first long-term application, over to noticeable enhancements in cloud-detection and compensation as well as inter-sensor comparisons, the thesis ultimately ended up presenting a new 13-yr pan-Arctic data set of daily gap-filled thin-ice thicknesses at a spatial resolution of 2km, which can now be further utilized in a variety of atmospheric and oceanographic applications. A logical next step regarding the potential effect on deep-water formation and the contributions to the cold halocline layer in the Arctic is the circumpolar derivation of salt-fluxes, enabling the quantification of the polynya-induced salinity increase in the Arctic shelf seas with a so far unmatched spatial detail. One of the main deficiencies of the current data set is the limited capability to derive IP in short-lived leads, which asks for a thoughtful combination with the data set / approach by Willmes and Heinemann [2015, 2016]. This would be the next major upgrade, as this wasn't possible in earlier passive microwave studies. Getting a glimpse on the quantitative effect of leads in the central Arctic on atmospheric and oceanic processes has the potential to be of high relevance not only for the scientific sea-ice community. Another topic that is worth to address is the utilization of new/better resolved atmospheric data sets in the TIT algorithm. The currently used coarse grid-sizes of around 80km (ERA-Interim) impose potentially significant error sources by not being able to resolve mesoscale spatial features in the wind field, including but not limited to tip-jets, channeling effects and other topography-induced phenomena [e.g. Moore et al. 2016]. Hence, future versions of the TIT retrieval should evaluate the usage of higher resolution data sets, such as the COSMO CLM [Gutjahr et al. 2016, 15km] or the soon to be released successor of ERA-Interim, ERA5 [Hirahara et al. 2016, 30km]. Finding ways to extend the data record by either incorporating available data from the Advanced Very High Resolution Radiometer (AVHRR) or preparing for data from new satellite instruments like the Sea and Land Surface Temperature Radiometer (SLSTR) onboard ESA's Sentinel-3 satellite platform is another aspect worth to strive for. However, the optimization of thin-ice retrievals from thermal infrared data can only be one puzzle-piece in the comprehensive characterisation of the (Arctic) sea-ice cover, as every sensor techniques has its distinct advantages and limitations. Finding ways to combine the strengths from a wide range of remote sensing products, while at the same time adequately addressing spatial and temporal scale-gaps, will ultimately be the key for further advances in the field of sea-ice remote sensing as well as an accurate quantification and monitoring of climatic changes in the polar regions.

## Bibliography

### Aagaard et al. 1981

AAGAARD, Knut ; COACHMAN, L.K. ; CARMACK, Eddy: On the halocline of the Arctic Ocean. In: *Deep Sea Research Part A. Oceanographic Research Papers* 28 (1981), jun, No. 6, 529–545. [http://dx.doi.org/10.1016/0198-0149\(81\)90115-1](http://dx.doi.org/10.1016/0198-0149(81)90115-1). – DOI 10.1016/0198-0149(81)90115-1

### Adams et al. 2013

ADAMS, S. ; WILLMES, S. ; SCHROEDER, D. ; HEINEMANN, G. ; BAUER, M. ; KRUMPEN, T.: Improvement and sensitivity analysis of thermal thin-ice retrievals. In: *IEEE Transactions on Geoscience and Remote Sensing* 51 (2013), No. 6, 3306–3318. <http://dx.doi.org/10.1109/tgrs.2012.2219539>. – DOI 10.1109/tgrs.2012.2219539

### Adams 2012

ADAMS, Susanne: *Monitoring of thin sea ice within polynyas using MODIS data*. Department of Environmental Meteorology, University of Trier, PhD. thesis, 2012

### Adams et al. 2011

ADAMS, Susanne ; WILLMES, Sascha ; HEINEMANN, Günther ; ROZMAN, Polona ; TIMMERMANN, Ralph ; SCHRÖDER, David: Evaluation of simulated sea-ice concentrations from sea-ice/ocean models using satellite data and polynya classification methods. In: *Polar Research* 30 (2011)

### Alexandrov et al. 2000

ALEXANDROV, Vitaly Y. ; MARTIN, Thomas ; KOLATSCHKE, Josef ; EICKEN, Hajo ; KREYSCHER, Martin ; MAKSHITAS, Alexandr P.: Sea ice circulation in the Laptev Sea and ice export to the Arctic Ocean: Results from satellite remote sensing and numerical modeling. In: *Journal of Geophysical Research* 105 (2000), No. C7, 17143–17159

### Andersen et al. 2007

ANDERSEN, Søren ; TONBOE, Rasmus ; KALESCHKE, Lars ; HEYGSTER, Georg ; PEDERSEN, Leif T.: Intercomparison of passive microwave sea ice concentration retrievals over the high-concentration Arctic sea ice. In: *Journal of Geophysical Research* 112 (2007), aug, No. C8. <http://dx.doi.org/10.1029/2006jc003543>. – DOI 10.1029/2006jc003543

### Arrigo 2004

ARRIGO, Kevin R.: Annual cycles of sea ice and phytoplankton in Cape Bathurst polynya, southeastern Beaufort Sea, Canadian Arctic. In: *Geophysical Research Letters* 31 (2004), No. 8. <http://dx.doi.org/10.1029/2003gl018978>. – DOI 10.1029/2003gl018978

### Barber and Massom 2007

BARBER, D. G. ; MASSOM, R. A.: The Role of Sea Ice in Arctic and Antarctic Polynyas. Version: 2007. [http://dx.doi.org/10.1016/s0422-9894\(06\)74001-6](http://dx.doi.org/10.1016/s0422-9894(06)74001-6). In: SMITH, W. O. (Hrsg.) ; BARBER, D. G. (Hrsg.): *Polynyas - Windows to the World*. Elsevier Oceanography Series, 2007. – DOI 10.1016/s0422-9894(06)74001-6, Kapitel The Role of Sea Ice in Arctic and Antarctic Polynyas, 1–54

**Barber et al. 2001**

BARBER, D.G. ; HANESIAK, J.M. ; CHAN, W. ; PIWOWAR, J.: Sea-ice and meteorological conditions in Northern Baffin Bay and the North Water polynya between 1979 and 1996. In: *Atmosphere-Ocean* 39 (2001), No. 3, 343–359

**Bauer et al. 2013**

BAUER, Martin ; SCHRÖDER, David ; HEINEMANN, Günther ; WILLMES, Sascha ; EBNER, Lars: Quantifying polynya ice production in the Laptev Sea with the COSMO model. In: *Polar Research* 32 (2013), No. 20922. <http://dx.doi.org/10.3402/polar.v32i0.20922>. – DOI 10.3402/polar.v32i0.20922

**Beitsch et al. 2014**

BEITSCH, Alexander ; KALESCHKE, Lars ; KERN, Stefan: Investigating High-Resolution AMSR2 Sea Ice Concentrations during the February 2013 Fracture Event in the Beaufort Sea. In: *Remote Sensing* 6 (2014), apr, No. 5, 3841–3856. <http://dx.doi.org/10.3390/rs6053841>. – DOI 10.3390/rs6053841

**Boisvert and Stroeve 2015**

BOISVERT, L. N. ; STROEVE, J. C.: The Arctic is becoming warmer and wetter as revealed by the Atmospheric Infrared Sounder. In: *Geophysical Research Letters* 42 (2015), No. 11, 4439–4446. <http://dx.doi.org/10.1002/2015GL063775>. – DOI 10.1002/2015GL063775. – ISSN 1944–8007. – 2015GL063775

**Bourassa et al. 2013**

BOURASSA, Mark A. ; GILLE, Sarah T. ; BITZ, Cecilia ; CARLSON, David ; CEROVECKI, Ivana ; CLAYSON, Carol A. ; CRONIN, Meghan F. ; DRENNAN, Will M. ; FAIRALL, Chris W. ; HOFFMAN, Ross N. ; MAGNUSDOTTIR, Gudrun ; PINKER, Rachel T. ; RENFREW, Ian A. ; SERREZE, Mark ; SPEER, Kevin ; TALLEY, Lynne D. ; WICK, Gary A.: High-Latitude Ocean and Sea Ice Surface Fluxes: Challenges for Climate Research. In: *Bulletin of the American Meteorological Society* 94 (2013), mar, No. 3, 403–423. <http://dx.doi.org/10.1175/bams-d-11-00244.1>. – DOI 10.1175/bams-d-11-00244.1

**Carmack 1986**

In: CARMACK, Eddy C.: *Circulation and Mixing in Ice-Covered Waters*. Boston, MA : Springer US, 1986. – ISBN 978–1–4899–5352–0, 641–712

**Cavalieri 1994**

CAVALIERI, Donald J.: A microwave technique for mapping thin sea ice. In: *Journal of Geophysical Research* 99 (1994), No. C6, 12561. <http://dx.doi.org/10.1029/94jc00707>. – DOI 10.1029/94jc00707

**Cavalieri and Martin 1994**

CAVALIERI, Donald J. ; MARTIN, Seelye: The contribution of Alaskan, Siberian, and Canadian coastal polynyas to the cold halocline layer of the Arctic Ocean. In: *Journal of Geophysical Research* 99 (1994), No. C9, 18343. <http://dx.doi.org/10.1029/94jc01169>. – DOI 10.1029/94jc01169

**Cohen et al. 2014**

COHEN, Judah ; SCREEN, James A. ; FURTADO, Jason C. ; BARLOW, Mathew ; WHITTLESTON, David ; COUMOU, Dim ; FRANCIS, Jennifer ; DETHLOFF, Klaus ; ENTEKHABI, Dara ; OVERLAND, James ; JONES, Justin: Recent Arctic amplification and extreme mid-latitude weather. In: *Nature Geoscience* 7 (2014), aug, No. 9, 627–637. <http://dx.doi.org/10.1038/ngeo2234>. – DOI 10.1038/ngeo2234

**Comiso 2010**

COMISO, Josefino C.: Variability and trends of the global sea ice cover. In: THOMAS, D.N. (Hrsg.) ; DIECKMANN, G.S. (Hrsg.): *Sea Ice*. Wiley-Blackwell, 2010, Kapitel 6, 205–246

**Dee et al. 2011**

DEE, D. P. ; UPPALA, S. M. ; SIMMONS, A. J. ; BERRISFORD, P. ; POLI, P. ; KOBAYASHI, S. ; ANDRAE, U. ; BALMASEDA, M. A. ; BALSAMO, G. ; BAUER, P. ; BECHTOLD, P. ; BELJAARS, A. C. M. ; BERG, L. van d. ; BIDLOT, J. ; BORMANN, N. ; DELSOL, C. ; DRAGANI, R. ; FUENTES, M. ; GEER, A. J. ; HAIMBERGER, L. ; HEALY, S. B. ; HERSBACH, H. ; HÖLM, E. V. ; ISAKSEN, L. ; KÅLLBERG, P. ; KÖHLER, M. ; MATRICARDI, M. ; McNALLY, A. P. ; MONGE-SANZ, B. M. ; MORCRETTE, J.-J. ; PARK, B.-K. ; PEUBEY, C. ; ROSNAY, P. de ; TAVOLATO, C. ; THÉPAUT, J.-N. ; VITART, F.: The ERA-Interim reanalysis: configuration and performance of the data assimilation system. In: *Quarterly Journal of the Royal Meteorological Society* 137 (2011), No. 656, 553–597. <http://dx.doi.org/10.1002/qj.828>. – DOI 10.1002/qj.828. – ISSN 1477–870X

**Deming et al. 2002**

DEMING, Jody W. ; FORTIER, Louis ; FUKUCHI, Mitsuo: The International North Water Polynya Study (NOW): a brief overview. In: *Deep Sea Research Part II: Topical Studies in Oceanography* 49 (2002), jan, No. 22-23, 4887–4892. [http://dx.doi.org/10.1016/S0967-0645\(02\)00168-6](http://dx.doi.org/10.1016/S0967-0645(02)00168-6). – DOI 10.1016/S0967-0645(02)00168-6

**Drucker et al. 2003**

DRUCKER, Robert ; MARTIN, Seelye ; MORITZ, Richard: Observations of ice thickness and frazil ice in the St. Lawrence Island polynya from satellite imagery, upward looking sonar, and salinity/temperature moorings. In: *J. Geophys. Res.* 108 (2003), No. C5, 3149. <http://dx.doi.org/10.1029/2001jc001213>. – DOI 10.1029/2001jc001213. – ISSN 0148–0227

**Drüe and Heinemann 2004**

DRÜE, C. ; HEINEMANN, G.: High-resolution maps of the sea-ice concentration from MODIS satellite data. In: *Geophys. Res. Lett.* 31 (2004), No. 20, L20403. – ISSN 0094–8276

**Drüe and Heinemann 2005**

DRÜE, C. ; HEINEMANN, G.: Accuracy assessment of sea-ice concentrations from MODIS using in-situ measurements. In: *Remote Sensing of Environment* 95 (2005), No. 2, 139–149. – ISSN 0034–4257

**Ebner et al. 2011**

EBNER, Lars ; SCHRÖDER, David ; HEINEMANN, Günther: Impact of Laptev Sea flaw polynyas on the atmospheric boundary layer and ice production using idealized mesoscale simulations. In: *Polar Research* 30 (7210) (2011), 16. <http://dx.doi.org/10.3402/polar.v30i0.7210>. – DOI 10.3402/polar.v30i0.7210

**Fetterer et al. 2002**

FETTERER, F. ; KNOWLES, K. ; MEIER, W. ; SAVOIE, M.: *Sea Ice Index*. – updated daily

**Francis and Hunter 2006**

FRANCIS, Jennifer A. ; HUNTER, Elias: New insight into the disappearing Arctic sea ice. In: *Eos, Transactions American Geophysical Union* 87 (2006), No. 46, 509. <http://dx.doi.org/10.1029/2006eo460001>. – DOI 10.1029/2006eo460001

**Francis and Vavrus 2012**

FRANCIS, Jennifer A. ; VAVRUS, Stephen J.: Evidence linking Arctic amplification to extreme weather in mid-latitudes. In: *Geophysical Research Letters* 39 (2012), mar, No. 6, n/a–n/a. <http://dx.doi.org/10.1029/2012gl051000>. – DOI 10.1029/2012gl051000

**Francis and Vavrus 2015**

FRANCIS, Jennifer A. ; VAVRUS, Stephen J.: Evidence for a wavier jet stream in response to rapid Arctic warming. In: *Environmental Research Letters* 10 (2015), No. 1, 014005

**Gutjahr et al. 2016**

GUTJAHR, O. ; HEINEMANN, G. ; PREUSSER, A. ; WILLMES, S. ; DRÜE, C.: Quantification of ice production in Laptev Sea polynyas and its sensitivity to thin-ice parameterizations in a regional climate model. In: *The Cryosphere* 10 (2016), No. 6, 2999–3019. <http://dx.doi.org/10.5194/tc-10-2999-2016>. – DOI 10.5194/tc-10-2999-2016

**Haas 2010**

HAAS, C.: Dynamics versus Thermodynamics: The Sea Ice Thickness Distribution. In: THOMAS, D.N. (Hrsg.) ; DIECKMANN, G.S. (Hrsg.): *Sea Ice*. Wiley-Blackwell, 2010, Kapitel 4, 113–151

**Haas et al. 2008**

HAAS, Christian ; PFAFFLING, Andreas ; HENDRICKS, Stefan ; RABENSTEIN, Lasse ; ETIENNE, Jean-Louis ; RIGOR, Ignatius: Reduced ice thickness in Arctic Transpolar Drift favors rapid ice retreat. In: *Geophysical Research Letters* 35 (2008), sep, No. 17. <http://dx.doi.org/10.1029/2008gl034457>. – DOI 10.1029/2008gl034457

**Hall et al. 2004**

HALL, D.K. ; KEY, J.R. ; CASEY, K.A. ; RIGGS, G.A. ; CAVALIERI, D.J.: Sea ice surface temperature product from MODIS. In: *Geoscience and Remote Sensing, IEEE Transactions on* 42 (2004), No. 5, 1076 – 1087. <http://dx.doi.org/10.1109/tgrs.2004.825587>. – DOI 10.1109/tgrs.2004.825587. – ISSN 0196-2892

**Hansen et al. 2013**

HANSEN, E. ; GERLAND, S. ; GRANSKOG, M. A. ; PAVLOVA, O. ; RENNER, A. H. H. ; HAAPALA, J. ; LØYNING, T. B. ; TSCHUDI, M.: Thinning of Arctic sea ice observed in Fram Strait: 19902011. In: *Journal of Geophysical Research: Oceans* 118 (2013), No. 10, 5202–5221. <http://dx.doi.org/10.1002/jgrc.20393>. – DOI 10.1002/jgrc.20393. – ISSN 2169-9291

**Hendricks et al. 2011**

HENDRICKS, Stefan ; GERLAND, S ; SMEDSRUD, LH ; HAAS, Christian ; PFAFFHUBER, AA ; NILSEN, F: Sea-ice thickness variability in Storfjorden, Svalbard. In: *Annals of Glaciology* 52 (2011), No. 57, 61–68

**Hirahara et al. 2016**

HIRAHARA, S. ; BALMASEDA, M. A. ; BOISSESON, E. de ; HERBACH, H.: *Sea Surface Temperature and Sea Ice Concentration for ERA5*. 2016. ( 26)

**Hirano et al. 2016**

HIRANO, Daisuke ; FUKAMACHI, Yasushi ; WATANABE, Eiji ; OHSHIMA, Kay I. ; IWAMOTO, Katsushi ; MAHONEY, Andrew R. ; EICKEN, Hajo ; SIMIZU, Daisuke ; TAMURA, Takeshi: A wind-driven, hybrid latent and sensible heat coastal polynya off Barrow, Alaska. In: *Journal of Geophysical Research: Oceans* (2016). <http://dx.doi.org/10.1002/2015JC011318>. – DOI 10.1002/2015JC011318

**Hobbs 1974**

HOBBS, P.V.: *Ice Physics*. Oxford : Clarendon Press, 1974

**Hollands and Dierking 2016**

HOLLANDS, Thomas ; DIERKING, Wolfgang: Dynamics of the Terra Nova Bay Polynya: The potential of multi-sensor satellite observations. In: *Remote Sensing of Environment* 187 (2016), dec, 30–48. <http://dx.doi.org/10.1016/j.rse.2016.10.003>. – DOI 10.1016/j.rse.2016.10.003

**Huntemann et al. 2014**

HUNTEMANN, M. ; HEYGSTER, G. ; KALESCHKE, L. ; KRUMPEN, T. ; MÄKYNEN, M. ; DRUSCH, M.: Empirical sea ice thickness retrieval during the freeze-up period from SMOS high incident angle observations. In: *The Cryosphere* 8 (2014), mar, No. 2, 439–451. <http://dx.doi.org/10.5194/tc-8-439-2014>. – DOI 10.5194/tc-8-439-2014

**Itkin et al. 2015**

ITKIN, Polona ; LOSCH, Martin ; GERDES, Rüdiger: Landfast ice affects the stability of the Arctic halocline: Evidence from a numerical model. In: *Journal of Geophysical Research: Oceans* 120 (2015), apr, No. 4, 2622–2635. <http://dx.doi.org/10.1002/2014jc010353>. – DOI 10.1002/2014jc010353

**Ivanova et al. 2014**

IVANOVA, Natalia ; JOHANNESSEN, Ola M. ; PEDERSEN, Leif T. ; TONBOE, Rasmus T.: Retrieval of Arctic Sea Ice Parameters by Satellite Passive Microwave Sensors: A Comparison of Eleven Sea Ice Concentration Algorithms. In: *IEEE Transactions on Geoscience and Remote Sensing* 52 (2014), nov, No. 11, 7233–7246. <http://dx.doi.org/10.1109/tgrs.2014.2310136>. – DOI 10.1109/tgrs.2014.2310136

**Iwamoto et al. 2013**

IWAMOTO, K. ; OHSHIMA, K.I. ; TAMURA, T. ; NIHASHI, S.: Estimation of thin ice thickness from AMSR-E data in the Chukchi Sea. In: *International Journal of Remote Sensing* 34 (2013), jan, No. 2, 468–489. <http://dx.doi.org/10.1080/01431161.2012.712229>. – DOI 10.1080/01431161.2012.712229

**Iwamoto et al. 2014**

IWAMOTO, Katsushi ; OHSHIMA, Kay I. ; TAMURA, Takeshi: Improved mapping of sea ice production in the Arctic Ocean using AMSR-E thin ice thickness algorithm. In: *Journal of Geophysical Research: Oceans* 119 (2014), No. 6, 3574–3594. <http://dx.doi.org/10.1002/2013jc009749>. – DOI 10.1002/2013jc009749

**Jakobsson et al. 2012**

JAKOBSSON, Martin ; MAYER, Larry ; COAKLEY, Bernard ; DOWDESWELL, Julian A. ; FORBES, Steve ; FRIDMAN, Boris ; HODNESDAL, Hanne ; NOORMETS, Riko ; PEDERSEN, Richard ; REBESCO, Michele ; SCHENKE, Hans W. ; ZARAYSKAYA, Yulia ; ACCETTELLA, Daniela ; ARMSTRONG, Andrew ; ANDERSON, Robert M. ; BIENHOFF, Paul ; CAMERLENGHI, Angelo ; CHURCH, Ian ; EDWARDS, Margo ; GARDNER, James V. ; HALL, John K. ; HELL, Benjamin ; HESTVIK, Ole ; KRISTOFFERSEN, Yngve ; MARCUSSEN, Christian ; MOHAMMAD, Rezwan ; MOSHER, David ; NGHIEM, Son V. ; PEDROSA, Maria T. ; TRAVAGLINI, Paola G. ; WEATHERALL, Pauline: The international bathymetric chart of the Arctic Ocean (IBCAO) version 3.0. In: *Geophysical Research Letters* 39 (2012), No. 12. <http://dx.doi.org/10.1029/2012gl052219>. – DOI 10.1029/2012gl052219

**Jardon et al. 2014**

JARDON, FP ; VIVIER, Frédéric ; BOURUET-AUBERTOT, Pascale ; LOURENÇO, Antonio ; CUYPERS, Yannis ; WILLMES, S: Ice production in Storfjorden (Svalbard) estimated from a model based on AMSR-E observations: Impact on water mass properties. In: *Journal of Geophysical Research: Oceans* 119 (2014), No. 1, 377–393

**Jensen 2007**

JENSEN, J. R.: *Remote Sensing of the Environment*. Pearson Education, Inc., 2007

**Jin et al. 2006**

JIN, Xin ; BARBER, David ; PAPAKYRIAKOU, Tim: A new clear-sky downward longwave radiative flux parameterization for Arctic areas based on rawinsonde data. In: *J. Geophys. Res.* 111 (2006),

No. D24, D24104. <http://dx.doi.org/10.1029/2005jd007039>. – DOI 10.1029/2005jd007039. – ISSN 0148–0227

**Kaleschke et al. 2010**

KALESCHKE, L. ; MAASS, N. ; HAAS, C. ; HENDRICKS, S. ; HEYGSTER, G. ; TONBOE, R. T.: A sea-ice thickness retrieval model for 1.4 GHz radiometry and application to airborne measurements over low salinity sea-ice. In: *The Cryosphere* 4 (2010), dec, No. 4, 583–592. <http://dx.doi.org/10.5194/tc-4-583-2010>. – DOI 10.5194/tc-4-583-2010

**Kaleschke et al. 2012**

KALESCHKE, L. ; TIAN-KUNZE, X. ; MAASS, N. ; MÄKYNEN, M. ; DRUSCH, M.: Sea ice thickness retrieval from SMOS brightness temperatures during the Arctic freeze-up period. In: *Geophysical Research Letters* 39 (2012), mar, No. 5, n/a–n/a. <http://dx.doi.org/10.1029/2012gl050916>. – DOI 10.1029/2012gl050916

**Kaleschke et al. 2016**

KALESCHKE, Lars ; TIAN-KUNZE, Xiangshan ; MAASS, Nina ; BEITSCH, Alexander ; WERNECKE, Andreas ; MIERNECKI, Maciej ; MÜLLER, Gerd ; FOCK, Björn H. ; GIERISCH, Andrea M. ; SCHLÜNZEN, K. H. ; POHLMANN, Thomas ; DOBRYNIN, Mikhail ; HENDRICKS, Stefan ; ASSENG, Jörlund ; GERDES, Rüdiger ; JOCHMANN, Peter ; REIMER, Nils ; HOLFORT, Jürgen ; MELSHEIMER, Christian ; HEYGSTER, Georg ; SPREEN, Gunnar ; GERLAND, Sebastian ; KING, Jennifer ; SKOU, Niels ; SØBJÆRG, Sten S. ; HAAS, Christian ; RICHTER, Friedrich ; CASAL, Tânia: SMOS sea ice product: Operational application and validation in the Barents Sea marginal ice zone. In: *Remote Sensing of Environment* 180 (2016), jul, 264–273. <http://dx.doi.org/10.1016/j.rse.2016.03.009>. – DOI 10.1016/j.rse.2016.03.009

**Kaleschke et al. 2015**

KALESCHKE, Lars ; TIAN-KUNZE, Xiangshan ; MAASS, Nina ; RICKER, Robert ; HENDRICKS, Stefan ; DRUSCH, Matthias: Improved retrieval of sea ice thickness from SMOS and Cryosat-2. In: *Geoscience and Remote Sensing Symposium (IGARSS), 2015 IEEE International IEEE, 2015*, 5232–5235

**Kanamitsu et al. 2002**

KANAMITSU, Masao ; EBISUZAKI, Wesley ; WOOLLEN, Jack ; YANG, Shi-Keng ; HNILO, JJ ; FIORINO, M ; POTTER, GL: NCEP-DOE AMIP-II Reanalysis (R-2). In: *Bulletin of the American Meteorological Society* 83 (2002), No. 11, 1631–1643

**Kassens et al. 1995**

KASSENS, Heidemarie ; PIEPENBURG, Dieter ; THIEDE, Jörn ; TIMOKHOV, Leonid ; HUBBERTEN, Hans-Wolfgang ; PRYAMIKOV, SM: Russian-German Cooperation: Laptev Sea System. In: *Berichte zur Polarforschung (Reports on Polar Research)* (1995), No. 176. <http://dx.doi.org/10013/epic.10177>. – DOI 10013/epic.10177

**Kern 2008**

KERN, Stefan: Polynya area in the Kara Sea, Arctic, obtained with microwave radiometry for 1979–2003. In: *Geoscience and Remote Sensing Letters, IEEE* 5 (2008), No. 2, 171–175

**Kern et al. 2007**

KERN, Stefan ; SPREEN, Gunnar ; KALESCHKE, Lars ; LA ROSA, Sara de ; HEYGSTER, Georg: Polynya Signature Simulation Method polynya area in comparison to AMSR-E 89 GHz sea-ice concentrations in the Ross Sea and off the Adélie Coast, Antarctica, for 2002–05: first results. In: *Annals of Glaciology* 46 (2007), No. 1, 409–418. <http://dx.doi.org/10.3189/172756407782871585>. – DOI 10.3189/172756407782871585



**Krumpen et al. 2016**

KRUMPEN, T. ; GERDES, R. ; HAAS, C. ; HENDRICKS, S. ; HERBER, A. ; SELYZHENOK, V. ; SMEDSRUD, L. ; SPREEN, G.: Recent summer sea ice thickness surveys in Fram Strait and associated ice volume fluxes. In: *The Cryosphere* 10 (2016), No. 2, 523–534. <http://dx.doi.org/10.5194/tc-10-523-2016>. – DOI 10.5194/tc-10-523-2016

**Krumpen et al. 2013**

KRUMPEN, Thomas ; JANOUT, Markus ; HODGES, KI ; GERDES, Rüdiger ; GIRARD-ARDHUIN, Fanny ; HÖLEMANN, Jens ; WILLMES, Sascha: Variability and trends in Laptev Sea ice outflow between 1992–2011. In: *The Cryosphere* 7 (2013), 1–15

**Kurtz et al. 2014**

KURTZ, N. T. ; GALIN, N. ; STUDINGER, M.: An improved CryoSat-2 sea ice freeboard retrieval algorithm through the use of waveform fitting. In: *The Cryosphere* 8 (2014), jul, No. 4, 1217–1237. <http://dx.doi.org/10.5194/tc-8-1217-2014>. – DOI 10.5194/tc-8-1217-2014

**Kwok et al. 2007**

KWOK, R. ; COMISO, J. C. ; MARTIN, S. ; DRUCKER, R.: Ross Sea polynyas: Response of ice concentration retrievals to large areas of thin ice. In: *J. Geophys. Res.* 112 (2007), No. C12, C12012. <http://dx.doi.org/10.1029/2006jc003967>. – DOI 10.1029/2006jc003967. – ISSN 0148–0227

**Kwok et al. 2009**

KWOK, R. ; CUNNINGHAM, G.F. ; WENSNAHAN, M. ; RIGOR, I. ; ZWALLY, H.J. ; YI, D.: Thinning and volume loss of the Arctic Ocean sea ice cover: 2003–2008. In: *Journal of Geophysical Research* 114 (2009), No. C7

**Kwok and Rothrock 2009**

KWOK, R. ; ROTHROCK, D. A.: Decline in Arctic sea ice thickness from submarine and ICESat records: 1958–2008. In: *Geophysical Research Letters* 36 (2009), aug, No. 15, n/a–n/a. <http://dx.doi.org/10.1029/2009gl039035>. – DOI 10.1029/2009gl039035

**Kwok et al. 2013**

KWOK, R. ; SPREEN, G. ; PANG, S.: Arctic sea ice circulation and drift speed: Decadal trends and ocean currents. In: *Journal of Geophysical Research: Oceans* 118 (2013), No. 5, 2408–2425

**Launiainen and Vihma 1990**

LAUNIAINEN, J. ; VIHMA, T.: Derivation of turbulent surface fluxes - An iterative flux-profile method allowing arbitrary observing heights. In: *Environmental Software* 5 (1990), No. 3, 113–124. [http://dx.doi.org/10.1016/0266-9838\(90\)90021-w](http://dx.doi.org/10.1016/0266-9838(90)90021-w). – DOI 10.1016/0266-9838(90)90021-w. – ISSN 0266–9838

**Laxon et al. 2013**

LAXON, Seymour W. ; GILES, Katharine A. ; RIDOUT, Andy L. ; WINGHAM, Duncan J. ; WILLATT, Rosemary ; CULLEN, Robert ; KWOK, Ron ; SCHWEIGER, Axel ; ZHANG, Jinlun ; HAAS, Christian ; HENDRICKS, Stefan ; KRISHFIELD, Richard ; KURTZ, Nathan ; FARRELL, Sinead ; DAVIDSON, Malcolm: CryoSat-2 estimates of Arctic sea ice thickness and volume. In: *Geophysical Research Letters* 40 (2013), feb, No. 4, 732–737. <http://dx.doi.org/10.1002/grl.50193>. – DOI 10.1002/grl.50193

**Lillesand et al. 2007**

LILLESAND, Thomas ; KIEFER, Ralph W. ; CHIPMAN, Jonathan: *Remote Sensing and Image Interpretation*. 6th edition. Wiley John + Sons, 2007

**Liu and Key 2014**

LIU, Yinghui ; KEY, Jeffrey R.: Less winter cloud aids summer 2013 Arctic sea ice return from 2012 minimum. In: *Environmental Research Letters* 9 (2014), No. 4, 044002. <http://dx.doi.org/10.1088/1748-9326/9/4/044002>. – DOI 10.1088/1748-9326/9/4/044002

**Lubin and Massom 2006**

LUBIN, Dan ; MASSOM, Robert: *Polar Remote Sensing, Volume I: Atmosphere and Oceans*. Bd. 1. Springer, 2006. – 775 S.

**Lüpkes et al. 2008**

LÜPKES, Christof ; VIHMA, T ; BIRNBAUM, Gerit ; WACKER, Ulrike: Influence of leads in sea ice on the temperature of the atmospheric boundary layer during polar night. In: *Geophysical Research Letters* 35 (2008), feb, No. 3. <http://dx.doi.org/10.1029/2007gl032461>. – DOI 10.1029/2007gl032461

**Markus and Burns 1995**

MARKUS, T. ; BURNS, B. A.: A method to estimate subpixel-scale coastal polynyas with satellite passive microwave data. In: *Journal of Geophysical Research* 100 (1995), No. C3, 4473–4487

**Markus and Cavalieri 2000**

MARKUS, T. ; CAVALIERI, D.J.: An enhancement of the NASA Team sea ice algorithm. In: *IEEE Transactions on Geoscience and Remote Sensing* 38 (2000), may, No. 3, 1387–1398. <http://dx.doi.org/10.1109/36.843033>. – DOI 10.1109/36.843033

**Markus et al. 2009**

MARKUS, Thorsten ; STROEVE, Julianne C. ; MILLER, Jeffrey: Recent changes in Arctic sea ice melt onset, freezeup, and melt season length. In: *J. Geophys. Res.* 114 (2009), dec, No. C12. <http://dx.doi.org/10.1029/2009jc005436>. – DOI 10.1029/2009jc005436

**Martin 2001**

MARTIN, S.: Polynyas. In: STEELE, John H. (Hrsg.) ; THORPE, Steve A. (Hrsg.) ; TUREKIAN, Karl K. (Hrsg.): *Encyclopedia of Ocean Sciences*. Academic Press, 2001, 22412247

**Martin et al. 2004**

MARTIN, Seelye ; DRUCKER, Robert ; KWOK, Ronald ; HOLT, Benjamin: Estimation of the thin ice thickness and heat flux for the Chukchi Sea Alaskan coast polynya from Special Sensor Microwave/Imager data, 1990–2001. In: *J. Geophys. Res.* 109 (2004), No. C10, C10012. – ISSN 0148-0227

**Martin et al. 2005**

MARTIN, Seelye ; DRUCKER, Robert ; KWOK, Ronald ; HOLT, Benjamin: Improvements in the estimates of ice thickness and production in the Chukchi Sea polynyas derived from AMSR-E. In: *Geophys. Res. Lett.* 32 (2005), No. 5, L05505. – ISSN 0094-8276

**Maslanik et al. 2007**

MASLANIK, J. A. ; FOWLER, C. ; STROEVE, J. ; DROBOT, S. ; ZWALLY, J. ; YI, D. ; EMERY, W.: A younger, thinner Arctic ice cover: Increased potential for rapid, extensive sea-ice loss. In: *Geophysical Research Letters* 34 (2007), No. 24, n/a–n/a. <http://dx.doi.org/10.1029/2007GL032043>. – DOI 10.1029/2007GL032043. – ISSN 1944-8007. – L24501

**Maslanik et al. 2011**

MASLANIK, James ; STROEVE, Julianne ; FOWLER, Charles ; EMERY, William: Distribution and trends in Arctic sea ice age through spring 2011. In: *Geophysical Research Letters* 38 (2011), jul, No. 13, n/a–n/a. <http://dx.doi.org/10.1029/2011gl047735>. – DOI 10.1029/2011gl047735

**Maykut 1978**

MAYKUT, Gary A.: Energy Exchange Over Young Sea Ice in the Central Arctic. In: *J. Geophys. Res.* 83 (1978), No. C7, 3646–3658. – ISSN 0148–0227

**Maykut 1982**

MAYKUT, Gary A.: Large-scale heat exchange and ice production in the central Arctic. In: *Journal of Geophysical Research* 87 (1982), No. C10, 7971. <http://dx.doi.org/10.1029/jc087ic10p07971>. – DOI 10.1029/jc087ic10p07971

**Melling et al. 2015**

MELLING, Humfrey ; HAAS, Christian ; BROSSIER, Eric: Invisible polynyas: Modulation of fast ice thickness by ocean heat flux on the Canadian polar shelf. In: *Journal of Geophysical Research, Oceans* 120 (2015), feb, No. 2, 777–795. <http://dx.doi.org/10.1002/2014jc010404>. – DOI 10.1002/2014jc010404

**Moore et al. 2016**

MOORE, G. W. K. ; BROMWICH, David H. ; WILSON, Aaron B. ; RENFREW, Ian ; BAI, Lesheng: Arctic System Reanalysis improvements in topographically forced winds near Greenland. In: *Quarterly Journal of the Royal Meteorological Society* 142 (2016), may, No. 698, 2033–2045. <http://dx.doi.org/10.1002/qj.2798>. – DOI 10.1002/qj.2798

**Morales-Maqueda et al. 2004**

MORALES-MAQUEDA, M. ; WILLMOTT, A.J. ; BIGGS, N.: Polynya dynamics: A review of observations and modeling. In: *Reviews of Geophysics* 42 (2004), No. 1, 1–37. <http://dx.doi.org/10.1029/2002rg000116>. – DOI 10.1029/2002rg000116

**Naoki et al. 2008**

NAOKI, Kazuhiro ; UKITA, Jinro ; NISHIO, Fumihiko ; NAKAYAMA, Masashige ; COMISO, Josefino C. ; GASIEWSKI, Al: Thin sea ice thickness as inferred from passive microwave and in situ observations. In: *Journal of Geophysical Research: Oceans* 113 (2008), No. C2, n/a–n/a. <http://dx.doi.org/10.1029/2007JC004270>. – DOI 10.1029/2007JC004270. – ISSN 2156–2202. – C02S16

**Overland et al. 2012**

OVERLAND, James E. ; FRANCIS, Jennifer A. ; HANNA, Edward ; WANG, Muyin: The recent shift in early summer Arctic atmospheric circulation. In: *Geophysical Research Letters* 39 (2012), No. 19

**Overland and Wang 2013**

OVERLAND, James E. ; WANG, Muyin: When will the summer Arctic be nearly sea ice free? In: *Geophysical Research Letters* 40 (2013), No. 10, 2097–2101

**Paul et al. 2015a**

PAUL, S. ; WILLMES, S. ; HEINEMANN, G.: Long-term coastal-polynya dynamics in the Southern Weddell Sea from MODIS thermal-infrared imagery. In: *The Cryosphere* 9 (2015), 2027–2041. <http://dx.doi.org/10.5194/tc-9-2027-2015>. – DOI 10.5194/tc-9-2027-2015

**Paul et al. 2015b**

PAUL, Stephan ; WILLMES, Sascha ; GUTJAHR, Oliver ; PREUSSER, Andreas ; HEINEMANN, Günther: Spatial Feature Reconstruction of Cloud-Covered Areas in Daily MODIS Composites. In: *Remote Sensing* 7 (2015), No. 5, 5042–5056. <http://dx.doi.org/10.3390/rs70505042>. – DOI 10.3390/rs70505042

**Perovich et al. 2016**

PEROVICH, D. ; MEIER, W. ; TSCHUDI, M. ; FARRELL, S. ; GERLAND, S. ; HENDRICKS, S. ; KRUMPEN, T. ; HAAS, C.: Sea Ice. In: *Arctic Report Card 2016*. available online, 2016

**Perovich et al. 2007**

PEROVICH, Donald K. ; LIGHT, Bonnie ; EICKEN, Hajo ; JONES, Kathleen F. ; RUNCIMAN, Kay ; NGHIEM, Son V.: Increasing solar heating of the Arctic Ocean and adjacent seas, 1979–2005: Attribution and role in the ice-albedo feedback. In: *Geophysical Research Letters* 34 (2007), No. 19

**Persson and Vihma 2017**

In: PERSSON, Ola ; VIHMA, Timo: *The atmosphere over sea ice*. 3. John Wiley & Sons, Ltd, 2017. – ISBN 9781118778371, 160–196

**Petrich and Eicken 2010**

PETRICH, C. ; EICKEN, H.: Growth, Structure and Properties of Sea Ice. In: THOMAS, D. (Hrsg.) ; DIECKMANN, G. (Hrsg.): *Sea Ice*. Wiley-Blackwell, 2010, Kapitel Sea Ice and Oceanography, 79–112

**Pithan and Mauritsen 2014**

PITHAN, Felix ; MAURITSEN, Thorsten: Arctic amplification dominated by temperature feedbacks in contemporary climate models. In: *Nature Geoscience* 7 (2014), feb, No. 3, 181–184. <http://dx.doi.org/10.1038/ngeo2071>. – DOI 10.1038/ngeo2071

**Preußner et al. 2016**

PREUSSER, A. ; HEINEMANN, G. ; WILLMES, S. ; PAUL, S.: Circumpolar polynya regions and ice production in the Arctic: results from MODIS thermal infrared imagery from 2002/2003 to 2014/2015 with a regional focus on the Laptev Sea. In: *The Cryosphere* 10 (2016), No. 6, 3021–3042. <http://dx.doi.org/10.5194/tc-10-3021-2016>. – DOI 10.5194/tc-10-3021-2016

**Preußner et al. 2015a**

PREUSSER, Andreas ; HEINEMANN, Günther ; WILLMES, Sascha ; PAUL, Stephan: Multi-Decadal Variability of Polynya Characteristics and Ice Production in the North Water Polynya by Means of Passive Microwave and Thermal Infrared Satellite Imagery. In: *Remote Sensing* 7 (2015), No. 12, 15844–15867

**Preußner et al. 2015b**

PREUSSER, Andreas ; WILLMES, Sascha ; HEINEMANN, Günther ; PAUL, Stephan: Thin-ice dynamics and ice production in the Storfjorden polynya for winter seasons 2002/2003–2013/2014 using MODIS thermal infrared imagery. In: *The Cryosphere* 9 (2015), No. 3, 1063–1073. <http://dx.doi.org/10.5194/tc-9-1063-2015>. – DOI 10.5194/tc-9-1063-2015

**Rees 2006**

REES, G.: *Remote Sensing of Snow and Ice*. CRC Press Taylor & Francis Group, 2006

**Renfrew et al. 2002**

RENFREW, Ian A. ; KING, John C. ; MARKUS, Thorsten: Coastal polynyas in the southern Weddell Sea: Variability of the surface energy budget. In: *J. Geophys. Res.* 107 (2002), No. C6, 3063. – ISSN 0148–0227

**Ricker et al. 2014**

RICKER, R. ; HENDRICKS, S. ; HELM, V. ; SKOURUP, H. ; DAVIDSON, M.: Sensitivity of CryoSat-2 Arctic sea-ice freeboard and thickness on radar-waveform interpretation. In: *The Cryosphere* 8 (2014), aug, No. 4, 1607–1622. <http://dx.doi.org/10.5194/tc-8-1607-2014>. – DOI 10.5194/tc-8-1607-2014

**Riggs et al. 2006**

RIGGS, G. ; HALL, DK ; SALOMONSON, VV: *MODIS Sea Ice Products User Guide to Collection 5*. University of Colorado, Boulder, CO 80309-0449 USA: National Snow and Ice Data Center, December 2006

**Rigor et al. 2002**

RIGOR, Ignatius G. ; WALLACE, John M. ; COLONY, Roger L.: Response of sea ice to the Arctic Oscillation. In: *Journal of Climate* 15 (2002), No. 18, 2648–2663

**Serreze and Barry 2011**

SERREZE, Mark C. ; BARRY, Roger G.: Processes and impacts of Arctic amplification: A research synthesis. In: *Global and Planetary Change* 77 (2011), may, No. 1-2, 85–96. <http://dx.doi.org/10.1016/j.gloplacha.2011.03.004>. – DOI 10.1016/j.gloplacha.2011.03.004

**Serreze and Stroeve 2015**

SERREZE, Mark C. ; STROEVE, Julienne: Arctic sea ice trends, variability and implications for seasonal ice forecasting. In: *Philosophical Transactions of the Royal Society A: Mathematical, Physical and Engineering Sciences* 373 (2015), jun, No. 2045, 20140159. <http://dx.doi.org/10.1098/rsta.2014.0159>. – DOI 10.1098/rsta.2014.0159

**Shindell and Faluvegi 2009**

SHINDELL, Drew ; FALUVEGI, Greg: Climate response to regional radiative forcing during the twentieth century. In: *Nature Geoscience* 2 (2009), mar, No. 4, 294–300. <http://dx.doi.org/10.1038/ngeo473>. – DOI 10.1038/ngeo473

**Shokr and Sinha 2015**

SHOKR, Mohammed ; SINHA, Nirmal: *Sea Ice: Physics and Remote Sensing*. John Wiley & Sons, Inc, 2015. <http://dx.doi.org/10.1002/9781119028000>. <http://dx.doi.org/10.1002/9781119028000>

**Skogseth et al. 2004**

SKOGSETH, R ; HAUGAN, PM ; HAARPAINTNER, J: Ice and brine production in Storfjorden from four winters of satellite and in situ observations and modeling. In: *Journal of Geophysical Research: Oceans (1978–2012)* 109 (2004), No. C10

**Skogseth et al. 2005**

SKOGSETH, Ragnheid ; FER, Ilker ; HAUGAN, Peter M.: Dense-Water Production and Overflow from an Arctic Coastal Polynya in Storfjorden. In: *The Nordic Seas: An Integrated Perspective* (2005), 73–88. <http://dx.doi.org/10.1029/158GM07>. – DOI 10.1029/158GM07

**Smedsrud et al. 2017**

SMEDSRUD, Lars H. ; HALVORSEN, Mari H. ; STROEVE, Julienne C. ; ZHANG, Rong ; KLOSTER, Kjell: Fram Strait sea ice export variability and September Arctic sea ice extent over the last 80 years. In: *The Cryosphere* 11 (2017), jan, No. 1, 65–79. <http://dx.doi.org/10.5194/tc-11-65-2017>. – DOI 10.5194/tc-11-65-2017

**Smith et al. 1990**

SMITH, Stuart D. ; MUENCH, Robin D. ; PEASE, Carol H.: Polynyas and leads: An overview of physical processes and environment. In: *Journal of Geophysical Research* 95 (1990), No. C6, 9461–9479. <http://dx.doi.org/10.1029/jc095ic06p09461>. – DOI 10.1029/jc095ic06p09461

**Smith and Barber 2007**

SMITH, W.O. ; BARBER, D.G.: Polynyas and Climate Change: A View to the Future. Version: 2007. [http://dx.doi.org/10.1016/s0422-9894\(06\)74013-2](http://dx.doi.org/10.1016/s0422-9894(06)74013-2). In: SMITH, W. O. (Hrsg.) ; BARBER, D. G. (Hrsg.): *Polynyas - Windows to the World*. Elsevier Oceanography Series, 2007. – DOI 10.1016/s0422-9894(06)74013-2, Kapitel 13, 411–419

**Spreen et al. 2008**

SPREEN, G. ; KALESCHKE, L. ; HEYGSTER, G.: Sea ice remote sensing using AMSR-E 89 GHz channels. In: *Journal of Geophysical Research* 113 (2008), No. C2. <http://dx.doi.org/10.1029/2005JC003384>. – DOI 10.1029/2005JC003384

**Spreen and Kern 2017**

In: SPREEN, Gunnar ; KERN, Stefan: *Methods of satellite remote sensing of sea ice*. 3. John Wiley & Sons, Ltd, 2017. – ISBN 9781118778371, 239–260

**Spreen et al. 2011**

SPREEN, Gunnar ; KWOK, Ron ; MENEMENLIS, Dimitris: Trends in Arctic sea ice drift and role of wind forcing: 1992-2009. In: *Geophysical Research Letters* 38 (2011), oct, No. 19, n/a-n/a. <http://dx.doi.org/10.1029/2011gl048970>. – DOI 10.1029/2011gl048970

**Stroeve et al. 2014**

STROEVE, JC ; MARKUS, Thorsten ; BOISVERT, Linette ; MILLER, J ; BARRETT, A: Changes in Arctic melt season and implications for sea ice loss. In: *Geophysical Research Letters* 41 (2014), No. 4, 1216–1225

**Stroeve et al. 2011**

STROEVE, Julienne C. ; SERREZE, Mark C. ; HOLLAND, Marika M. ; KAY, Jennifer E. ; MALANIK, James ; BARRETT, Andrew P.: The Arctics rapidly shrinking sea ice cover: a research synthesis. In: *Climatic Change* 110 (2011), No. 3-4, 1005–1027

**Tamura and Ohshima 2011**

TAMURA, Takeshi ; OHSHIMA, Kay I.: Mapping of sea ice production in the Arctic coastal polynyas. In: *J. Geophys. Res.* 116 (2011), No. C7, C07030. <http://dx.doi.org/10.1029/2010jc006586>. – DOI 10.1029/2010jc006586. – ISSN 0148–0227

**Tamura et al. 2007**

TAMURA, Takeshi ; OHSHIMA, Kay I. ; MARKUS, Thorsten ; CAVALIERI, Donald J. ; NIHASHI, Sohey ; HIRASAWA, Naohiko: Estimation of Thin Ice Thickness and Detection of Fast Ice from SSM/I Data in the Antarctic Ocean. In: *J. Atmos. Oceanic Technol.* 24 (2007), No. 10, 1757–1772. <http://dx.doi.org/10.1175/jtech2113.1>. – DOI 10.1175/jtech2113.1. – ISSN 0739–0572

**Tamura et al. 2008**

TAMURA, Takeshi ; OHSHIMA, Kay I. ; NIHASHI, Sohey: Mapping of sea ice production for Antarctic coastal polynyas. In: *Geophys. Res. Lett.* 35 (2008), No. 7, L07606. <http://dx.doi.org/10.1029/2007g1032903>. – DOI 10.1029/2007g1032903. – ISSN 0094–8276

**Tedesco 2015**

TEDESCO, Marco: *Remote Sensing of the Cryosphere*. John Wiley & Sons Inc, 2015. – ISBN 1118368851

**Tetzlaff et al. 2015**

TETZLAFF, A. ; LÜPKES, C. ; HARTMANN, J.: Aircraft-based observations of atmospheric boundary-layer modification over Arctic leads. In: *Quarterly Journal of the Royal Meteorological Society* 141 (2015), jun, No. 692, 2839–2856. <http://dx.doi.org/10.1002/qj.2568>. – DOI 10.1002/qj.2568

**Tian-Kunze et al. 2014**

TIAN-KUNZE, X. ; KALESCHKE, L. ; MAASS, N. ; MÄKYNEN, M. ; SERRA, N. ; DRUSCH, M. ; KRUMPEN, T.: SMOS-derived thin sea ice thickness: algorithm baseline, product specifications and initial verification. In: *The Cryosphere* 8 (2014), may, No. 3, 997–1018. <http://dx.doi.org/10.5194/tc-8-997-2014>. – DOI 10.5194/tc-8-997-2014

**Timco and Frederking 1996**

TIMCO, GW ; FREDERKING, RMW: A review of sea ice density. In: *Cold Regions Science and Technology* 24 (1996), No. 1, 1–6. [http://dx.doi.org/10.1016/0165-232X\(95\)00007-X](http://dx.doi.org/10.1016/0165-232X(95)00007-X). – DOI 10.1016/0165-232X(95)00007-X

**Tschudi and Meier 2016**

TSCHUDI, C. Fowler J. Maslanik J. S. S. M. ; MEIER, W.: *EASE-Grid Sea Ice Age, Version 3*. Boulder, Colorado USA: NASA National Snow and Ice Data Center Distributed Active Archive Center, 12 2016. <http://dx.doi.org/http://dx.doi.org/10.5067/PFSVFZA9Y85G>. <http://dx.doi.org/http://dx.doi.org/10.5067/PFSVFZA9Y85G>

**Wadhams 2000**

WADHAMS, Peter: *Ice in the Ocean*. CRC Press, 2000

**Weeks and Ackley 1986**

WEEKS, Wilford F. ; ACKLEY, Stephen F.: The growth, structure, and properties of sea ice. In: *The geophysics of sea ice*. Springer, 1986, 9–164

**Weeks 2010**

WEEKS, Willy F.: *On Sea Ice*. P.O. Box 756240, Fairbanks, AK 99775-6240 : University of Alaska Press, 2010. – ISBN 160223079X

**Willmes et al. 2010**

WILLMES, S. ; KRUMPEN, T. ; ADAMS, S. ; RABENSTEIN, L. ; HAAS, C. ; HOELEMANN, J. ; HENDRICKS, S. ; HEINEMANN, G.: Cross-validation of polynya monitoring methods from multisensor satellite and airborne data: a case study for the Laptev Sea. In: *Canadian Journal of Remote Sensing* 36 (2010), No. S1, S196–S210. <http://dx.doi.org/10.5589/m10-012>. – DOI 10.5589/m10-012

**Willmes et al. 2014**

WILLMES, S. ; NICOLAUS, M. ; HAAS, C.: The microwave emissivity variability of snow covered first-year sea ice from late winter to early summer: a model study. In: *The Cryosphere* 8 (2014), No. 3, 891–904. <http://dx.doi.org/10.5194/tc-8-891-2014>. – DOI 10.5194/tc-8-891-2014

**Willmes et al. 2011**

WILLMES, Sascha ; ADAMS, Susanne ; SCHRÖDER, David ; HEINEMANN, Günther: Spatio-temporal variability of polynya dynamics and ice production in the Laptev Sea between the winters of 1979/80 and 2007/08. In: *Polar Research* 30 (5971) (2011), 16. <http://dx.doi.org/10.3402/polar.v30i0.5971>. – DOI 10.3402/polar.v30i0.5971

**Willmes and Heinemann 2015**

WILLMES, Sascha ; HEINEMANN, Günther: Pan-Arctic lead detection from MODIS thermal infrared imagery. In: *Annals of Glaciology* 56 (2015), No. 69, 29–37

**Willmes and Heinemann 2016**

WILLMES, Sascha ; HEINEMANN, Günther: Sea-Ice Wintertime Lead Frequencies and Regional Characteristics in the Arctic, 2003–2015. In: *Remote Sensing* 8 (2016), No. 1, 4

**Winsor and Björk 2000**

WINSOR, Peter ; BJÖRK, Göran: Polynya activity in the Arctic Ocean from 1958 to 1997. In: *Journal of Geophysical Research* 105 (2000), No. C4, 8789–8803

**Wood et al. 2013**

WOOD, Kevin R. ; OVERLAND, James E. ; SALO, Sigrid A. ; BOND, Nicholas A. ; WILLIAMS,

William J. ; DONG, Xiquan: Is there a “new normal” climate in the Beaufort Sea? In: *Polar Research* 32 (2013), oct, No. 0. <http://dx.doi.org/10.3402/polar.v32i0.19552>. – DOI 10.3402/polar.v32i0.19552

**Woodhouse 2006**

WOODHOUSE, Iain H.: *Introduction to Microwave Remote Sensing*. Taylor & Francis Ltd, 2006. – ISBN 0415271231

**Yu and Lindsay 2003**

YU, Y. ; LINDSAY, R.W.: Comparison of thin ice thickness distributions derived from RADARSAT Geophysical Processor System and advanced very high resolution radiometer data sets. In: *J. Geophys. Res.* 108 (2003), No. C12, 3387. <http://dx.doi.org/10.1029/2002jc001319>. – DOI 10.1029/2002jc001319. – ISSN 0148-0227

**Yu and Rothrock 1996**

YU, Y. ; ROTHROCK, D. A.: Thin ice thickness from satellite thermal imagery. In: *J. Geophys. Res.* 101 (1996), No. C11, 25753–25766. <http://dx.doi.org/10.1029/96jc02242>. – DOI 10.1029/96jc02242. – ISSN 0148-0227

**Yu et al. 2014**

YU, Yanling ; STERN, Harry ; FOWLER, Charles ; FETTERER, Florence ; MASLANIK, James: Inter-annual Variability of Arctic Landfast Ice between 1976 and 2007. In: *Journal of Climate* 27 (2014), jan, No. 1, 227–243. <http://dx.doi.org/10.1175/jcli-d-13-00178.1>. – DOI 10.1175/jcli-d-13-00178.1

**Zhang and Rothrock 2003**

ZHANG, Jinlun ; ROTHROCK, D. A.: Modeling Global Sea Ice with a Thickness and Enthalpy Distribution Model in Generalized Curvilinear Coordinates. In: *Monthly Weather Review* 131 (2003), may, No. 5, 845–861. [http://dx.doi.org/10.1175/1520-0493\(2003\)131<0845:mgsiwa>2.0.co;2](http://dx.doi.org/10.1175/1520-0493(2003)131<0845:mgsiwa>2.0.co;2). – DOI 10.1175/1520-0493(2003)131<0845:mgsiwa>2.0.co;2

**Zwally et al. 2002**

ZWALLY, H.J. ; SCHUTZ, B. ; ABDALATI, W. ; ABSHIRE, J. ; BENTLEY, C. ; BRENNER, A. ; BUFTON, J. ; DEZIO, J. ; HANCOCK, D. ; HARDING, D. ; HERRING, T. ; MINSTER, B. ; QUINN, K. ; PALM, S. ; SPINHIRNE, J. ; THOMAS, R.: ICESat's laser measurements of polar ice, atmosphere, ocean, and land. In: *Journal of Geodynamics* 34 (2002), oct, No. 3-4, 405–445. [http://dx.doi.org/10.1016/s0264-3707\(02\)00042-x](http://dx.doi.org/10.1016/s0264-3707(02)00042-x). – DOI 10.1016/s0264-3707(02)00042-x



## **Curriculum Vitae - Andreas Preußer, M.Sc.**

# Andreas Preußner, M.Sc.

Bruchhausenstraße 11 || 54290 Trier (Germany)

*Phone (mobile)* +49 (0)176/63107752  
*Phone (work)* +49 (0)651/201-4630  
*Email* preusser@uni-trier.de  
*Date of birth* 03 June 1986  
*Place of birth* Dernbach (Germany)  
*Nationality* German

---

## Work & Education

- 04/2016 – 12/2016 **Ocean and Sea Ice Dynamics Group**, Institute of Low Temperature Science, Hokkaido University, Sapporo, Japan  
*Japan Society for the Promotion of Science (JSPS) – Postdoctoral Fellowship Short-term (dt.: “JSPS-Forschungskurzstipendium für Doktoranden und Postdoktoranden nach Japan”)*
- 09/2013 – present **Dept. of Environmental Meteorology**, University of Trier, Trier, Germany  
*Ph.D. candidate and Research Associate (Project “Laptev Sea Transdrift 2013-2016”)*
- 10/2010 – 08/2013 **University of Trier**, Trier, Germany  
*Course of study: M.Sc. Environmental Assessment and Management: Remote Sensing and Modeling (Awarded as Top-Student of this course in 2013)*  
*Master thesis: “Remote sensing of polynya characteristics in the Arctic” (Grade: 1.0)*
- 10/2007 – 09/2010 **University of Trier**, Trier, Germany  
*Course of study: B.Sc. Environmental Geosciences*  
*Bachelor thesis: “Investigation of the dynamics of the North Water Polynya for 1996-2010 using satellite data” (Grade: 1.3)*
- 10/2006 – 09/2007 **Trier University of Applied Sciences**, Trier, Germany  
*Course of study: Mechanical Engineering (not graduated)*
- 08/1997 – 03/2005 **Mons-Tabor Gymnasium**, Montabaur, Germany  
*Principal Subjects: Geography, Mathematics, English*

## Internships and further training

- 09/2013                    **Summer School “Glaciology and Remote Sensing of Ice”**  
16 – 26 September 2013, St. Ottilien, Germany.  
Supervisors: Prof. Dr. Angelika Humbert (Alfred Wegener Institute, Bremerhaven) and Prof. Dr. Matthias Braun (University of Erlangen-Nürnberg, Germany)
- 08/2012 – 09/2012    **Max Planck Institute for Chemistry**, Satellite Group, Mainz, Germany  
(Investigation of the effect of missing detector pixels on trace-gas retrievals using Ozone Monitoring Instrument (OMI) satellite data)
- 08/2009 – 09/2009    **Max Planck Institute for Chemistry**, Satellite Group, Mainz, Germany  
(Spectral measurements of vegetation using a MiniMax DOAS instrument)

## Previous Occupations

- 01/2013 – 07/2013    **Student/Research assistant in the department of Environmental Meteorology**, University of Trier, Trier, Germany (Project “Laptev Sea Transdrift”)
- 11/2012 – 12/2012    **Student/Research assistant in the department of Environmental Meteorology**, University of Trier, Trier, Germany (Project “Weddell Sea”)
- 05/2012 – 07/2012    **Research assistant in the department of Sea-ice physics / Climate sciences, Alfred Wegener Institute, Bremerhaven**, Germany (Designing maps and data products of Arctic sea-ice for [www.meereisportal.de](http://www.meereisportal.de))
- 10/2010 – 04/2012    **Student/Research assistant in the department of Environmental Meteorology**, University of Trier, Trier, Germany (Tutor “Introduction to Meteorology” & Project “Experimental study of the interaction of the atmosphere with polynyas/sea ice near Greenland - IKAPOS”)

## Languages

**German** (native speaker)  
**English** (high level in spoken and written English)  
**French** (basic communication and reading skills)  
**Japanese** (simple communication and reading skills)

## Field experience

- 03/2014                    **Aircraft campaign LEAST** (*Lead and ABL study in the Transpolar System*), operating from Longyearbyen (Svalbard), Norway.  
*Type of Aircraft: Basler BT-67 (POLAR 5), owned by the Alfred-Wegener Institute (AWI), Bremerhaven, Germany*

## Service

- 07/2016 - present    **Association of Polar Early Career Scientists Germany (National Committee)**  
*Co-founder and current board member*
- 05/2015            **Association of Polar Early Career Scientists**  
*Representative to the Annual Meeting of the German National Committee SCAR / IASC in Erlangen, Germany*

## Professional memberships

**Association of Polar Early Career Scientists (APECS)**  
**European Geosciences Union (EGU)**  
**German Society for Polar Research** (*Deutsche Gesellschaft für Polarforschung e.V.* – DGP)

## Publications and Conference Proceedings

### *Peer-reviewed:*

**Preußner, A.**, Heinemann, G., Willmes, S., and Paul, S. (2016): Circumpolar polynya regions and ice production in the Arctic: results from MODIS thermal infrared imagery from 2002/2003 to 2014/2015 with a regional focus on the Laptev Sea. *The Cryosphere*, 10, 3021-3042, doi: 10.5194/tc-10-3021-2016.

Gutjahr, O., Heinemann, G., **Preußner, A.**, Willmes, S., and Drüe, C. (2016): Quantification of ice production in Laptev Sea polynyas and its sensitivity to thin-ice parameterizations in a regional climate model. *The Cryosphere*, 10, 2999-3019, doi: 10.5194/tc-10-2999-2016.

**Preußner, A.**, Heinemann, G., Willmes, S., and Paul, S. (2015): Multi-Decadal Variability of Polynya Characteristics and Ice Production in the North Water Polynya by Means of Passive Microwave and Thermal Infrared Satellite Imagery. *Remote Sensing*, 7(12), 15844-15867, doi: 10.3390/rs71215807.

Paul, S., Willmes, S., Gutjahr, O., **Preußner, A.**, and Heinemann, G. (2015): Spatial Feature Reconstruction of Cloud-Covered Areas in Daily MODIS Composites. *Remote Sensing*, 7(5), 5042-5056, doi: 10.3390/rs70505042.

**Preußner, A.**, Willmes, S., Heinemann, G., and Paul, S. (2015): Thin-ice dynamics and ice production in the Storfjorden polynya for winter-seasons 2002/2003–2013/2014 using MODIS thermal infrared imagery. *The Cryosphere*, 9, 1063-1073, doi: 10.5194/tc-9-1063-2015.

### *Talks:*

**Preußner, A.**, Willmes, S., Heinemann, G., and Ohshima, K.I. (2016): Pan-Arctic polynya and salt flux dynamics between 2002/2003 and 2010/2011 – a multi-sensor intercomparison project. The Seventh Symposium on Polar Science at NIPR, Tokyo, Japan, November 29-December 02, 2016.

**Preußner, A.**, Heinemann, G., Willmes, S., and Paul, S. (2015): Pan-Arctic polynya dynamics and thermodynamic ice production estimates for 2002/2003-2014/2015 based on MODIS thermal infrared imagery and ERA-Interim reanalysis. 26<sup>th</sup> Congress on Polar Research, Munich, Germany, September 06-11, 2015.

**Preußner, A.,** Heinemann, G., Willmes, S., Drüe, C., and Paul, S. (2015): Long-term dynamics of the North Water polynya by means of passive microwave and thermal infrared imagery. Arctic Science Summit Week (ASSW) 2015, Toyama, Japan, April 27-30, 2015.

**Preußner, A.,** Heinemann, G., Willmes, S., and Paul, S. (2015): Thin-ice dynamics and ice production in the Storfjorden polynya for winter-seasons 2002/2003–2013/2014 using MODIS thermal infrared imagery. High Latitude Dynamics Workshop, Rosendal, Norway, March 23-27, 2015.

**Preußner, A.,** Willmes, S., Heinemann, G., and Paul, S. (2014): Linking MODIS satellite and airborne thermal infrared imagery to assess polynya characteristics in Storfjorden, Svalbard. Integrating spatial and temporal scales in the changing Arctic System (ISTAS), Plouzané/Brest, France, October 22, 2014.

**Preußner, A.,** Willmes, S. and Heinemann, G. (2014): Thin ice thickness distribution and ice production in the North Water and Laptev Sea polynya regions using MODIS thermal infrared imagery. European Geosciences Union (EGU), General Assembly, Vienna, Talk, April 29, 2014.

Heinemann, G. and **Preußner, A.** (2013): Long-term dynamics of the North Water Polynya: Comparison of different satellite data sets and methods. Arctic Science Summit Week (ASSW) 2013, Kraków, Poland, April 13-19, 2013.

Heinemann, G. and **Preußner, A.** (2012): A study of the dynamics of the North Water Polynya using different satellite data sets and models. Arctic Net 8<sup>th</sup> Annual Scientific Meeting (ASM2012), Vancouver (B.C.), Canada, December 10-14, 2012.

**Poster:**

**Preußner, A.,** Willmes, S., Heinemann, G., and Paul, S. (2016): Circumpolar polynya and fast-ice dynamics in the Arctic for 2002/2003-2014/2015 based on MODIS thermal infrared imagery and ERA-interim reanalysis. ESA Living Planet Symposium 2016, Prague, Poster, May 10-12, 2016.

**Preußner, A.,** Willmes, S., Heinemann, G., and Paul, S. (2016): Circumpolar polynya characteristics in the Arctic between 2002/2003 and 2014/2015 as derived from MODIS thermal infrared imagery and ERA-Interim reanalysis. European Geosciences Union (EGU), General Assembly, Vienna, Poster, April 18, 2016.

**Preußner, A.,** Willmes, S. and Heinemann, G. (2014): Thin ice thickness distribution and ice production in the Storfjorden Polynya for 2002/2003 - 2011/2012 using MODIS thermal infrared imagery. European Geosciences Union (EGU), General Assembly, Vienna, Poster, April 29, 2014.

**Preußner, A.,** Heinemann, G., Drüe C., (2011): Investigation of the dynamics of the North Water Polynya for 1996-2010 using satellite data, Geophysical Research Abstracts, 13, 2011, European Geosciences Union (EGU), General Assembly, Vienna, Austria, April 03–08, 2011.



Trier, 07<sup>th</sup> February 2017

Andreas Preußner

## Acknowledgements

I would like to take this opportunity to express my appreciation to some of the people who have contributed significantly to the success of this work.

I am highly grateful to Prof. Dr. Günther Heinemann for the supervision of my work, helpful and constructive consultations as well as the possibility to participate in the LEAST campaign in March 2014. Furthermore, I would like to thank him for the encouraging support to participate at international conferences as well as during the application for a JSPS fellowship to conduct research in Japan and APECS-related activities.

I would also like to thank Dr. Sascha Willmes for his continuous help and support for all kinds of science- and work-related matters, as well as the great time we had together as office mates in F48.

I highly appreciate the helpful and productive discussions with Dr. Stephan Paul, that helped a lot to shape the TIT-retrieval in its current form. Additional thanks for his steady motivation to become better at climbing up boulder-routes.

Furthermore, I would like to thank all my colleagues at the Department of Environmental Meteorology for the great working atmosphere, with a special mention of Anne Menkhaus, Uwe Baltes and Mercedes Peter for handling a huge proportion of organizational and logistical matters.

Also, I am very grateful for the hospitality of Prof. Kay I. Ohshima and the Ocean and Sea Ice Dynamics group at the Institute of Low Temperature Science, Hokkaido University. Their generous and helpful support and fruitful discussions during the final months of my thesis are highly appreciated.

Special thanks to my family Iris, Ulli, Markus, Elli and Titus Preußner for their endless support and motivation, and for being the definition of the term 'quality time'.

Finally, thanks to all my friends around the globe for everything beyond work, be it football, climbing, snowboarding or the joys of hop and grapes. Cheers!

---

The author wants to thank the National Snow and Ice Data Center (NSIDC), as well as the European Center for Medium-Range Weather Forecasts (ECMWF) for providing the passive microwave brightness temperature data, the MODIS Sea Ice product and the ERA-Interim atmospheric reanalysis data. The University of Bremen and the University of Hamburg are also kindly acknowledged for providing the passive microwave sea ice concentration data. This work was funded by the Federal Ministry of Education and Research (Bundesministerium für Bildung und Forschung - BMBF) under Grant 03G0833D. Additional financial support was provided by the Japan Society for the Promotion of Science (JSPS).

## Eidesstattliche Erklärung

Hiermit erkläre ich, Andreas Preußner, geb. am 03. Juni 1986 in Dernbach/Westerwald, dass ich die vorliegende Dissertation mit dem Thema

*Multi-sensor remote sensing of long-term circumpolar polynya characteristics in the Arctic*

selbständig verfasst und keine anderen als die angegebenen Quellen und Hilfsmittel benutzt habe, wobei ich alle wörtlichen und sinngemäßen Zitate als solche gekennzeichnet habe. Die Arbeit wurde bisher keiner anderen Prüfungsbehörde vorgelegt und auch nicht veröffentlicht. Bei einer anderen Hochschule wurde bisher noch kein Promotionsverfahren beantragt.

Trier, 13. Februar 2017

---

ANDREAS PREUSSNER